UiT
THE ARCTIC UNIVERSITY OF NORWAY

Faculty of Science and Technology

Department of Geosciences

Controls on fluid-flow systems in the Loppa High, SW Barents Sea

ANDERS CLAUSEN WOLLBERG

Master thesis in Geology, Geo-3900
May 2018

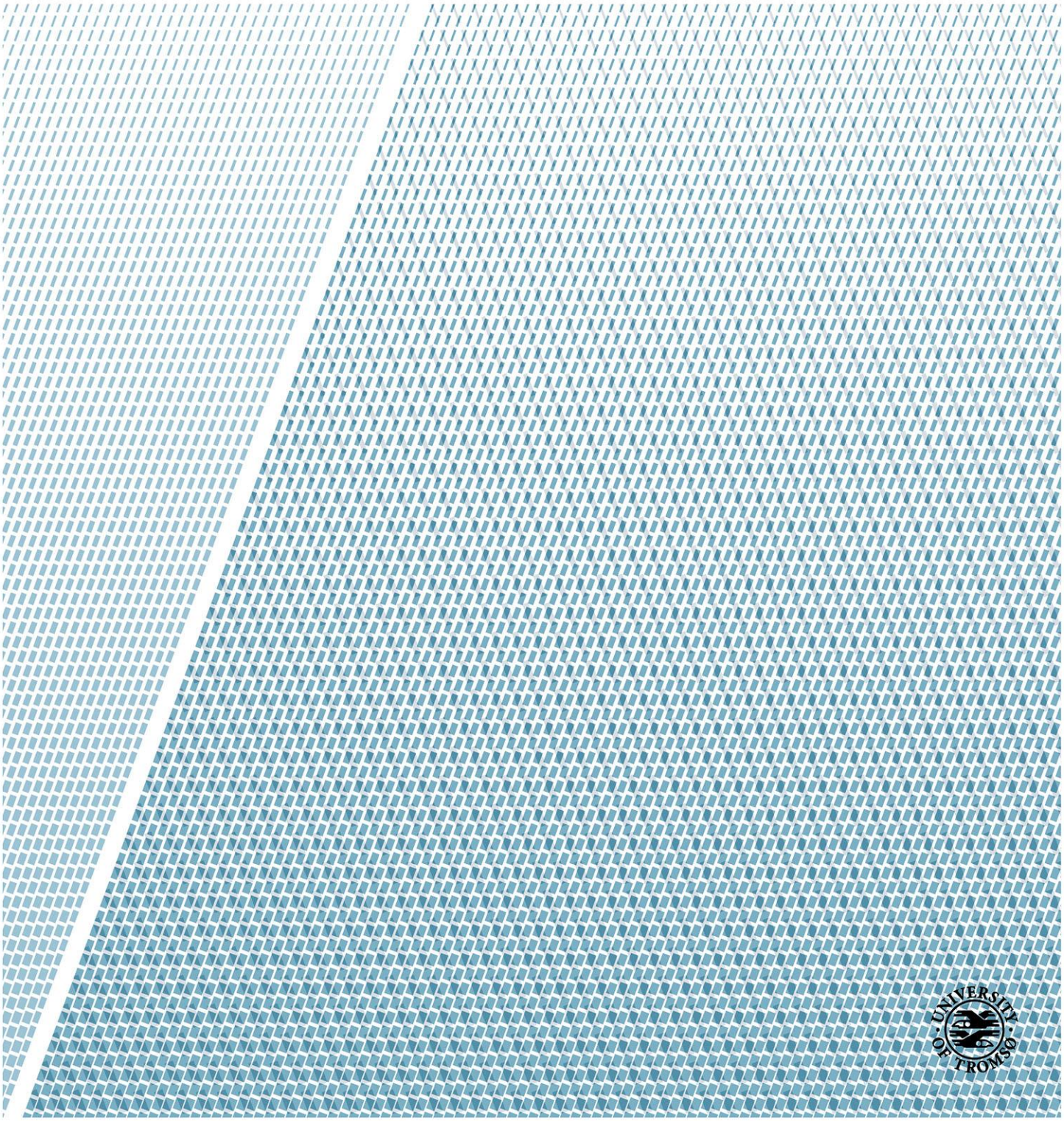

Abstract

The SW Barents Sea is a large hydrocarbon-prone epicontinental Sea comprised of a complex mosaic of deep sedimentary basins and structural highs. Uplift and erosion have been affecting the area on a large scale since the Cenozoic and have had a major impact on the petroleum systems in the area, resulting in spillage of hydrocarbons. The origin of the hydrocarbons are from deep source rocks, which have leaked or migrated into the shallow subsurface, forming gas hydrates and shallow gas accumulations, often accumlated in extensional fault blocks and the flanks of basins. This makes the Loppa High, bound by major faults complexes and basins on all sides, a potential target for hydrocarbon exploration. The distribution of fluid flow systems may improve our understanding of the sedimentary basins in the area. Numerous fluid flow features (e.g. fluid leakage along faults, gas chimneys, amplitude anomalies, pockmarks), and their relationship to tectonic elements and geological history have therefore been analyzed from 3D/2D seismic data.

The faults in the area are divided into deep-seated faults and shallow faults, based on their vertical extent and the strata they are confined in. The deep-seated faults were probably initiated during the Permian - Early Triassic rifting and/or the Kimmerian tectonic phase in the Middle – Late Jurassic when the Atlantic rifting propagated northwards. The shallow faults are most likely the result from tectonic readjustments related to the opening of the Norwegian-Greenland Sea, in Late Cretaceous – Paleocene. This event and multiple glacial cycles resulted in multiple episodes of reactivation.

Fluid migration from deeper reservoirs is evidenced by nine large gas chimneys, representing excellent migration pathways for gas. High amplitude anomalies within the Torsk Formation most likely represent accumulations of free gas below a sealing layer of gas hydrates. The occurrence of shallow gas is also probably controlled by the Opal A to Opal CT transition zone. Free gas accumulations are also represented along the URU as the unconformity may act as an impermeable barrier. Fluid expulsion events have led to the formation of circular to sub-circular depressions (pockmarks) on the seafloor.
The fluid flow features occur mainly above major deep-seated faults, suggesting that the faults and occurrence of mature source rocks control the fluid flow in the area.

Acknowledgement

Det siste året har vært en travel og opptatt tid, og jeg har lyst å takke alle som har bidratt og hjulpet meg med denne oppgaven. Dette gjelder både faglig og ikke-faglig. Uten deres hjelp og støtte hadde dette ikke vært mulig.

Først har jeg lyst å takke min veileder, Sunil Vadakkepuliyambatta for muligheten til å skrive denne oppgaven. Tusen takk for din veiledning!

Jeg vil takke alle de fantastiske studentene som jeg har blitt kjent med i min studietid. En spesiell takk til min «Petrel-Guru» Sigurd, Stine og Frank som har vært gode støttespillere - tiden på seismikk-laben hadde ikke vært den samme uten dere! Jeg vil også takke Mariann, Andre, Daniel og Håvard for gode samtaler og som har hjulpet meg holde motet oppe!

Takk til guttaboys hjemme i Stavanger, og takk til min familie som alltid stiller opp for meg. Dere har alltid vært tilgjengelige over telefonen med oppmuntrende og motiverende ord!

Anders Clausen Wollberg
Tromsø, Mai 2018

Contents

1. Introduction

1.1 Motivation and objectives

The SW Barents Sea represent a petroliferous basin which consists of a complex mosaic of deep sedimentary basins and structural highs. It is a glaciated margin and uplift and erosion has been affecting the area on a large scale since the Cenozoic (Faleide et al., 1996). Uplift and erosion of up to 2 km sediments have had a major impact on the petroleum systems in the area, causing the spillage of oil and gas into the shallow subsurface (A. G. Doré & L. N. Jensen, 1996). The widespread occurrence of shallow gas, gas hydrates and pockmarks has been reported from all over the SW Barents Sea (Andreassen et al., 1990; Andreassen et al., 2017; Vadakkepuliyambatta et al., 2013; Vadakkepuliyambatta et al., 2017). Although faults seem to provide a structural control for the fluid flow, there are significant exceptions and the origin and evolution of these fluid-flow systems are still poorly understood.

The Loppa High, bound by major fault complexes on all sides, is a major structural high reported to have seepage of gas into the water column indicating active gas migration through open faults (Chand et al., 2012). The locations of these anomalies may indicate potential targets for hydrocarbon exploration. The objectives of this master thesis is therefore to map and classify the fluid-flow anomalies and structural elements, such as faults, on and around the Loppa High region using 3D/2D seismic and well data to characterize their distribution and analyze the dominating mechanisms controlling fluid flow in the study area (Figure 1.1). Their relationship to shallow gas accumulations will also be discussed. Other aims include identifying potential source for fluid migration and the evolution of the fluid flow systems with respect to the tectonic history. Different seismic attributes will be used to map and visualize the vertical and lateral distribution of fluid flow features and fault structures.

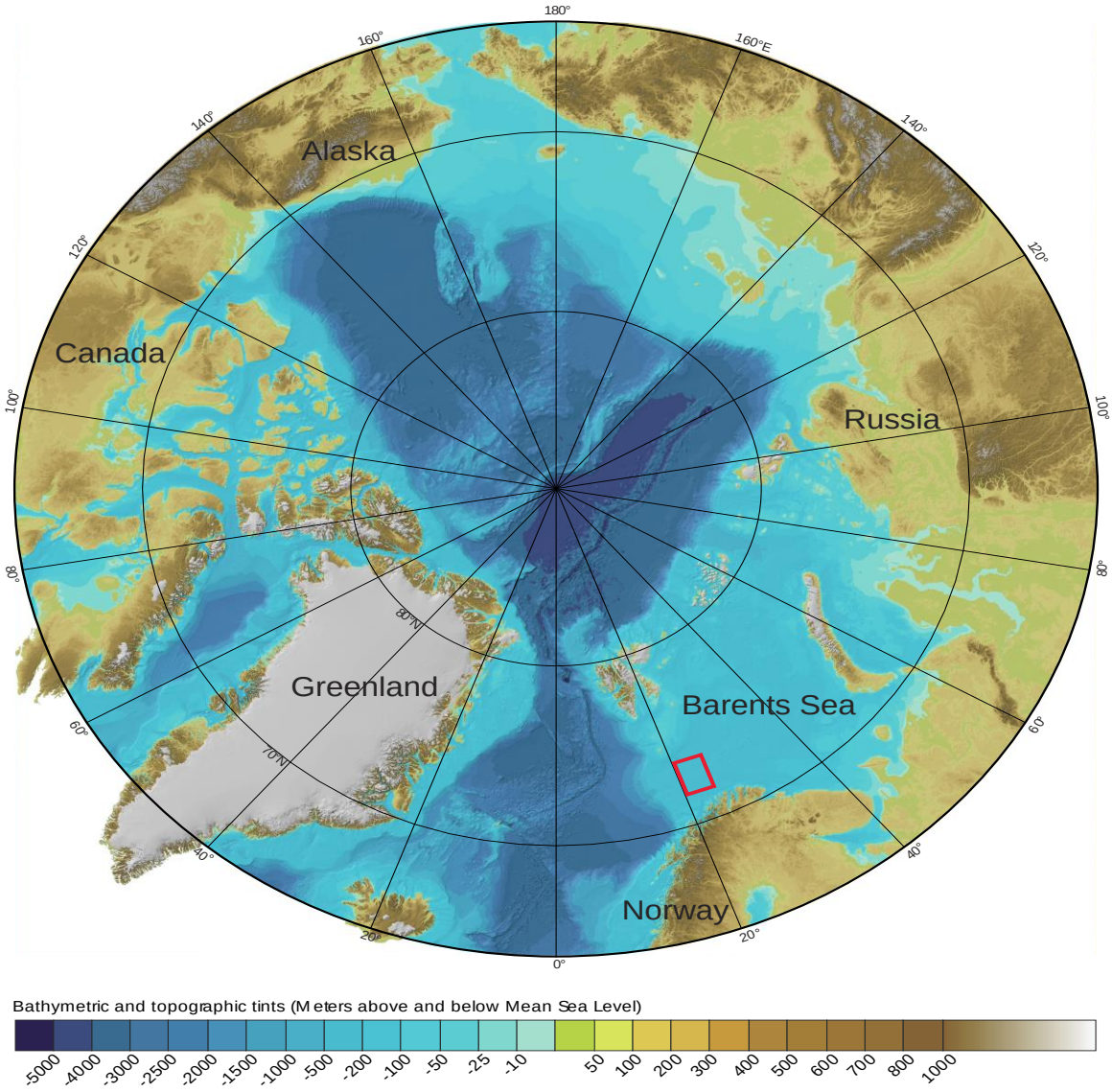

Figure 1.1: Bathymetry map of the Arctic Sea and its surroundings. The approximate location of the study area is indicated in red. Figure modified from Jakobsson et al. (2012).

1.2 The petroleum system

Many geological factors have to be in place in order for hydrocarbons to form and accumulate. This includes geologic elements like a source rock, reservoir rock, cap rock and an overburden rock, and processes like trap formation and the generation-migration-accumulation of hydrocarbons. These essential elements and processes must be correctly placed in time and space for organic matter inside the source rock to be converted into hydrocarbons. A petroleum system (Figure 1.2) will only exist wherever all these elements and processes are present. The geological evolution will then determine the preservation of the hydrocarbon reservoir over time (Magoon, 2003).

1.2.1 Source rock

A source rock is a sediementary unit capable of generating hydrocarbons that will subsequently migrate into a reservoir. This rock needs to contain organic matter (kerogen) preserved by deposition in an environment that inhibits oxidation. The organinc matter will then be turned into hydrocarbons under the right conditions regarding temperature and pressure (Selley & Sonnenberg, 2014). The organic material has to be buried to a depth with a sufficient temperature, and if all these criteria's are met, the source rock will start generating oil and can be defined as oil-mature (Selley & Sonnenberg, 2014). At an even greater depth and temperature will it start generating gas. Oil is in general generated on lower temperatures (60-120°C) than gas (120-225°C). If the depth and temperature is exceeded even more will the potential of hydrocarbons be absent and the source rock will be burned out. Temperatures above 225°C will transform the remaining carbons into graphite through metamorphosis (Selley & Sonnenberg, 2014). The petroleum systems need high concentrations of organic matter, which tend to accumulate in environments with stagnant water and a high organic productivity (nutrient rich coastal upwelling, lakes, swamps and shallow seas).

1.2.2 Reservoir rock

A reservoir rock works as a storage for hydrocarbons. It needs to be very porous and permeable for hydrocarbons to be able to move into the rock. In other words, a reservoir rock needs sufficient pore space to be able to contain moveable fluids. An optimal depth of burial and temperature is important to preserve these qualities. Petroleum reservoirs occur mainly within the so-called "Golden Zone", which is limited to the temperature interval 60-120 °C. Reservoir rocks need to be connected to a source rock with a migration pathway, which makes the hydrocarbons able to move freely (Selley & Sonnenberg, 2014).

1.2.3 Traps (Cap rocks)

The formation of hydrocarbon traps are dependent on a permeable reservoir rock covered by an impermeable cap rock to prevent leakage and further migration (Selley & Sonnenberg, 2014). These traps are classified according to the mechanism that produced the hydrocarbon accumulation and can be divided into four main groups: (1) Structural traps (formed by structural deformation of rocks, e.g. anticlines, faults), (2) stratigraphic traps (related to depositional or diagenetic features in the sedimentary sequence, e.g. truncated), (3) combination traps (formed as a result of both the above mentioned factors, e.g. stratigraphic

pinch-out) and (4) hydrodynamic traps (hydrodynamic movement of water prevent upward movement of the fluids).

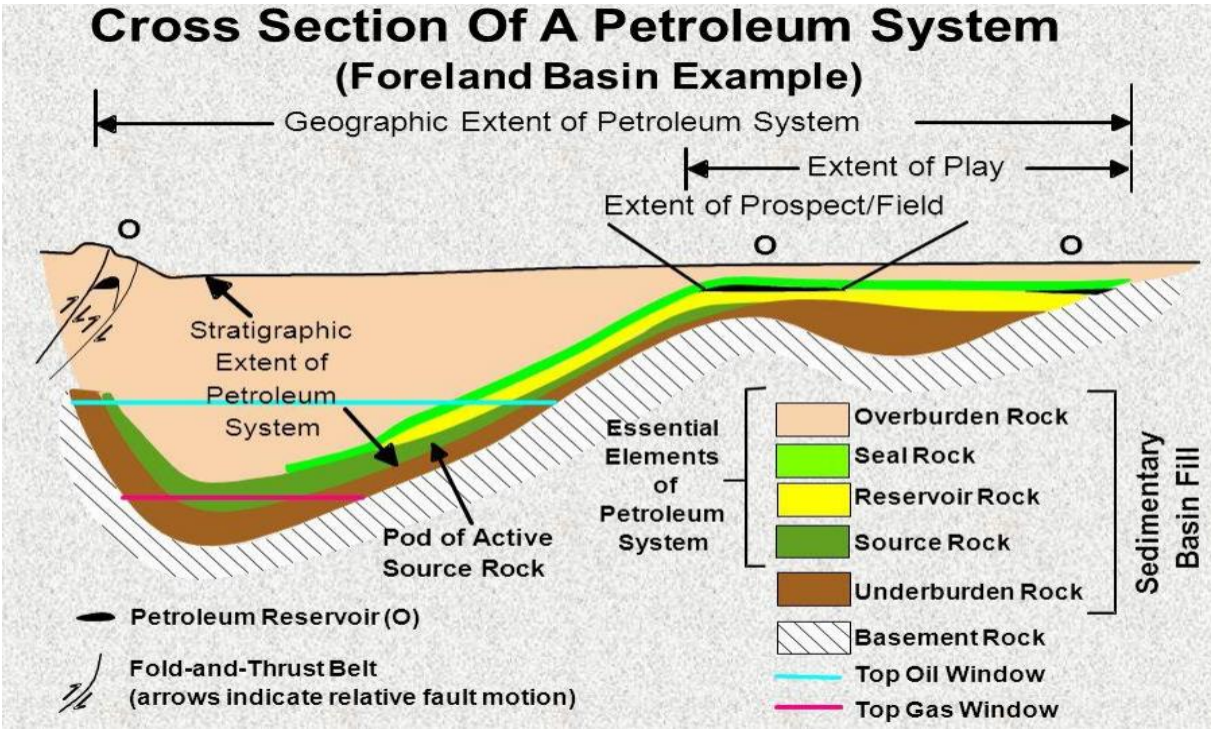

Figure 1.2: Cross section of a petroleum system. Figure is modified from Magoon and Dow (1994).

1.3 Faults

Faults are fractures formed in the rocks of the Earth's crust. They are structures resulted from compressional or tensional forces, which cause a relative displacement of the rocks on the opposite sides of the fracture. In other words, a fault is a surface or a narrow zone in the Earth's crust where one side has moved relative to the other, parallel to the surface. Faults can be described as discontinuities with offsets of more than one meter. Fault vary in size from a few centimeters to hundreds of kilometres. The faults of bigger proportions are of special interest since these can act as prominent migration pathways for fluids. The migration of fluids along the fault planes makes it possible for deeper-seated reservoirs to expel fluids to shallower-level stratigraphy (Fossen & Gabrielsen, 2005; Ligtenberg, 2005).

1.3.1 Fault types

Faults can be classified by looking at their angle of dip, slip and their relative displacement (Figure 1.3). A fault is considered a high-angle fault or low-angle fault depending whether the dip of the fault is more or less than 45°. The slip, which is the net distance and the direction the hanging wall has moved relative to the footwall, divide faults into dip-slip, strike-slip and

oblique-slip (Twiss & Moores, 2007). The relative displacement, or shear sense, along the faults subdivide them into normal, reverse and strike-slip (Figure 1.3).

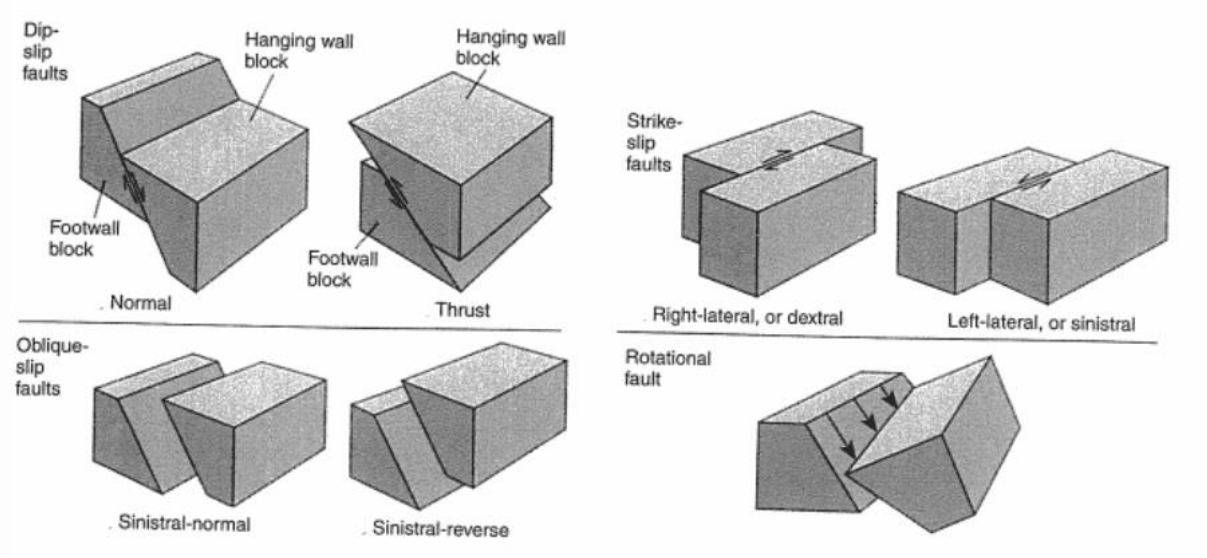

Figure 1.3: Faulted blocks showing the characteristic displacement for the different fault types. Figure is modified from Twiss and Moores (2007).

Normal faults are dip-slip faults formed by vertical compression as the Earth's crust lengthens. In an extensional tectonic regime will therefore the hanging wall slide down relative to the footwall. The displacement is mostly parallel to the dip of the fault surface, but might vary if the strike of the fault changes. Normal faults tend to be about 60°, but they can also be vertical or horizontal (Twiss & Moores, 2007). Normal faults are quite common and are normal in mountain ranges and rift valleys along spreading margins of tectonic plates. Horst-and-graben structures are formed by normal faulting and are characterized by alternating uplifted (horst) and down-dropped (graben) fault blocks (Figure 1.4). In other words, a block dropped relatively downward between two normal faults dipping toward each other is called a graben while a block that has been relatively uplifted between two normal faults dipping away from each other is called a horst. Half-graben are only bounded at one side by a normal fault. Formations of horst-and-graben strutures gives good accommodation space for sediments to accumulate. By studying these deposits and faults can periods of rifting be determined (Twiss & Moores, 2007). Faults that are steep at the surface and flattens with depth are termed listric normal faults. These faults can merge or turn into a horizontal fault/detachment at depth.

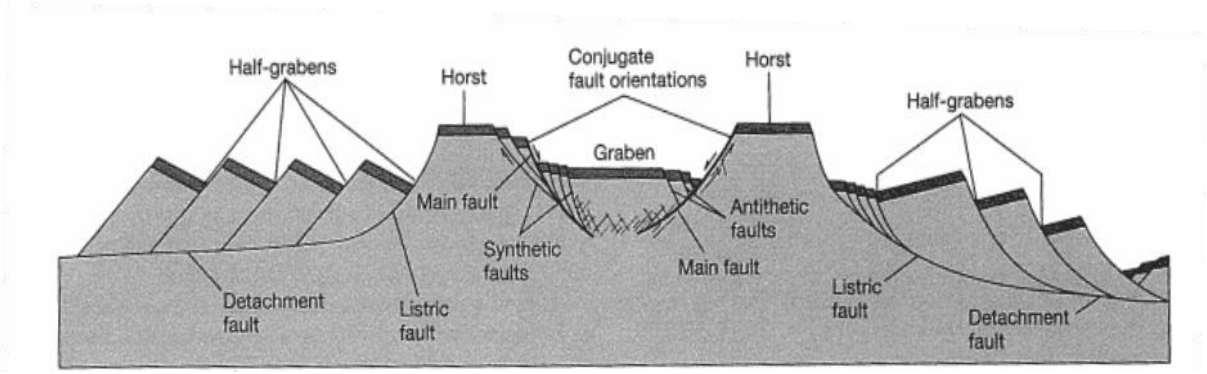

Figure 1.4: Normal faults are characterized by a main fault with associated subsidiary faults and by low-angle detachment faults. Figure from Twiss and Moores (2007).

Reverse dip-slip faults are faults formed by horizontal compression due to a shortening/contraction of the Earth's crust. The hanging wall will move up and over the footwall. The dip of the faults are greater than 45° for reverse faults and less than 45° for thrust faults, which can be divided further into overthrusts/detachments if the angle is low enough and total displacement is sufficient (Fossen & Gabrielsen, 2005; Twiss & Moores, 2007). Thrust faults can be found in compressive tectonic plate boundaries.

Strike-slip faults are faults like reverse dip-slip faults caused by horizontal compression, but the energy by rock displacement is instead released in a horizontal direction (almost parallel to the compressional force). They consist of numerous segments with various lengths. These faults have a vertical fault plane and are termed right-lateral (dextral) or left-lateral (sinistral) based on the relative movement of the fault blocks (Twiss & Moores, 2007). They can normally be found at the boundary between obliquely converging oceanic and continental tectonic plates. Oblique-slip faults have a simultaneous displacement up or down the dip and along the strike. This displacement of the blocks on the opposite sides of the fault plane is often measured by looking at its relation to the sedimentary strata.

1.3.2 Fault initiation and reactivation

Rocks will experience stress from all directions in the sub-surface. This will give rise to a stress field, which can be represented as an infinite number of traction vector of any orientation. On the surface, the stress is a vector (σ) defined by the relationship between the force and the area the force is acting upon. There are two main stress vectors, the normal stress vector (σ_n) and is the shear stress vector (σ_s), which are oriented to the surface differently. While the normal stress vector (σ_n) is oriented normal to the surface is the shear stress vector (σ_s) parallel with the surface. Fractures and faults occur when the effective stress overcomes the internal strength of

the rock (Fossen & Gabrielsen, 2005). To display the stresses acting on a plane of any given point at a surface is the Mohr stress diagram (Figure 1.5) very useful. Values of normal stress (σ_n) and shear stress (σ_s) components are plotted on a vertical and horizontal axis respectively (Twiss & Moores, 2007). In a Mohr circle is the maximum (σ_1) and minimum (σ_3) principal stress plotted along the horizontal axis. The distance between σ_1 and σ_3 forms the diameter in a circle with centre (($\sigma_1 - \sigma_3$) /2). This will visualize the stress field along a plane of interest in two dimensions, which makes it possible to find the shear stress acting upon any surface containing σ_2. The differential stress, the difference between maximum (σ_1) and minimum (σ_3) principal stress, which is the diameter of the circle determines whether the rock will fracture or not (Fossen & Gabrielsen, 2005). What separates stable state from an unstable state of stress is the failure envelope (Figure 1.5). If the Mohr circle touches the envelope will it be in a critical state, and if it crosses the envelope will it become unstable. In an unstable state, the rock cannot withstand the stress, and thus fracture.

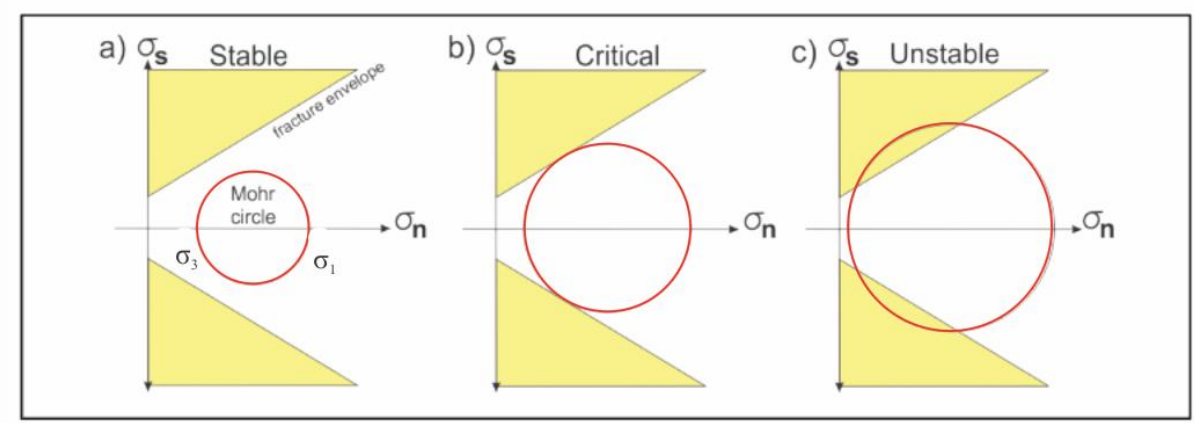

Figure 1.5: Mohr stress diagram showing failure envelope and Mohr circle.
States of stress: a) Stable, b) Critical, c) Unstable. Figure is modified from Fossen and Gabrielsen (2005).

To illustrate how the different stress components act on each of the surfaces in three dimensions can we imagine a cube (Figure 1.6). The normal stress components are found along the diagonal while the shear stress components are under and above the diagonal (Fossen & Gabrielsen, 2005).

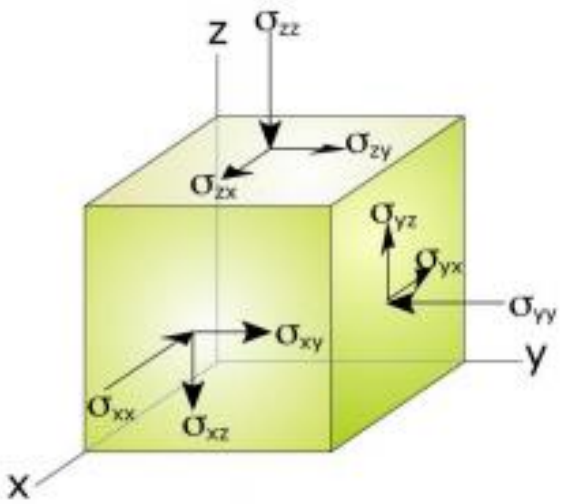

Figure 1.6: Cube showing the different stress components working on each of the surfaces. Only positive stress components are shown. σ_{xx}, σ_{yy} and σ_{zz} represents normal stress while the rest represents shear stress along the axis. Figure from Fossen and Gabrielsen (2005).

The fracture envelope for porous rocks are based on the Coulombs fracture criterion (Equation 1.1) and is used for brittle failture (Fossen & Gabrielsen, 2005). The Coulomb failure criteria predicts when a rock with given physical properties will fracture.

$$\sigma s = C + (\tan\phi) * \sigma n \qquad \textit{(Equation 1.1)}$$

In this case, σ_s and σ_n are the normal and shear stresses on a potential fracture plane in the moment of initiation of fracture. The cohesion (C) is the resistance to shear fracture on a plane experiencing no normal stress, the point where the fracture envelope crosses the σ_s-axis and equals zero. It is also described as the rocks uniaxial compressive strength. Φ is the angle of internal friction, a constant of the slope angle of the same envelope (Twiss & Moores, 2007). Rocks containing fluids experience pore pressure. If the pore pressure is increased, can a rock that normally would be stable, be forced to the initiation of failure.

For faults to reactivate is much less energy (differential stress) required than initiating new ones. This is because faults and fractures lower the cohesion strength of the rock. As a result will reactivation of faults often occur. Stress will be accommodated by sliding on already existing fracture planes rather than initiation of new fractures (Twiss & Moores, 2007).

1.3.3 Polygonal faults

Polygonal fault systems (Figure 1.7) are a relatively new discovered class of non-tectonic faults. They occur in fine-grained (clay-sized) sediments and are related to sediment compaction and fluid expulsion (Cartwright, 2011). It is important to get a better understanding of these fault systems since they play an important role regarding fluid flow, fluid accumulation and hydrocarbon reservoir dynamics. Polygonal faults can serve as conduits for fluids in shallow plays with sufficient overpressure.

On high resolution seismic, sedimentary basins may show polygonal faults as uniformly developed fault arrays. These are laterally extensive arrays of extensional faults with polygonal expressions on the surface (Cartwright, 2011). The mechanisms behind the formation of polygonal faults are poorly understood, but several theories are proposed: (1) Syneresis of colloidal sediments, (2) density inversion and (3) low coefficients of residual friction (Cartwright & Lonergan, 1996; Dewhurst et al., 1999; Goulty, 2008; Henriet et al., 1989).

Polygonal faults are normal dip-slip faults with fault planes usually ranging from approximately 50-80°. However, deeper situated faults tend to have lower angles (20-50°). A common assumption is that polygonal faults are generated as compressional or extensional faults, which is incorrect. Nevertheless, they may act as zones of weakness under late tectonic events and can be reactivated as compressional or extensional faults (Ostanin et al., 2012).

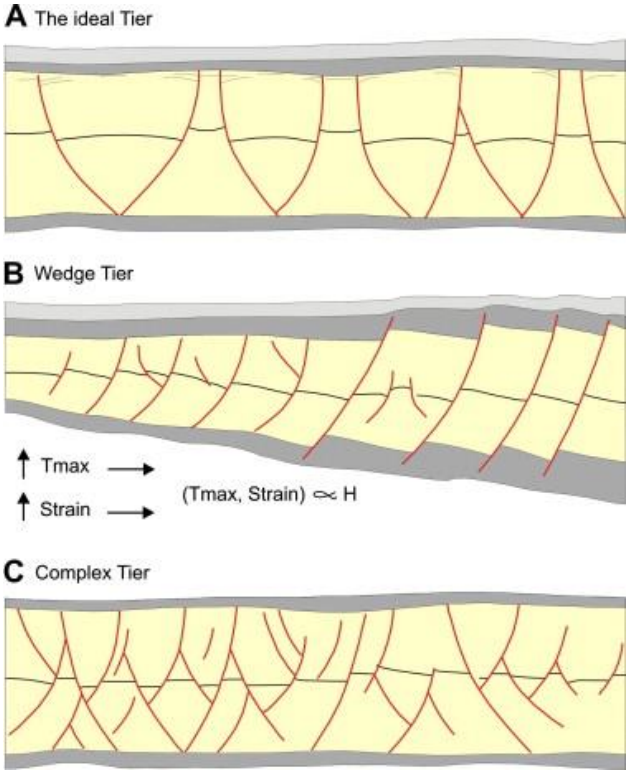

Figure 1.7: Schematic cross sections through different types of tiers (polygonal faults). ***A:*** *The ideal tier consisting of regular and even numbers of oppositely dipping faults.* ***B:*** *Wedge tier, where the preponderant dip component is upslope and towards the thin end of the wedge.* ***C:*** *Complex tier, only a few large faults transects the full thickness of the tier. The smaller faults fill the space in-between and intersects them at different levels. Figure from Cartwright (2011).*

1.4 Fluid migration dynamics

In the subsurface plays porosity a great factor regarding fluid flow. This is because fluids occupy the pore spaces and fractures in sediments and rocks and determines the reservoir storage capacity. The fluids usually occur in a gaseous or liquid phase (Guzzetta & Cinquegrana, 1987). For fluids to be able to migrate or flow through a rock is it essential that the rock has sufficient porosity (amount of open space) and permeability (ability to permit fluid flow, connected pore spaces). Fluid migration is a process driven by pressure and temperature gradients in the subsurface (Berndt, 2005).

Petroleum fluid migration (Figure 1.8) may be divided into two stages: (1) Primary migration, which is the migration of hydrocarbons out of the source rock to more permeable rocks, and (2) secondary migration, which is the migration along porous and permeable layers (or faults) into an area of accumulation or from the seabed to the water column (Tissot & Welte, 1984). It is important to mention that a third stage of migration (tertiary migration), which occurs when hydrocarbons migrate from a trap to another or a seep site, also exists. However, this stage is not that common to include.

Primary migration is mainly driven by diffusion (movement of gas molecules from high to low concentrated areas), micro fracturing (related to over-pressuring during compaction) and solution (methane solubility increases with depth). Secondary migration is dominantly driven by buoyancy and the density difference between hydrocarbons and fluids.

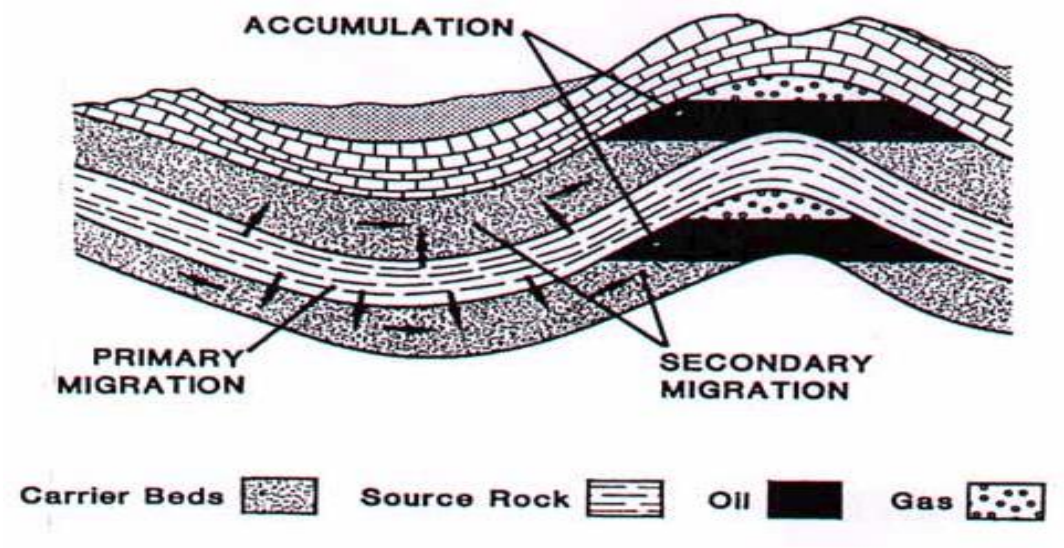

Figure 1.8: Definitions of primary and secondary migration. Figure from Tissot and Welte (1984).

The amount of fluids flowing through a permeable medium is determined by the rock properties and the difference in pore-water pressure. This is expressed in Darcy's law (Equation 1.2) in response to a hydraulic potential field (Bjørlykke, 1993). It is important to add that the equation is only valid when the medium is filled with only one fluid phase with no chemical reactions between the fluid and the medium. In addition, the fractures should not be too big compared to the area of interest. By interpreting the equation is it possible to conclude that fluid flow favors a short migration pathway with a high permeability and high pressure difference. It also suggests a fluid of low viscosity flow better than one of high viscosity (Selley & Sonnenberg, 2014). The viscosity in fluids controls how the fluid responds to the changes in pressure.

$$Q = \frac{k\,(P1-P2)A}{\mu\,L} \qquad \textit{(Equation 1.2)}$$

Q = Fluid flux (m^3/s)

k = Permeability (m^2)

P1 – P2 = Pressure difference (Pa)

A = Area (m^2)

μ = Viscosity of the medium (Pa*s)

The pressure gradient in the subsurface is related to the compaction history of the sediments. In general will sediments over time become more and more compacted as new sediments accumulate on top, increasing the load of overburden. This can result in a change in the grain configuration and hence a decrease in their porosity and permeability. Lithology is a deciding factor together with temperature on how the sediments respond to the compaction. The lithostatic pressure (pressure from the weight of the overburden) will together with the pore pressure (pressure from the weight of the fluid column) affect the diagenetic properties of the rock (Berndt, 2005). The hydrostatic pressure (Equation 1.3) is equal to the force exerted by the overlying water column:

$$P = pgh + Pa \qquad \textit{(Equation 1.3)}$$

P = Pore pressure (bar)

p = Density of pore water (kg/m^3)

g = Gravitational constant (9.81 m/s^2)

h = Height of fluid column (m)

Pa = Atmospheric pressure (1 bar)

Hydrostatic pressure (Equation 1.3) is the pressure exerted by a fluid at equilibrium at a given point within the fluid. This is due to gravity and is why hydrostatic pressure increases in proportion to depth. Overpressure is the pressure fluids experience when it exceeds that of hydrostatic proportions at a specific depth. Underpressure is the pressure that occurs when the pore pressure is less than normal of the hydrostatic pressure. A high overpressure may influence fluids to enhance the permeability of weak zones and fracture in order to release pressure to reach an equilibrium state (Berndt, 2005). In other words, fluid flow changes from diffuse to focused. Overpressure is linked to the fracture gradient (Figure 1.9), and it can fracture rocks allowing fluids to migrate laterally and vertically before the fluid pressure eventually becomes hydrostatic (Berndt, 2005). The fracture gradient marks the pressure required to induce fractures in a rock at a given depth.

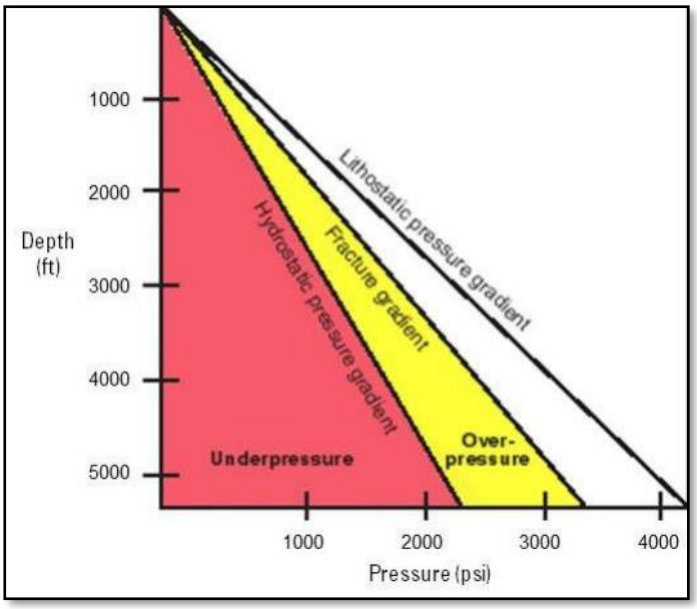

Figure 1.9: Diagram showing subsurface pressure related to depth. Figure from Schlumberger (2018b).

Mechanisms like differential compaction, sedimentation and generation of biogenic and thermogenic gas can all create overpressure regimes (Osborne & Swarbrick, 1997). Since oil and gas are less dense than water will buoyancy be one of the main factors for migration. Buoyancy increases as the density gradient increases between fluids and it enables fluids with lower densities to migrate against the hydrodynamic gradient. The Capillary pressure is the pressure difference between oil and water in pores, which determines if the pores are whether oil- or waterwet. Capillary pressure arise at the interface between two fluid phases filling the pores. The flow of fluids is in addition to Darcy's law affected by the fluids ability to overcome the capillary entry pressure (Equation 1.4). It is important for the understanding of saturation distribution in the reservoir and is one of the driving forces of fluid flow.

$$\text{Capillary pressure} = \frac{2i\cos\theta}{r} \qquad \textit{(Equation 1.4)}$$

i = Interfacial tension

θ = Contact angle between the fluids and the capillary tube

r = Radius of the capillary

1.5 Mechanisms of fluid migration

Fluids can migrate both vertically and laterally. Petroleum migration occurs under a sealing surface with factors like fracturing and fluid potential controlling the migration pathway. The fluid potential is derived from excess water pressure, capillary pressure differences and natural occurring buoyancy forces (England et al., 1987; Hindle, 1997).

1.5.1 Lateral fluid migration

Lateral fluid migration is mostly seen in sedimentary basins which has experienced no or little tectonic activity. The petroleum found here has probably travelled from a petroleum reservoir several hundreds of kilometres away (Thrasher et al., 1996). This is why petroleum can migrate into permeable layers on the sides of the fault zones where they appear as a stacking of high amplitude anomalies. The migration will continue as long as there is a sufficient sealing horizon (Hindle, 1997). Lateral fluid migration is normal along clinoforms.

1.5.2 Vertical fluid migration (Seal bypass systems)

Vertical fluid migration may occur if the petroleum fluids overcome the excess capillary pressure of the seals overlying the horizontal carrier beds. The fluid migration will continue as long as it does not encounter an impermeable seal. As the petroleum moves upward, it may damage the sedimentary layering, which can result in a permanent alteration of the affected rocks (England et al., 1987).

Seal bypass systems are essential regarding vertical fluid migration. Seal bypass systems makes it possible for fluids to migrate through impermeable layers. These systems are described as geological features embedded within the sealing sequences that promotes cross-strata fluid migration, and are classified into three groups: (1) Fault related, (2) Intrusion related and (3) Pipe related (Cartwright et al., 2007).

The first group of seal bypass systems is fault related. In sedimentary basins act fault zones as good fluid conduits and are the main migration pathway for fluids. An active, or recently active fault is more likely to be able to act as a conduit for fluid flow than a non-active fault. Other important factors are age, sealing and burial processes. Polygonal fault systems are normal in this setting. Leakage in the fault zones occur along local, weak sections within each zone and is why small faults may have the same leakage potential as larger faults (Cartwright et al., 2007). Each fault zones leakage potential are controlled by its complexity and if they intersect with each other. In addition, factors like the shape and roughness of the fault planes need to be taken into account (Ligtenberg, 2005). When the fault plane is crushed into a fine-grained, claylike substance by tectonic forces (fault gouge), will the permeability and connectivity of fractures and pores be affected. This can further lead to leaking when the fluid pressure is increased (Cartwright et al., 2007; Ligtenberg, 2005). Migration along faults can be challenging to identify and map on seismic data since the fault zones are usually uneven distributed and with a limited extent. However, features like carbonate build-ups, gas plumes in the water column and pockmarks can help indicate where the migration has taken place (Cartwright et al., 2007; Løseth et al., 2009).

The second group of seal bypass systems is intrusion related. Intrusions are structures that pierce through a sealing sequence, which helps fluids to migrate through. Fluids are transmitted through the sequences together with intrusive material and they can also develop fractures and deform the strata, making it easier for migration to occur. Intrusions can breach the sealing sequence in three different ways: (1) The intrusion itself may contain fluids (this is how mud volcanoes form), (2) The intruded material has a higher permeability than the seal and may act as a bypass (e.g. sandstone intrusions) and (3) The intrusive event results in deformation and fracturing of the seal (normal around salt diapirs).

The third group of seal bypass systems is pipe related. Pipes are sub-vertical, circular, narrow zones of acoustic masking, and are considered to be very much related to fluid migration. In seismic data are pipes identified as vertical reflections caused by the gas-bearing sediments' low velocity (Berndt et al., 2003). The origin of these pipes are usually from polygonal fault systems which can work as pathways for upward migration of accumulated gases/fluids. In other words, these fault systems can feed fluids to the overlying sediments (Løseth et al., 2009).

1.5.3 Surface expressions of fluid flow release

The most typical surface expression of fluid expulsion is probably pockmarks (Figure 1.10). These are circular to sub-circular and elongated depressions in the seabed marking the area where fluids/gas are released from the subsurface into the water column (Hovland et al., 2002). Pockmarks are one of the main indicators of fluid flow which is why they are often connected to active chimneys and/or pipes in the subsurface. Pockmarks can occur in both active and passive continental margins (Hovland et al., 2002).

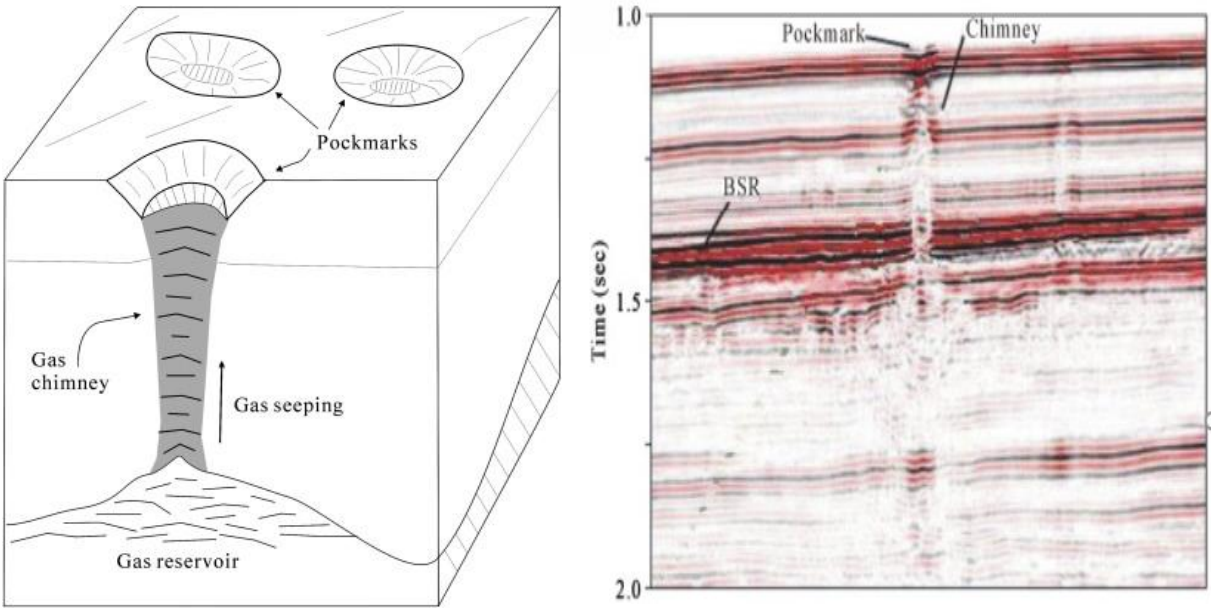

Figure 1.10: ***Left****: Gas is seeping upwards through the gas chimney creating pockmarks.* ***Right****: Seismic profile of a gas chimney that links the pockmark to an underlying bottom simulating refelector (BSR) from the flanks of the Storegga slide off Norway. Figure from Cathles et al. (2010).*

The size and shape of pockmarks varies between areas, and they may merge into each other creating bigger composite pockmarks. According to Løseth et al. (2009) do pockmarks mostly have a diameter of tens of metres, but they may vary from a few metres to over 400m. The depth is normally 1-45 metres. A pockmark's properties is related to what kind of sediments it is comprised of. Small pockmarks usually form in silts, while largers ones form in clays. The fine-grained composition is not a coincidence. The formation of pockmarks require disturbance of sedimentary matrix by moving fluids upward while at the same time removing mobilized material by the activity of bottom currents. Fine-grained material is more susceptible for disturbance of these currents, and is why pockmarks are rarely comprised of coarser sediments, such as sand. A very high energetic environment would be required, which rarely happens in environments with the formation of pockmarks (Judd & Hovland, 2009).

1.6 Reflection and refraction seismic

Seismic waves travels through the earth as body and surface waves (Figure 1.11). Regarding seismic interpretation is the body waves of most interest. These waves can either travel as pressure- (P-waves) or shear waves (S-waves). S-waves do not have the ability to travel through water (no shear strength) and is why P-waves are used in this setting. When the energy in form of P-waves hit a surface/interface will it be scattered and transmitted. When an incident ray hits a horizontal plane at normal incidence will the energy be portioned into refracted and reflected waves (Andreassen, 2009). The geometry of these waves is described using Snell's law (Equation 1.5). This equation explains how they travel through different media where the waves are transmitted at different velocities:

$$\frac{Sin\theta 1}{Sin\theta 2} = \frac{V1}{V2} = \frac{n1}{n2} \qquad \textit{(Equation 1.5)}$$

Sinθ1 = Sine of the angle of incidence

Sinθ2 = Sine of the angle of refraction

V1 = Velocity of medium 1

V2 = Velocity of medium 2

n1 = Refractive index of medium 1

n2 = Refractive index of medium 2

This formula illustrates that when a wave passes from one medium to another will both the sines of the angles (incidence and refractions, θ1 and θ2) have a constant number. This constant number will be equal to the ratio of the velocities (V1, V2) in the mediums. In addition, it will be equal to the inverse ratio of the exponent of the refraction of the two mediums (n1, n2).

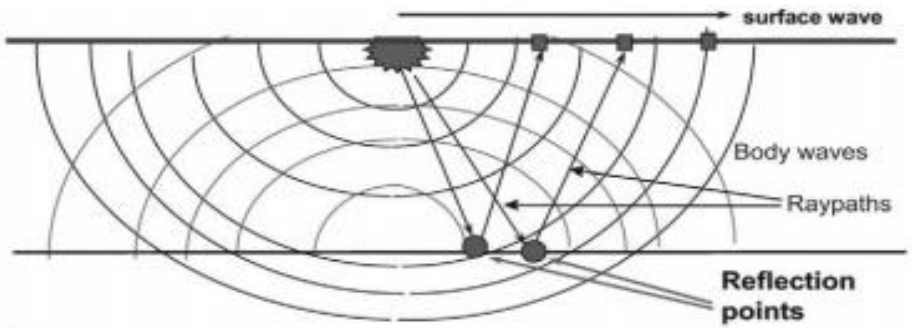

Figure 1.11: Illustration on how energy travels from a source within an isotropic media. Spherical lines indicate wavefronts which represents surfaces of equal travel time. Figure from Andreassen (2009).

1.7 Seismic indications of fluids and gas

Seismic exploration involves mapping geological structures by creating seismic waves with an artificial source (watergun, airgun etc.) and observe the arrival time of the waves reflected from interfaces in the rocks (Andreassen, 2009). The downward-travelling seismic energy that is reflected back is then detected by seismic receivers in a hydrophone cable.

The seismic reflections originate from interfaces with a sufficient density-velocity contrast which is called acoustic impedance (Equation 1.6), which is defined as:

$$Acoustic\ Impedance = P\ x\ V \qquad \textit{(Equation 1.6)}$$

P = Density (kg/m^3)

V = P-wave velocity (m/s)

The acoustic impedance contrasts are related to sedimentary bedding planes, unconformities and pore fill characteristics. These pulses, or seismic waves, travel through the Earth at a speed governed by the acoustic impedance of the medium. When a seismic wave encounters an interface between two materials with different acoustic impedances will some of the energy reflect off this interface while some of it will refract through (Figure 1.12). Seismic reflection is the method used in this thesis, which can generate detailed images of layers and structures of the subsurface. It is often used to reveal stratigraphy and structural features.

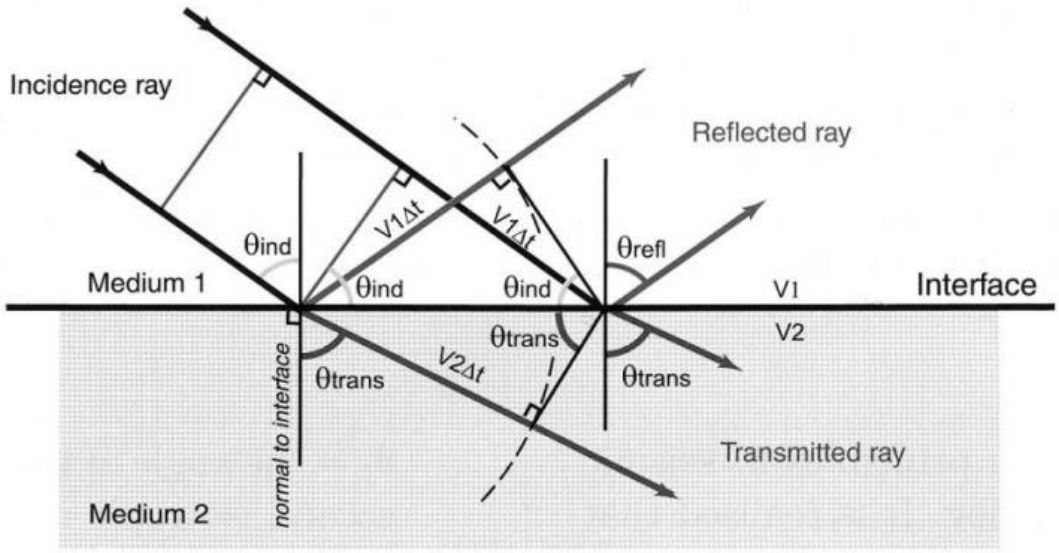

Figure 1.12: Acoustic sound waves are affected by the velocity-density interface between medium 1 and medium 2. The way the rays are behaving suggests a sufficient acoustic impedance contrast. P- and S-wave energy energy is ignored. Figure from (Andreassen, 2009).

Gas trapped in the sediments will affect the acoustic response since it tends to scatter the sonic energy. Gas bubbles will therefore change the speed of sound propagation drastically, and the sound attenuation is increased (Equation 1.7). This can be expressed relative to the acoustic wavelength (Judd & Hovland, 2009):

$$\lambda = \frac{Vp}{f} \qquad \textit{(Equation 1.7)}$$

λ = Wavelength (m)
Vp = P-wave velocity (m/s)
f = Frequency (Hz)

Hydrocarbons can be detected in seismic data since oil and gas reduce the P-wave velocity, giving rise to a negative change in acoustic impedance. This change will give result in an amplitude anomaly, which is a known hydrocarbon indicator. Since oil does not have the same significant effect on seismic properties as gas will oil only produce a minor reduction in acoustic impedance. Oil looks quite similar to that of water is a seismic profile. However, oil in sediments can effect diagenetic processes and lead to different mineralogical properties across the oil/water-interface (Karin Andreassen et al., 2007).

Not all amplitude anomalies are true hydrocarbon indicators. To distinguish these do we have certain criteria: (1) Amplitude variation with offset, (2) Bright or dim spots in amplitude as a result of variations in lithology and pore fluids, (3) Phase reversal due to velocity changes, (4) Conformity with local structures, (5) Diffractions that arise from fluid contacts, (6) Flat spots representing a fluid contact, (7) Gas chimneys above leaking reservoirs, (8) Shadow zones below accumulation, (9) Push-down due to lower velocity in hydrocarbons compared to adjacent rocks and (10) Difference in response between reflected pressure and shear energy (Schlumberger, 2018a).

Direct hydrocarbon indicators include features like bright spots, flat spots, dim spots, phase reversal, velocity effects and masking/pipes, which will be discussed in the next subchapters. Other indicators of gas are loss of high frequencies (natural increase of absorption of seismic energy with depth and within gas/fluid-bearing layers beneath bright spots) and diffractions (difference in impedance contrast can be seen on flanks of gas/fluid-pockets).

1.7.1 Bright spots

When free gas is present in the sediment pore space will the wave velocity decrease and give rise to reflections with high amplitude from the top of the gas, called a bright spot (Figure 1.13). In other words, bright spots occur where there is a strong acoustic impedance contrast. These high amplitude anomalies will have a significant decrease in acoustic impedance in hydrocarbon-filled reservoirs compared to those that are brine-filled. In a seismic profile will the bright spots normally occur close to leaking faults and gas chimneys, usually within or on top of the reservoir (Ligtenberg, 2005). It is important to add that changes in lithology also can cause negative changes in acoustic impedance, and should not be confused for bright spots (Andreassen, 2009).

1.7.2 Phase reversal

At the top of a gas reservoir can the reflection change from a bright spot lead to an increase in acoustic impedance across the fluid contact. This reflection can have a negative reflection coefficient, a phase reversal, which is a good indicator for gas (Karin Andreassen et al., 2007). A phase reversal (Figure 1.13) is characterized as a phase shift of 180° along a continuous reflection at the gas-oil or gas-water contact, resulting in the peak becoming a trough and the trough becoming the peak (Løseth et al., 2009). A phase reversal is normal when for example a brine-filled reservoir is harder than the shale on top.

1.7.3 Dim spots

Dim spots (Figure 1.13) are low amplitude reflections caused by a local decrease in the acoustic impedance contrast. The contrast is normally small, and can indicate that some gas has replaced the water in the pores. These features usually appears when the hydrocarbon-filed reservoir is harder than the overburden. Dim spots are the bright spots of high depth and compaction (Løseth et al., 2009).

1.7.4 Flat spots

A feature which has many of the same characteristics of a bright spot. It occurs when a gas-filled reservoir has a sufficient thickness with an acoustic impedance contrast between the gas and the underlying sediments of fluids. In the pore space will it create a reflection from the base of the gas zone, called a flat spot (Figure 1.13). Flat spots are likely to only be found down to about 2.5 km since the effect of gas on velocity is less marked below this depth, the chance of getting a good reflection from a gas contrast is therefore reduced. Flat spots will always have

positive reflection coefficients and usually have a flat orientation (Karin Andreassen et al., 2007).

1.7.5 Push-downs

If the gas column is sufficiently thick, a push-down may be observed on underlying reflectors. This is a feature caused by low velocity in the gas-bearing sediments. The low velocity will create an increase in travel time and the reflection will appear deeper than it actually is on the seismic data. Although gas contacts are usually horizontal in depth, will they not always appear horizontal in time due to the push-down effect of the lower velocity in the gas interval (Andreassen, 2009).

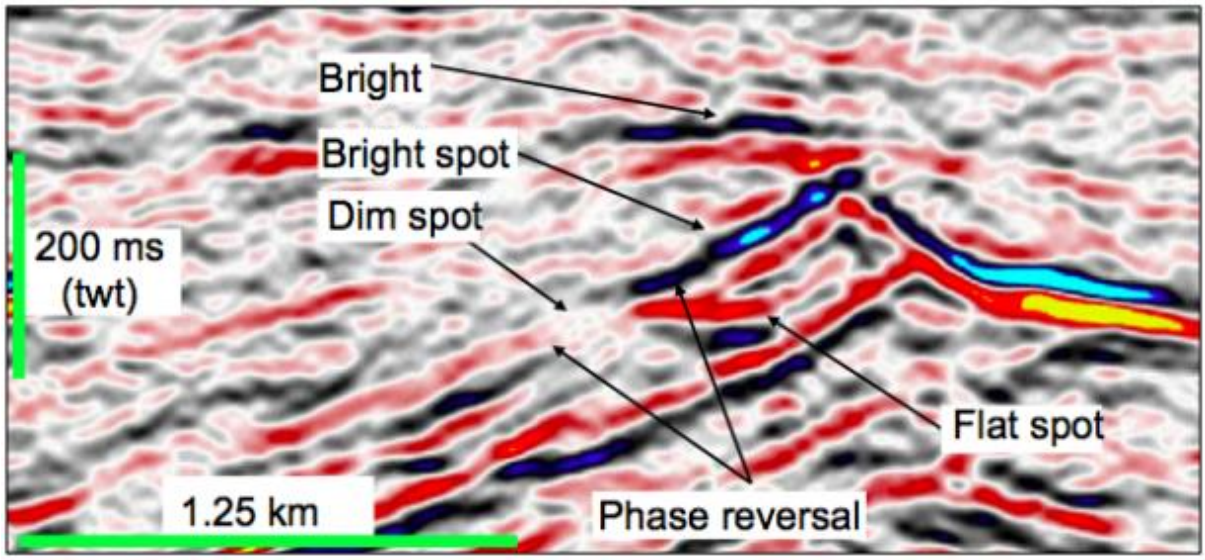

Figure 1.13: Seismic indications of fluid flow and fluid accumulation (bright spots, dim spot, flat spot, phase reversal). Figure from Løseth et al. (2009).

1.7.6 Gas chimneys

Acoustic masking appears in vertical zones with wipe-out of seismic reflections. It is an area with a low reflectivity, but it can also be distorted or disturbed. It is one of the most common evidence for presence of free gas in shallow marine sediments. Even though natural seepage of gas occurs will most of the gas be trapped on its way to the surface. This creates shallow gas accumulations with seepage from deeper-lying hydrocarbon reservoirs from a thermogenic origin. These areas can indicate a scattering of acoustic energy caused by gas bubbles in the sediments. Vertical zones of acoustic masking can indicate "high fluid-flux paths" initiated by an overpressure regime and can be referred to as gas chimneys (Karin Andreassen et al., 2007). Gas chimneys are wipe-out zones located in low-permeable cap rocks representing area of leakage (leakage zones). They can represent a fractured cap rock with irregularly distributed low-velocity gas zones.

1.7.7 Acoustic pipes

Acoustic pipes are a feature strongly related to acoustic masking. These appear as sub-vertical, circular, narrow zones of acoustic masking with disrupted reflection continuity. These represent migration pathways for fluid flow from underlying reservoir and can work as connections between bright spots where they in the end terminate at the seabed in large pockmark craters. They can also be used to detect zones of hydrocarbon expulsion and to see which faults are leaking (Ligtenberg, 2005).

1.7.8 Gas hydrates

Gas hydrates are methane or other hydrocarbon gas molecules trapped within a water-structure lattice. It is an ice/snow-like substance which is only stable at low temperatures and high pressures, restricting them to the upper 500-600m of the sediments (Sloan, 1998; Vadakkepuliyambatta et al., 2017). Salinity of the pore-waters and pore-space availability also controls its occurrence in marine sediments. They occur in large parts of the world's continental margins and high latitude permafrost regions onshore and offshore. Gas hydrates can only be found in the gas hydrate stability zone (Figure 1.14), which is where all these conditions are met. These conditions are most common is deep marine basins. The gas hydrate stability zone is found above the BSR (Bottom Simulating Reflector), which marks both the base of the GHSZ (Gas Hydrate Stability Zone) and the boundary between the GHSZ and the free gas zone (gas from deep reservoirs)(Chand & Minshull, 2003). The GHSZ may in addition to the BSR be identified by using P-T (Pressure-Temperature) relations. The BSR is characterized by a negative-polarity reflection mimicking the seabed. The BSR occurs as a response to the abrupt change in the acoustic impedance on the interface between gas hydrate bearing sediments and the underlying free gas sediments (Andreassen, 2009).

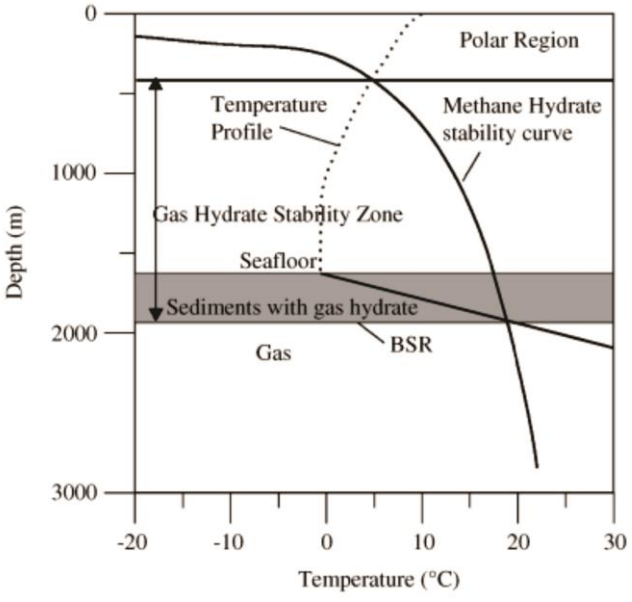

Figure 1.14: Phase diagram showing the stability field of gas hydrates in Polar Regions, where the geothermal gradient is 50°C km^{-1}. The methane hydrate stability curve is calculated from hydrostatic pressures. Figure from Chand and Minshull (2003).

The reason why gas hydrates (Figure 1.15) are regarded as so important and interesting is because they may represent a major future energy source, they can be used as an indicator of deeper reservoirs (Heggland, 1998), have a strong influence on the climate (methane is the second most important greenhouse gas), may reduce the shear strength of the sediments and they are connected to geohazards (methane can alter the seafloor sediment stability and cause submarine landslides during petroleum exploration).

Gas hydrates are often found in association with gas chimneys and authigenic carbonates since it has suitable amounts of gas in the correct P-T conditions (Heggland, 1998).

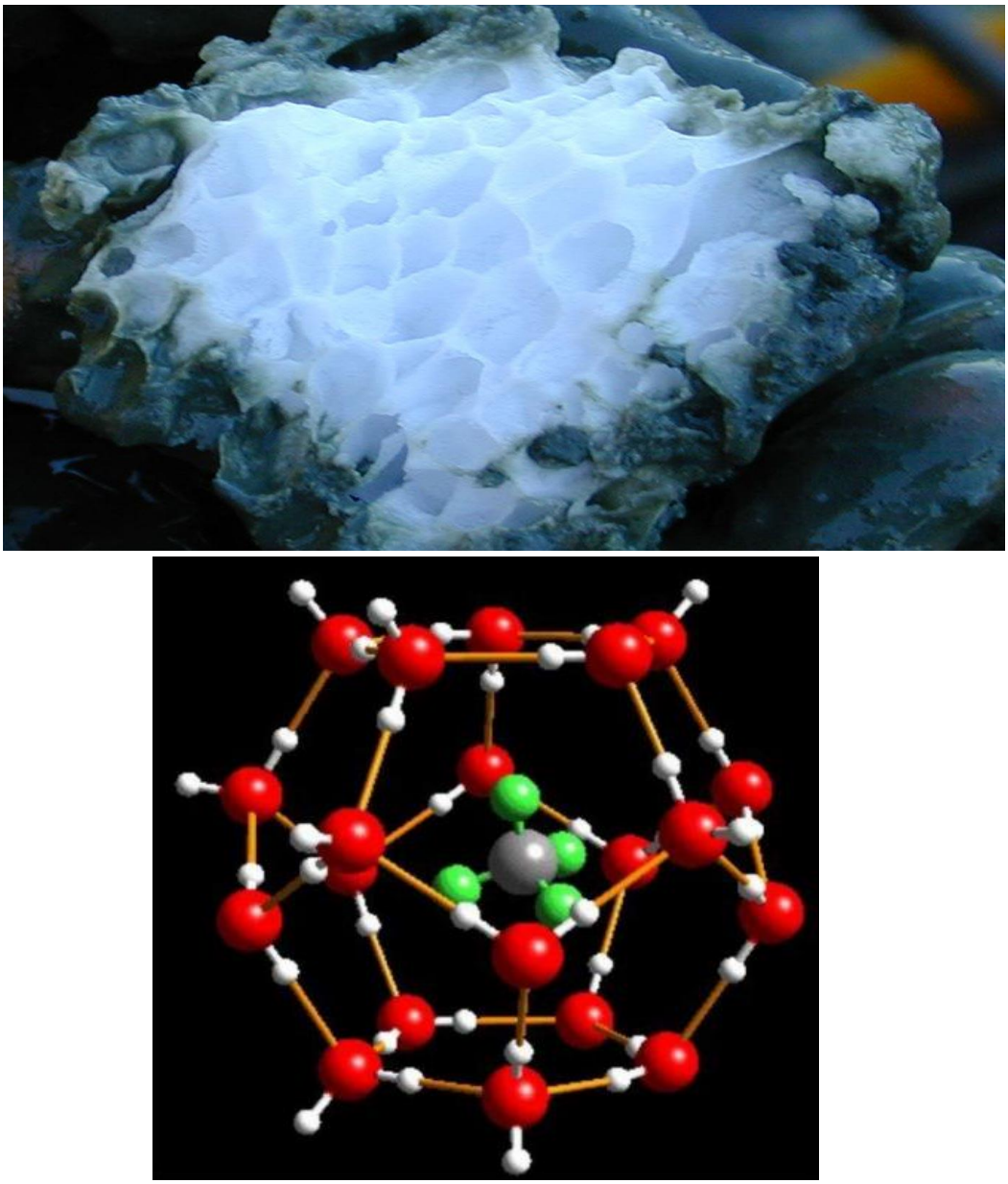

Figure 1.15: ***Upper****: Visualization of gas hydrates.* ***Lower****: Methane (CH_4) trapped in a complex of water. Figure from Studentenergy (2018) and Andreassen (2009).*

2. Study area

The Barents Sea is a wide shallow epicontinental sea (approximately 300m), which is a region bracketed by the eastern border of the Norwegian-Greenland Sea, the north Norwegian and Russian coasts, and the Novaya Zemlya, Franz Josef Land and Svalbard archipelagos (Figure 2.1). It is situated on the north-western corner of the Eurasian continental shelf and it covers about 1.3 million km^2. This makes it one of the largest areas of continental shelf on the globe and its position makes it a testing ground for a better understanding of the geological development of Europe, and of the entire Arctic Ocean (Doré, 1995; Smelror et al., 2009).

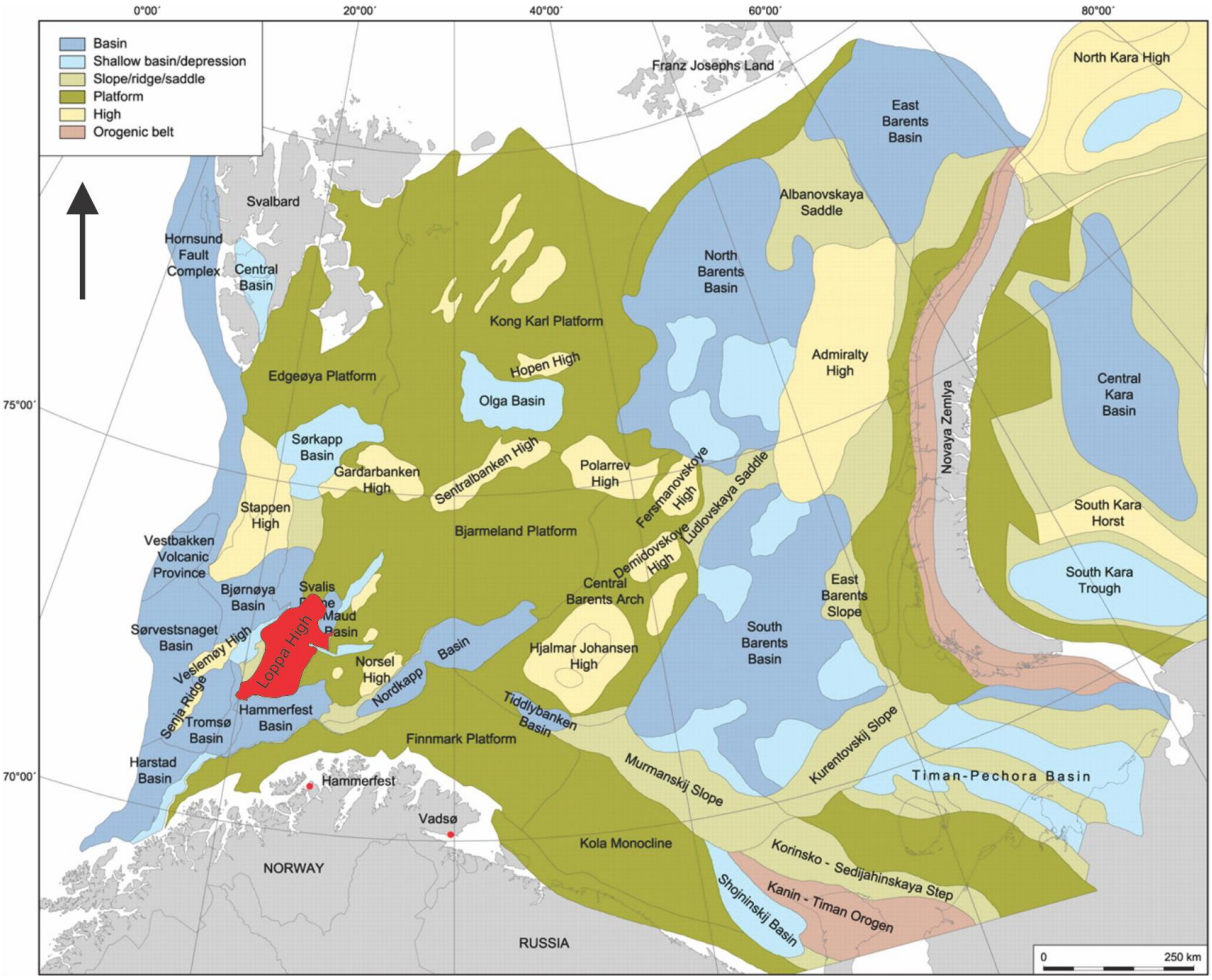

Figure 2.1: Overview of the Barents Sea off the coast of northern Norway. The main structural elements in the region are shown together with the study area (Loppa High) colored in red. Figure is modified from Henriksen, Ryseth, et al. (2011).

In the 1970's, the offshore areas were investigated for the first time using geophysical methods. This resulted in the first well being drilled in the 1980's after it was discovered that the Barents Sea had a large complex network of sedimentary basins with features and structures that could potentially indicate accumulations of hydrocarbons (Doré, 1995).

Bounded by Cenozoic passive margins to the west and north, it preserves a relatively complete succession of sedimentary strata ranging in age from Late Palaeozoic to Quaternary, locally exceeding 15 km in thickness. The Mesozoic-Cenozoic structure and tectonic history of the south-western part of this region is relatively well known through a number of studies based mainly on seismic reflection data correlated to offshore boreholes and onshore outcrops (Faleide et al., 1993; Gabrielsen et al., 1990).

The Late Palaeozoic geology is less understood, mainly because of the deterioration in seismic quality with depth and the few boreholes penetrating into Palaeozoic strata not giving sufficient information. To get a complete pircture of the geological development in this region, we need to look at the onland exposures surrounding the shelf. An example is the Svalbard Archipelago, which displays a comprehensive overview of the geology of the entire region. The formations here is a good analogy to the formations in the Barents Sea. Only a synthesis of these, together with available knowledge of the subsurface of the shelf itself, can help us understand the geological development of this vast province. Advances in seismic processing and the release of pertinent borehole information are also gradually improving this situation (Gudlaugsson et al., 1998).

The Barents Sea has been tectonically affected by major continental collisions and a complex rifting history, which ultimately led to continental break-up and formation of the Norwegian-Greenland Sea and Arctic Ocean. This can be interpreted from the deep bathymetry.

The Barents Sea is a complex mosaic of basins and platforms. By looking at the large-scale structures (platforms, sag-basins, graben features, basement highs etc.) on the Barents Shelf, it has been normal to divide the area into an Eastern and Western province. These provinces are also separated by a huge monoclinal structure. The Eastern province, with its massive south and north basins, is mainly influenced by the Uralian orogeny and the tectonic history of Novaya Zemlya and the Timan-Pechora basin. The Western province, which this master thesis will focus on, has a much more complex tectonic development. The western Barents Sea is a large Perm-Triassic platform and has been formed by different rifting events, mainly by the Caledonian rifting phase. At least five phases of basin development can be recognized in the western Barents Sea area before the final crustal break-up and seafloor spreading occurred in Early Eocene (Ryseth et al., 2003). The southwestern Barents Sea has been tectonically active multiples times in the past, which has led to a complex structural setting with development of different set of faults affecting various stratigraphic levels. The large-scale structures in this province reflect the tectonic processes along northwestern margin of the Eurasian plate.

Sørvestnaget, Bjørnøya, Tromsø and Harstad Basin defines the eastern flank of the last phase of rifting before it led to crustal break-up of Laurentia and Baltica and the formation of the oceanic crust (Gudlaugsson et al., 1998). The Barents sea has since Silurian time gone through major changes regarding climate, deposition and structure (Smelror et al., 2009).

2. 1 Geological history of the Barents Sea

The geology of the Barents Sea area can be explained by a complex combination of large-scale processes controlled by plate movements and varying climatic and depositional conditions from hundreds of millions years of continental drift. The seismic stratigraphy calibrated with lithostratigraphic units in exploration wells, has provided timing on the main tectonic events (Faleide et al., 1993).

The south-western Barents Sea (Figure 2.2) contains some of the deepest sedimentary basins worldwide. These formed in response to several phases of regional tectonics within the North Atlantic-Arctic region together with continental separation of Eurasia and Greenland and accretion of the oceanic crust in the Early Tertiary. The post-Caledonian geological history of the western Barents Sea is dominated by three major rift phases: Late Devonian-Carboniferous, Middle Jurassic – Early Cretaceous and Early Tertiary. These rift phases are connected to several minor tectonic events which locally led to large variations in deposition and palaeographic history (Faleide et al., 1993; Smelror et al., 2009).

2.1.1 Paleozoic (541-254Ma)

The Barents Sea has a complex geological history, which extends over a long period of time. However, it was originally formed from two major events: The Caledonian orogeny and the Uralian orogeny. These are two major continental collisions, the Caledonian orogeny being the closure of the Iapetus Ocean approx. 400ma as the result of Laurentia and Baltica colliding to form Laurasia, and the Uralian orogeny being the result of a subsequent collision between Laurasia and Western Siberia culminating approx. 240ma. Novaya Zemlya, which is a northern extension of the Urals mountain chain marks the suture zone of this closure. Caledonian and Uralian trends dominate the basement substructure of the Barents Sea. We can clearly see Caledonian and Uralian influences in the structural grain orientation in both provinces. Caledonian influences are seen in the N-S structural grains of the western Barents margin and Svalbard, and the NE-SW grains of the southwestern Barents Sea and Finnmark (Doré, 1995). In the Devonian to early Carboniferous time period, the Caledonian orogeny stopped and

exhumation and extensive erosion of the area started. This led to accumulation of Old Red Sandstone deposits in the western part of the Barents Sea before post-Caledonian rifting.

By Early Devonian times, the crystalline basement of the Barents Sea was consolidated and large-scale transcurrent movements within the Caledonian Innuitian domain had probably stopped. The fundamental structural framework for later tectonic development dominated by crustal extension, subsidence and sediment accumulation, which is thought to primarily be a response to northeast Atlantic-Arctic rifting. Heavily eroded extensional structures like rollovers and tilted fault blocks are thought to record a phase of late-orogenic or early post-orogenic collapse of the Barents Sea Caledonides. Due to denudation and erosion of the Caledonides, the extensive land areas over most of the western Barents Sea were gradually peneplaned (flat due to erosion). In the east, the pre-existing marine basin expanded during the Late Devonian (Doré, 1995; Smelror et al., 2009; Worsley, 2008).

During middle carboniferous times, a 300km wide rift zone extending at least 600km in a northeastern direction was formed. This rift zone is a direct continuation of the north-east Atlantic rift between Norway and Greenland and is composed of rift basins and intrabasinal highs with orientations ranging from northeastern in the main rift zone to northern at the present western continental margin. Regional extension dominated the western part of the Barents Sea during this period. At the end of Carboniferous times, the tectonic development was dominated by regional subsidence, which gradually made the entire Barents Sea region part of a huge Permian-Triassic interior sag basin. However, Permian-Early Triassic rifting and formation of north-trending structures stopped this development (Faleide et al., 1993; Gudlaugsson et al., 1998). The Barents Sea is in other words at the end of Palaeozoic mostly affected by crustal extension. This extension would later migrate westward and start the formation of well-defined rifts and pull-apart basins in the southwest, and the development of a belt of strike-slip faults in the north (Faleide et al., 1993).

From Late Carboniferous times, the tectonic development in the south-western Barents Sea (Figure 2.2) was dominated by regional subsidence. The close correlation between Carboniferous rift structures on the one hand, and the areal distribution of evaporites and carbonate buildups in the overlying Permian succession on the other hand, is interpreted to result from a component of differential thermal subsidence induced by the earlier phase of crustal extension (Gudlaugsson et al., 1998). In other words, Permian to Early Triassic rifting

stopped the regional subsidence. During the end of Carboniferous drifted Pangea northward which resulted in a climatic shift from tropical humid to semi-arid throughout most of the Barents Sea. Combined with an overall regional transgression, the climatic change had significant effects on the depositional environments in the area. Dramatic changes in the sea level were a response to the glaciations on the southern hemisphere. A major consequence of these events was an expansion of the carbonate shelf and widespread evaporite deposition in deep marine basins.

2.1.2 Mesozoic (252-72Ma)

The tectonic history of the Barents Sea was in late Palaeozoic and Mesozoic primarily dominated by extensional tectonic movements, first representing the collapse of the newly formed Caledonian and Uralian orogenic belts, and later due to stages in the progressive break-up of Pangea. In other words, the tectonic movement started to change to an extensional tectonic regime. Such episodes are recorded in many different time periods from seismic stratigraphy calibrate with lithostratigraphic units in exploration wells. These events created major rift basins traversing the Barents Shelf, and intervening series of platforms and structural highs (Doré, 1995). It is also important to mention that this area underwent intracontinental sedimentation during this whole period

In the early Triassic would an extensive supply of sediments from the Uralian orogeny cause an extensive northwestward progradation of non-marine deposits in the eastern Barents Sea. The greatest subsidence took place within the South Barents Basin and in the eastern part of Franz Josef Land, resulting in a continuous sedimentation of non-marine, near-shore and minor shallow-marine deposits. However, the western parts of the Barents Sea was in Triassic in general a tectonically quiet period, marked by passive regional subsidence. More active faults are found along the Western Margin. The Loppa High, the study area, which is located in this area was uplifted and eroded in the early Triassic as a result of rifting to the west. This is indicated by a thickening in the Bjørnøya Basin (Smelror et al., 2009).

During Mid-Triassic times, the Barents Sea comprised a central marine shelf bordered by land areas to the northwest, east and south. Open marine connections probably existed southwestwards into the North Atlantic rift system. The mudstones in this area are assigned to the Steinkobbe Formation. The total organic carbon content of these deposits reaches up to 9%,

and the mudstones are interpreted to have been deposited in anoxic conditions in a similar restricted basin as the Botneheia Formation on Svalbard (Smelror et al., 2009).

Uplift and erosion in the eastern Barents Sea-Kara Sea region led to extensive westward coastal progradation and the development of continental and coastal-plain environments over the major part of the Barents Sea area, while marine environments were restricted to the westernmost parts. Lower to Middle Triassic strata reflects this deltaic progradation from a westerly Laurentian source. Triassic tectonism in the Bjørnøya area most likely comprised a series of uplifts. This interpretation is supported by a slight angular unconformity between the Triassic strata and underlying Upper Permian carbonates, and the fact that the succession is highly discontinuous. During Norian, a sea-level rise known as the Rhaetian transgression would establish marine connections, which led to a major shift in structural regimes and depositional systems (Worsley, 2008). Mid-Late Triassic time is in other words characterised by post-rift thermal subsidence in the North Atlantic and Arctic basins and transgressive-regressive cycles which deposited marine, deltaic and continental clastic sediments (Smelror et al., 2009).

In the southwestern Barents Sea area (Figure 2.2), an Early Toarcian transgression led to a change from flood-plain environments to prograding coastal settings. Shallow-marine depositional environments were established and sandstones, siltstones and minor shale of the Stø Formation were deposited in the Hammerfest, Nordkapp and Bjørnøya Basins. The Stø Formation generally consists of stacked shoreface deposits with excellent reservoir qualities. Later, in the Bajocian, the Middle Jurassic regression reached its maximum. Large parts of the shelf were exposed to erosion, and a depositional gap is observed over most of the western Barents Shelf. Marine environments were restricted to western and eastern areas, but the presence of Bajocian shallow-marine deposits may suggest an open seaway connecting the western and eastern marine basins (Smelror et al., 2009).

The structural evolution in the south-western Barents Sea (Figure 2.2) since middle Jurassic comprises two main stages: Late Mesozoic rifting and basin formation, and early Tertiary rifting and opening of the Norwegian-Greenland Sea. This basin formation was controlled by pre-existing structural elements probably established in late Palaeozoic. The Late Mesozoic-Cenozoic evolution is related to major plate tectonic events in the Atlantic and Arctic. As the continental breakup started in the central Atlantic would Middle-Late Jurassic rifting initiate into the south-western Barents Sea (Figure 2.2). The structuring were characterized by regional

extension accompanied by strike-slip adjustments along old structural lineaments. Successive rifting episodes during the Cretaceous led to rapid subsidence and development of major deep basins like Bjørnøya, Tromsø, Sørvestnaget and Harstad basins (Smelror et al., 2009). These were the major depocentres (sites of maximum deposition within a sedimentary basin) in this area and were separated from the more stable areas to the east by major fault complexes (Faleide et al., 1993).

The final Early Cretaceous rift phase was followed by rapid subsidence and infill of the mentioned depocentres. This rifting is seen in several places on the shelf and a major Cretaceous thinning of the crust affected the Bjørnøya and Sørvestnaget basins. Uplift continued towards the north, and by Late Cretaceous time large parts of the Barents Shelf were uplifted. This an overall regression and development of more continental conditions (Smelror et al., 2009). Large deltas prograded from the uplifted areas in the north towards the subsiding basins in the south. The The Late Cretaceous to Palaeocene rifting phase between Norway and Greenland was progressively taken up by strike-slip movements and deformation within the De Geer Zone, leading to the formation of pull-apart basins in the westernmost parts of the Barents Sea (Smelror et al., 2009). The De Geer Zone was rejuvenated as a major dextral continental megashear zone (Faleide et al., 1993).

2.1.3 Cenozoic (66Ma-present)

The beginning of Cenozoic is marked by the Paleocene-Eocene transition which involves early tertiary rifting. This led to the continental break-up of the North Atlantic margins and opening of the Norwegian-Greenland Sea and the Eurasian basin. This opening occurred after the formation of the compressive Tertiary orogenic belt of Spitsbergen and the north-western shelf (Worsley, 2008). Deep sedimentary basins formed in response several phases of regional tectonincs in this area together with this continental seperation and accretion of the oceanic crust in the Early Tertiary (Faleide et al., 1993). This period is also characterized by a big magmatic event indicated by massive basaltic traps and the formation of volcanic rifted margins identified in Lofoten and the northeastern Greenland shelves (Smelror et al., 2009).

The formation of the sheared western Barents Sea-Svalbard continental margin was due to the continental break-up which would experience both transtensional and transpressional deformation during Eocene. It was in other words taken up by strike-slip movements and

deformation within the De Geer Zone, leading to the formation of pull-apart basins in the westernmost parts of the Barents Sea (Smelror et al., 2009). This resulted in the opening of the Lofoten basin, which caused extensional faulting and a dextral stress field created along the Senja-Hornsund lineament. These are two individual sheared segments which separated this margin by a central rift segment. The compressional component of the movements along the Hornsund Fault Zone, between the Svalbard region and North Greenland, is demonstrated by the Fold- and Thustbelt on Svalbard. Seafloor spreading would begin in the Norwegian-Greenland Sea in the early Eocene, and significant reorganisation of the spreading patterns occurred as the spreading expanded farther north (Faleide et al., 1993; Smelror et al., 2009). Due to the seperation of the Barents Sea were the eastern and northern parts of shelf uplifted while the western parts continued to subside. Sediments from the newly uplifted areas in the east would end up being deposited here in Eocene times. This includes the Tromsø basin, Harstad basin, sørvestnaget basin, Vestbakken volcanic province and the areas west of the the Knølegga and Hornsund Fault Zones (Worsley, 2008). Later in Oligocene would the margin become tectonically quiet. Together with a regional subsidence resulted this in the creation of a big sedimentary wedge comprising of late Pliocene-Pleistocene glacial deposits (Faleide et al., 1993).

The following events were followed by large-scale plate movements, which caused uplift and erosion along the western Barents shelf. This led to Neogene depositions of thick clastic wedges related to repeated phases of glaciation and deglaciation of the shelf (Worsley, 2008). The geological development of the Barents Sea was in other words largely controlled by Northern Hemisphere glaciations. In Neogene is the entire shelf characterized by these events which led to sedimentation of major, submarine, depositional fans restricted to the western shelf margins. A major unconformity is present between the Mesozoic-Tertiary strata and the overlying glacial deposits which marks the onset of the Northern Hemisphere glaciations in the Late Pliocene in this area. In northern platform areas and on Svalbard caused maximum uplift and erosion 2-3 km of sediments to be removed. In the late quaternary, parts of the area experienced renewed volcanism. The northwestern part of Spitsbergen is thought to be related to the Yermak hot spot to the north-west of the archipelago (Worsley, 2008).

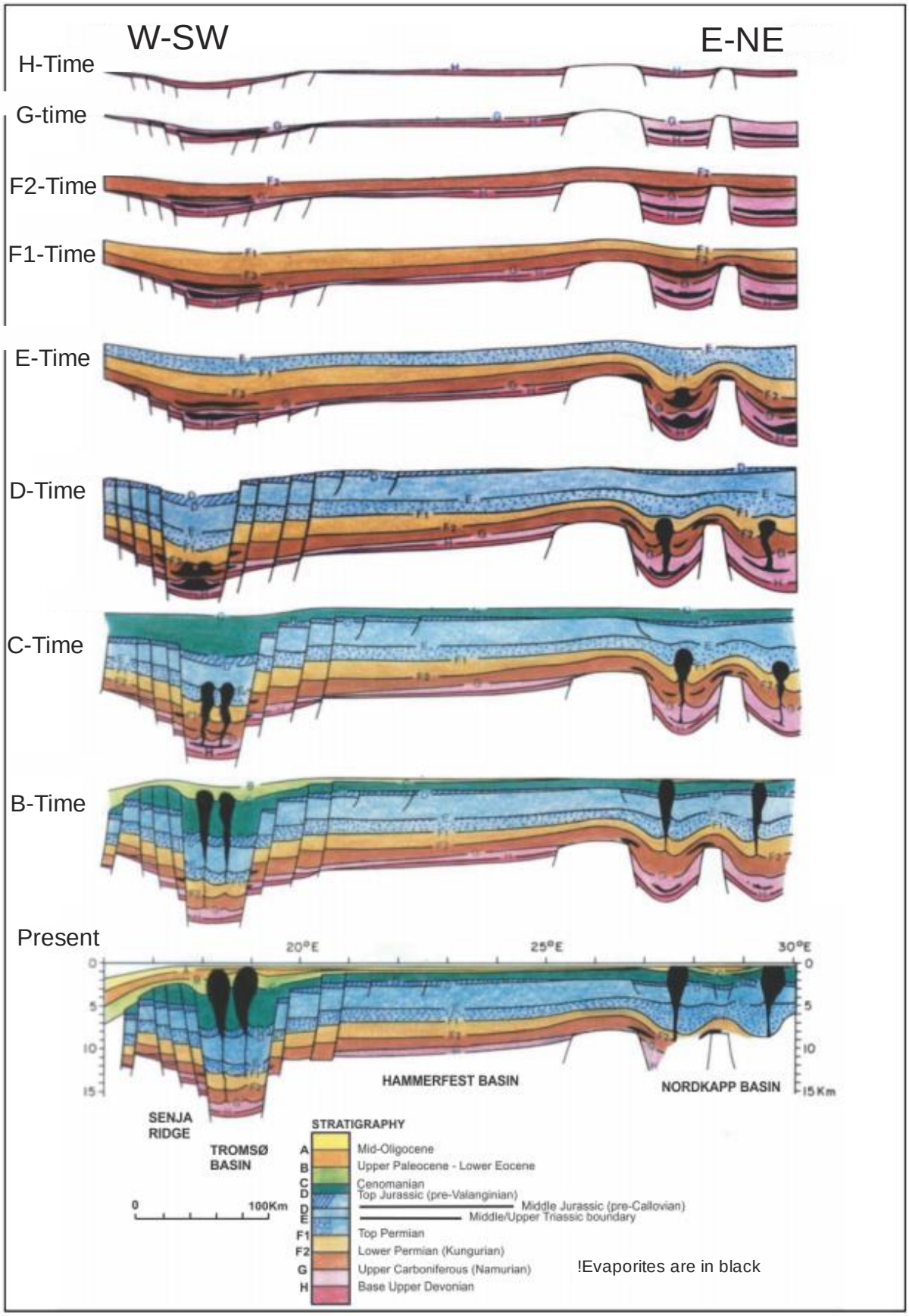

Figure 2.2: Evolution of the southwestern Barents Sea, from Devonian to present. The Senja Ridge is located to the west, the Nordkapp Basin to the east. Figure is modified from Faleide et al. (1984).

2.2 Loppa High

The Loppa High is a N-S trending structural feature separated by the East-West trending Asterias Fault Complex from the Hammerfest Basin to the south and by the Ringvassøy-Loppa and the Bjørnøyrenna fault complexes (Tromsø and Bjørnøya basins) to the west (Gabrielsen et al., 1990). It also grades gently downwards into the Bjameland Platform to the east.

The Loppa High has been through a complex geological history characterized by several phases of uplift, subsidence, tilting and erosion (Figure 2.3). However, Mesozoic highs like Loppa High has not experienced the pronounced Cretaceous-Tertiary subsidence. It has a Mid-Carboniferous rift topography, which has been filled by Upper Palaeozoic siliciclastic deposits, evaporates and carbonates. After the tectonic tilting and uplifting during Late Permian/Early Triassic, gradual onlaping took place before rapid subsidence and the deposition of the Upper Triassic succession (Larssen et al., 2002). Another name for this succession is the Snadd formation. In the southern crest of the Loppa High, eroded remnants of Paleogene shale (Sotbakken Group) is overlying Middle-Triassic claystones (NPD, 2018a).

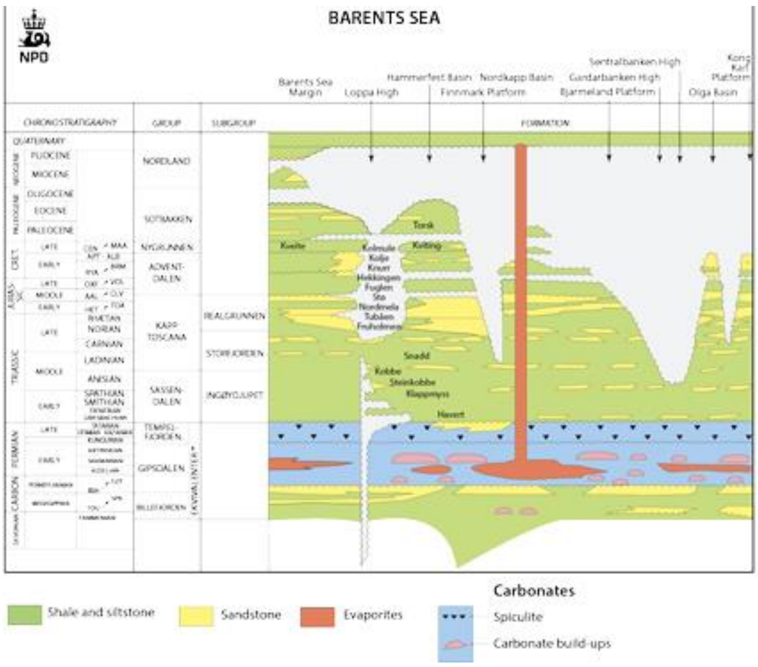

Figure 2.3: Lithostratigraphic chart of the Barents Sea showing absence of a few formations on the Loppa High. Figure from NPD (2018b).

2.3 Stratigraphy and paleoenvironment

The late Paleozoic to present-day development of the Barents Sea reflects the continuing northwards movement of the Eurasian plate from the equatorial zone in mid-Devonian/early-carboniferous to its present-day high arctic latitudes. From Paleozoic to present-day, it has drifted from approx. 50° S to 70° N (Torsvik & Cocks, 2005). This has resulted in a significant climatic change through time. Tectonic processes along the shelf-margin have controlled the sedimentation while sea variations have determined the depositional history of the province (Worsley, 2008).

The Svalbard Archipelago, which represents the subaerially exposed north-western margins of the shelf, gives a comprehensive overview of the geology of the region (Harland et al., 1997; Steel & Worsley, 1984). With a position south of the Euramerican Basin and east of the Norwegian-Greenland Sea makes it excellent for the study of the main features controlling the development of the western Barents Shelf. These features are relevant for the understanding of the entire subsurface of the south-western shelf (Nøttvedt et al., 1993).

The western Barents Sea is in general underlain by rocks of Upper Palaeozoic to Cenozoic age constituiting three different regions. The first region is the Svalbard platform, which is covered by a relatively flat succession of Upper Palaeozoic and Mesozoic sediments. The second region is a basin province between the Svalbard platform and the Norwegian coast. This region is characterized by its many highs and has a prominent structural relief westwards (Jurassic-Cretaceous). The third region is the continental margin consisting of three main segments. The first segment is the southern sheared margin along the Senja Fracture Zone, the second segment is a volcaninc rifted complex south-west of Bjørnøya, and the third segment is sheared/rifted margin along the Hornsund Fault Zone (Faleide et al., 1993).

2.3.1 Paleozoic

The Barents Sea is divided regarding structural elements like geological basins, platforms and highs, but this region has more or less a continuous sedimentary succession ranging from upper Palaeozoicum to Eocene. The northeastern orientation of the basins and highs in the southern Barents Sea is assumed to be controlled by reactivation of older weakness-zones. The origin of these structural highs is probably due to compressional movement in late Permian, late Jurassic and early Cretaceous (NPD, 2017).

Devon and the beginning of Carbon are periods clearly affected by extension due to the presence of riftbasins. From these time periods are continental clastic sediments like shale and siltstone with conglomerates and coal layers dominating. The Billefjorden Group from Devonian-Early Carboniferous consists mostly of fluvial and lacustrine sediments deposited in human and warm terrestrial environments. Sediment-filled half-grabens in this area show a generally coarsening-upwards trend, from meandering river sandstones and floodplain fines, into braided stream and alluvial fan sandstones, and conglomerates (Worsley, 2008).

In late Devonian-Mid Permian is the origin of a carbonate platform. This is seen in sequences from the Norwegian Barents Shelf in lithostratigraphic groups like the Gipsdalen- and the Bjarmeland-Group. The Gipsdalen-Group is dominated by shallow marine carbonates, sabkha-evaporites and local siliciclastics on the extensive platform areas of the shelf. The sediments of the group were deposited in a warm and arid climate, during a period characterized by distinct depositional regimes with abrupt changes in tectonic and climatic conditions (NPD, 2017).
In the end of Carbon and Permian would the Barents Sea experienced extension/rifting. The dry climate with rapid sea level changes caused carbonates to be exposed to air, and is why carstification is normal during this period. Limestone, Mg-rich dolomite, carbonates and evaporates (gypsum, anhydrite, salt) would dominate in the marine environment. The origin of reefs in this period can have played an important factor for the creation of reservoir-rocks in late carbon and Permian, especially on the horst and highs around the evaporate basins (NPD, 2017).

During the late Palaeozoic and early Mesozoic would deposition of a continental nature take place locally in the syn- and post-orogenic collapse basins. The marine depositional environment was strongly influenced by the specific tectonic setting, but also by climatic factors. As the Barents Sea drifted northwards, carbonate depositions (with some important evaporate intervals) prevailed over wide areas of the shelf in Devonian, Carboniferous and Permian times (Doré, 1995). In Mid-Permian would this evaporitic deposition cease and there would be a shift first to cool-water carbonates and then to clastic and organoclastic deposition. This would be accompanied by a general decrease in tectonic activity along the western margins. The subsidence rate would then increase as a response to the Uralide orogeny (Doré, 1995).

2.3.2 Mesozoic

The Mesozoic structuring is characterized by regional extension accompanied by strike-slip adjustments along old structural lineaments. The Barents Sea experienced a decrease of the subsidence rate throughtout the Triassic. This resulted in major deltaic progradations in many areas, which led to a more stable environment. This is observed in the lower to middle Triassic succession which comprises transgressive-regressive cycles of marine, deltaic and continental clastic sediments. Early Triassic extension also initiated salt-tectonic activity in the Nordkapp Basin and diapirs grew passively until Mid-Triassic times (Worsley, 2008). This was done by maintaining their crest close to the seafloor, while sediment accumulated in adjacent salt-withdrawal basins.

The Early Triassic was primarily dominated by the Sassendalen Group, which represents non-siliceous fine clastics (Figure 2.4). The Havert, Klappmyss and Kobbe formations are part of this group that is also known as the "Early Triassica silica gap" (Worsley, 2008). The Southwestern Barents Sea got isolated from the Central European basins at this time. This was due to the closing of the Permian Zechstein seaway as a result of the uplift of the mid-Norwegian and eastern Greenland shelves (Doré, 1991). Restriced anoxis basins south of the shelf gave rise to organic rich formations like Kobbe and Snadd (Smelror et al., 2009; Worsley, 2008). The Barents Sea region also experienced progressive uplift. This can be clearly seen in the significant westward thickening of the Carnian strata, representing clastic influx from the Fennoscandian Shield and probably form a western Laurentian source. Much of the western Barents Shelf would later be covered by widespread alluvial plains, and coastal and shelf-break settings (Smelror et al., 2009).

A sea level rise in the early Norian, known as the Rhaetian transgression, flooded central Europe and gave the origin of marine connections between the Tethyan Boreal oceans along the proto-atlantic seaway. This affected the structural regimes and depositional systems in the arctic provinces, which led to a great decrease in both subsidence and sedimentational rate. Shallow marine and coastal environments were now dominant instead of Uralian-sourced progradational systems (Worsley, 2008). During the Lower-Middle Jurassic were the Tubåen, Nordmela and Stø formations deposited. The Tubåen Formation is restricted to the western Barents Shelf due to uplift and erosion in the Lower Jurassic and represents tidal inlets, estuaries and lagoons, with portions of shale and coal (Smelror et al., 2009). The Nordmela Formation is comprised of silty shales and fine-grained sandstones deposited in a floodplain environment. The

environment later changed to a shallow-marine environment which resulted in the deposition of stacked shoreface deposits of the Stø Formation (Smelror et al., 2009).

The sedimentation rate decreased due to extensional tectonism in the Mid-Late Jurassic. This resulted in the origin of major platform and basin pattern we see today (Bjørnøya, Tromsø, Harstad bains etc) (Faleide et al., 1993; Worsley, 2008). These basins would eventually in the early Cretaceous rift phase be affected by a rapid subsidence and experience infill basins by a 5-6 km thick shaly sequence covering most of the structural relief by Cenomanian time.

The Jurassic-Cretaceous time period reflects the development of the polar Euramerican Basin on the northern margins of the shelf. This depositional phase contains several sandstone units with significant hydrocarbon reservoir potential. This is especially in the lower section which is more shale-dominated upwards. This sequence is seen in the lower Storfjorden Subgroup and in the Adventdalen Group. The lower Storfjorden Subgroup has a deltaic character, with sandstone provenance from widely differing areas while the Adventdalen Group (Figure 2.4) is shale dominated with a significant organinc carbon content due to regional transgression in the Bathonian/Callovian (NPD, 2017; Smelror et al., 2009; Worsley, 2008; Worsley et al., 1988). The organic-rich shales of the Hekkingen Formation is considered the main oil-prone source rock in the area with organic contents of up to 20 % (Faleide et al., 1993; Smelror et al., 2009). The Knurr and Kolje formations are mostly claystones with thin stringers of limestone and dolomite deposited in a distal marine environment.A later transgression resulted in deposition of shales, mudstones and siltstones of the Kolmule Formation.

In Late Cretaceous was the calcareous units of the Kviting Formation and the claystone dominated Kveite Formation of the Nygrunnen Group deposited in a deep to shallow shelf environment (Worsley et al., 1988).

2.3.3 Cenozoic

Paleogene was primarily dominated by alternating transpressive and transtensional regimes. This development was dominated by the tectoninc activity along the western shelf margins before the Eocene/Oligocene break-up and opening of the Norwegian–Greenland Sea. This led the progradation of shallow marine to alluvial sands from the west that filled the basin in the Eocene. The Paleogene Torsk Formation (Sotbakken Group) was deposited in the open and deep marine shelf environment, dominated by claystones interbedded with siltstones, tuffs and

carbonates (Figure 2.4) (Faleide et al., 1993). It is worth mentioning that the final opening of the Norwgian-Greenland Sea occurred after the formation of the Tertiary orogenic belt of Spitsbergen and the northwestern shelf.

In Neogene did massive wedge deposits develop over the western shelf margins. These deposits recieved clastics derived from glacially related repeated shelf depressions and uplift (Dimakis et al., 1998; J. I. Faleide et al., 1996). This characterized the enitre shelf together with sedimentation restricted to the western shelf margins. Spills onto the newly formed oceaninc crust is the origin of the Nordland group (Figure 2.4**),** which accumulated up to 5km fine-grained deposits along the western Barents Shelf margin (J. I. Faleide et al., 1996). In other words, these deposits reflect the glacial erosion and periodic isostatic uplift caused by erosional unloading during the Pliocene and Pleistocene (Mangerud et al., 1996; Vorren et al., 1991).

As a result of erosion and redeposition on the slope associated with glaciations (J. I. Faleide et al., 1996) did the southwestern Barents Sea continental margin prograde 30-40km westward. Along this margin have three main prograding sediment packages (GI – GIII) and seven seismic reflectors (R7-R1) been identified. The deepest sediment package, GI, is thought to represent a glaciomarine environment with dipping clinoforms and a strong continuity of seismic reflections. The other packages, GII and GIII, have a chaotic reflection pattern and interpreted to represent mass-movement desposits related to nearby grounded glaciers (K Andreassen et al., 2007). The deepest reflector, R7, has been interpreted to be the mark of the glacially dominated deposition at 2.3ma (K Andreassen et al., 2007; J. I. Faleide et al., 1996).

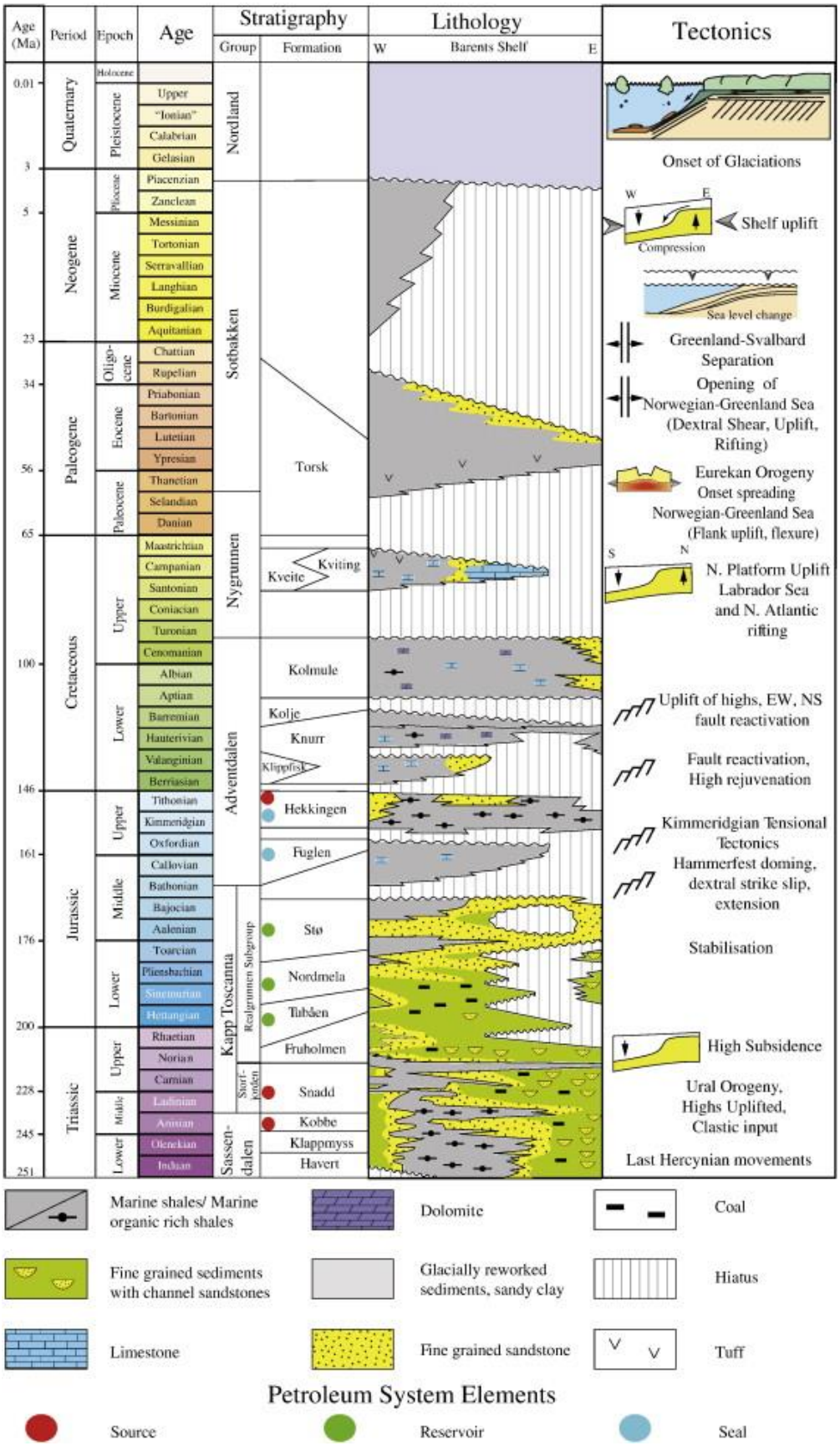

Figure 2.4: Lithostratigraphy of the Barents Sea. Major tectonic events are also shown. Figure from Ostanin et al. (2012).

2.4 Hydrocarbon exploration of the Barents Sea

The first explorations wells were drilled in 1963 by Norsk Polarnavigasjon and in 1965-1966 by the Amoseas Group. Since this time have 71 licenses been certified. This includes 157 wells whereas 126 of these are exploration wells in the Norwegian sector of the Barents Sea. 49 discoveries have been made from 1980-2016 and two fields remain in production to this day, Snøhvit and Goliat (NPD, 2017). Drilling has proven 260-300 billion cubic meters of gas (with minor oil) in Norwegian waters. This accumulation of gas over oil is an exploration problem and is together with the leakage of hydrocarbons through traps, connected to the intense erosion and uplift of the Barents Shelf that took place during Cenozoic (Doré, 1995). Residual oil columns have been found beneath the gas field in the Hammerfest Basin, which indicate that these structures once have been filled to a certain extent. The removal of the sedimentary overburden also has severe consequences for the accumulation. Expulsion of oil form traps, seal spillage and cooling of the source rocks have all led to the predominance of gas over oil in the Barents Sea (Doré, 1995).

Despite the mentioned difficulties, exploration of the Barents Sea is at an immature stage compared to the other petroleum provinces worldwide, and there is still a significant potential. A circumpolar chain of known petroleum basins surrounds the area, which makes the Barents Sea an obvious target for hydrocarbon exploration (Doré, 1995).

2.4.1 Source rocks

The presence of source rocks with a good hydrocarbon potential is crucial for the understanding of the migration and accumulation of hydrocarbons within the study area. Source rocks have earlier been described in chapter 1.2.1 as sedimentary units capable of generating hydrocarbons. These rocks need to contain organic matter preserved in an anoxic environment, which will be turned into hydrocarbons given enough time and the right conditions (temperature and pressure). Several possible source rocks (Figure 2.5) have been described by Ohm et al. (2008) and the Lower Hekkingen is regarded as the most promising source rock, which has been sampled in 32 different wells. This formation is comprised of organinc rich shales of Late Jurassic age which is known for its good reservoir quality. However, this formation is thought to only be mature in certain areas. This includes a narrow belt at the western margin of the Hammerfest basin and along the western fringe of the Loppa High (Doré, 1995).

The intervals from Middle and Lower Jurassic have a potential of expelling oil along with the underlying Triassic shales (Ohm et al., 2008). As the Triassic shales are buried deeper will they mature earlier than the Jurassic (Ohm et al., 2008). Lower-Middle Triassic potential source rocks include the Snadd- and Kobbe formation which are deposited in terrestrial environments in the southern part of the Barents Sea (Ohm et al., 2008).

Other potential source rocks include Billefordgruppen, Gipsdalgruppen, Tempelfjordgruppen and the Steinkobbe/Botneheia formation (NPD, 2017). Billefjordgruppen contains coal and carbon-rich shale from the beginning of Carbon and its geological history suggests that the source has been buried at a sufficient depth to generate gas in the basin-areas and oil at the highs. Gipsdalgruppen is mainly comprised of carbon-rich organic mud of Carbon-Permian age and Tempelfjordgruppen is mainly marine shale of Permian age. Gipsdalgruppen has probably the biggest oil-generation potential since the presence of Tempelfjordgruppen is uncertain in parts of the area. The Permian source rocks are overmature over large parts of the Barents Sea, but appear to be in the oil window on the upper part of the Loppa High and along the margins of the Finnmark Platform (Ohm et al., 2008). The Steinkobbe/Botneheia formation contains organic rich shale of Olenek, Anis and Ladin age and has been proven to be oil generating in certain areas. These accusations are based on information from Svalbard and exploration wells/shallow drilling in the southern Barents Sea (NPD, 2017).

The source rocks in the Barents Sea show large differences in maturity level and does not follow the same trends in maturity versus depth like elsewhere on the Norwegian continental shelf (Ohm et al., 2008). A reason for this could be that the Barents shelf has higher temperature gradients, but it is important to add that repeated phases of uplift and erosion also have affected this to a certain degree (Doré, 1995). This makes it difficult to predict the maturity. Areas with the highest uplift have most likely had a colling of the source rock that stopped the generation of hydrocarbons, while areas with no uplift have resulted in an overmature source rock (Ohm et al., 2008).

2.4.2 Reservoir rocks and traps

The hydrocarbon resources in the Barents Sea are mainly contained within the strata of Jurassic age. The biggest discoveries in the Norwegian sector (Snøhvit, Askeladden and Albatross) all have reservoirs consisting of Lower-Middle Jurassic sandstone. This unit is called the Stø formation and was deposited in a coastal marine setting. It is estimated to contain about 85% of the resources in Norwegian Barents Sea. Most of the hydrocarbon traps in the Barents Sea are in general fault-bounded positive blocks sealed by overlying upper Jurassic shales (Doré, 1995).

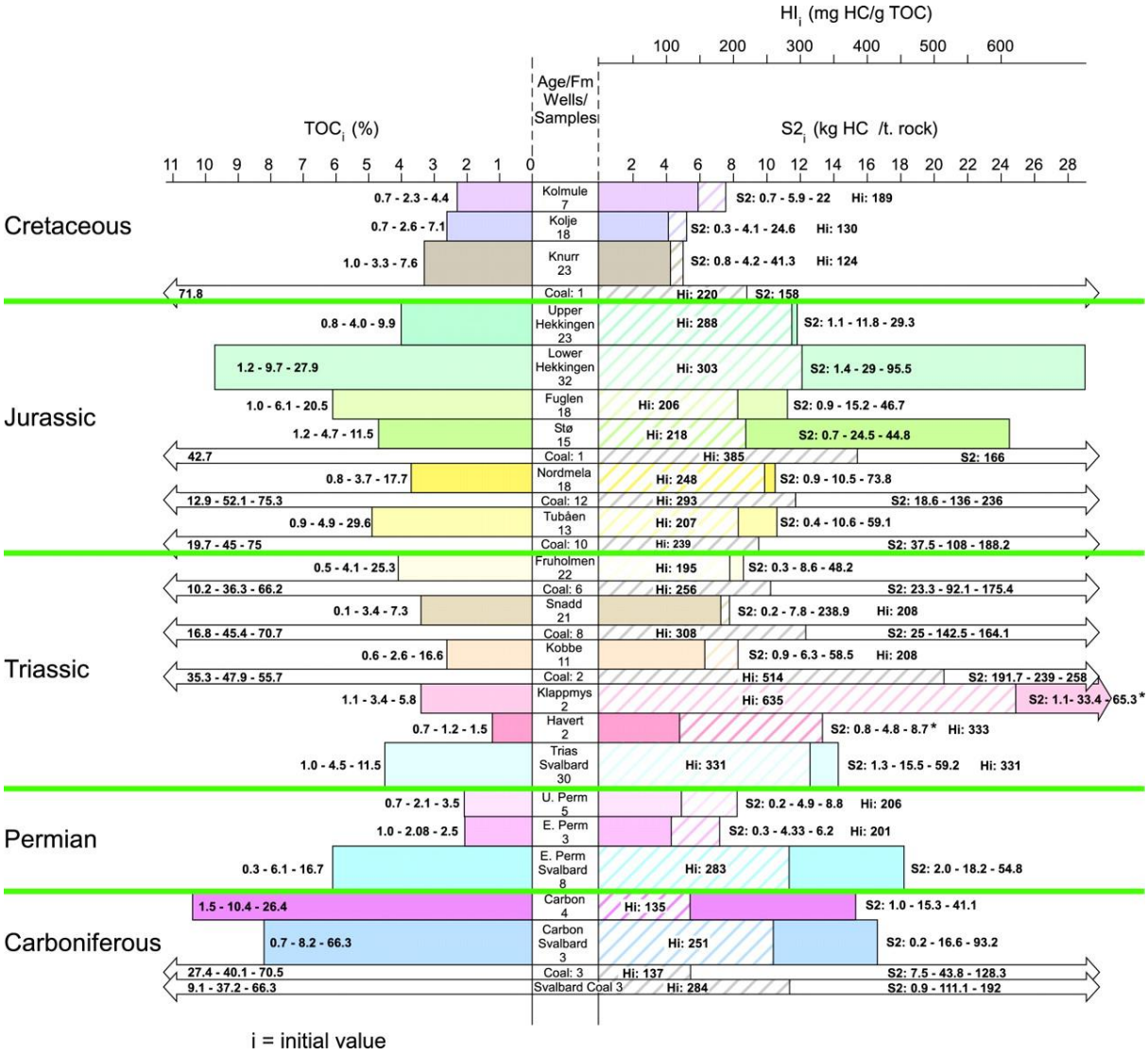

Figure 2.5: Diagram showing source rock characteristics in intervals from Carboniferous to Cretaceous, presenting the initial total organic carbon content (TOC), S2 (amount of HC generated) and hydrogen index (HI). The Lower Hekkingen is the most profilic source rock, which is based on data from 32 wells. Since few wells have penetrated pre-triassic sources are the extent of these less known. Figure from Ohm et al. (2008).

3. Data & methods

This study is based on conventional 3D and 2D seismic data from the Loppa High area in the southwestern Barents Sea. Exploration wells are used to correlate some of the seismic units and its boundaries. 2D seismic profiles are used to determine geological setting and amplitude anomalies. Some 2D surveys were used for quality control on well correlations (Figure 3.1).

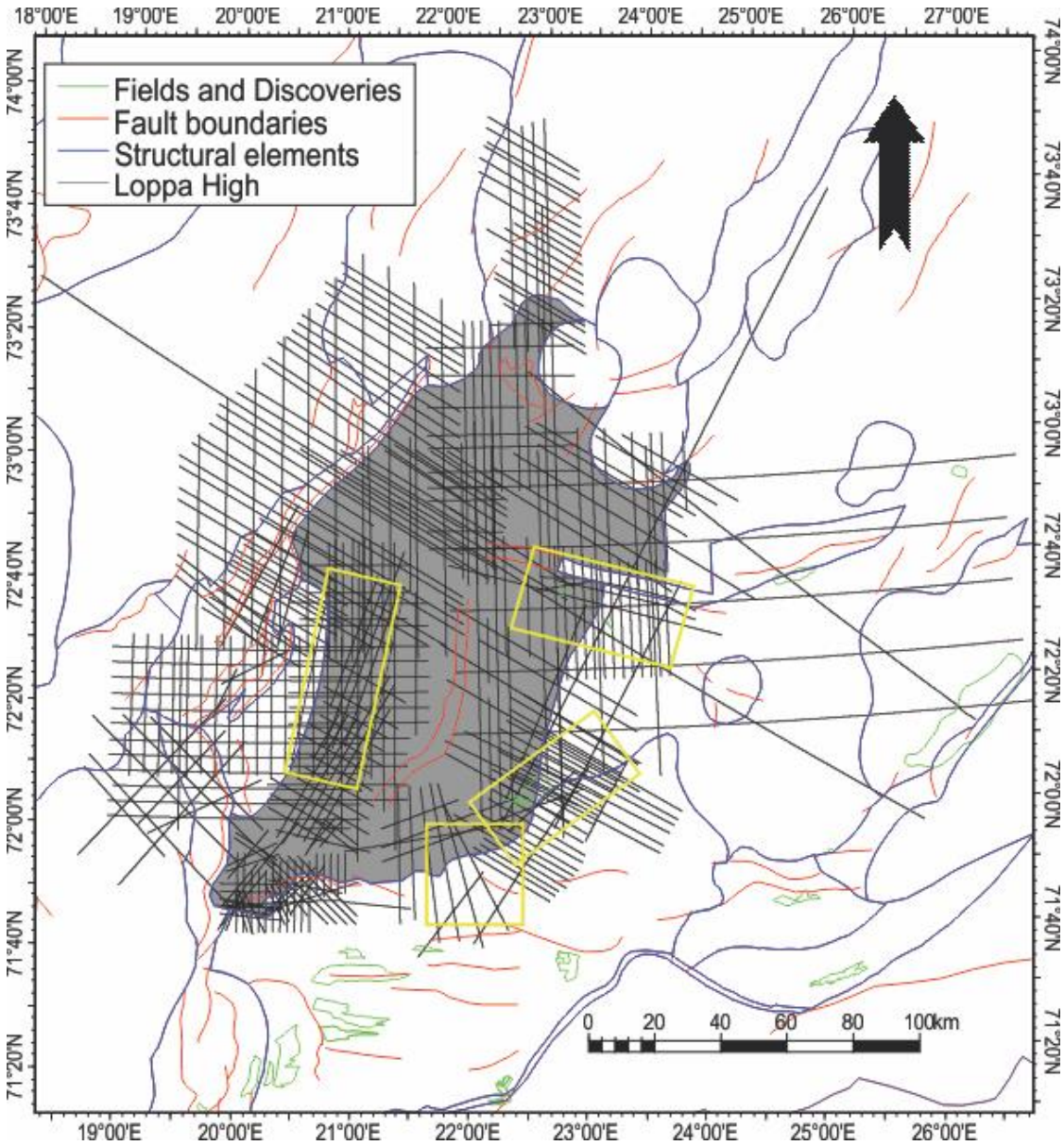

Figure 3.1: Overview of the study area showing the location of the seismic datasets. The 3D data is indicated by yellow squares while the 2D data is indicated by black lines.

3.1 Dataset

Four 3D seismic surveys and twenty-one 2D seismic datasets were used in this thesis (Table 3.1 and Table 3.2).

The polarity standard used is the SEG of Sheriff (2006). This SEG convention is an international standard which display positive peaks as positive reflection coefficients and negative peaks as negative reflection coefficients (Figure 3.2). This is known as normal or positive polarity. It can also be reversed when it is beneficial. . In this study will the positive amplitude be given a red/yellow color while the negative amplitude a blue color.

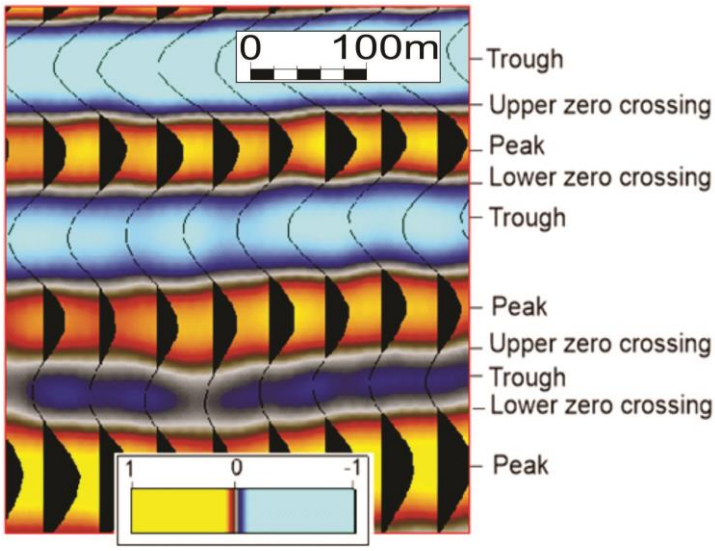

Figure 3.2: Seismic section from the SG9804 survey. The wavelet is processed to zero phase with normal polarity (SEG standard polarity). The data is acquired in an E-W direction (inline). The figure shows peak, trough, upper and lower zero crossing. The polarity of a negative and positive reflector is indicated.

A zero-phase wavelet with normal polarity (SEG normal) will be symmetrical with its peak at the central point corresponding to an increase in acoustic impedance, or positive reflection coefficient (Figure 3.3). For a reversed polarity (SEG reverse) will the opposite be true.

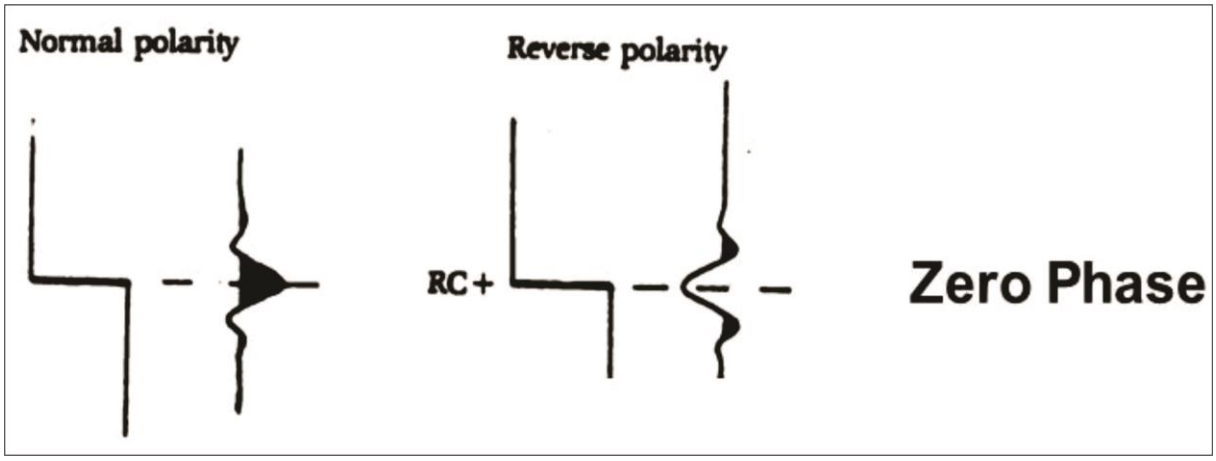

Figure 3.3: Polarity conventions for plotting seismic signals used in this study (SEG). Figure is modified from Sheriff (2006).

Survey name	Polarity	Phase	Bandwidth (Hz)	Peak frequency (Hz)	Area (km^2)	Inline Orientation
SG9810	Normal	Zero-phase	9-46	19	1281	E-W
SG9804	Normal	Zero-phase	7-30	17	1104	E-W
SG9803	Normal	Zero-phase	8-34	28	1035	NE-SW
OMV09M01	Normal	Zero-phase	6-18	12	513	N-S

Table 3.1: Overview of polarity, phase, frequency, size and orientation of the 3D datastes used in this study.

Survey name	Data type	Number of lines in survey	Gathered by	Year	Total length (cdp km)
AN88-9Q6-4	2D	30	Amoco Norway Oil Company	1988	1166
LHSG-89	2D	47	Den norske stats oljeselskap a.s	1989	1802
NH8403	2D	35	Norsk Hydro Produksjon AS	1984	1636
NH8506	2D	55	Norsk Hydro Produksjon AS	1985	2908
NH8514	2D	26	Norsk Hydro Produksjon AS	1985	907
NH8610	2D	22	Norsk Hydro Produksjon AS	1986	395
NH8904	2D	9	Norsk Hydro Produksjon AS	1989	132
NPD-BJRE-84	2D	1	Oljedirektoratet	1984	6380
NPD-NOLO-85	2D	12	Oljedirektoratet	1985	10363
SG8737	2D	4	Saga Petroleum ASA	1987	1048
SG9309	2D	48	Saga Petroleum ASA	1993	1889
SG9714	2D	14	Saga Petroleum ASA	1997	603
SG9715	2D	11	Saga Petroleum ASA	1997	488
SG9817	2D	1	Saga Petroleum ASA	1998	63
SH8601	2D	12	A/S Norske Shell	1986	223
SH9103	2D	12	A/S Norske Shell	1991	179
ST8813	2D	11	Den norske stats oljeselskap a.s	1988	566
ST8906	2D	24	Den norske stats oljeselskap a.s	1989	845
ST8823	2D	16	Den norske stats oljeselskap a.s	1988	742
BARE02	2D	10	-	-	-

Table 3.2: Overview of the 2D seismic datasets used in the study.No information about "BARE02" was found.

3.1.1 Well data

Ten wells are located within the vicinity of the study area which were used to tie lithostratigraphic units to the seismic data (Figure 3.4). This was done to get a more comprehensive understanding of the stratigraphy and depositional environment. The thickness of geological features and fault throw can be determined by estimating the velocity for each lithostratigraphic unit by combining the depths of units with a velocity-depth profile. In this master thesis, a velocity-depth profile by Storvoll et al. (2005) will be used, which was created using 13 exploration wells within the southwestern Barents Sea (Figure 3.5). The velocity for the Loppa High area was calculated using the average depths for the top of each geological formation (TWT and TVD), using data from the ten wells and well data from the NPD fact pages (NPD, 2018c). A velocity of 1500 m/s for the water column and 1700 m/s for the Quaternary sediments above the URU are used (Chand et al., 2008). The velocity of pre-Quaternary sediments is shown in Table 3.3.

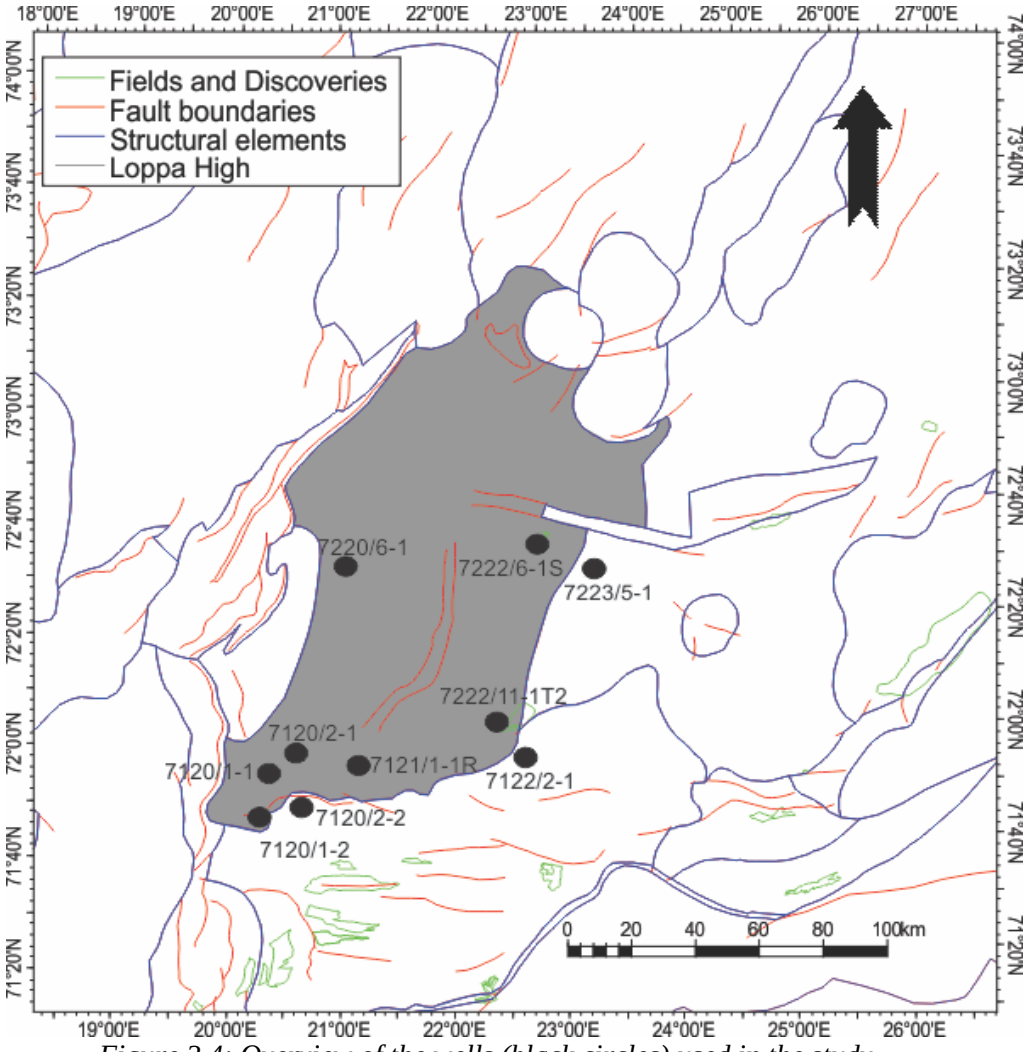

Figure 3.4: Overview of the wells (black circles) used in the study.

Interval	Top depth TWT (ms)	Top depth (TVD) m	Velocity (m/s)
Water column	-	-	1500
Nordland Group	496	375	1700
Torsk FM	568	458	2000
Kviting/Kveite FM	1170	1249	2300
Kolmule FM	1179	1067	2200
Kolje FM	1612	1846	2600
Hekkingen FM	1782	2147	3200
Stø FM	1875	2323	3500
Snadd FM	755	667	2100
Kobbe FM	1613	2038	3000
Klappmyss FM	1795	2458	3700
Havert FM	1967	2611	3800
Ørn FM	1820	2358	3600

Table 3.3: Overview of the velocity that will be used for calculating fault throw and thickness of geologic features in the study area. Older formations will occassionaly appear shallower than younger formations due to uplift and erosion where younger formations are absent.

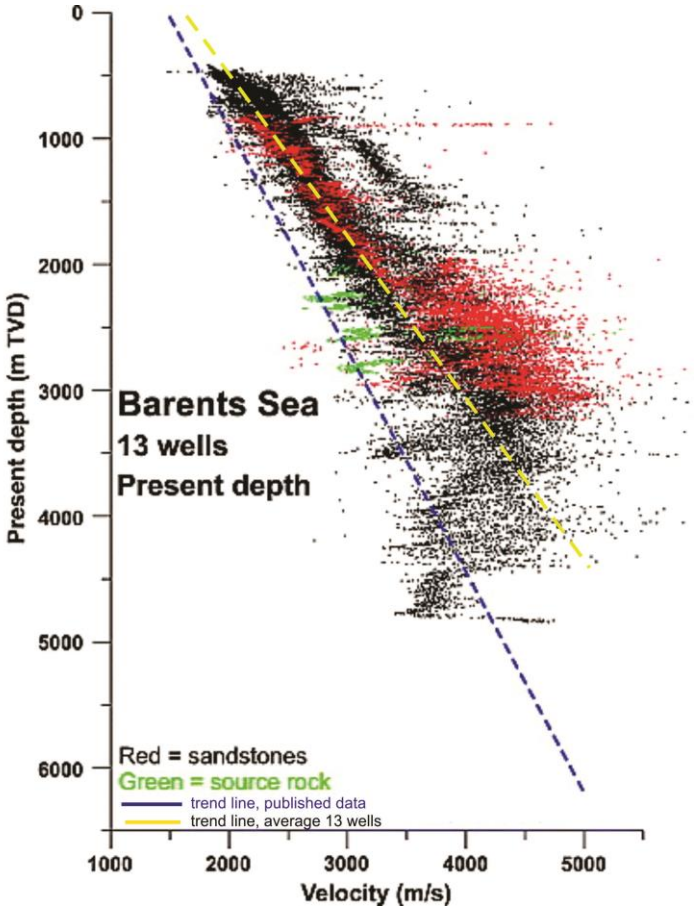

Figure 3.5: Sonic velocity profile at present depth from 13 wells.Blue line represents the average velocities from well from the North Sea, Norwegian Sea and Barents Sea. Yellow line represents average velocities from 13 wells in the Barents Sea. Velocities of sandstones are shown in red, shales in black, and the organic-rich Hekkingen FM in green. Figure modified from Storvoll et al. (2005).

3.1.2 Artefacts

Artefacts appear as of acquisition footprints in the seismic datasets (Figure 3.6). These footprints occur as lines parallel to the survey direction on the seismic images. Coherent noise is normal in finished seismically processed datasets, which correlates with the acquisition geometry (same orientation as inlines) (Bulat, 2005). These artefacts may arise from a faulty acquisition geometry from the streamers and guns. It can also be due to towing depth differences causing differences in the two-way travel time. It is important to not mistake these for actual features. Even though processing is a method designed to eliminate noise and correct systematic errors a certain degree of error will always be present. In old surveys artefacts are more prominent which should be kept in mind when interpreting the seismic data.

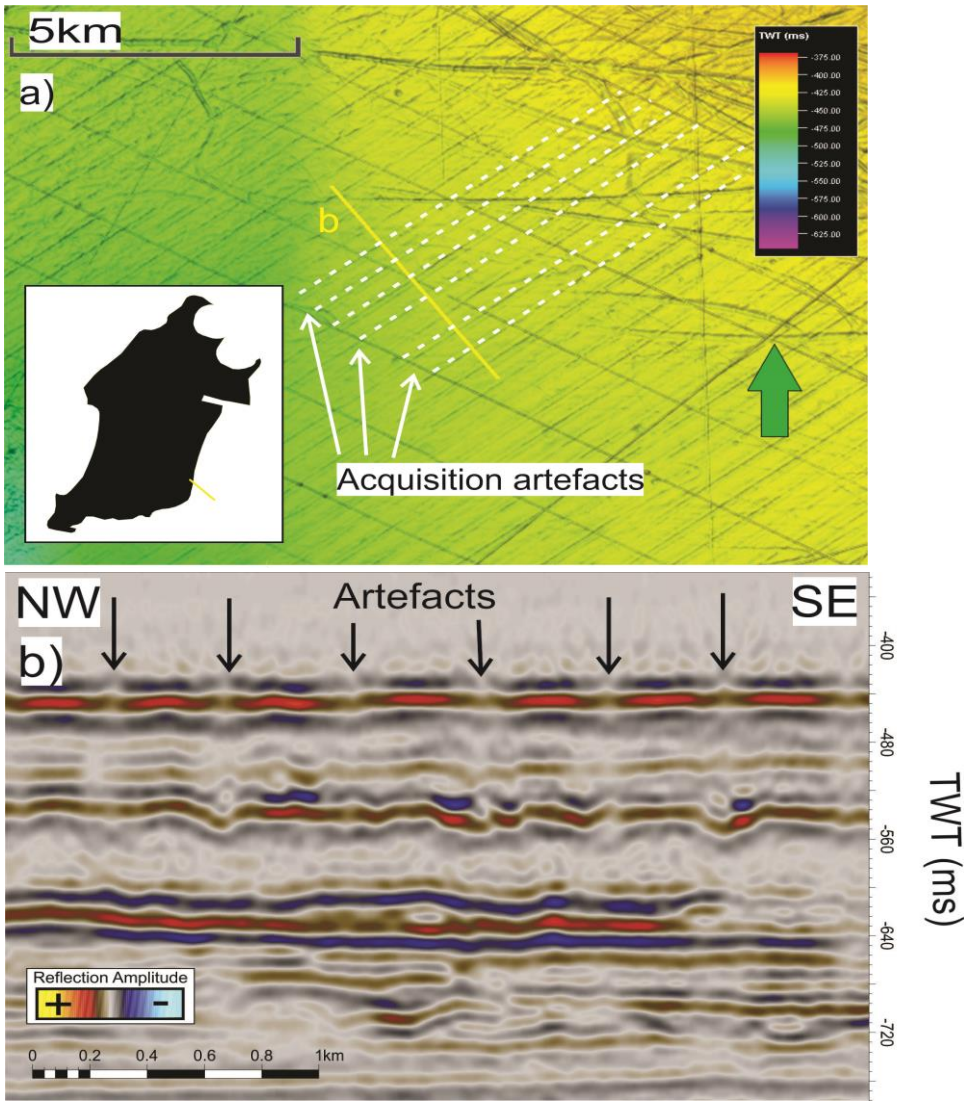

Figure 3.6: ***a)*** *Acqusition footprints (white dashed lines) parallel to the inlines of survey SG9803. Position indicated by yellow line in black polygon.* ***b)*** *Seismic section (xline) perpendicular to the footprints in* ***a****.*

3.2 Seismic resolution

Seismic resolution is defined as the ability to distinguish between two individual reflectors. It can be measured both vertical and horizontal (Sheriff, 1985). The seismic resolution decreases with depth as the wavelength increases (Figure 3.7). This is due to rocks becoming more compacted as they get older. As a result will the velocity increase. The frequency will decrease with depth due to a weaker seismic signal at a faster rate (attenuation of higher frequencies) (Brown, 2011). The seismic resolution depends on the seismic wavelength (Equation 3.1):

$$\lambda = \frac{v}{f} \qquad \textit{(Equation 3.1)}$$

λ= Wavelength (m)

v = Seismic velocity (m/s)

f = Seismic frequency (Hz)

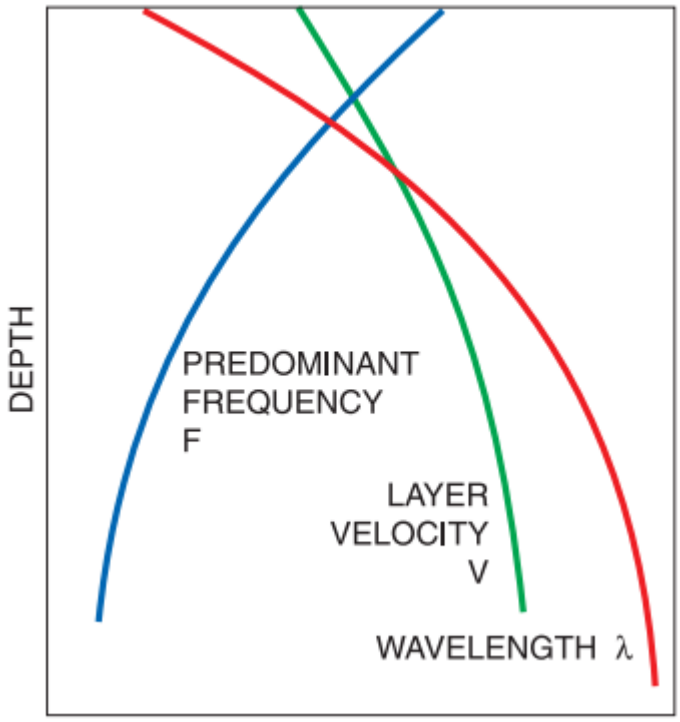

Figure 3.7: The wavelength increases with depth which reduces the resolution. Figure from Brown (2011).

3.2.1 Vertical resolution

In seismic data determines vertical resolution the smallest size a feature can have before it no longer can be observed in the dataset. It is referred to as the limit of seperability. It can be derived from the length of the acoustic wave which is normally ¼ of the wavelength. The dominant wavelength has to be considered in order to calculate the vertical resolution (Equation 3.2):

$$Vr = \frac{\lambda}{4} \qquad \textit{(Equation 3.2)}$$

Vr = Vertical resolution (m)

λ = Wavelength (m)

The equation for vertical resolution implies that if the thickness of layer/feature is less than ¼ of the wavelet, the top and base of the layer may merge into one waveform and produce an amplitude increase. In other words, this is the threshold distance for distinguishing between two reflectors. This is called the interference or tuning effect, which is the result of destructive interference that will occur until the limit of visibility is reached and the signal gets obscured by the background noise (Brown, 2011; Sheriff, 1985). If the two reflecting interfaces are separated by more than half of a wavelength will the wavelets not interfere and two separate reflections will be produced. The vertical resolution for the 3D seismic datasets is shown in Table 3.4. An average velocity of 2600 m/s (Kolje FM) is used to calculate the resolution (Table 3.3).

Survey name	**Peak frequency (Hz)**	**Wavelength (m): λ = v /f**	**Vertical resolution (m): Vr = λ/4**
SG9810	19	137	34.3
SG9804	17	153	38.3
SG9803	28	93	23.3
OMV09M01	12	217	54.3

Table 3.4 Overview of the vertical resolution for the 3D seismic datasets used. The velocity of the subsurface sediments Kolje FM (2600 m/s) is from table 3.3.

3.2.2 Horizontal resolution

The horizontal resolution refers to the minimum horizontal distance between two reflecting points needed to be recognized as two separate points. The pre-migration horizontal resolution is determined by the size of the Fresnel zone (Figure 3.8), which is the area the wave front reaches within ¼ λ. It is the subsurface area that reflects energy that arrives at the geophone/hydrophone within a half-cycle (Bulat, 2005; Sheriff, 1985). The radius of the area is determined by the wavelength of the acoustic signal. The wavefront will spread with increasing depth. The horizontal resolution of the dataset is affected by the two-way traveltime to the top of the reflector, interval velocity and the frequency content of the pulse (Veeken, 2013). An increased frequency will result in an improved horizontal resolution, but high frequencies will have trouble penetrating sufficient depths. This is why low frequency seismic waves are often used which results in a reduced resolution with depth. The formula for the Fresnel zone's radius in unmigrated seismic data is given by Equation 3.3:

$$rf = \frac{v}{2}\sqrt{\frac{t}{f}} \qquad \textit{(Equation 3.3)}$$

rf = Radius of Fresnel zone (m)

v = Velocity (m/s)

t = Two-way traveltime (s)

f = Dominant frequency (Hz)

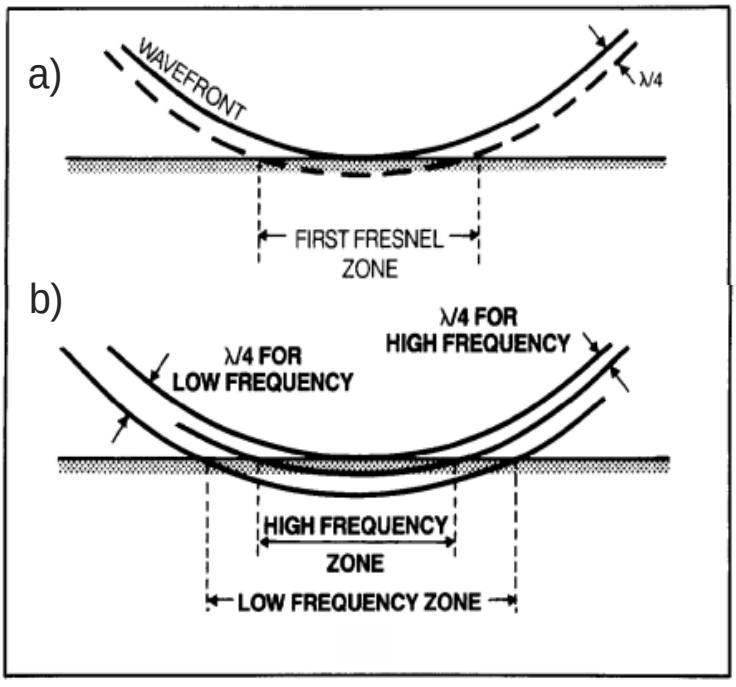

Figure 3.8: ***a)*** *The Fresnel zone defines the area where the wavefront is tangent to the reflector. It is limited by the area the wavefront circle makes with the interface after 1/4 λ.*

b) *Size of the Fresnel zone depends on frequency/wavelength. Figure modified from Sheriff (1985).*

Shrinking the Fresnel zone will give an increased horizontal resolution with migration of the seismic data. For 2D seismic data may the migration only collapse the Fresnel zone in the inline direction to an ellipse (Bulat, 2005; Sheriff, 1985). In 3D can the Fresnel circle be shrunk down to a small circle giving a better resolution as the energy is more focused (Figure 3.9). For migrated seismic data can the horizontal resolution be illustrated using the following formula (Equation 3.4):

$$Hr = \frac{\lambda}{4} \qquad \textit{(Equation 3.4)}$$

Hr = Horizontal resolution (m)

λ= Wavelength (m)

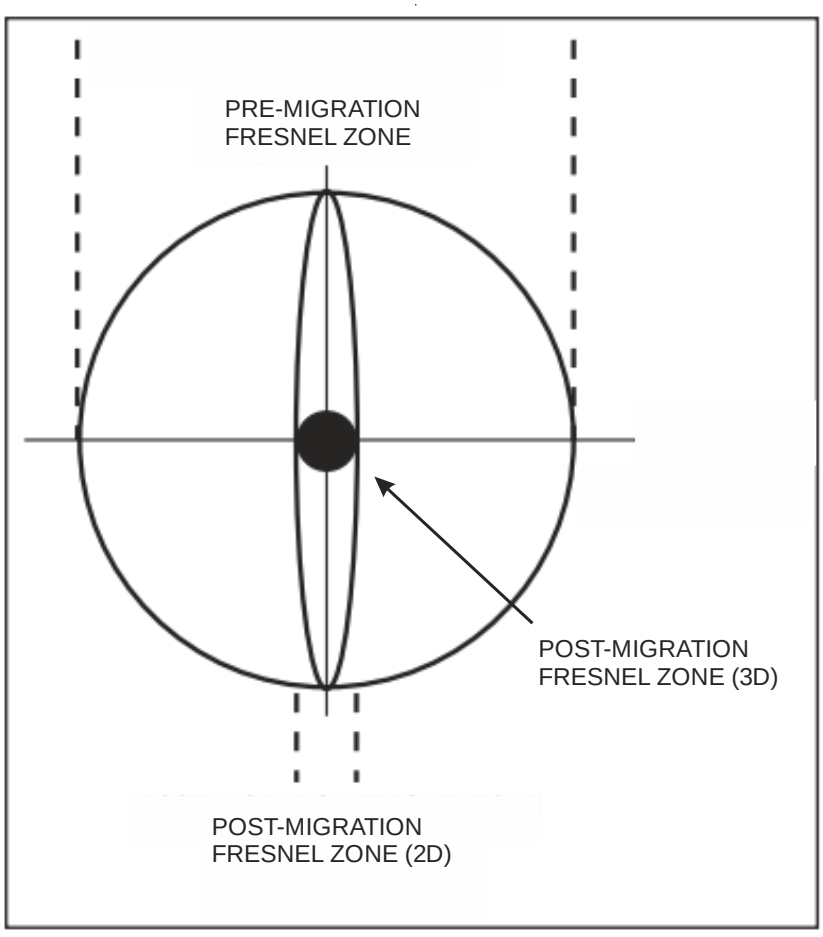

Figure 3.9: Effect on the Fresnel zone size/shape regarding 2D and 3D migration. Figure modified from Brown (2011).

Survey name	Peak frequency (Hz)	Wavelength (m): $\lambda = v / f$	Horizontal resolution, pre-migration (m)	Horizontal resolution, post-migration (m)
SG9810	19	137	398.1	34.3
SG9804	17	153	420.9	38.3
SG9803	28	93	328	23.3
OMV09M01	12	217	501	54.3

Table 3.5 Overview of the horizontal resolution for the 3D seismic datasets used. The velocity of the subsurface sediments Kolje FM (2600 m/s) is used which is from Table 3.3. Equation 3.3 is used to calculate the horizontal resolution (pre-migration).

3.3 Interpretation methods

The interpretations in this thesis have been carried out using the petrel software version 2016. This software is developed by Schlumberger with the intention for hydrocarbon exploration. It was used to visualize and interpret the seismic data using tools and features to make horizons and generate attribute-maps.

Corel draw 2017 was used to create and modify figures in this thesis. Corel draw is a graphic software allowing the user to work in different layers which simplifies the figure generating process.

3.3.1 Seismic interpretation

Seismic volumes can be visualized from created surfaces using horizons. These horizons have been made using the seeded 2D auto tracking. This tool can interpret continuous reflectors, which are determined by the amplitude values in a seismic trace. This trace will follow a reflector based on continuity and signal strength, but other parameters can also be used. The seeded 3D auto tracking and the paintbrush function were used to fill in the areas between the inlines and crosslines. The manual auto tracker has been used for less continuous reflectors. Interpretation of fault has also been done by placing faults sticks in the seismic profiles.

3.3.2 Seismic attributes

From the imported data can different attributes and calculations be extracted. The dataset is a time-migrated dataset. In other words, all interpreted horizons, structural elements and anomalies are interpreted in the time-domain using cross sections, 2D- and 3D-windows.

Different parameters like seismic traces, attribute maps and volumes were used. A seismic attribute is defined as a “quantitative measure of a seismic characteristic of interest” (Chopra & Marfurt, 2005). These attributes can be displayed on seismic sections, random intersections,

time slices, different volumes and surfaces. In this thesis was seismic attributes calculated to map faults, ampltide anomalies and different features.

3.3.2.1 Structural smoothing

Structural smoothing is an attribute, which increases the continuity of seismic reflections. In other words, it smoothes the input data in a given volume. The reflection continuity is increased while important discontinuities are preserved.

3.3.2.2 Variance

The variance attribute represents the trace-to-trace variability over a certain sample interval. The method isolates discontinuties in the horizontal continuity of amplitudes, which is often used on faults and stratigraphic features (Chopra & Marfurt, 2005). It produces interpretable lateral changes in acoustic impedance in three dimensions. In addition, it can be used to map the outer rim of fluid flow features. This attribute is very useful regarding seismic facies analysis and the depositional environment can be interpreted from the seismic data. A three-dimensional variance map allows the user to move to time periods and depths of interest. Time-slices were created at various depths to confirm accurate and detailed mapping.

3.3.2.3 RMS amplitude

RMS (Root Mean Square) amplitude is an attribute used to highlight strong amplitudes in a specific volume. It calculates the square root of the sum squared amplitudes divided by the number of samples within the specified interval. It is normally calculated for a seismic volume or used as a surface attribute. It may be used to map geological features which are isolated from background features by the amplitude response. The RMS amplitude maps can be used as hydrocarbon indicators and to do seismic facies analysis.

4. Results

In this chapter all the observations and interpretations done for the datasets located in the Loppa High region (Figure 4.1) will be presented. The fluid flow systems in the area have been interpreted from key seismic horizons/units together with the analysis of various attribute maps and time-slices. The main focus has been to map the distribution of fluid flow features and see how these are related to the structural elements (potential leaking faults). The features mainly appear as vertical zones of distorted reflections and high amplitude anomalies, often associated with polarity reversal and velocity effects in the seismic data. The linkage between shallow gas accumulations and deeper-seated reservoirs is poorly understood and a better understanding of how focused fluid flow contribute to these accumulations is of great interest. Interpretation of the seafloor will help link the deeper structures to the shallow morphological features. The large extent of the study area, formations being truncated due to erosion and the structural setting prevents complete interpretations of the seismic stratigraphy and to some degree detailed descriptions of the individual features. Some of the faults, gas chimneys and other related structures have previously been described and interpreted by other published works (e.g. (Larsen, 2011; Vadakkepuliyambatta et al., 2013).

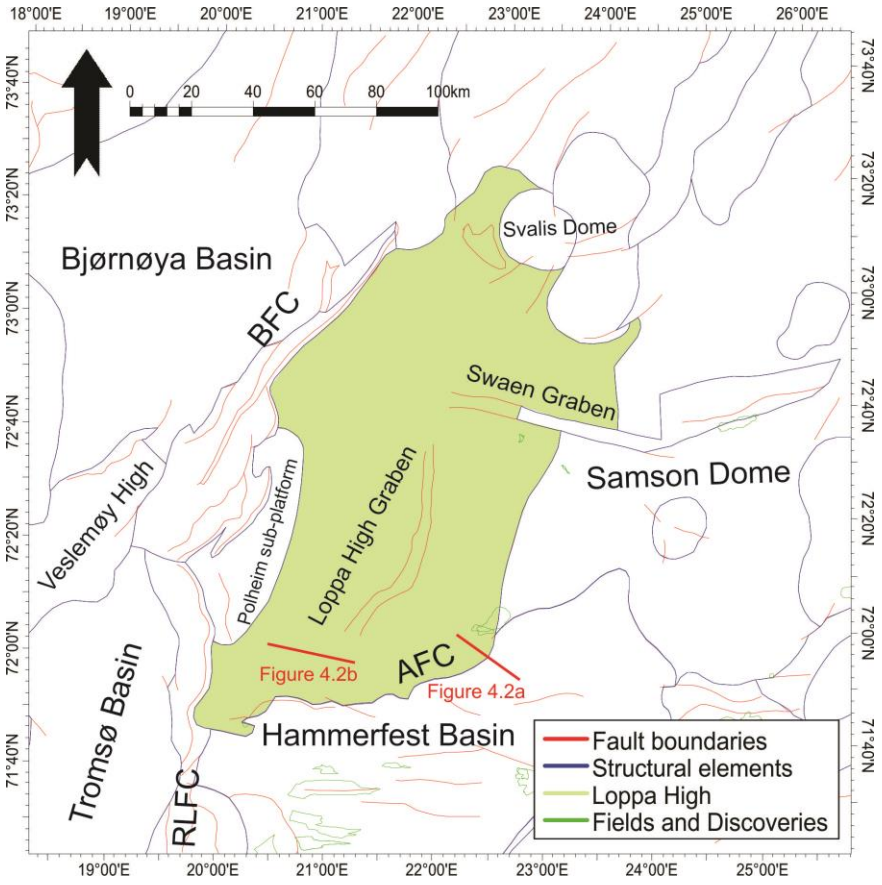

Figure 4.1: Overview of the study area showing the location of the seismic sections in Figure 4.2

4.1 Seismic stratigraphy

The geological history of the Barents Sea is revealed by multiple strong reflectors. These reflectors can be linked to the well data within the study area to determine the seismic stratigraphy in the Loppa High. However, the focus of this study has not been to determine the stratigraphy but rather see how the different formations are related to fluid flow in the area. The formations can in other words be used to find the origin and transport of fluids (where the fluids are migrating upwards) by acting as a source/reservoir rock. Formation tops from NPD has been obtained for this task which contains well tops from the Basement up to the Top Torsk formation and the Nordland Group. Formation-depths in the western area are uncertain due to lack of wells. Interpretations in this area will therefore be based on other articles (Chand et al., 2012; Rajan et al., 2013). The Loppa High has a structural geometry with enclosed basins and onlapping subsurface formations. Due to uplift and erosion are Jurassic, Cretaceous and Paleogene formations missing on top of the high. The stratigraphic units varies in the datasets and are difficult to identify over large areas due to truncation (Figure 4.2).

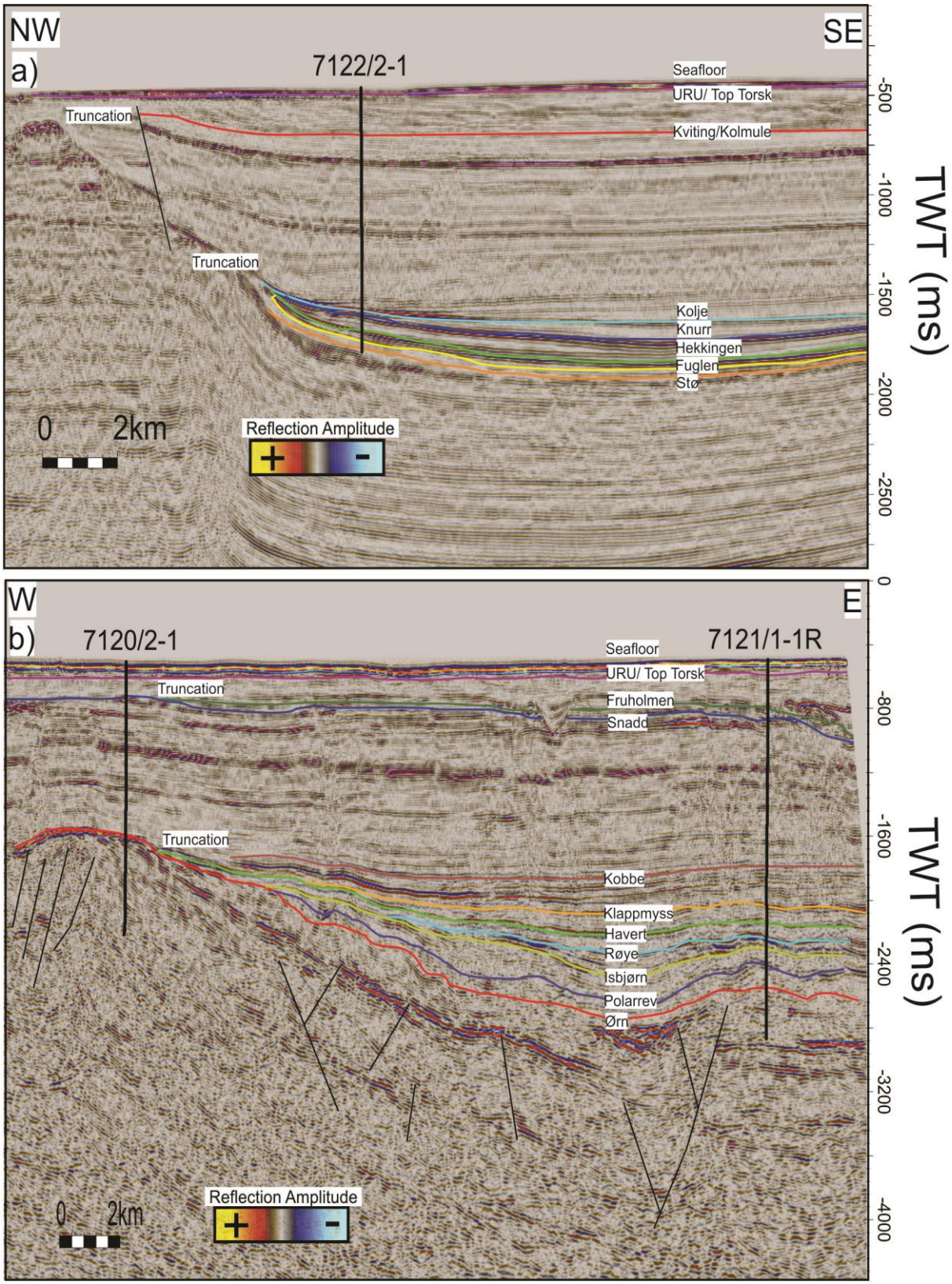

Figure 4.2: ***a-b)*** *Seismic sections showing the stratigraphic units and well positions in the Loppa High region. Positions of a-b is indicated in Figure 4.1.*

4.1.1 Seafloor

The seafloor in the Loppa High region is to a high degree affected by glacial erosion and is in general characterized by two types of features with different geometries. The first type appear as elongated, curved and linear depressions while the other type appear as circular to sub-circular depressions. This is illustrated in Figure 4.3 and Figure 4.4.

The first type appear as furrows and lineations imprinted on the seafloor and is interpreted to be plough marks (Figure 4.4**a,b)** and scours formed by the movement of icebergs driven by wind, tide and ocean currents (K Andreassen et al., 2007). Features like these are normal at the edges of continental shelves in high latitude zones which have earlier been covered by ice. The plough marks show two dominant directions: SW-NE and NW-SE which reflects the main direction of the glaciers movement. There are also a couple of plough marks oriented in all directions. This indicates other periods with different directions of the iceberg. It is important to clarify that these features varies greatly in size, but will in general be 20-375m wide, up to 30km in length and 10-30 ms (TWT) deep coreesponding to 5-22.5m (TVD) (Vp = 1500 m/s, Table 3.3). These features could also potentially be interpreted to be mega-scale glacial lineations (MSGL). The curvilinear furrows are interpreted as scours which have a random to preferred orientation. They are produced as a result of erosion of a sediment surface by a current flowing over it. Features like these are common in bank areas and seem to often be curved (V- or U-shaped) in a cross profile with levees at their sides. Scouring is normal in front of marine glaciers where the keel of the iceberg may erode the seafloor together with rocks trapped under the ice. The location of the glacial features are limited to the shallowest eastern and western areas in the study area.
The second type of features located on the seabed is interpreted to be pockmarks (Figure 4.4**c,d**) (Judd & Hovland, 2009). Pockmarks indicate postglacial fluid emissions, but visual fluid flow indicators may be absent (Figure 4.4**e,f**). These circular-subcircular depressions will be discussed further in chapter 4.5.

The seabed reflector is strong over the whole area and morphological features can easy be interpreted due to its high spatial resolution (Figure 4.4). However, this is only the case for the obtained 3D data. The water depth in the area varies from 375-625 ms (TWT), corresponding to 281-469 m (TVD) assuming a water velocity of 1500 m/s (Table 3.3). The water depths somewhat gradually increase towards north. The shallowest areas are to the southwest while the deepest parts are in the northwest. The deepest water depths are related to Bjørnøyrenna

and the Bjørnøya basin which marks the end of the Barents Sea continental shelf. The southwestern Barents Sea was part of a large ice sheet where Bjørnøyrenna acted as the main pathway for ice streams.

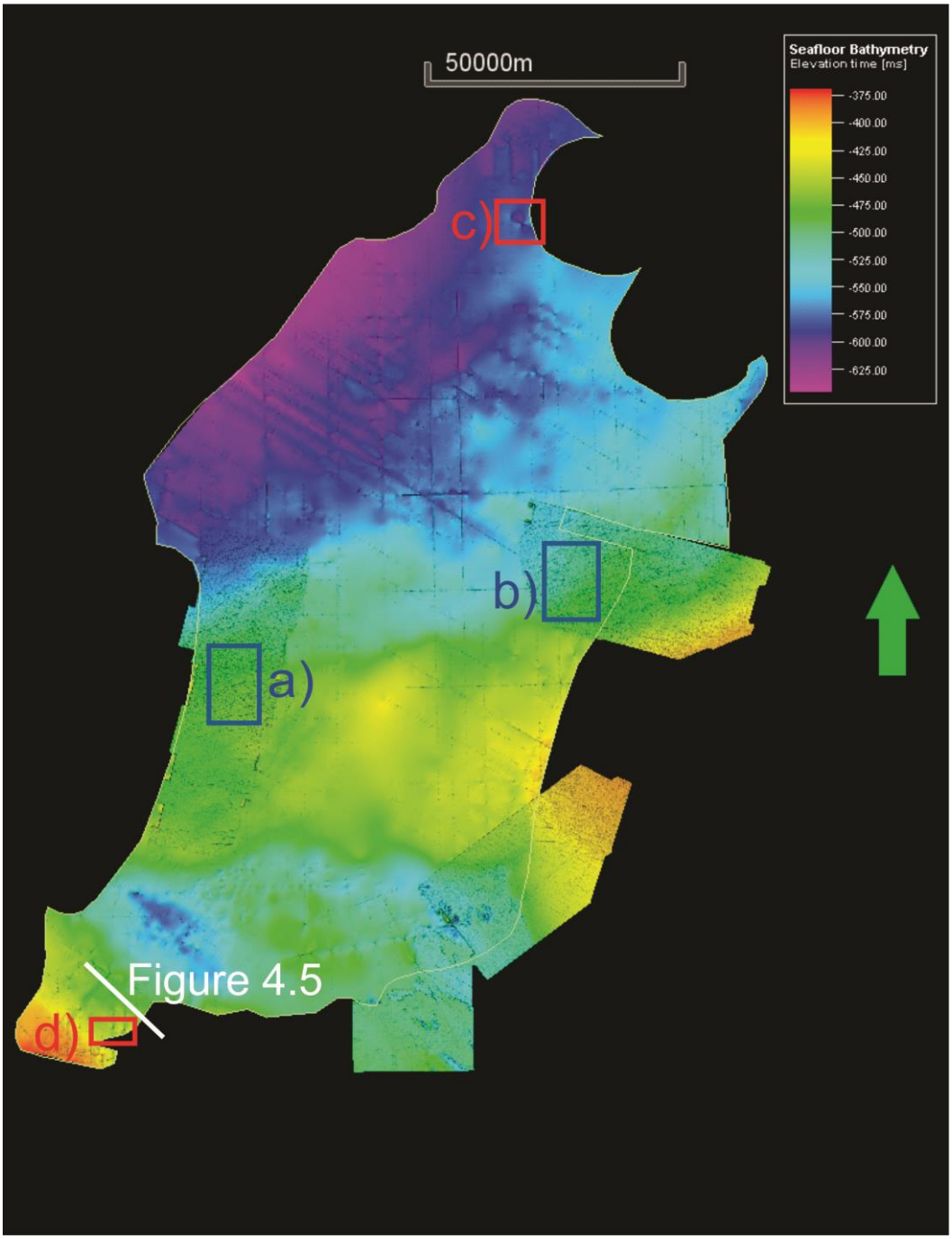

Figure 4.3: Map of the seafloor on the Loppa High based on seismic interpretation of the seabed reflector. Legend is measured in TWT (ms). The blue and red squares indicates the areas shown in Figure 4.4.

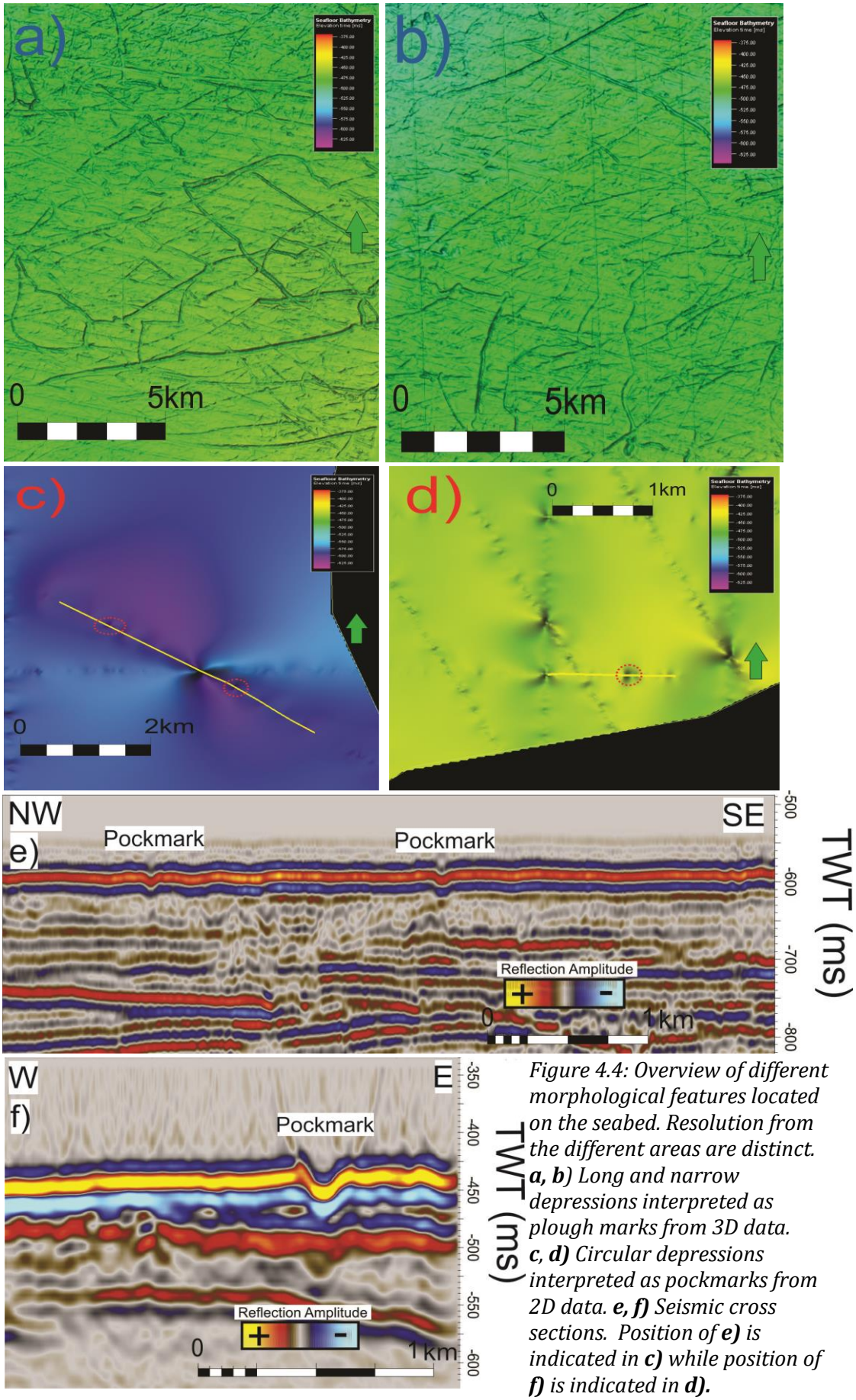

Figure 4.4: Overview of different morphological features located on the seabed. Resolution from the different areas are distinct. ***a, b****) Long and narrow depressions interpreted as plough marks from 3D data.* ***c****,* ***d)*** *Circular depressions interpreted as pockmarks from 2D data.* ***e, f)*** *Seismic cross sections. Position of* ***e)*** *is indicated in* ***c)*** *while position of* ***f)*** *is indicated in* ***d).***

4.1.2 Upper Regional Unconformity

Several periods of glaciations have occurred since Plio-Pleistocene which have influenced the Barents Sea (K Andreassen et al., 2007; Vorren et al., 1991). A regional reflector, the upper regional unconformity (URU), represents the interface between the underlying sedimentary bedrocks (Paleogene – Neogene sediments) and the overlying Pleistocene glacigenic deposits. It is in other words a significant erosive surface. This reflection marks the base of the Nordland Group and is characterized by a high amplitude reflection (Figure 4.5). The reflection representing the URU is in general easy to identify and map due to its high continuity, but will occasionally be affected by truncated clinoforms of the underlying Torsk Formation.

In the southwestern area is the URU typically located between 50-80 ms (TWT) below the seabed (Figure 4.5).

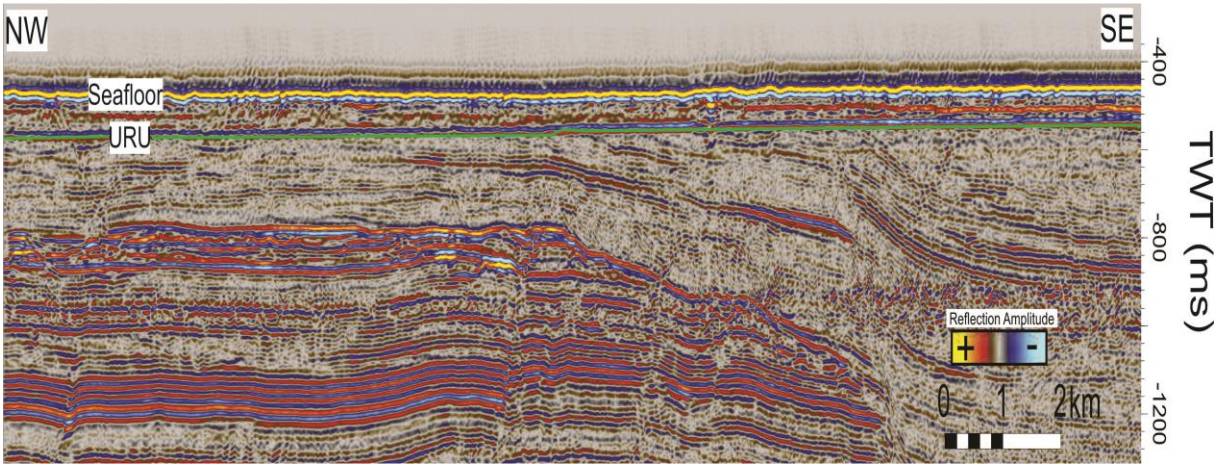

Figure 4.5: Seismic cross section showing reflector (green) interpreted as URU. Southeastern dipping strata is truncated against the URU. Position is indicated in Figure. 4.3.

4.2 Faults

The Loppa High region is highly affected by faulting. The high itself is surrounded by various faults and geologic basins and is in addition comprised of two grabens (Swaen Graben and Loppa High Graben) which is indicated in Figure 4.1. Several faults have been identified, but they have not been mapped over the whole region due to the size of the study area and scope of this study. The identified faults are gathered from the available 3D-data (Figure 3.1) which allows the use of time slices.

The identified faults may be divided into two groups based on their vertical extent: Deep-seated faults and shallow faults. Deep-seated faults are in this thesis defined as faults terminating below the Upper Regional Unconformity. These kind of faults affect different stratigraphic levels across the Loppa High. Some deep-seated fault may reach the URU, but are not classified as shallow faults due to their larger vertical extent. The shallow faults are faults terminating at or right below the URU. These are faults restricted to the younger strata.

4.2.1 Deep-seated faults

The seismic data reveals faults extended in the deep parts of the stratigraphy (Figure 4.6). However, some of the deep-seated faults also tend to penetrate shallower strata and possibly also the URU (Figure 4.7**b**). The deep-seated faults appear as extensional discontinuities/features with a varied fault throw along the strike- and dip-direction. The interpreted deep-seated faults seem to have four dominating strike orientations: ESE-WNW, SE-NW, NE-SW and E-W. All faults are interpreted as parallel normal faults where fault blocks have created horst-graben structures. The fault throws varies greatly, but the largest throws appear to occur in the deeper levels. Faults with small-scale throws may not show in the seismic as the horizontal and vertical resolution is not sufficient to distinguish these.

The deep-seated faults probably helped creating the Loppa Highs diamond-shaped outline and can be described as first/second class faults responsible for structures on a regional setting (Gabrielsen, 1984).

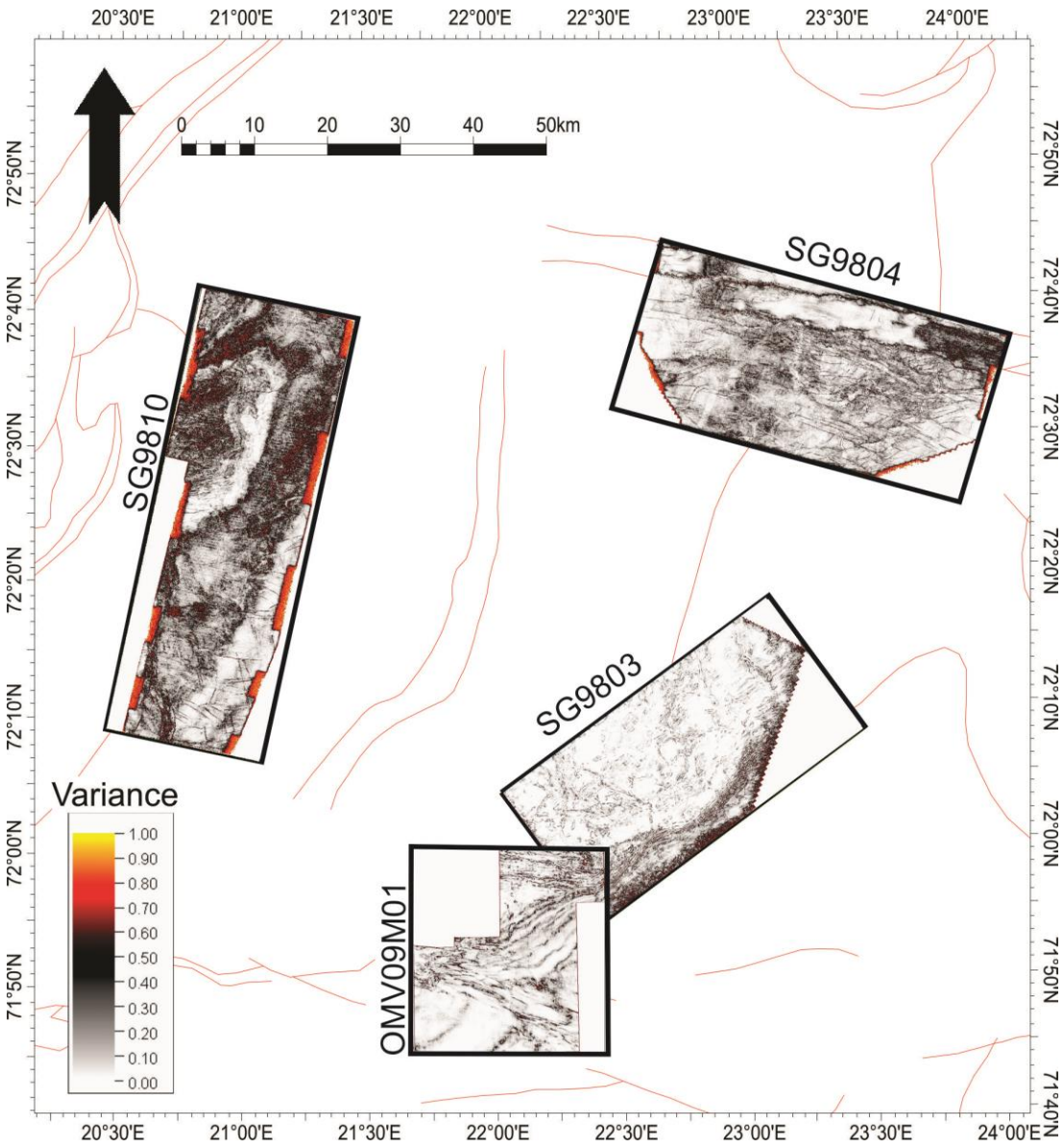

Figure 4.6: Overview picture of the deep-seated faults in the study area. Variance time slices are used to map and identify faults. Depth (TWT) of time slices indicated in Table 4.1.

Survey name	**Time slice depth in TWT (ms)**
SG9810	1140
SG9804	988
SG9803	3292
OMV09M01	3516

Table 4.1. Depth (TWT) used for the variance time slices in Figure 4.6.

The majority of the deep-seated faults in survey SG9810 extend from the Basement and displace the strata up to the Ørn Formation (Carboniferous/Permian) where they terminate. They have in general an ESE-WNW strike orientation and are identified mainly in the northern and southeastern part of the survey (Figure 4.7**a**). The faults appear very vertical, but have slight dip directions towards the north and south, forming steep horst and graben structures. The faults have in general a vertical extent of 500 ms (TWT). In Figure 4.7**a** do the faults look to consist of closely spaced segments between 3-11 km long and spaced 1-5 km apart. The fault throws varies between 10-15 ms (TWT), corresponding to 18-27 m (TVD) (V_p = 3600 m/s, Table 3.3). However, a larger throw of 40 ms (TWT), corresponding to 72 m (TVD) (V_p = 3600 m/s, Table 3.3) is also observed related to the fault reaching more shallow strata. It is important to add that the Ørn Formation is located at very shallow depths in this area, probably giving too high values when going from ms (TWT) to m (TVD).

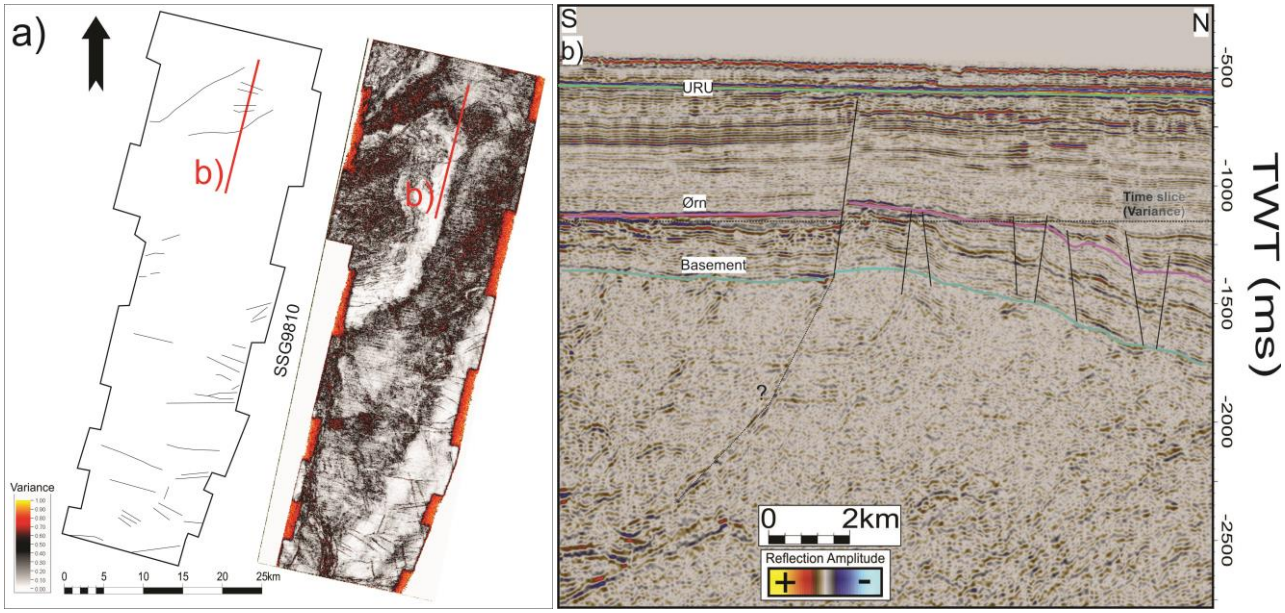

*Figure 4.7: **a)** Overview of deep-seated faults in survey SG9810. Variance time slice is indicated in **b** (1140 ms TWT). **b)** Seismic section showing deep-seated faults. Position indicated in **a**.*

The deep-seated faults in survey SG9804 extend in general from the Havert Formation and displace the strata up to the Snadd Formation (Upper Traissic) where they terminate. They have a SE-NW strike orientation. The deep-seated faults are identified mainly in the northern part of the survey (Figure 4.8**a**). The faults appear vertical with slight dip directions towards the northeast and southwest. The faults have in general a vertical extent of 1000-1500 ms (TWT). In Figure 4.8**a** do majority of the faults seem to consist of closely spaced segments between 3-13 km long and spaced 1-5 km apart. The fault throws varies between 10-15 ms (TWT) in the

southern areas, corresponding to 18.5-28m (TVD) (V_p = 3700 m/s, Table 3.3). However, larger throws up to 300 ms (TWT) in the northern areas, corresponding to 315m (TVD) (V_p = 2100 m/s, Table 3.3), is also observed. These large fault throws are related to the Swaen Graben. The graben is made of two opposing normal falts trending in an SE-NW direction, highly oblique to the Loppa High Graben (Figure 4.1) which trends in a more N-S direction. It spans the northeastern corner of the Loppa High and seem to continue on through the Eastern Flexure and towards the Norvarg Dome. It is quite narrow relative to its length. The Swaen Graben extends throughout the whole survey except the westernmost areas. The formation of the Swaen Graben most likely occurred during the Early- to Mid-Jurassic as Trassic formations (Havert, Klappmyss, Snadd) are clearly affected.

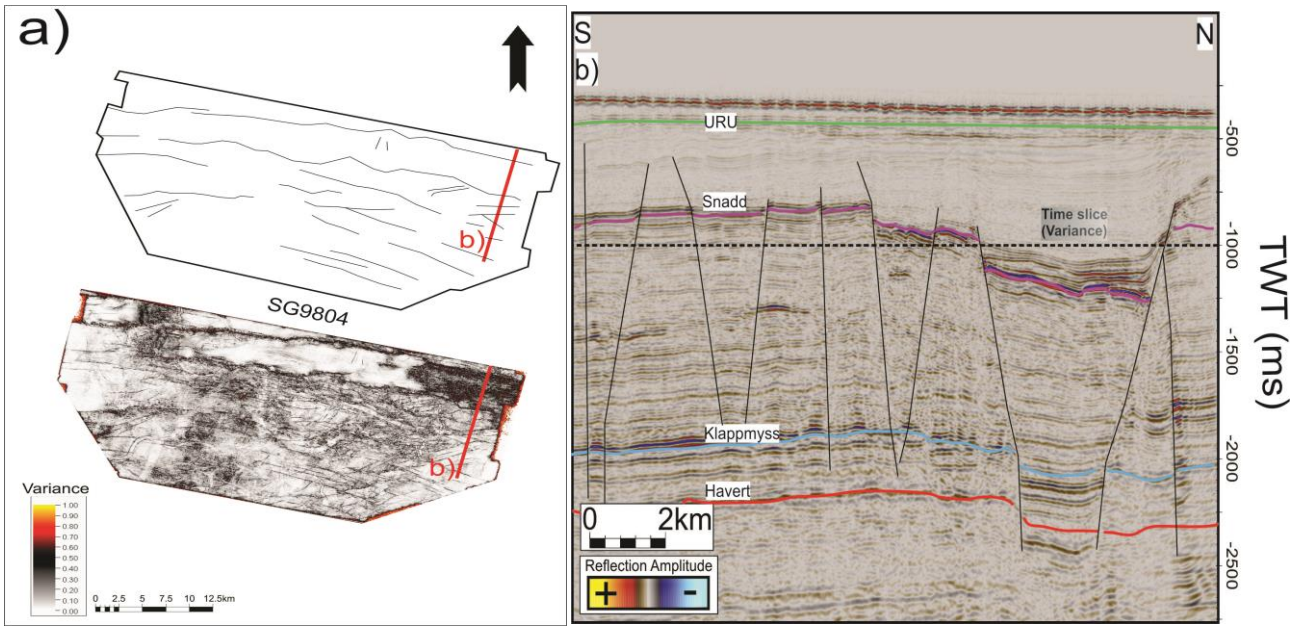

*Figure 4.8: **a)** Overview of deep-seated faults in survey SG9804. Variance time slice is indicated in **b** (988 ms TWT). **b)** Seismic section showing deep-seated faults. Position indicated in **a**.*

The deep-seated faults in survey SG9803 extend and terminate below the Kobbe Formation. They have in general a NE-SW strike orientation. The faults have slight dip directions towards the south/southeast with a vertical extent of 1000-2000 ms (TWT). In Figure 4.9a do the faults look to consist of spaced segments in general between 3-10 km long and spaced 1-6 km apart. The fault boundaries occur longer. The fault throws varies between 10-50 ms (TWT), corresponding to 15-75 m (TVD) (V_p = 3000 m/s, Table 3.3).

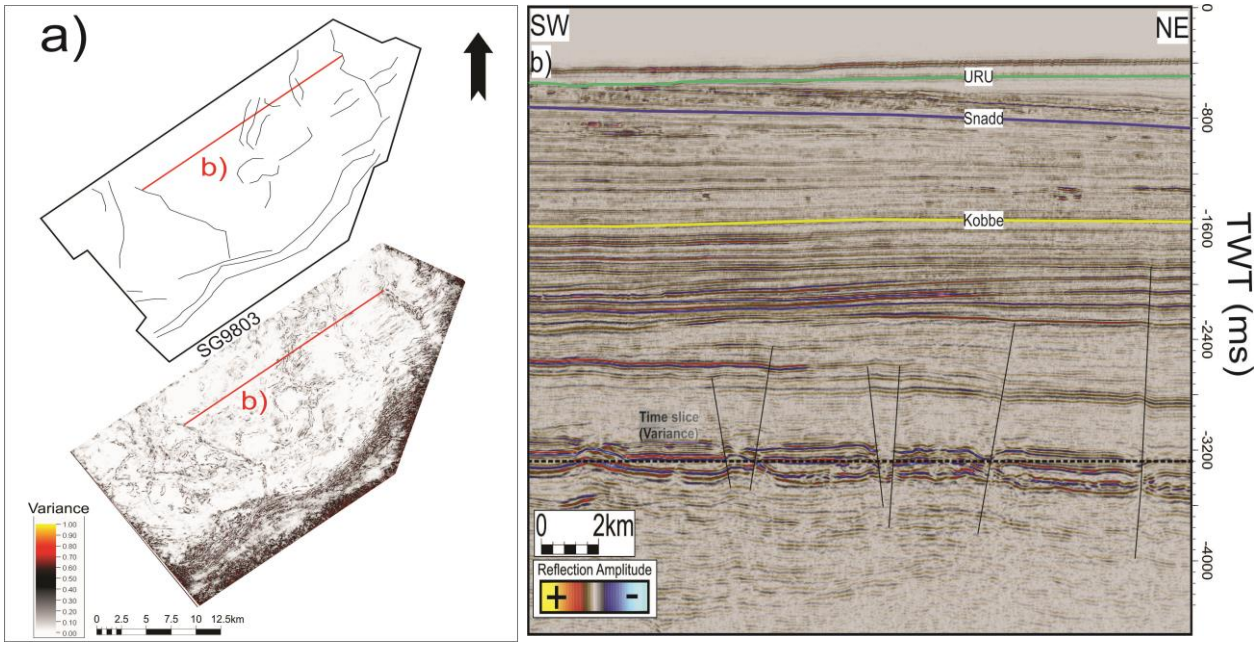

*Figure 4.9: **a)** Overview of deep-seated faults in survey SG9803. Variance time slice is indicated in **b** (3292 ms TWT). **b)** Seismic section showing deep-seated faults. Position indicated in **a**.*

The deep-seated faults in survey OMV09M01 extend in general through the Kobbe Formation. They have in general an E-W strike orientation with dip directions towards the south. The faults have a vertical extent of 500-3000 ms (TWT). In Figure 4.10 do the faults look to consist of spaced segments up to 10 km long and spaced 1-5 km apart. The fault throws varies between 10-125 ms (TWT), corresponding to 15-188m (TVD) (V_p = 3000 m/s, Table 3.3). These faults are part of the Asterias Fault Complex.

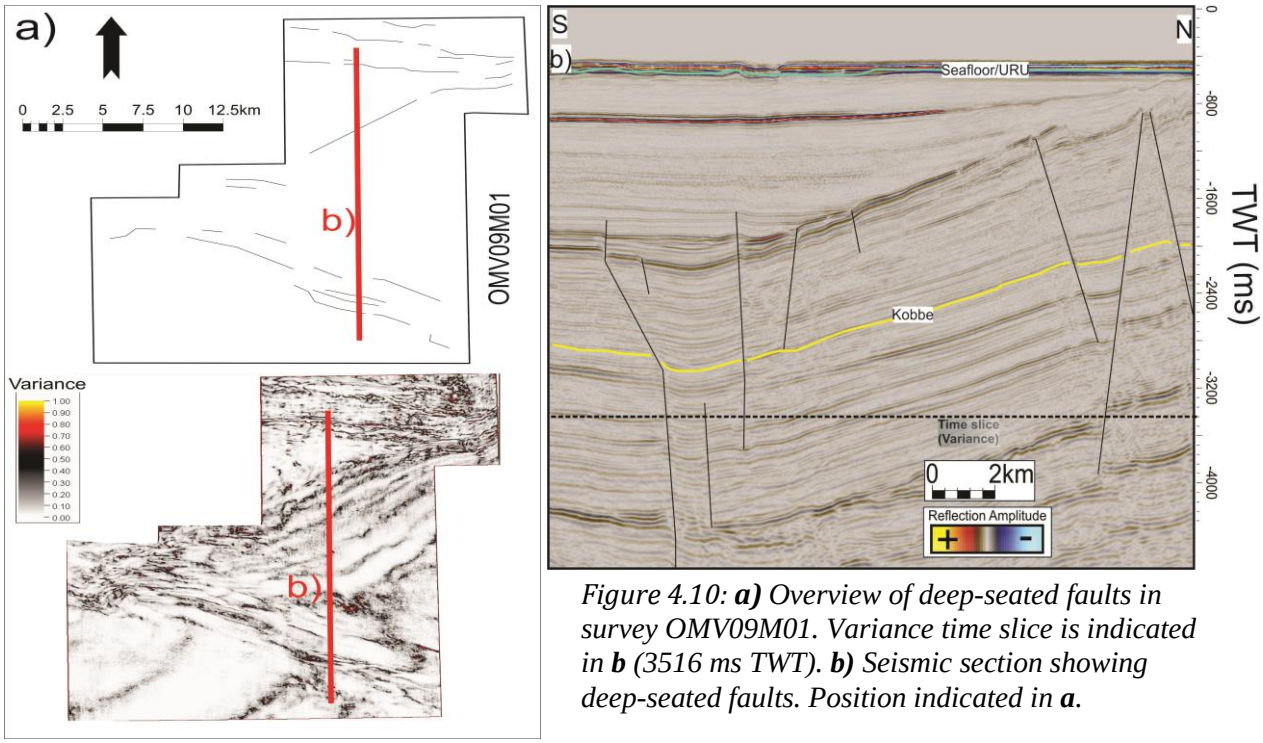

*Figure 4.10: **a)** Overview of deep-seated faults in survey OMV09M01. Variance time slice is indicated in **b** (3516 ms TWT). **b)** Seismic section showing deep-seated faults. Position indicated in **a**.*

4.2.2 Shallow faults

Looking at time slices within the URU reveals numerous shallow faults (Figure 4.11). These extensional features are normally confined to the upper part of the Torsk Formation which is a formation of Paleocene-Eocene age. Shallow faults terminate at or just below the URU. The shallow faults are normal fault systems with dominant strike directions E-W, NE-SW and SE-NW. Most of the fault occur within the upper 1500 ms (TWT) with a varied fault throw along the strike- and dip-direction.

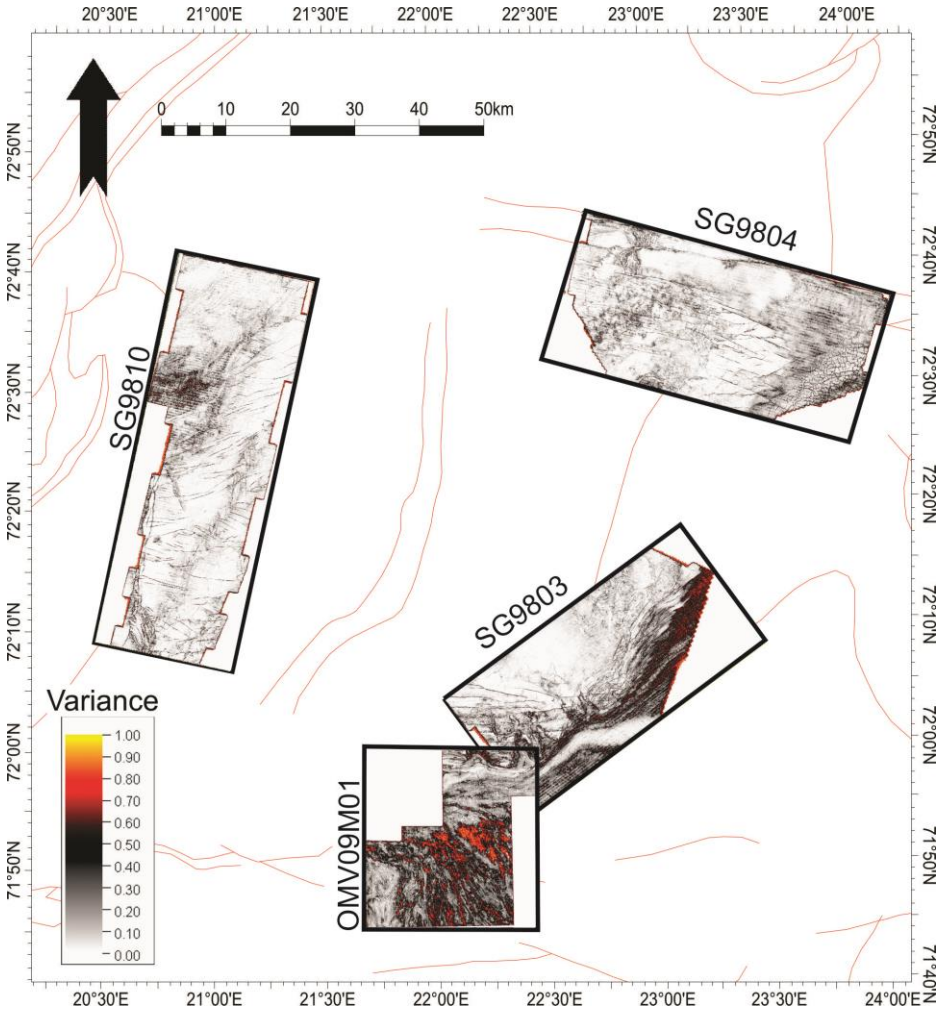

Figure 4.11: Overview picture of the shallow faults in the study area. Variance time slices are used to map and identify faults. Depth (TWT) of time slices indicated in Table 4.2.

Survey name	Time slice depth in TWT (ms)
SG9810	664
SG9804	696
SG9803	748
OMV09M01	688

Table 4.2. Depth (TWT) used for the variance time slices in Figure 4.11.

The shallow faults in survey SG9810 extend and terminate right below the URU. They have an E-W and NE-SW strike orientation (Figure 4.12). The faults have slight dip directions towards the northweet and southeast. These faults occur between 1500-500 ms (TWT) (Figure 4.12), a vertical extent of approx. 1000ms (TWT) and have a linear to curved shape. They have a length of 4-11km and are closely spaced together with 1-5km between each segment. The fault throws varies between 5-15 ms (TWT), corresponding to 5-15m (TVD) (V_p = 2000 m/s, Table 3.3).

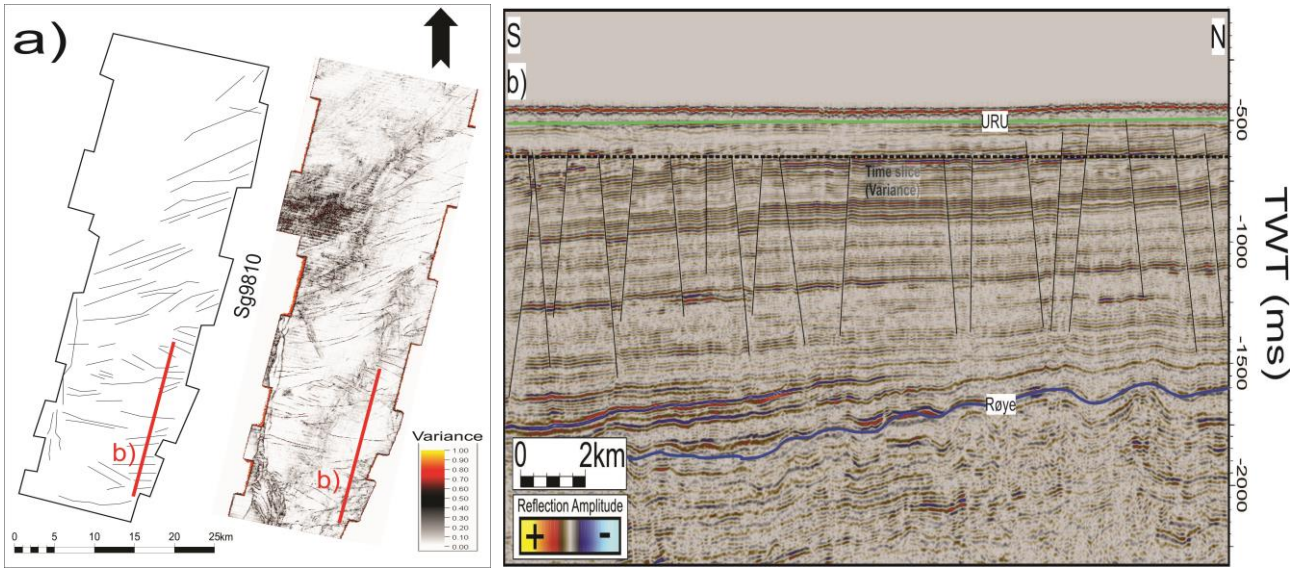

Figure 4.12: ***a)*** *Overview of shallow faults in survey SG9810. Variance time slice is indicated in* ***b*** *(664 ms TWT).* ***b)*** *Seismic section showing shallow faults. Position indicated in* ***a****.*

The shallow faults in survey SG9804 extend and terminate right below the URU. They have an SE-NW strike orientation (Figure 4.13). The faults have dip directions towards the northeast and southwest and occur between 1100-600 ms (TWT), a vertical extent of approx. 500ms (TWT). They have in general a length of 3-10km and are closely spaced together with 1-3km between each segment. The fault throws varies between 10-20 ms (TWT), corresponding to 10-20m (TVD) (V_p = 2000 m/s, Table 3.3). The time slice from the variance attribute reveal a polygonal pattern southeast in the survey which is interpreted to be a tier of polygonal faults due to their seismic character and closely spacing.

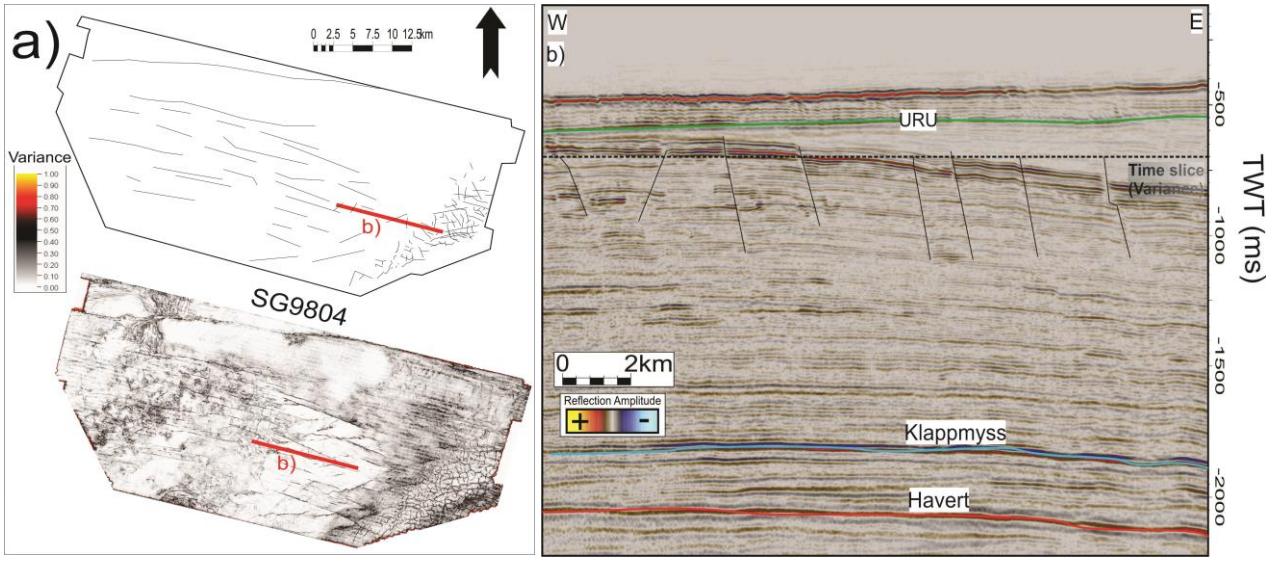

Figure 4.13: ***a)*** *Overview of shallow faults in survey SG9804. Variance time slice is indicated in* ***b*** *(696 ms TWT).* ***b)*** *Seismic section showing shallow faults. Position indicated in* ***a****.*

To the northeast, the shallow faults in survey SG9803 terminate right below the seafloor/URU. They have an E-W and a NE-SW strike orientation (Figure 4.14). The faults have dip directions towards the south/southeast. These faults occur between 1600-500 ms (TWT), a vertical extent of 1100ms (TWT). They will in general have a length of 5-10km, but occur longer at the fault boundaries. They are closely spaced together with 1-5km between each segment. The fault throws varies between 10-30 ms (TWT), corresponding to 10-30m (TVD) (V_p = 2000 m/s, Table 3.3).

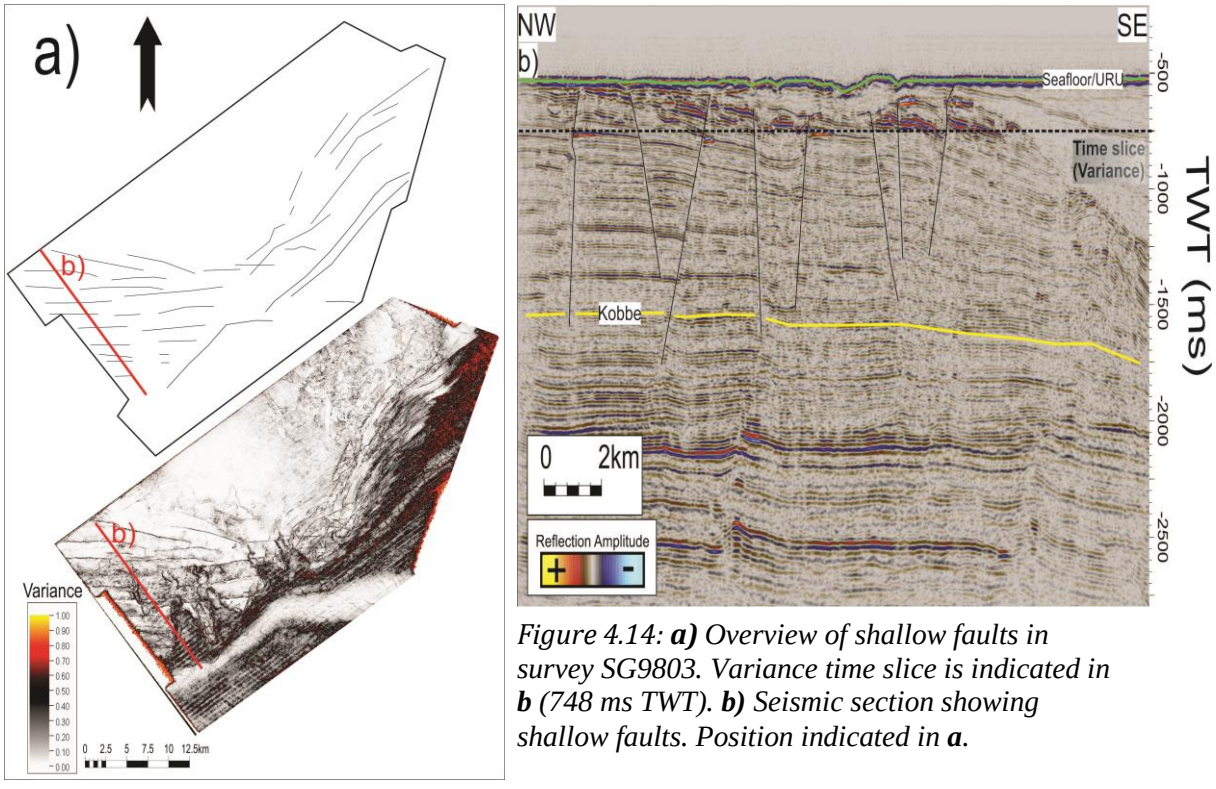

Figure 4.14: ***a)*** *Overview of shallow faults in survey SG9803. Variance time slice is indicated in* ***b*** *(748 ms TWT).* ***b)*** *Seismic section showing shallow faults. Position indicated in* ***a****.*

The shallow faults in survey OMV09M01 extend and terminate at or below the URU (the URU reflection coincices with the seabed reflection). They have an E-W strike orientation and only occur in the northern areas (Figure 4.15). The E-W faults have dip directions towards the south. They occur between 2300-500 ms (TWT) and the vertical extent is varying from 500-1500 ms (TWT). They have a length of 2-4km and are closely spaced together with 1-2km between each segment. The fault throws varies between 10-80 ms (TWT), corresponding to 10-80m (TVD) (V_p = 2000 m/s, Table 3.3).

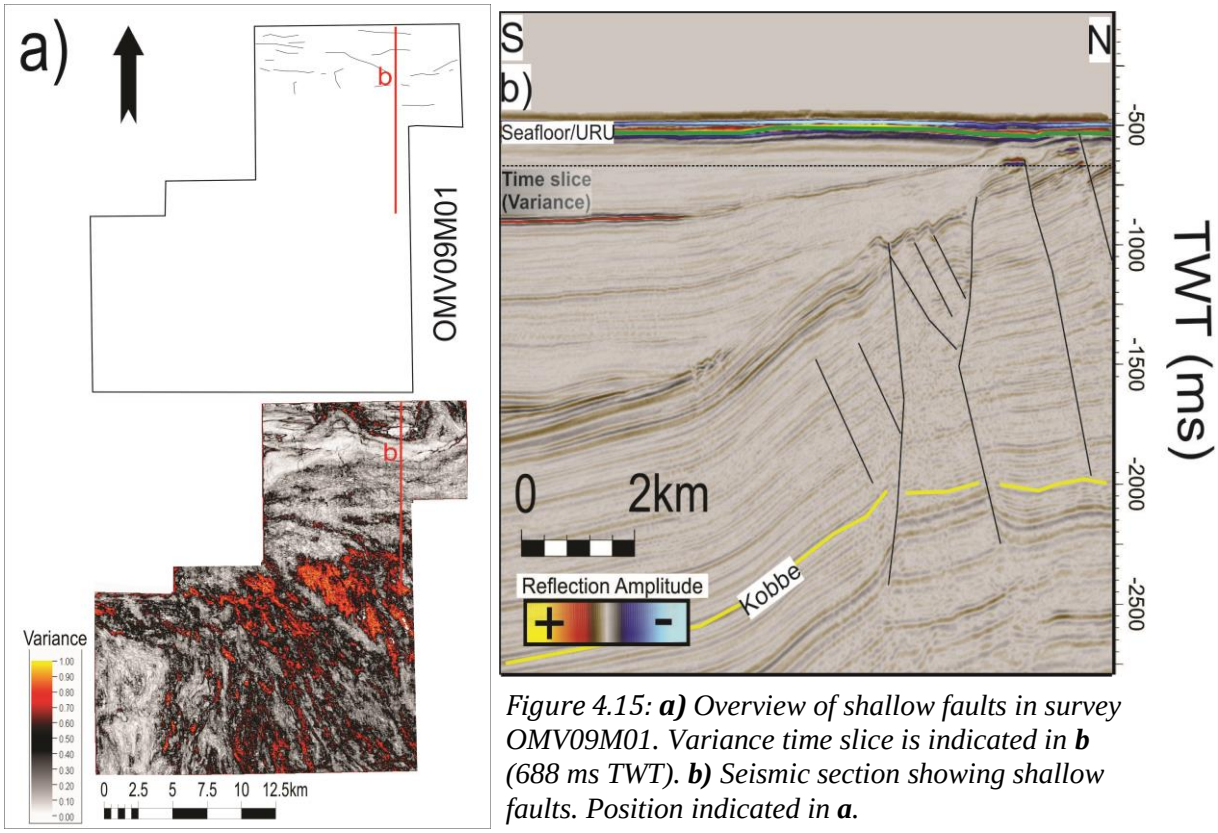

*Figure 4.15: **a)** Overview of shallow faults in survey OMV09M01. Variance time slice is indicated in **b** (688 ms TWT). **b)** Seismic section showing shallow faults. Position indicated in **a**.*

4.3 Seismic evidence for fluid migration

In the subsurface where fluids are present, sub-vertical faults and zones of highly fractured sediments act as conduits for the migration of gas-bearing fluids. This allows fluids to travel to the shallower strata, where it may accumulate or continue towards the surface. Tectonic faulting and fracturing are often regarded as the main controlling mechanisms for the location and distribution of fluid flow features. Potential leakage along faults are often connected to shallow amplitude anomalies, push-downs and pockmarks. The presence of these features together increases the possibility of a fluid flow system.

Areas with acoustic masking and high amplitudes are common in the study area which are typical for fluid migration. Acoustic masking can indicate the presence of gas while high amplitudes may indicate trapped fluids. These features vary in shape, both in horizontal and vertical extent. In this study are they identified as vertical zones of distorted seismic reflections, interpreted as focused fluid flow features (Løseth et al., 2009). In the Loppa High region is the source of the fluids most likely from deeper-seated reservoirs that has been expelling hydrocarbons along permeable faults. Different features related to fluid migration are observed in the seismic data which will be described in this chapter.

4.3.1 Potential leakage zones along faults (PLZ)

Faults related to potential leakage are observed all over the study area, concentrated along the flanks of the Loppa High (Figure 4.16). This is related to the flanks representing big fault boundaries. The potential leakage in the northeastern part is mainly related to the Swaen Graben. The seismic data show that these faults are often associated with chaotic reflections and high amplitude anomalies. In other words, fault systems may feed fluids to overlying sediments. It is important to add that the interpretations of potential leakage zones along faults are strongly affected by the quality of the seismic data. Poor seismic quality limits the observations and interpretations and has probably influenced the number and distribution of features identified and mapped. Fluids are hard to detect within fault zones due to horizontal resolution. Due to limitation of deeper seismic and well data is the possible origin of hydrocarbons hard to detect in certain areas. Potential leakage zones are separated from gas chimneys by their more narrow and vertical continuity of the acoustic anomaly. It is not considered as an object, but rather as an array of bright and dim spots.

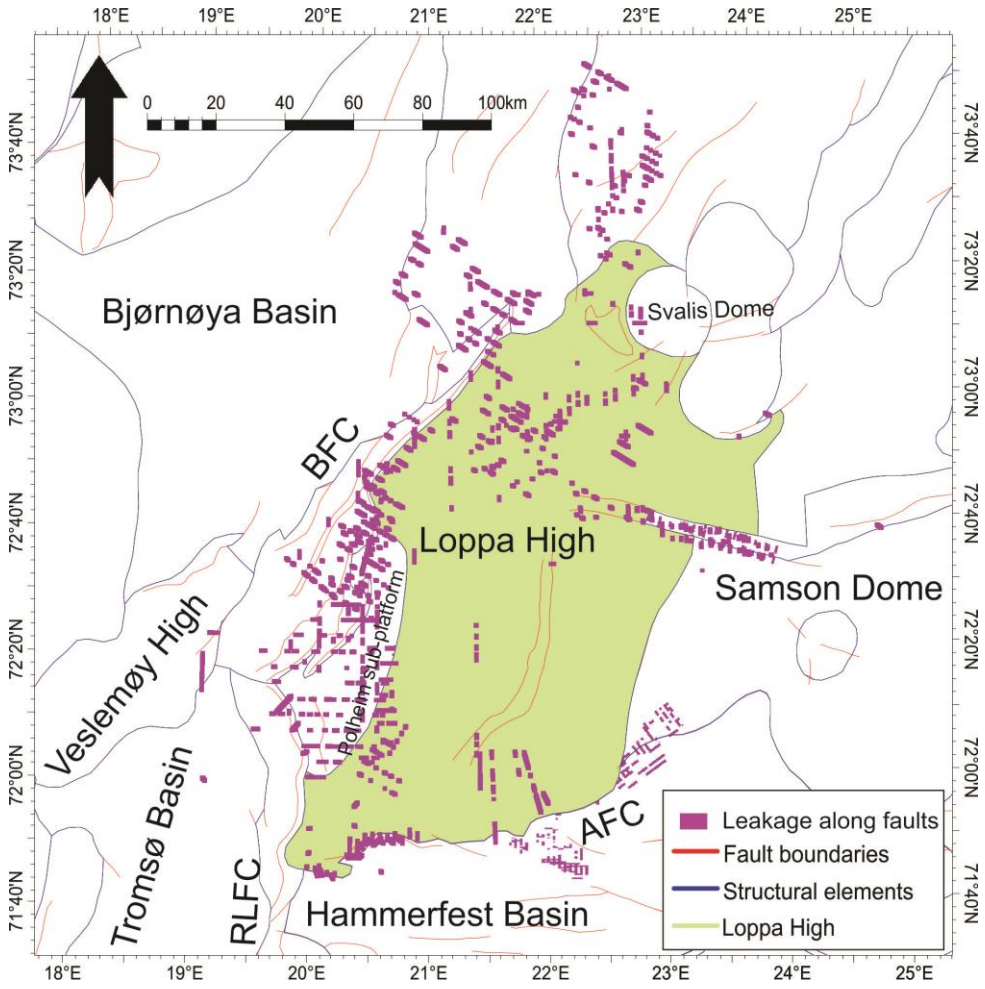

Figure 4.16: Overview picture of potential leakage zones along faults within the study area. Size of the leakage zones has been increased to some degree in order to be processed in Corel Draw.

4.3.1.1 PLZ 1

Figure 4.17 is a seismic profile from the eastern part of the study area. It is related to the Swaen Graben where faults have been described earlier. The two major deep-seated faults penetrate the Snadd- and Havert-formations. The Havert formation (Triassic) may represents the source of the fluids. However, there is a great possibility that the origin of the fluids are from formations at an even greater depth, from a more prolific source rock. The faults have an SE-NW strike orientation, sharing the same characteristics as the mentioned deep-seated faults in Survey SG9804 in chapter 4.2.1. This also includes the size of fault throws. The shallow faults are traceable for about 500 ms (TWT) while the deeper faults are traceable for about 1500 ms (TWT), from base to top termination. The transparency of the seismic makes it difficult to determine it precisely. High amplitude reflections (some with reverse polarity) are present along the faults indicating trapped fluids. Shallow gas accumulations are visible above some of the high amplitude reflections, indicating further leakage. Chaotic reflections indicate fluid migration while push-downs indicate a low velocity material, most likely gas.

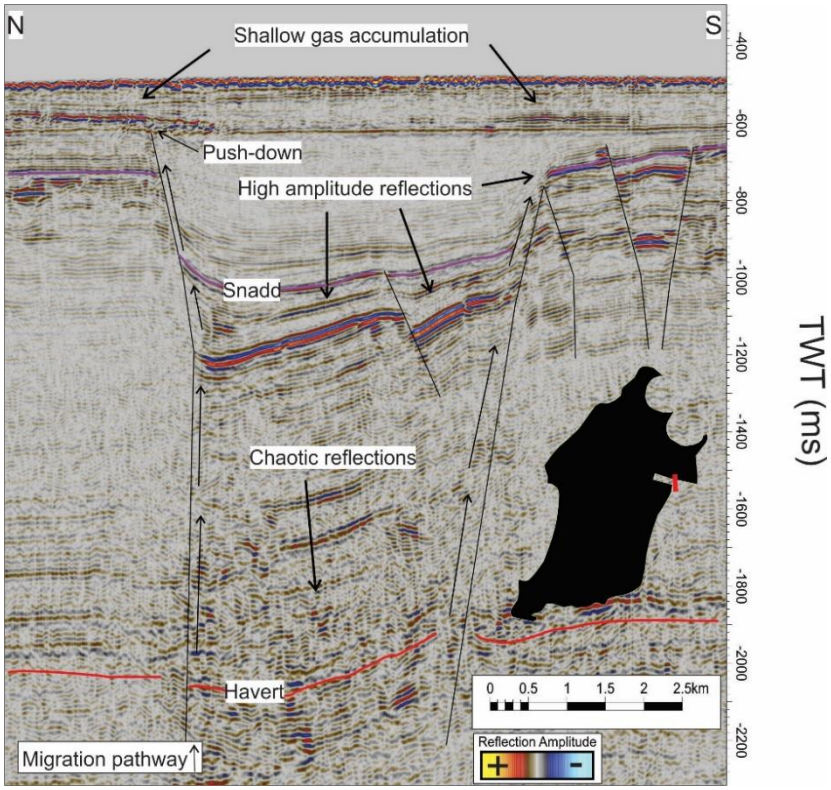

Figure 4.17: Potential leakage along faults bisecting the Havert and Snadd reflectors showing the fluid migration pathway. Push-down, chaotic reflections and shallow gas accumulation indicate leakage to shallower stratigraphy. The red line in the polygon indicates the seismic profile.

4.3.1.2 PLZ 2

The southern part of the Loppa High is a heavily faulted region (Figure 4.18). Chaotic reflections are observed along the faults with high amplitude reflections on top where the faults terminate. This may indicate the presence of gas. Vertical columnar structures are visible in the shallow strata which coincide with push-downs. These structures might be the result of vertical

pipes working as pathways for fluid flow. Small depressions are observed on the seafloor above the terminated faults. This could indicate gas seepage, a pockmark, but without 3D seismic data this task is difficult to resolve. The three major faults are traceable for about 1700 ms (TWT) while the smaller shallower faults extends for about 800-1100 ms (TWT). The fault throws are up to 50 ms (TWT), corresponding to 75m (V_p = 3000 m/s, Table 3.3). It seems the origin of most of the high amplitude reflections are from the three major deeper faults, which look to be connected to the shallower smaller faults. The source of the leakage could be the Kobbe Formation (Triassic) or the underlying Paleozoic strata.

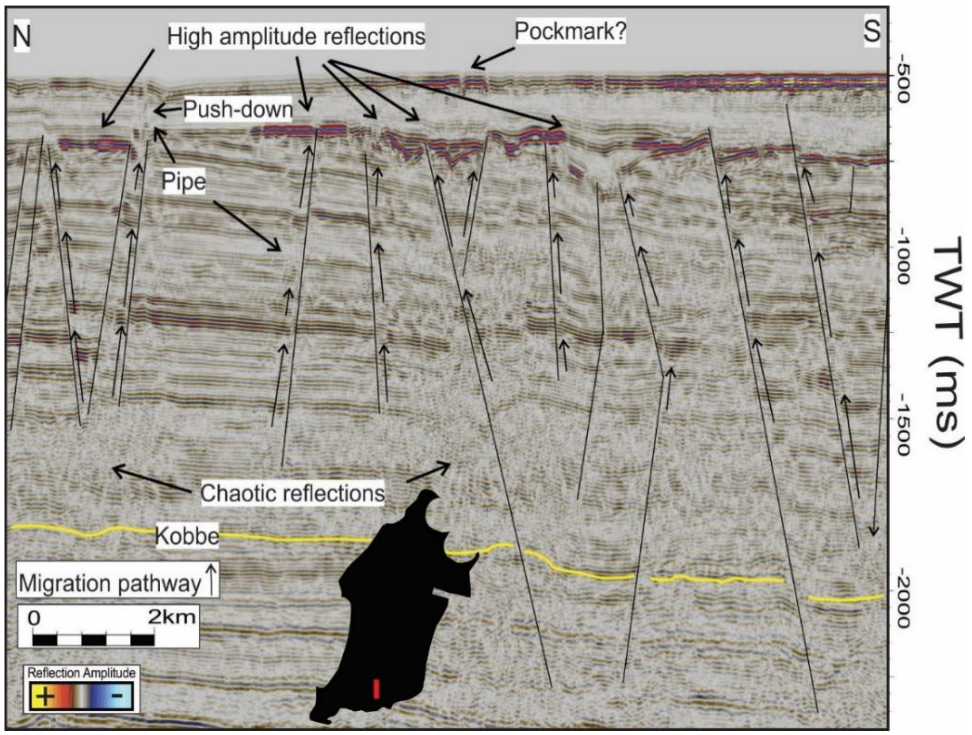

Figure 4.18: Potential leakage along faults showing the fluid migration pathway. Push-down and pipe-structures indicate fluid flow. A pockmark on the seafloor increases the chance of a fluid flow system. The red line in the polygon indicates the seismic profile.

4.3.1.3 PLZ 3

To the west of the Loppa High is another faulted area with potential leakage. The faults have a N-S strike orientation and extends up to 1200 ms (TWT) vertically. Fault throws are up to 150 ms (TWT). The strata shows a dip towards the west. A pipe structure is potentially present in the seismic profile (Figure 4.19). The pipe is approximately 200 ms in vertical length (TWT) and terminates 400 ms (TWT) below the URU. It has higher amplitudes than the surrounding reflectors. Close to the pipe is a high amplitude anomaly observed which is interpreted to be a bright spot. Strong chaotic reflections underneath the feature suggest fluid migration and presence of gas. The Tertiray reflection is retrieved from Chand et al. (2012).

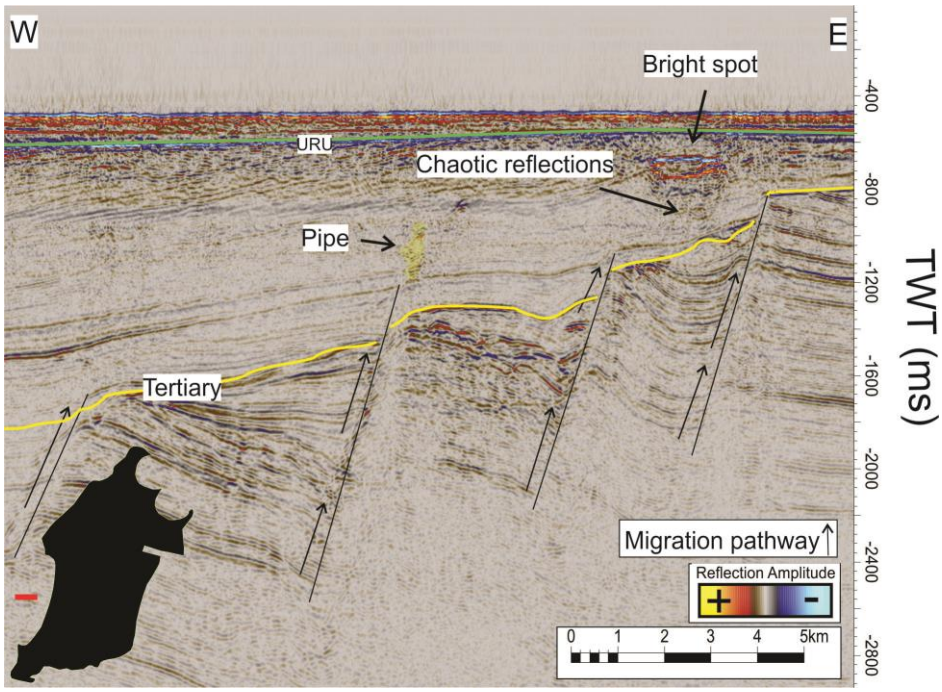

Figure 4.19: Potential leakage along faults showing the fluid migration pathway. A pipe-structure marked in yellow and a bright spot with chaotic reflections underneath indicate fluid flow. The red line outside the polygon indicates the seismic profile.

4.3.1.4 PLZ 4

A seismic profile from the northern part of the study area (Figure 4.20) shows two major deep-seated faults penetrating the Havert-formation (Triassic) which may represents the source of the fluids. Although, deeper formations could also contribute to the the origin of the fluids. The area has large throws in the shallow parts, varying from 50 to ~200 ms (TWT) which is 50-200m (TVD) (V_p = 2000 m/s, Table 3.3) while the deep parts have smaller throws, varying from 30-80 ms (TWT)m, corresponding to 57-152m (V_p = 3800 m/s, Table 3.3). The shallow faults are traceable for about 400 ms (TWT) while the deeper faults are traceable for about 1600 ms (TWT), from base to top termination. High amplitude reflections are present at the top termination points of the faults indicating trapped fluids. Masking and push-downs indicate the presence of gas.

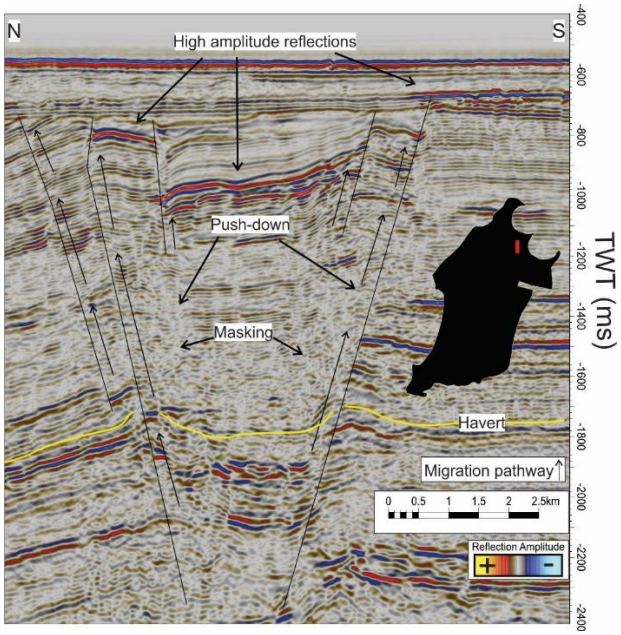

Figure 4.20: Potential leakage along faults showing the fluid migration pathway. Push-downs and masking may indicate fluids present in the stratigraphy. The red line in the polygon indicates the seismic profile.

4.3.1.5 PLZ 5

To the north of the Loppa High is a horst-graben fault system (Figure 4.21). These faults extend 500 ms (TWT) and terminate up to the URU. The fault throws vary from 10-40 ms (TWT), corresponding to 10-40m (V_p = 2000 m/s, Table 3.3). Chaotic reflections are present under high amplitude reflections indicating an upward migration of fluids. Small depressions on the seabed are found coincidence with many of these faults which suggest fluid flow along the fault planes.

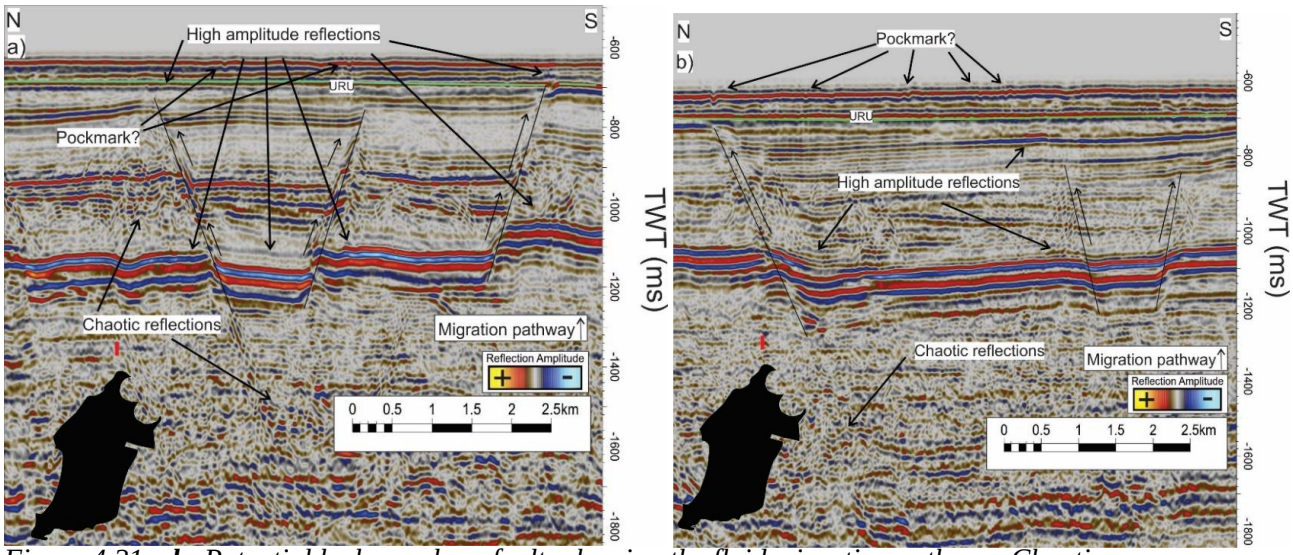

*Figure 4.21**a, b**: Potential leakage along faults showing the fluid migration pathway. Chaotic reflections underneath high amplitudes indicate fluids present in the stratigraphy. Pockmarks are oberserved on the seafloor increasing the possibility of fluid flow. **a** is a continuation of the same seismic profile further north shown in figure **b**. The red line outside the polygon indicates the seismic profile.*

4.3.1.6 PLZ 6

Figure 4.22 shows faulting in the southwestern part of the Loppa High. The faults are traceable for approximately 900 ms (TWT). The transparency of the seismic makes it difficult to determine how far the western-most fault extends. The fault throws vary mostly from 15-30 ms (TWT), corresponding to 15-30m (V_p = 2000 m/s, Table 3.3). The area represent a big fault zone separating the Loppa High and the Polheim Subplatform. This results in much older formations situated on shallower levels to the east compared to the west. The high amplitude reflections look to be connected to deeper-seated faults. Masking and push-downs indicate low-velocity material, probably gas. The source of the fluids is possibly from the Isbjørn Formation in the east. In the west is it harder to evaluate the origin of the fluids due to their deep origin and the limitation of seismic data.

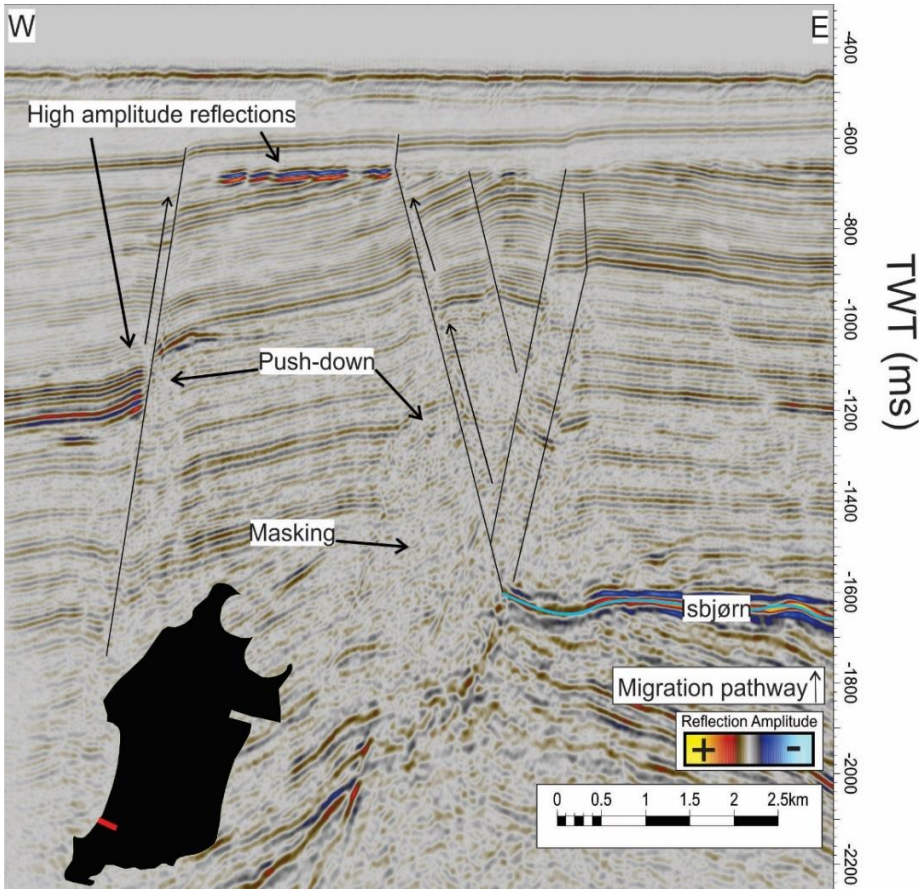

Figure 4.22: Potential leakage along faults showing the fluid migration pathway. Push-downs and masking may indicate fluids present in the stratigraphy. The red line in the polygon indicates the seismic profile.

4.3.1.7 Seepage pipe

In the northern part of the Loppa High is a vertical, narrow columnar zone of disrupted reflection with localized amplitudes anomalies (Figure 4.23). Enhanced reflections are visible along the feature which can indicate that the feature is in fact working as a zone of fluid leakage. It is approximately 900m wide at its greatest width and 1600 ms (TWT) in vertical length. The feature is interpreted as a seepeage pipe. The source of the fluid leakage is probably of Triassic or older age since the leakage extends far deeper than the Havert Formation.

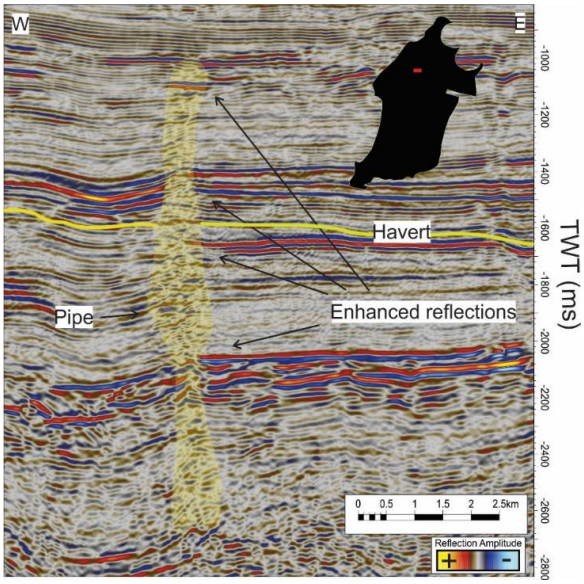

Figure 4.23: Pipe-structure marked in yellow. The red line in the polygon indicates the seismic profile.

4.3.2 Gas Chimneys

Large zones of low, dim and chaotic reflectors are observed in the study area (Figure 4.24). The size and shape of these zones varies widely. These will often terminate at a shallow stratigraphic level (Torsk FM) with high amplitude anomalies on top while push-down features are observed beneath the feature. They are typical in sedimentary basins and are often correlated to major faults, distributed mostly west of Loppa High. Features like these are interpreted as gas chimneys based on the published article from Løseth et al. (2009) and Karin Andreassen et al. (2007). Gas chimneys are defined as a region of distorted seismic signals as a result of low-velocity gas-charged zones, formed due to an upward migration of fluids/gas (Vadakkepuliyambatta et al., 2013). The Loppa High and adjacent faulted areas show a high concentration of gas chimneys. Due to the size of the study area will only some of the largest and most prominent gas chimneys be described. A summary (Table 4.3) of the interpreted gas chimneys will be given at the end of the chapter.

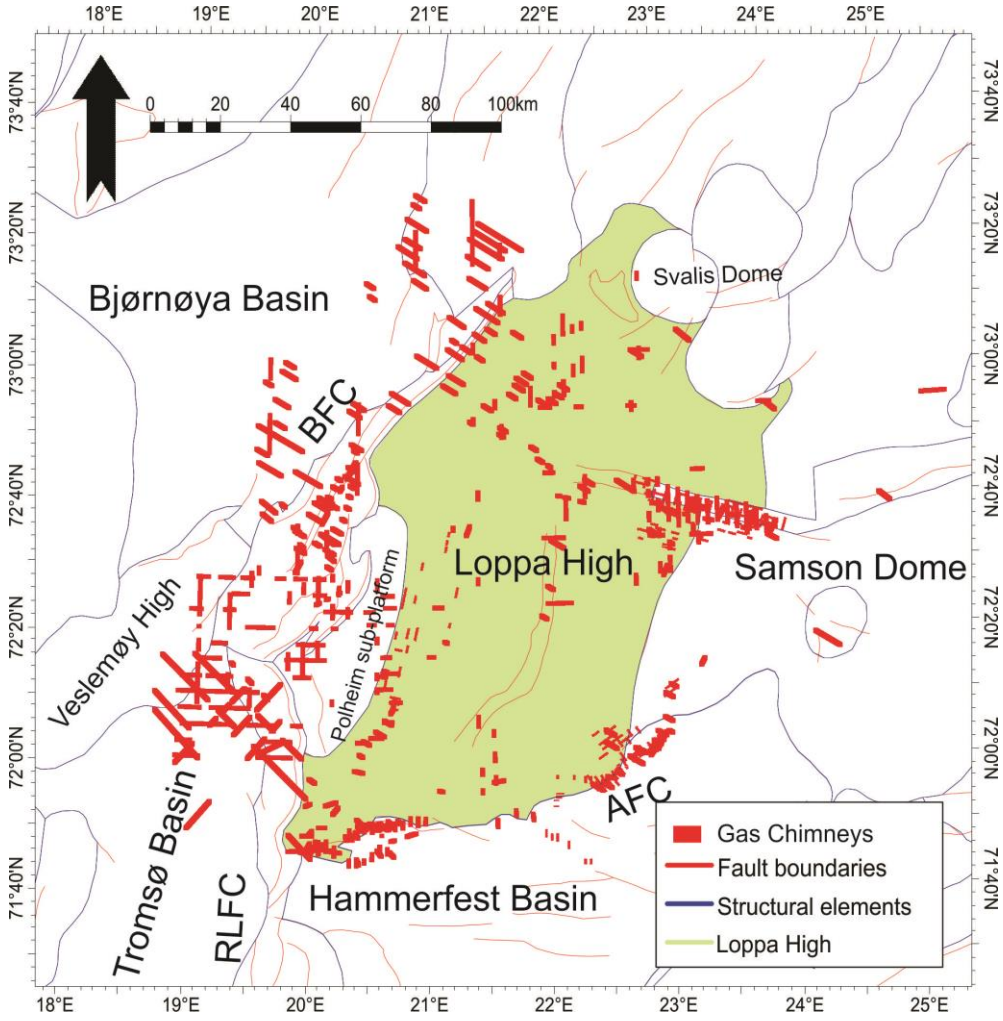

Figure 4.24: Overview picture of gas chimneys within the study area. Size of the gas chimneys has been increased to some degree in order to be processed in Corel Draw.

4.3.2.1 Gas Chimney 1 and 2

Elongated gas chimneys are located in the Bjørnøya Basin, to the northwest of Loppa High (Figure 4.25). The largest gas chimney (GC1) has a long axis of 8km striking N-S and a short axis of 5km, respectively. It covers an area of 40 km^2. These features show zones of distorted dimmed seismic signals and terminate 400 ms (TWT) below Top Cretaceous (1000 ms TWT). The transition between the dimmed reflection zones inside the chimneys looks to be more prominent at greater depths. GC1 looks to extend down to ~4000 ms (TWT). High amplitude reflections are observed above both chimneys. Both features are located in the Bjørnøyrenna Fault Complex (BFC) area. The small gas chimney (GC2) seems to be connected to a deeper-seated fault where gas has probably migrated upward. It has a long axis of of 2km and a short axis of 1.5km, covering an area of 3km^2. The upper termination is at Top Cretaceous at ~1000ms (TWT). The acoustic masking extends down to ~2000ms (TWT).

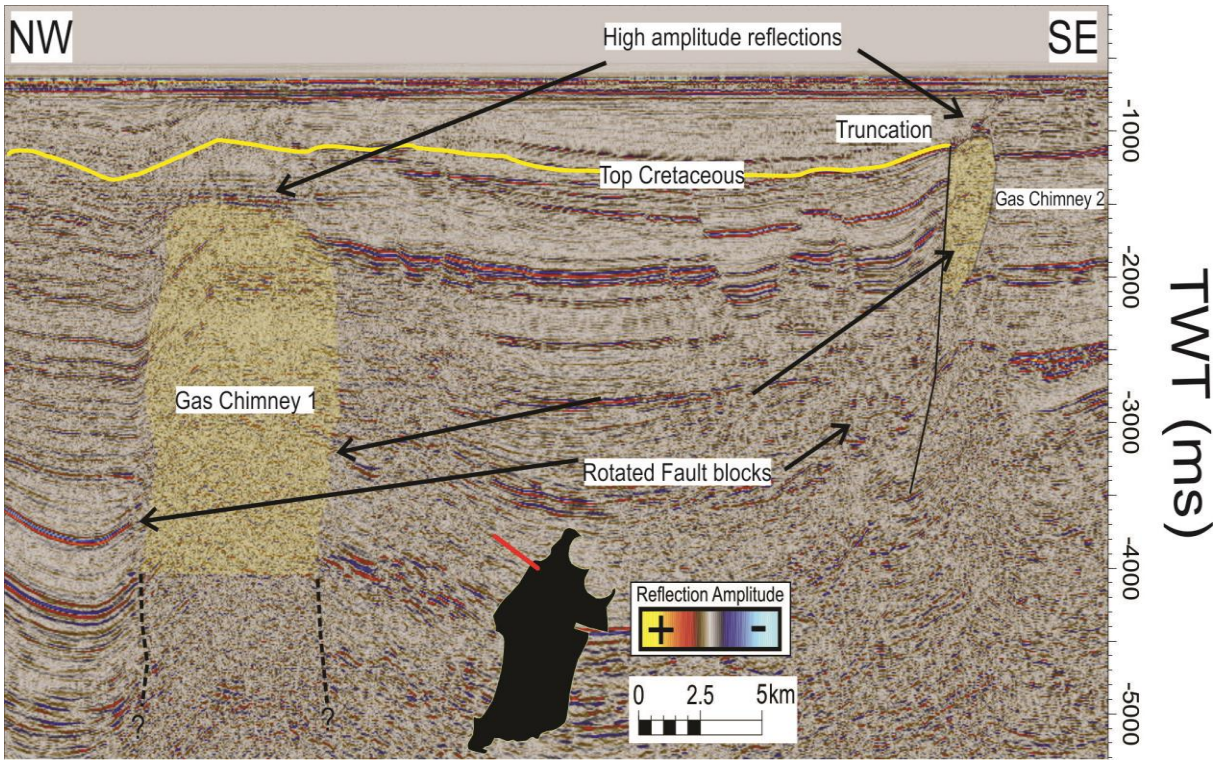

Figure 4.25: Fluid flow in the northwestern part of Loppa High. The large fluid flow feature (GC1) has a leakage zone of approximately 8 km in the widest areas. The small fluid flow feature (GC2) has a leakage zone of approximately 2km. Both features have high amplitude anomalies present on top of the leakage zone. Gas chimneys marked in yellow. The red line in the polygon indicates the seismic profile.

4.3.2.2 Gas Chimney 3

A gas chimney (GC3) is located west of Loppa High, close to the Polheim Subplatform within the BFC (Figure 4.26). It has a cicular shape surrounded by cross-cutting high amplitude anomalies in the shallow strata, located mostly between the intervals 700-800 ms (TWT),

corresponding to depths of 700-800m (TVD) (V_p = 2000 m/s, Table 3.3). This is also where the chimney terminates (Torsk Formation). It is hard to tell exactly how deep the chimney extends, but a vertical extent of at least 3000 ms (TWT) looks to be the case. The long/short-axis is 5km which gives an area of 19.6km^2 using the formula for a circular body ($\pi*r^2$). The high amplitude anomalies show reverse polarity with respect to the seafloor indicating presence of gas. Highly chaotic reflections define the zone of fluid flow which show downward bending reflectors indicating push-downs due to low-velocity material (gas). Acoustic masking is also present beneath the shallow high amplitude anomalies which is most likely caused by gas migrating upwards. The seismic signal is very chaotic inside the chimney, making it difficult to identify the source of gas leakage, but is most likely from a formation older than Fuglen. The source might be from faults since the gas chimney is located in a high-faulted area with rotated fault blocks.

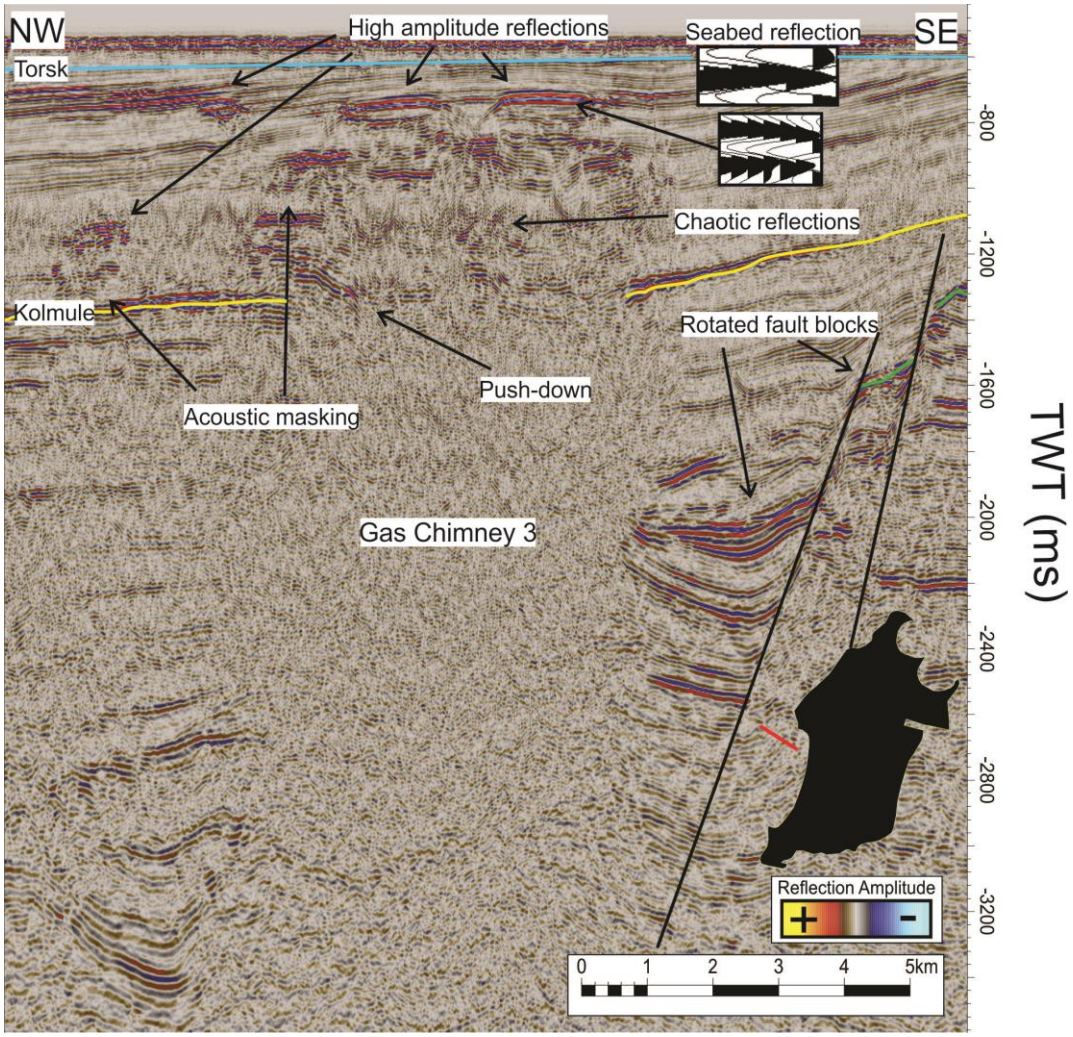

Figure 4.26: Fluid flow west of Loppa High. The large fluid flow feature (GC3) has a leakage zone of approximately 5 km in the widest areas. High amplitude anomalies are present on top of the leakage zone. The shallow high amplitude reflections show reverse polarity with respect to the seafloor. Chaotic reflections indicate fluid flow. The red line in the polygon indicates the seismic profile.

4.3.2.3 Gas Chimney 4 and 5

Two big gas chimneys are located southwest of Loppa High in the Tromsø Basin (Figure 4.27). These gas chimneys are located on the Ringvassøy-Loppa Fault Complex (RLFC) and covers a huge area. They are characterized by acoustic masking and the northwestern gas chimney (GC4) has a long/short-axis of 12km in the widest areas, giving an area of 113km^2. GC5 has a long/short axis of 11km^2, covering an area of 95km^2. They have a circular shape with high amplitude anomalies located at their upper termination. These high amplitude anomalies are also present on other stratigraphic boundaries adjacent to the gas chimneys, suggesting lateral migration. The source of leakage is hard to identify due to chaotic reflections inside the chimneys, but it might be the RLFC feeding gas to the overlying sediments. The shallow high amplitude anomalies have a reverse polarity compared to the seafloor, which may indicate gas/fluids. The gas chimneys terminate at shallow depths (Top Kolmule) close to the URU. The vertical extent of the chimneys is hard to say due to weak reflections deep in the seismic, but it looks to be very deep (~4000 ms TWT). It is important to mention that these gas chimneys might be big salt structures. GC5 has reflections tilting upwards, which might indicate intrusion.

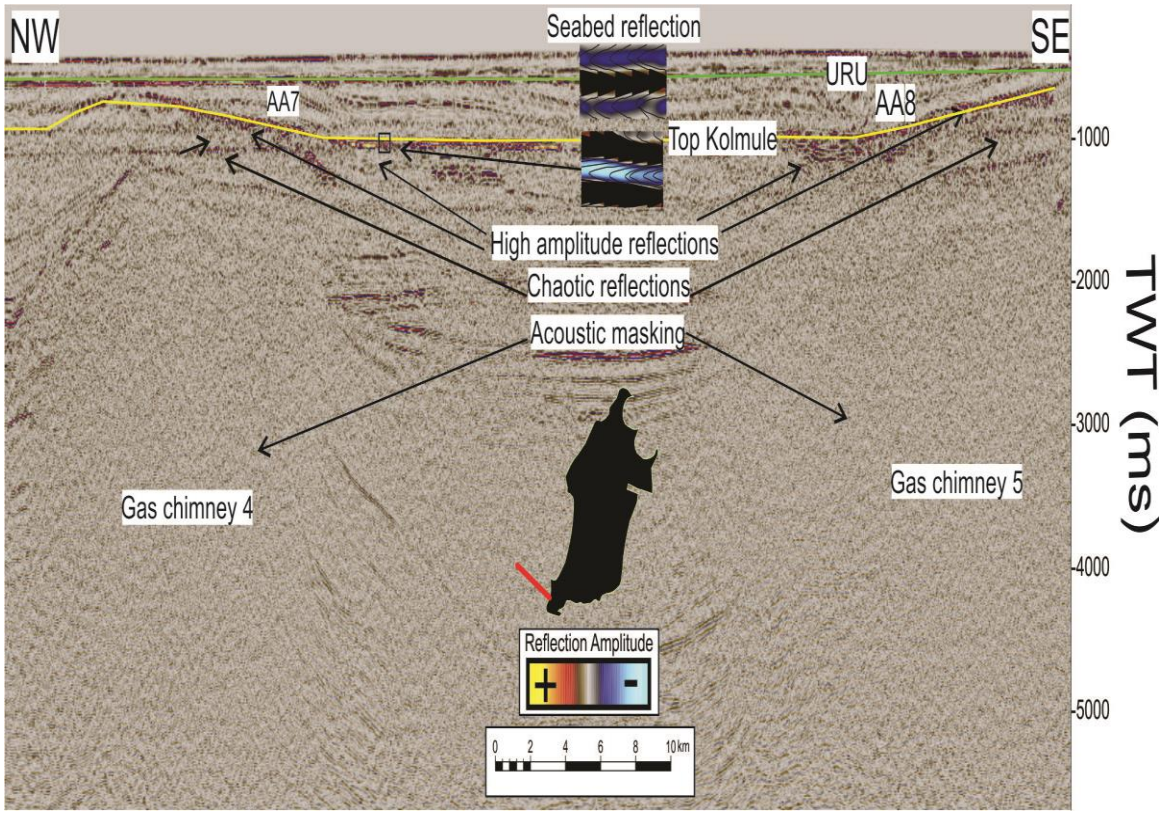

Figure 4.27: Fluid flow southwest of Loppa High. The largest fluid flow feature (GC4) has a leakage zone of approximately 12 km in the widest areas. GC5 has a leakage zone of 11 km. The high amplitude anomalies are present on top of the leakage zone. The shallow high amplitude reflections show reverse polarity with respect to the seafloor. Chaotic reflections indicate fluid flow. The red line in the polygon indicates the seismic profile.

Figure 4.28 shows the northwestern and southeastern gas chimneys in Figure 4.27 in different orientations. The high amplitude reflections in the northwestern gas chimney are located shallower (truncated at 800 ms TWT) and have distinct chaotic reflections and acoustic masking beneath it.

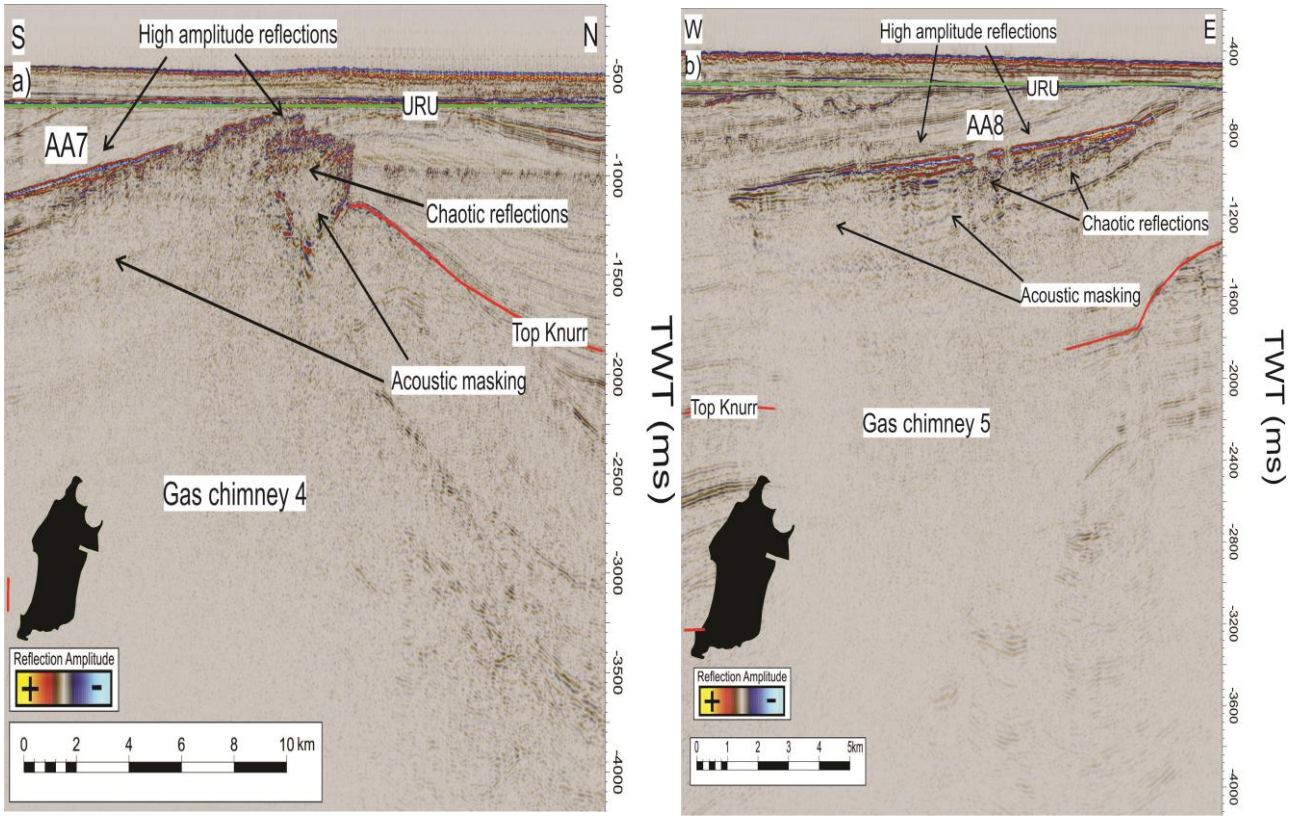

Figure 4.28: ***a)*** *The northwest gas chimney (GC4) in figure (Figure 4.27) in a N-S orientation.* ***b)*** *The southeast gas chimney (GC5) in figure (Figure 4.27) in an E-W orientation. The red line in the polygon indicates the seismic profile.*

4.3.2.4 Gas Chimney 6 and 7

Two gas chimneys are located at the southern flank of "Bjørnøya trough" west of Loppa High, in the western transition of the Polheim Subplatform (Figure 4.29). GC6 is circular while GC7 has an elongated shape. They represent large leakage zones of acoustic masking. The southernmost gas chimney (GC6) has a long/short-axis of 7km, covering an area of 38km^2. The northern gas chimney (GC7) is ~5km in the widest areas with a short axis of 3km. This gives an areal of 15km^2. These leakage zones terminate at approximately 600 ms (TWT) showing high amplitude reflections on top. These show a reverse polarity in respect to the seafloor indicating accumulations of gas which is supported by chaotic regions suggesting upward migration of fluids. The origin of the source is unknown, but fluids have probably migrated along faults (the chimneys are situated on major faults). The southern gas chimney has a top with an elongated shape with narrow depressions in between the high amplitudes cross-cutting parts of the lithology. This cross-cutting event could potentially indicate a gas-hydrate-related BSR where hydrocarbon-gases are migrating together with other fluids through the gas chimney and form gas hydrates (Chand et al., 2008). Both chimneys have relative flat tops according to the seabed and are located right below the URU. The extent of the gas chimneys are generally characterized by low amplitudes, but how far deep they extend is difficult to determine on the provided seismic. A lower termination of 3500 ms (TWT) is suggested.

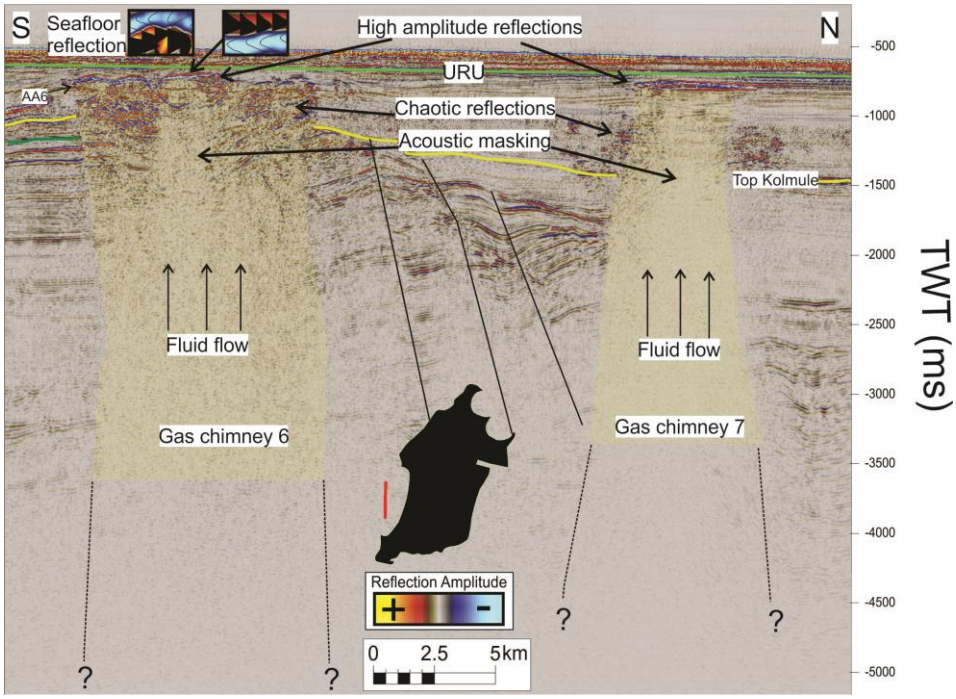

Figure 4.29: Fluid flow west of Loppa High. The southern gas chimney (GC6) has a leakage zone of approximately 7 km in the widest areas. The northern gas chimney (GC7) has a leakage zone of approximately 5km. Both features have high amplitude anomalies present on top of the leakage zone with a reverse polarity. Gas chimneys marked in yellow. The red line in the polygon indicates the seismic profile.

Figure 4.30 shows the southern and northern gas chimneys in Figure 4.29 in different orientations. The high amplitude reflections in the southern gas chimney (GC6) are clearly cross-cutting the lithology. An isolated bright spot is present west for GC6. The E-W orientation show major fault boundaries more clearly. Faults seem to be present inside the chimneys.

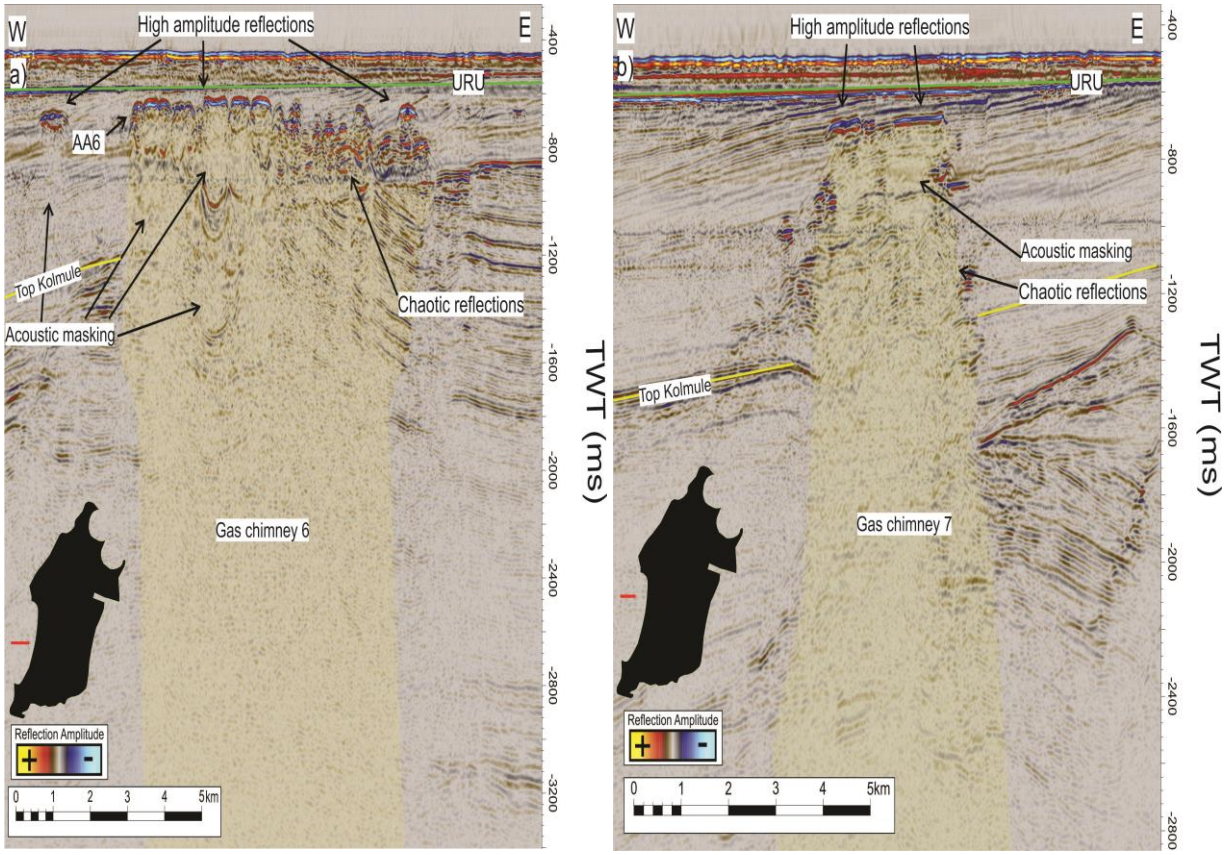

Figure 4.30: ***a)*** *The southern gas chimney (GC6) in figure (Figure 4.29) in an E-W orientation.* ***b)*** *The northern gas chimney (GC7) in figure (Figure 4.29) in an E-W orientation. The red line in the polygon indicates the seismic profile.*

4.3.2.5 Gas Chimney 8

A potential gas chimney (GC8) is located in the southeastern part of Loppa High (Figure 4.31**b**). The acoustic masking is not as prominent as the others and the gas chimney is therefore highly speculative. The chimney terminates at 900 ms (TWT). High amplitude reflections are located here and the URU (600 ms TWT). The chimney has a circular shape in plan view and represents zone of fluid leakage supported by acoustic masking. It has short/long-axis of 2.5km in the widest areas, covering an area of 4.9km^2. Chaotic reflections and push-downs indicate the presence of a low-velocity material (gas). It is hard to tell how deep it extends due to the limited seismic. The source could be coming from the interpreted Kobbe-Formation which is located at approximately 1600 ms (TWT). The gas chimney could be related to the oil/gas discovery Caurus. A time-slice is generated at 1052 ms (TWT) (Figure 4.31**a**).

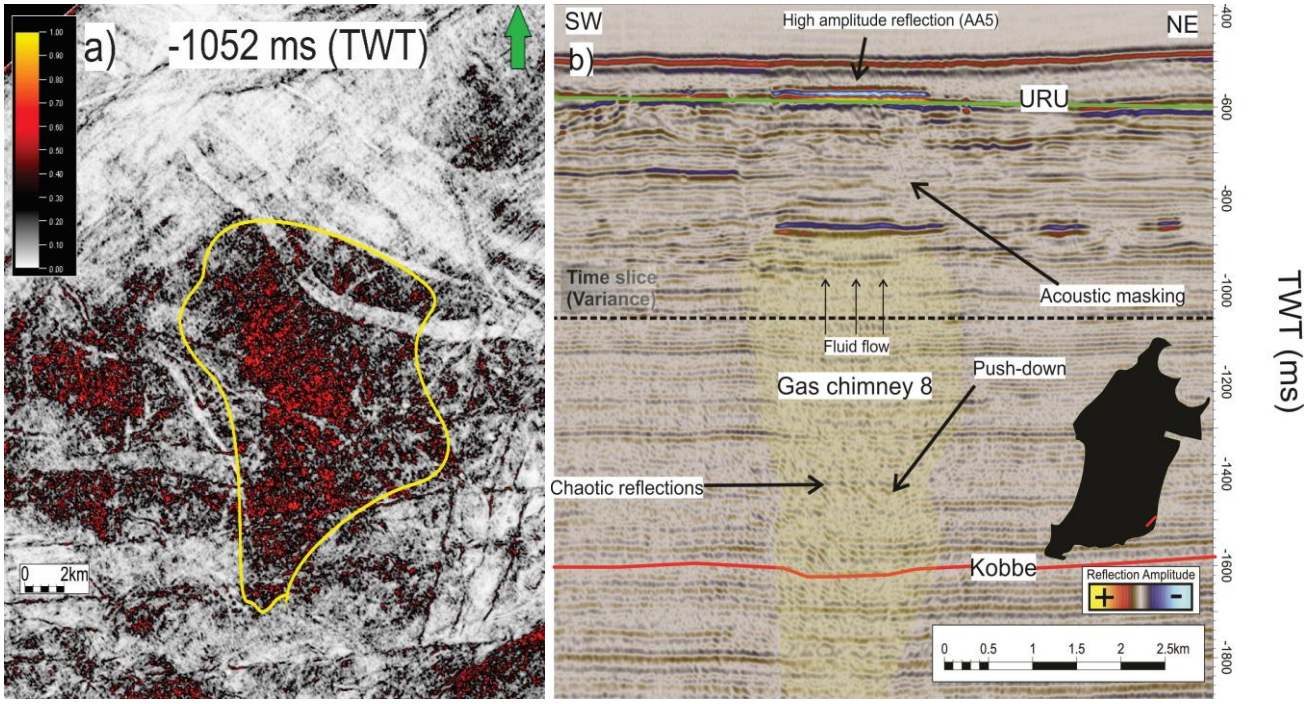

*Figure 4.31: **a)** Variance map of the gas chimney at 1052 ms (TWT). The chimney is outrimmed with a yellow line. **b)** Fluid flow in the southeastern part of Loppa High. The chimney has a leakage zone of approximately 2.5 km in the widest areas. A high amplitude anomaly is present on top of the leakage zone. Gas chimney marked in yellow. The red line in the polygon indicates the seismic profile.*

4.3.2.6 Gas Chimney 9

Southwest on Loppa High is a gas chimney (GC9) identified (Figure 4.32). It has an elongated shape with its longest axis striking in N-S direction. It covers an area of 12.5km^2 where the long axis measures 5km while the short axis measure 2.5km. The top of the chimney is characterized by high amplitude reflections, located at 700 ms (TWT), within the Torsk formation. The chimney looks to extend down to 1800 ms (TWT), and is most likely related to the oil/gas discovery Alta.

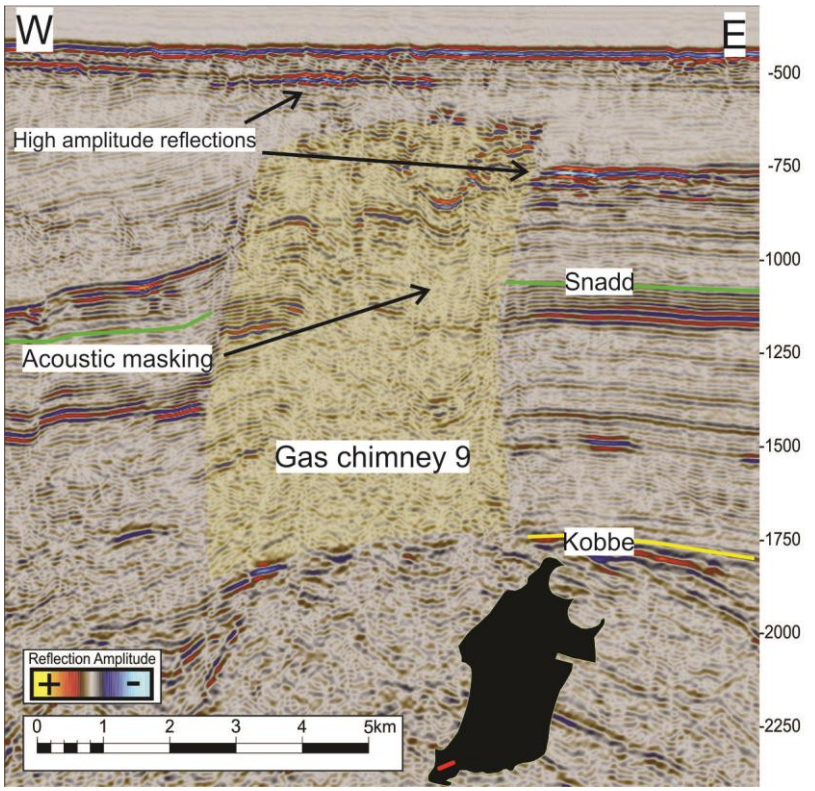

Figure 4.32: Fluid flow in the southwestern Loppa High. The chimney has a leakage zone of approximately 5km in the widest areas. High amplitude reflections are present on top of the leakage zone. Gas chimney marked in yellow. The red line in the polygon indicates the seismic profile.

Chimney	**Shape**	**Long axis (km)**	**Short axis (km)**	**Area (km^2)**	**Top TWT (ms)**	**Base TWT (ms)**
GC1	Elongated tube	8	5	40	1000	4000
GC2	Elongated tube	2	1.5	3	1000	2000
GC3	Circular	5	5	19.6	700-800	3000
GC4	Circular	12	12	113	800	4000
GC5	Circular	11	11	95	800	4000
GC6	Circular	7	7	38	600	3500
GC7	Elongated tube	5	3	15	600	3500
GC8	Circular	2.5	2.5	4.9	900	2000
GC9	Elongated tube	5	2.5	12.5	700	1800

Table 4.3: Summary of acoustic chimneys (GC1-GC9). The top is defined as the depth where acoustic masking terminates into an amplitude anomaly. The measurements of GC1-GC7 and GC9 are measured in 2D-data spaced 4-8km apart and should be viewed as approximate numbers.

4.4 Amplitude anomalies

High amplitude anomalies occur throughout the study area (Figure 4.33) and are observed at different stratigraphic levels. The amplitude anomalies in the survey area show the highest concentration along the flanks of the Loppa High and in adjacent basins. These features vary in size (horizontal distribution/vertical extent) and shape. The anomalies are in general characterized with anomalous high amplitudes where the reflections have a reverse polarity in respect to the seafloor reflection. The wave velocity decrease and give rise to reflections with high amplitude from the top of the gas. They are often associated with chaotic reflections and acoustic masking located beneath the features. Push-downs are also normal in areas with high amplitude anomalies and they often coincide with one or several faults. The interpreted gas chimneys are observed directly beneath some of the anomalies. These anomalies which are related to gas chimneys (west for Loppa High) tend to be the most prominent. High amplitude anomalies are interpreted as an indicator of focused fluid flow from deeper to shallower strata, but could also be due lithological boundaries. These seismic anomalies can be observed by using RMS amplitude mapping which enhances strong seismic. In this chapter will some of the most prominent mapped amplitude anomalies be described. Amplitude anomalies 6-10 are from 2D-profiles which makes it not possible to generate time slices. A short summary of all observations will be presented at the end of the chapter (Table 4.4).

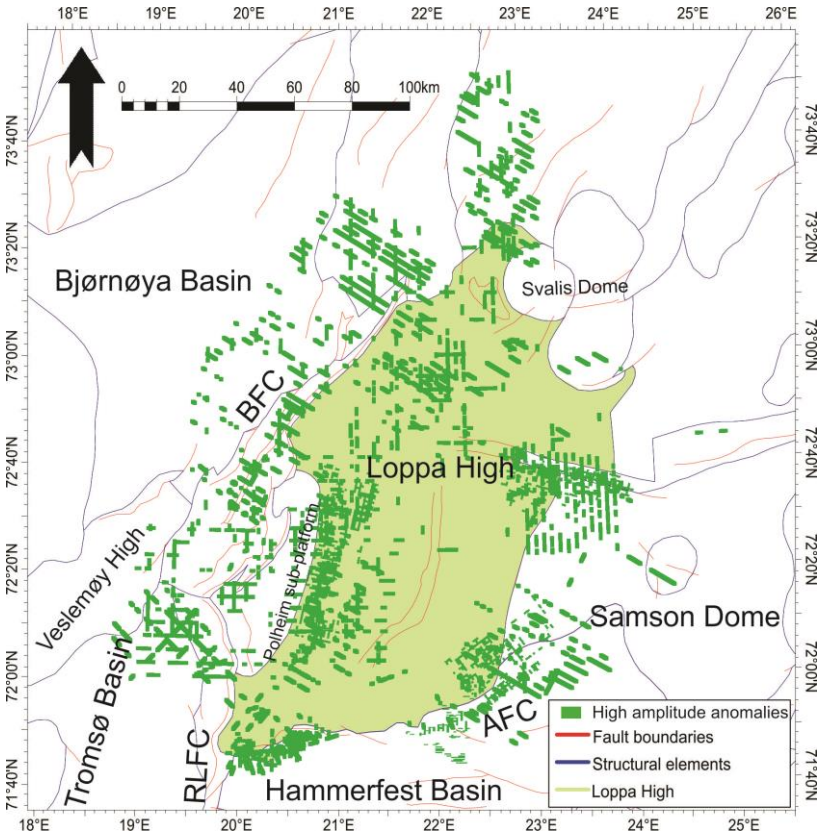

Figure 4.33: Overview picture of high amplitude anomalies within the study area. Size of the amplitude anomalies has been increased to some degree in order to be processed in Corel Draw.

4.4.1 Amplitude Anomaly 1

Amplitude anomaly 1 (AA1) occurs within the northern part of the dataset SG9810 (Figure 4.34). Two strong reflection amplitudes appear as laterally continuous reflections. They appear approximately at the same depth (at or right below the Snadd-Formation/URU), but are separated by 8.5km. It is possible they are part of the same shallow gas accumulation. Acoustic masking is observed underneath the anomalies. The Ørn-Formation is located quite shallow in the area (~ 1100 ms TWT) and could potentially be the source of the features. The top of the high amplitude reflections are located at ~625 ms (TWT) with a base at ~775 ms (TWT), giving a vertical extent of 150 ms (TWT). The western feature has an E-W orientation. It has a length of 4km and a width of 2km in the widest areas. It is hard tell the size and orientation of the eastern feature due to the limitation of data, but it looks to extend even further to the east. This feature has a length of 8km and a width of 5km in the widest areas. They cover an area of 48km^2. It is dipping toward the east. Both features have an oval shape.

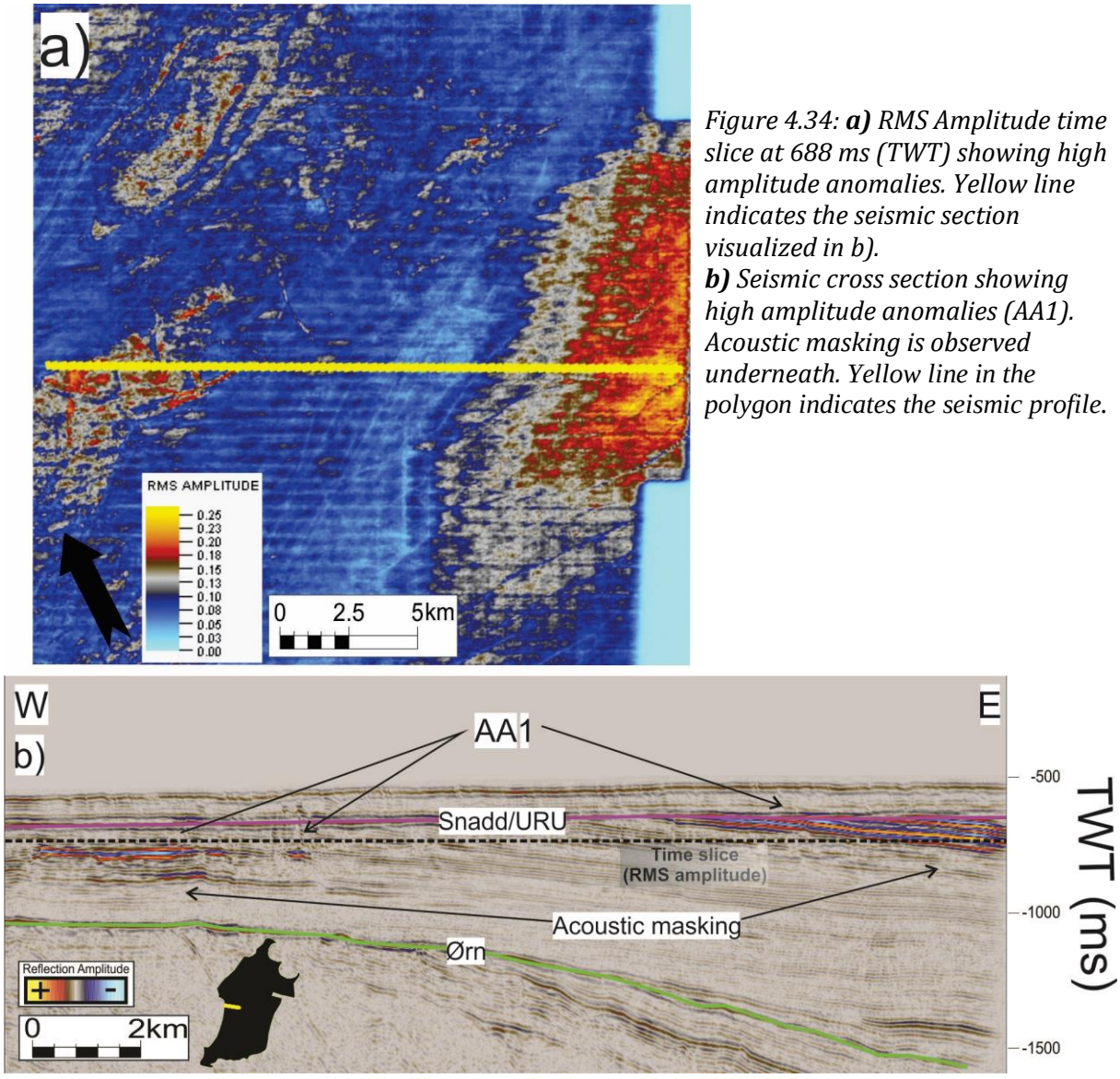

Figure 4.34: ***a)*** *RMS Amplitude time slice at 688 ms (TWT) showing high amplitude anomalies. Yellow line indicates the seismic section visualized in b).*
b) *Seismic cross section showing high amplitude anomalies (AA1). Acoustic masking is observed underneath. Yellow line in the polygon indicates the seismic profile.*

4.4.2 Amplitude Anomaly 2

Amplitude anomaly 2 (AA2) occurs in the southern part of survey SG9810 (Figure 4.35). It is situated in the PLZ 6 interpreted in chapter 4.3.1.6, located on top of the Ørn-Formation. In plan view the anomaly covers an area of roughly 8km^2. It has an elongated shape oriented in a NE-SW direction. The longest axis measures approximately 4km while the short axis measures 2km. It is located between 1600 and 1900 ms (TWT), giving a vertical extent of 300 ms (TWT). On seismic profiles, the anomaly is recognized as a laterally strong reflector with a weak reflectivity (acoustic masking) underneath. It is important to add that it may represent a lithological boundary and not gas. The anomaly has much weaker reflections in the western area, probably due to the transition from Loppa High to the Polheim Subplatform. The strata changes from dipping towards the east to dipping towards the west. The transition zone is a highly-faulted area and fluids have probably migrated upwards along these faults. High amplitude reflections observed on top of these faults support this theory.

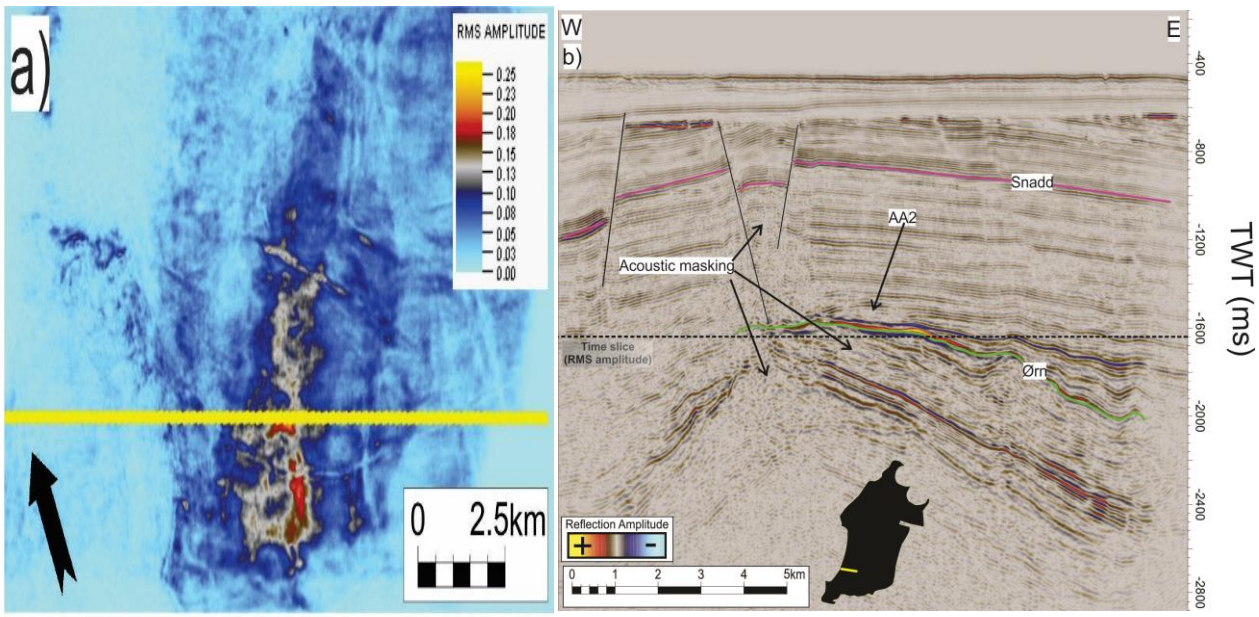

*Figure 4.35: **a)** RMS Amplitude time slice at 1628 ms (TWT) showing high amplitude anomaly. Yellow line indicates the seismic section visualized in b). **b)** Seismic cross section showing high amplitude anomaly (AA2). Acoustic masking is observed underneath. Yellow line in the polygon indicates the seismic profile.*

4.4.3 Amplitude Anomaly 3

Amplitude anomaly 3 (AA3) is located in the northern part of dataset SG9804, located in the Snadd-Formation (Figure 4.36). It is situated in the PLZ 1 interpreted in chapter 4.3.1.1. It has an oval shape oriented in a SE-NW direction. The longest axis is approximately 3.5km while the short axis measures 2.5km. The anomaly is located between 1100 and 1250 ms (TWT), giving it a vertical extent of 150 ms (TWT). In plan view does it cover an area of roughly 9km^2. The seismic shows the anomaly appearing as a laterally strong reflector surrounded by E-W striking faults interpreted in chapter 4.2. The origin of the anomaly might be from leakage along these faults from the Klappmyss formation or other deeper-seated formations, but it may also be a lithological boundary. Weak reflection underneath the anomaly might indicate a gas chimney.

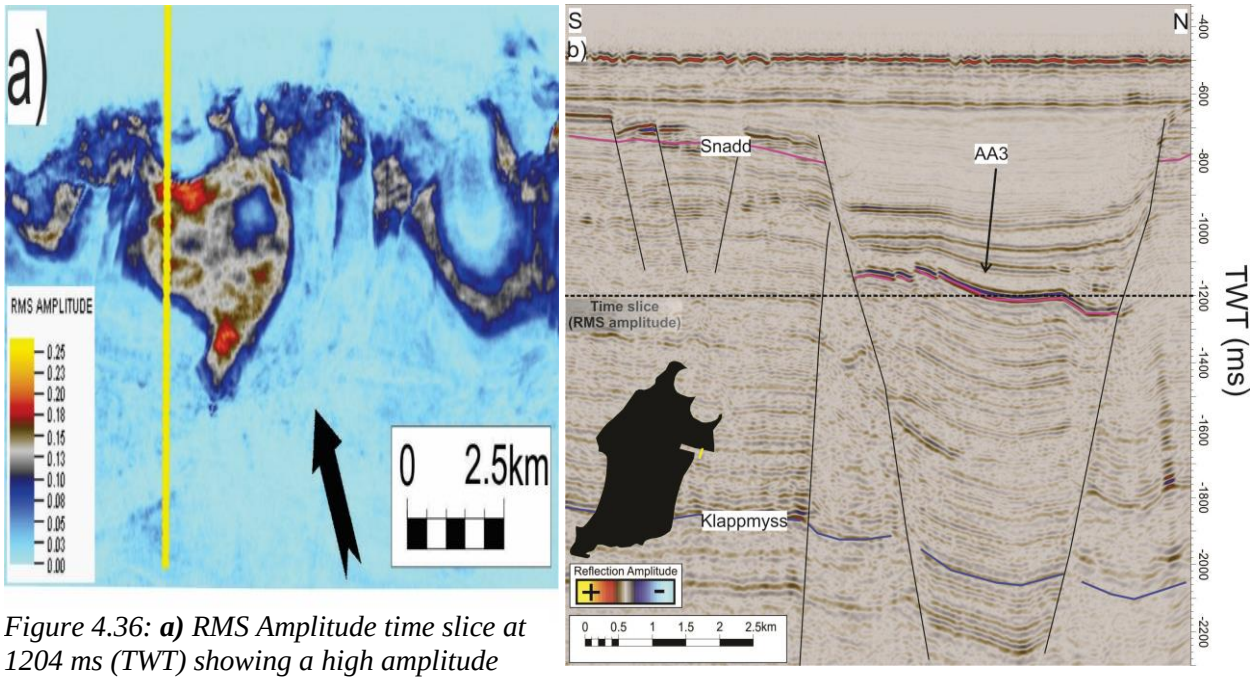

Figure 4.36: ***a)*** *RMS Amplitude time slice at 1204 ms (TWT) showing a high amplitude anomaly. Yellow line indicates the seismic section visualized in b).* ***b)*** *Seismic cross section showing high amplitude anomaly (AA3). Yellow line in the polygon indicates the seismic profile.*

4.4.4 Amplitude Anomaly 4

Amplitude anomaly 4 (AA4) is observed in the southeastern part of survey SG9803 (Figure 4.37**)**, located in the Hekkingen-Formation and other formations (compacted strata). Lithological boundaries truncating in a basin might be the cause of this anomaly. It has an elongated shape oritented in an E-W direction. The long axis measures 15km while the short axis measures 2km. The anomaly is located between 1400 and 1700 ms (TWT), a vertical extent of 300 ms (TWT). In plan view it covers an area of 30km^2, but (Figure 4.37**c**) clearly shows that it extends even further. The seismic cross section shows strong lateral reflections with weak reflection underneath (acoustic masking). The area marks the transition between Loppa High in the northwest and the Hammerfest Basin to the southeast. The strata dips towards southeast. This zone is marked by a major fault which shows structural truncation.

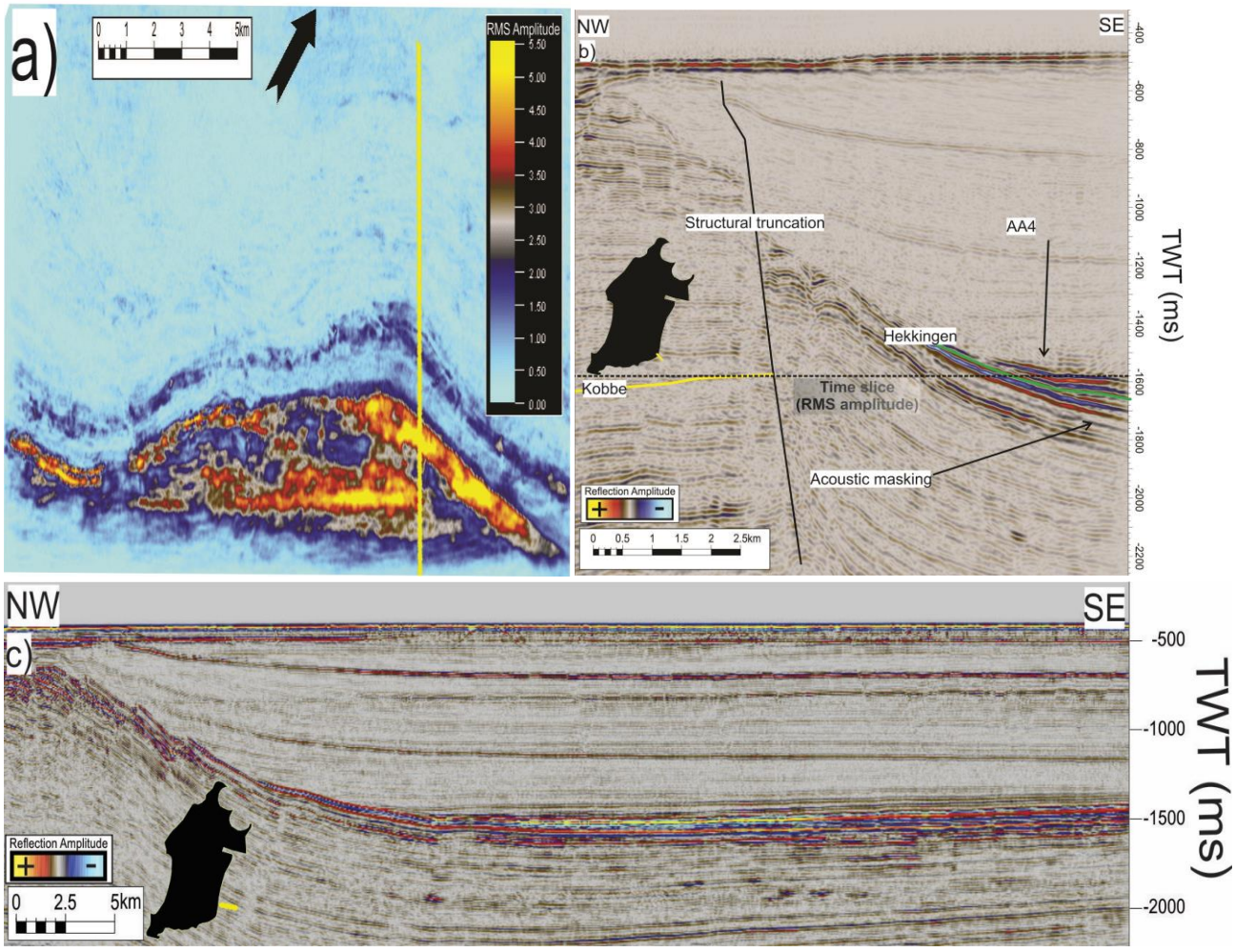

*Figure 4.37: **a)** RMS Amplitude time slice at 1588 ms (TWT) showing a high amplitude anomaly. Yellow line indicates the seismic section visualized in b). **b)** Seismic cross section showing high amplitude anomaly (AA4). Yellow line in the polygon indicates the seismic profile. **c)** Seismic cross section showing the amplitude in a different orientation.*

4.4.5 Amplitude Anomaly 5

Amplitude anomaly 5 (AA5) is located in the southern part of survey SG9803 (Figure 4.38). It is situated on top of the gas chimney (GC8) from chapter 4.3.2.5 (Figure 4.31), approximately 900 ms (TWT) shallower and 6km northwest of amplitude anomaly 4. The lateral reflection is found in the Kappa Toscana Formation at 550-600 ms (TWT) (Figure 4.38**b**), a vertical extent of 50 ms (TWT). In map view, AA5 has an elongated shape oriented in a SE-NW direction. The longest axis measures 7.5km while the short axis measures 2.5km. The anomaly covers an area of 18.75 km^2. Acoustic masking is observed directly beneath the anomaly. The origin of the anomaly could be coming from upward migrating fluids/gas from the deeper-seated Kobbe Formation.

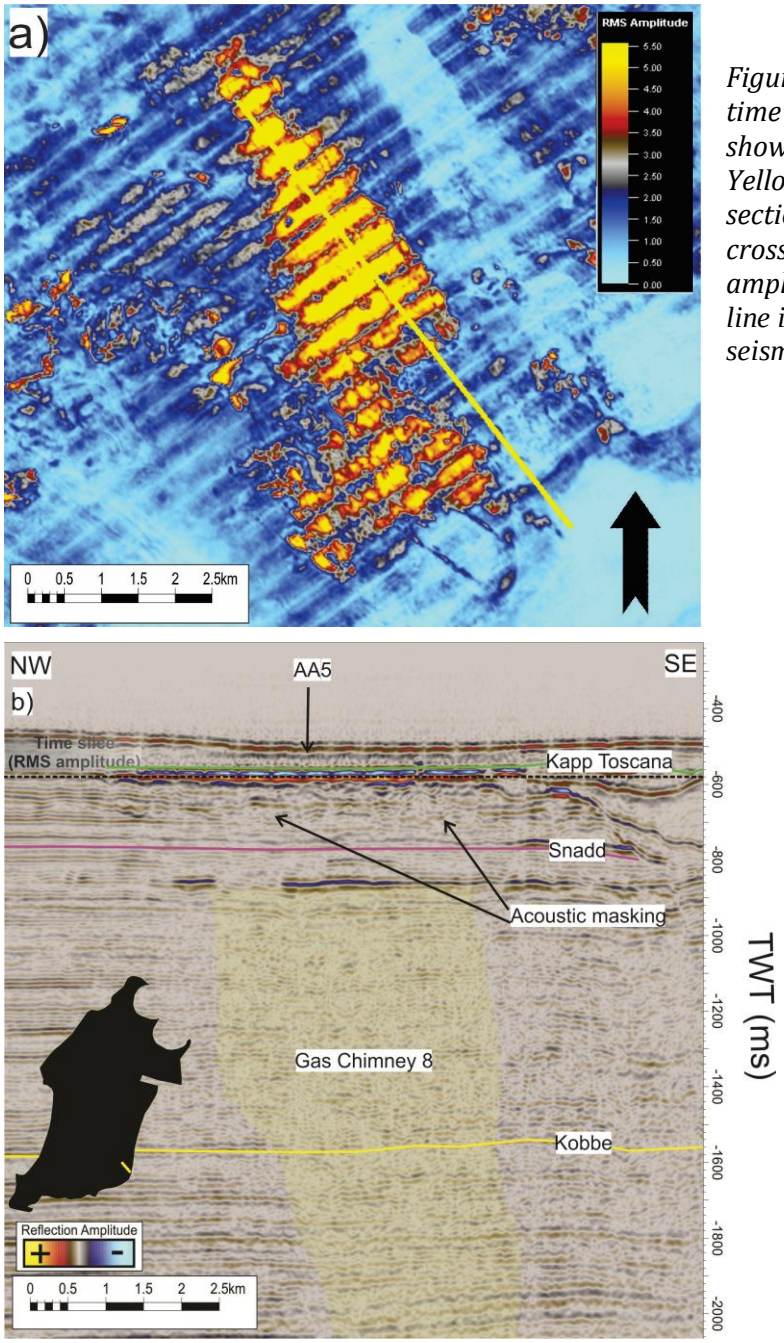

*Figure 4.38: **a)** RMS Amplitude time slice at 580 ms (TWT) showing high amplitude anomaly. Yellow line indicates the seismic section visualized in b). **b)** Seismic cross section showing high amplitude anomaly (AA5). Yellow line in the polygon indicates the seismic profile.*

4.4.6 Amplitude Anomaly 6

Amplitude anomaly 6 (AA6) is located 100 ms (TWT) below the URU, in the Torsk Formation on top of gas chimney 6 (GC6) from chapter 4.3.2.4 (Figure 4.30), southwest of Loppa High in survey NH8403-107 (Figure 4.39**a**) and NH8403-309 (Figure 4.39**b**). The anomaly has a 600 top TWT (ms) while the base TWT is 900 ms (TWT). The anomaly has its long/short-axis measuring 10km covering an area of roughly 79km2. It has a size greater than the other interpreted amplitude anomalies. Indicators of fluids/gas are found below the anomaly in form of acoustic masking, chaotic reflections, reverse polarity (compared to the seabed reflection) and push-downs. The anomaly seems to be a sub-horizontal event occurring at slightly different depths cross-cutting the lithology suggesting formation of gas hydrates.

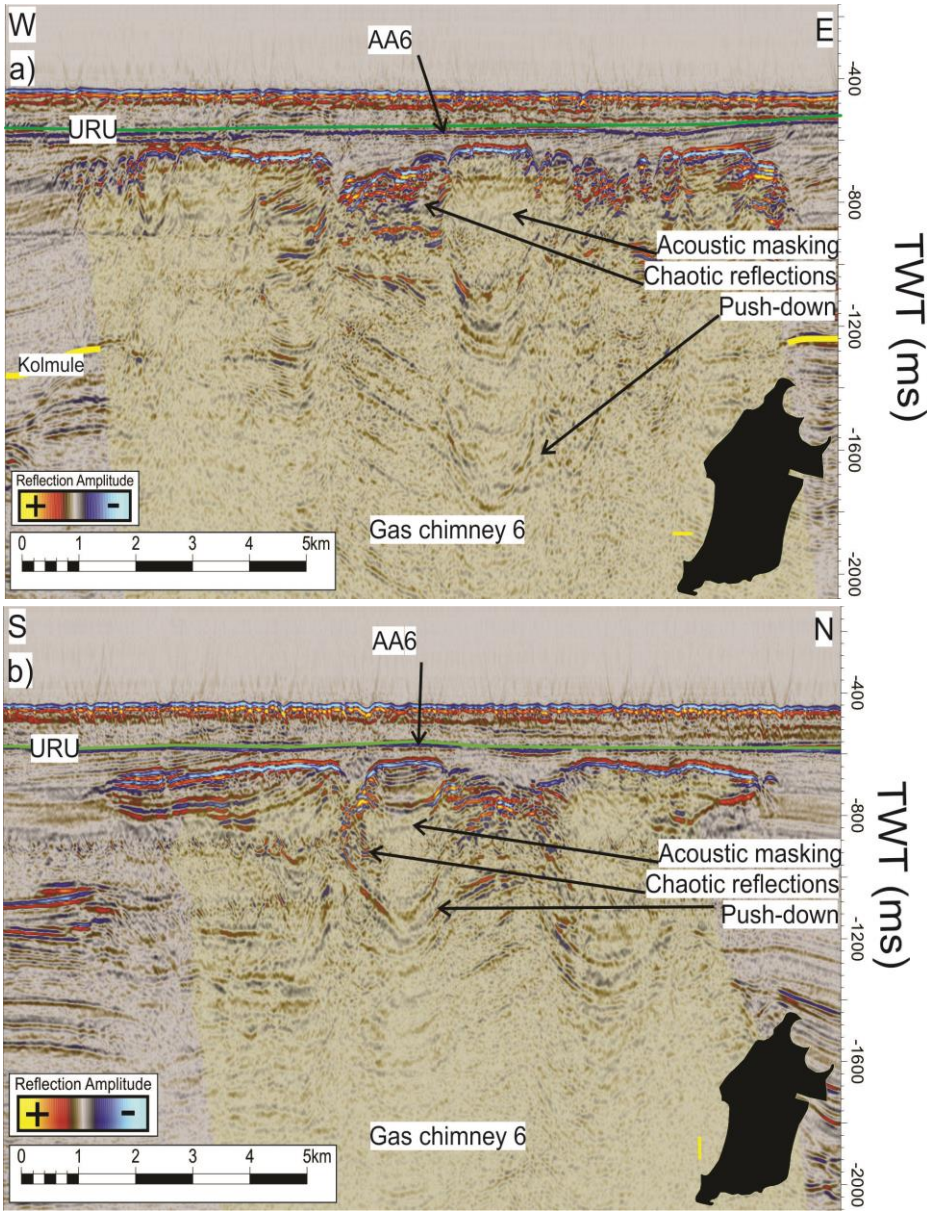

*Figure 4.39: **a)** Seismic cross section showing high amplitude anomaly (AA6) in an E-W direction. Yellow line close to the polygon indicates the position of the seismic profile. **b)** Seismic cross section showing high amplitude anomaly (AA6) in a N-S direction. Yellow line close to the polygon indicates the position of the seismic profile.*

4.4.7 Amplitude Anomaly 7

Amplitude anomaly 7 (AA7) is located 50-500 ms (TWT) below the URU (Figure 4.40), on top of the gas chimney 4 (GC4) from chapter 4.3.2.3 (Figure 4.29). It is found southwest of Loppa High in surveys NH8403-301 (Figure 4.40**a**) and LHSG89-403 (Figure 4.40**b**), on top of the Kolmule FM, in the Torsk FM. The anomaly has its upper termination at 650 ms (TWT) and its base at 1100 ms (TWT), a vertical extent of 450 ms (TWT). It is comprised of three separate bodies which looks to be part of the same anomaly and layer. The distance between them is approximately 700m. The anomaly appears "flat" in the southern part of the seismic and could potentially be interpreted as a flat spot. It has a circular shape with a long/short-axis of roughly 12km, covering an area of 113km^2. Acoustic masking, chaotic reflections and a reverse polarity of the anomaly (compared to the seabed reflection) indicate the presence of fluids. The anomaly seems to be a sub horizontal event in a SE-NW direction, while it has a more circular-shape in a N-S direction.

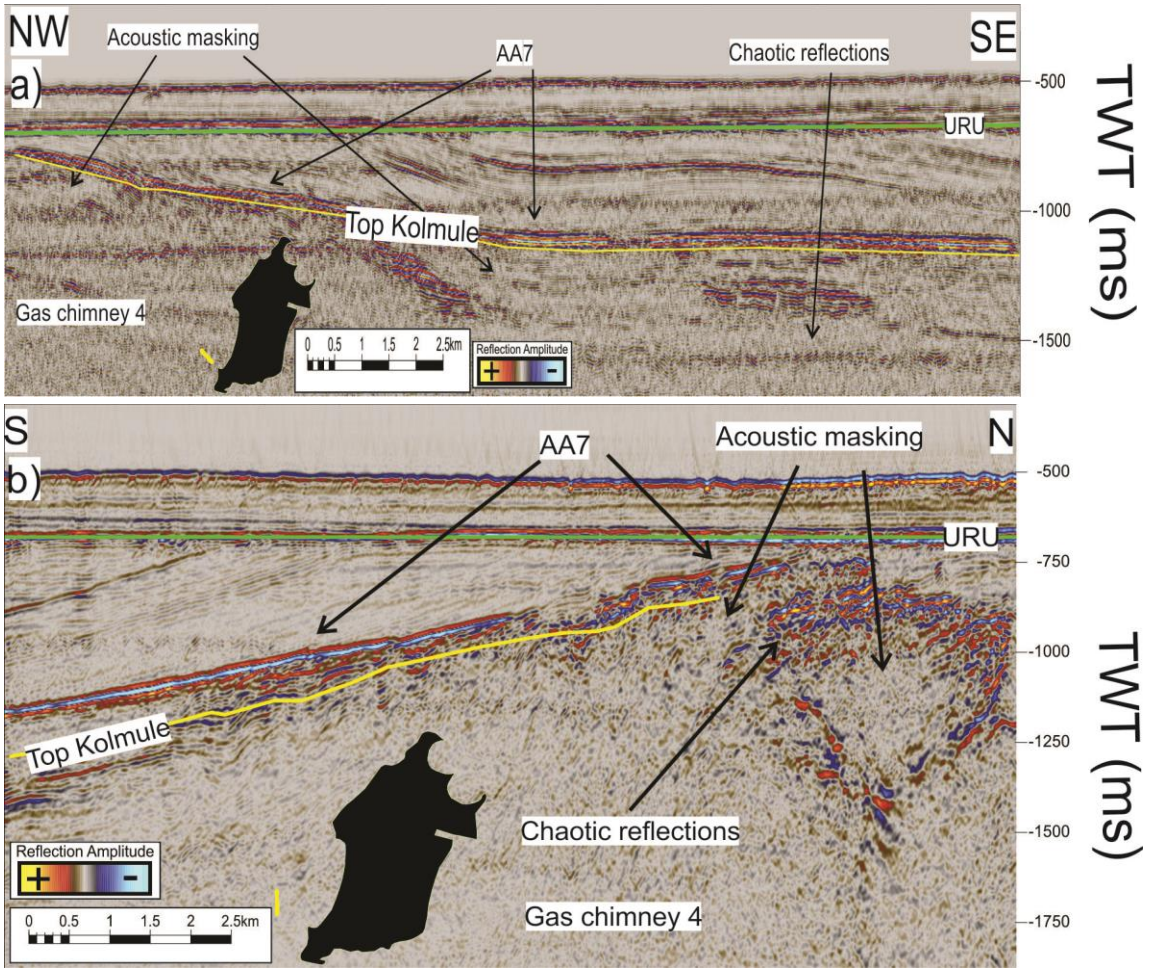

Figure 4.40: ***a)*** *Seismic cross section showing high amplitude anomaly (AA7) in an SE-NW direction.* ***b)*** *Seismic cross section showing high amplitude anomaly 7 in a N-S direction. Yellow line close to the polygon indicates the position of the seismic profile.*

4.4.8 Amplitude Anomaly 8

Amplitude anomaly 8 (AA8) is located 125-475 ms (TWT) below the URU (Figure 4.41) and has a curvilinear shape. Geographically, the anomaly is found southwest in the study area, in the transition zone between Loppa High and Bjørnøya Basin, 8km southeast of AA7. It is found in dataset NH8403-101. The amplitude anomaly is strongest in the upper eastern part where it appears shallower than the western part. The top of the bright spot is located between 725-1050 ms (TWT) and the base is located between 750-1075 ms (TWT). It is situated on top of the Kolmule FM, and is probably part of the Torsk FM. The bright spot show a reversed polarity in respect to the seabed. It has a circular shape with a long/short-axis of 11km, covering an area of 95km^2. Beneath the amplitude anomaly is gas chimney 5 (GC5) from chapter 4.3.2.3. Acoustic masking and chaotic reflections are also observed. The high amplitude anomaly seems to follow the strata which looks like western-dipping clinoforms.

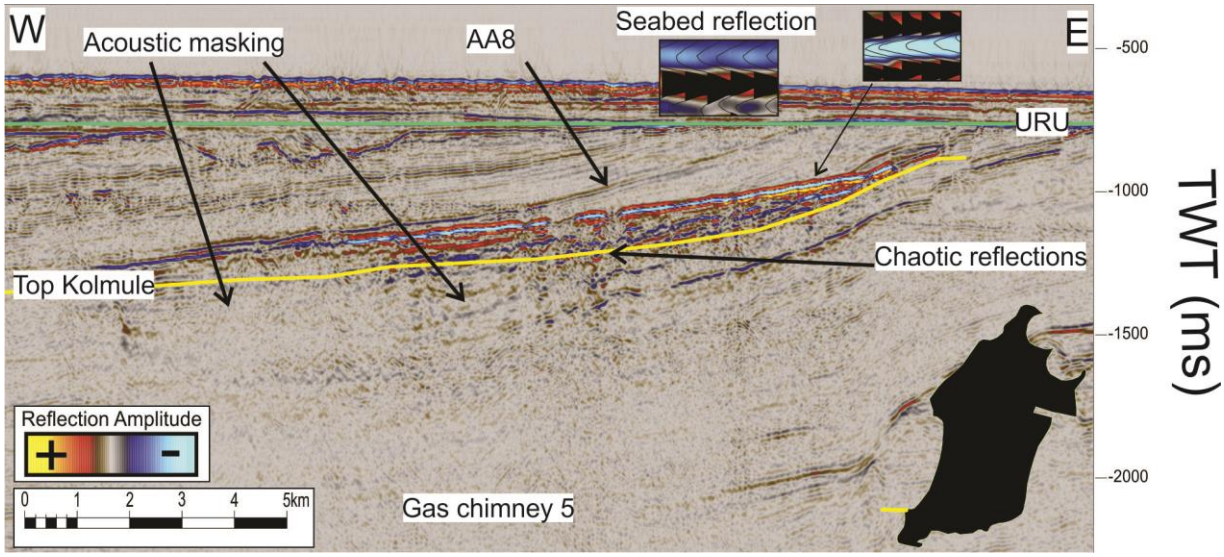

Figure 4.41: Seismic cross section showing high amplitude anomaly (AA8) in an E-W direction. Yellow line on the polygon indicates the position of the seismic profile.

4.4.9 Amplitude Anomaly 9

Amplitude Anomaly 9 (AA9) is located 300-550 ms (TWT) below the URU, in the northwestern part of Loppa High in dataset NH8506-411 (Figure 4.42**a**) and NH8506-305A (Figure 4.42**b**). It has an elongated shape in a SE-NW direction. The top of the anomaly is first visible in the southeastern part from 850 ms (TWT) while the base occurs at 1100 ms (TWT). This gives a vertical extent of 250 ms (TWT). It is situated on top of the top Kolmule FM. The anomaly has a length of 8km and a maximum width of 4.5km. It covers an area of roughly 36km^2. It appears shallower in the southeastern part where it eventually weakens and truncates against the Loppa High. Below the anomaly, there appears to be acoustic masking disturbing the reflectors. The high amplitude reflection could also indicate a lithological contrast and bedding spacing. High amplitudes can suggest a vertical alternation of contrasting lithologies while a low amplitude suggests a similar lithology on both sides of the interface. The anomaly is situated in a basin between Loppa High and the BFC (Bjørnøya Fault Complex).

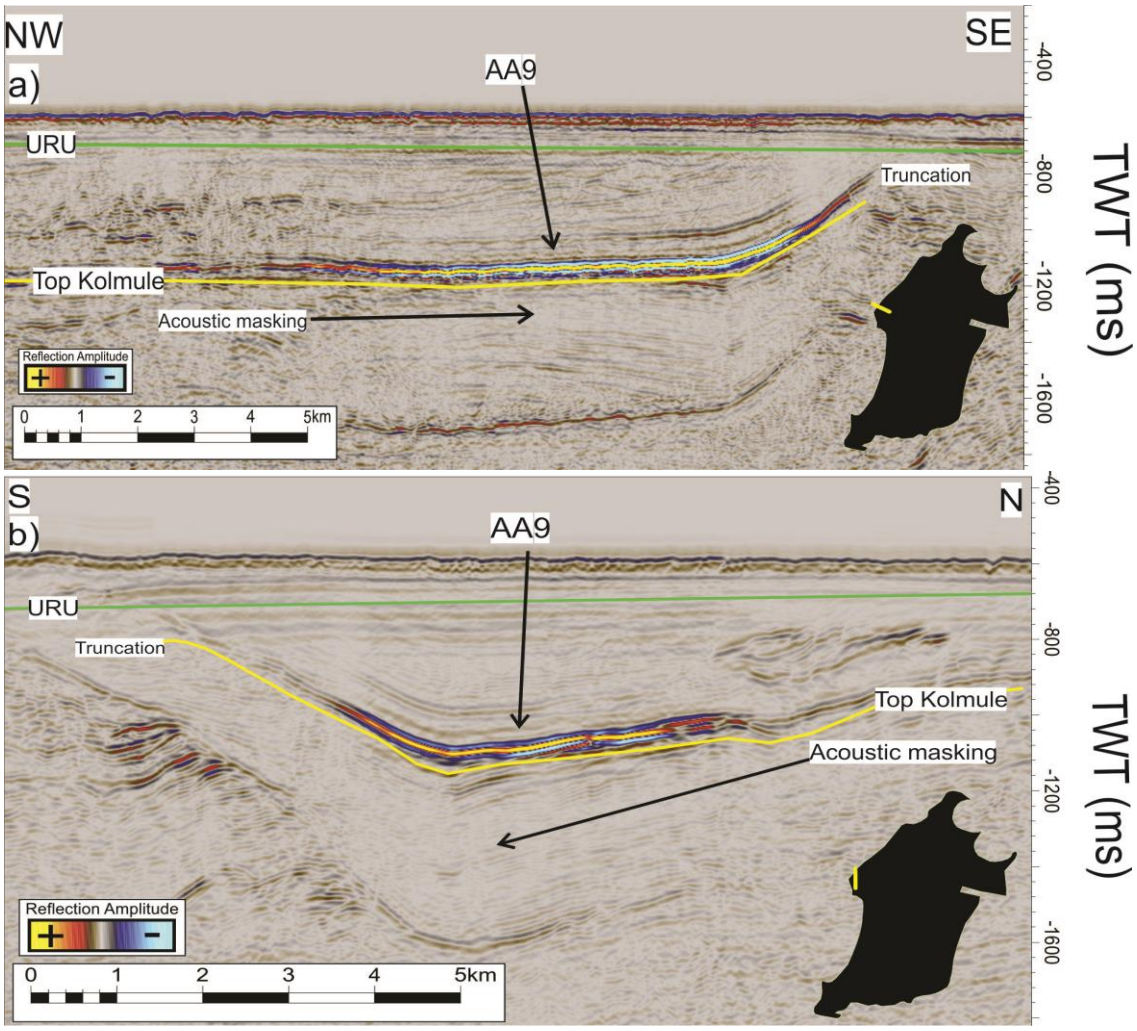

*Figure 4.42: **a)** Seismic cross section showing high amplitude anomaly (AA9) in a SE-NW direction..*

***b)** Same anomaly in a N-S direction. Yellow line on the polygon indicates the position of the seismic profile.*

4.4.10 Amplitude Anomaly 10

Amplitude Anomaly 10 (AA10) is located in surveys NH8403-111 and NH8403-312 (Figure 4.43). The anomaly has a lateral elongated shape in a N-S direction with a length of 5km and a more oval shape in E-W direction with a width of 1.5km covering an area of 7.5km^2. It is 6.5km east of gas chimney 7 from chapter 4.3.2.4 (Figure 4.30). AA10 is characterized with a reversed polarity compared to the seabed reflection and appears to be a relatively flat event that mimics the seabed, crosscutting the western-dipping strata. It is located 100 ms (TWT) below the URU between 650-775 ms (TWT). This gives a vertical extent of 125 ms (TWT). It is located above the Kolmule Fm, inside the Torsk FM. The seismic reflections below and adjacent to the anomaly are to a degree influenced, as they have a low continuity and weak amplitudes oriented relatively to the anomaly. Directly beneath and inside the anomaly is acoustic masking observed. Two NE-SW striking faults are identified below the anomaly where acoustic masking is observed along the fault planes. They look to be connected to the anomaly and have probably fed the anomaly fluids through leakage along these faults.

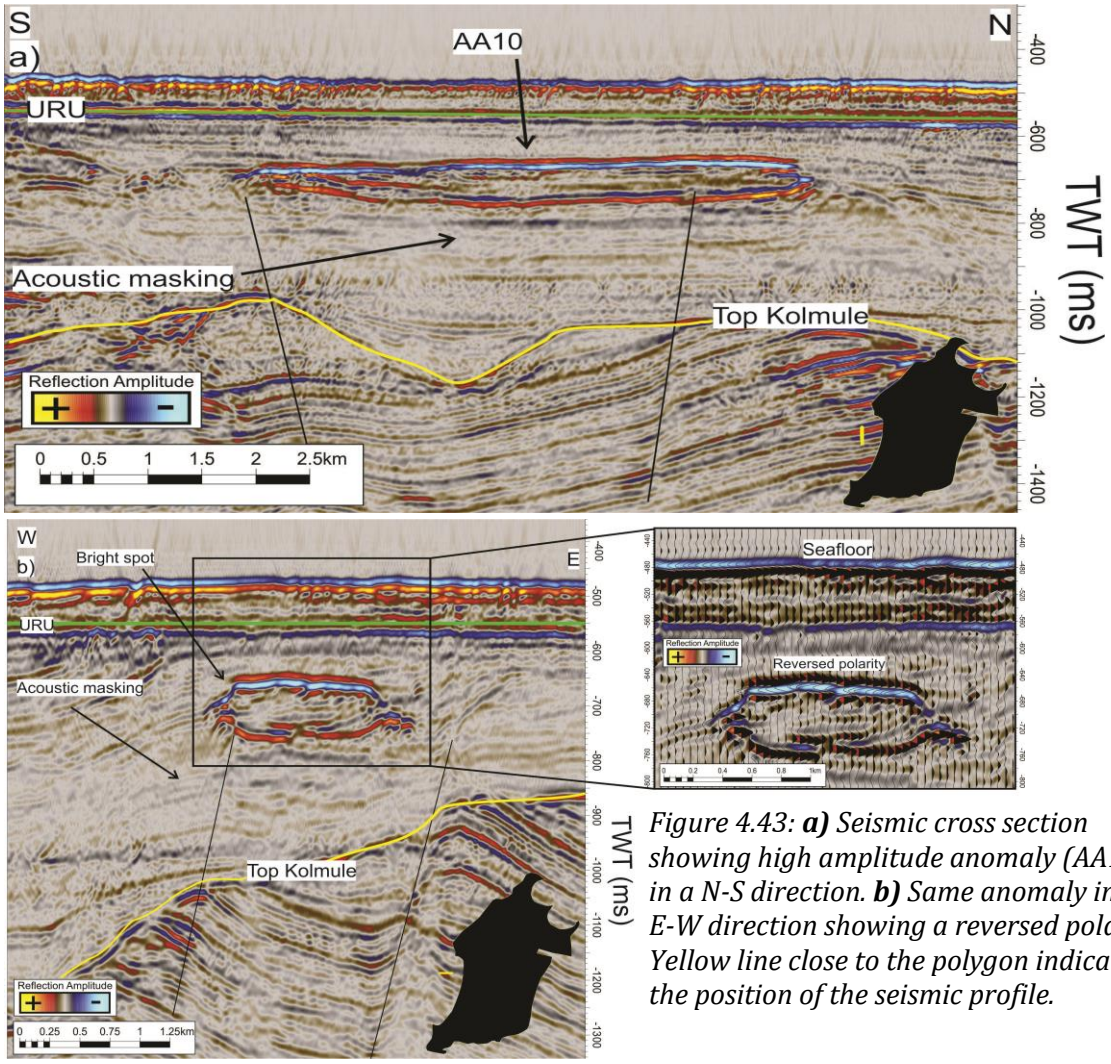

*Figure 4.43: **a)** Seismic cross section showing high amplitude anomaly (AA10) in a N-S direction. **b)** Same anomaly in an E-W direction showing a reversed polarity. Yellow line close to the polygon indicates the position of the seismic profile.*

Anomaly	**Survey**	**Length (km)**	**Width (km)**	**Area (km^2)**	**Top TWT (ms)**	**Base TWT (ms)**	**Formation**
AA1	SG9810	8, 4	5, 2	48	625	775	Snadd
AA2	SG9810	4	2	8	1600	1900	Ørn
AA3	SG9804	3.5	2.5	7	1100	1250	Snadd
AA4	SG9803	15	2	30	1400	1700	Hekkingen
AA5	SG9803	7.5	2.5	18.75	550	600	Kappa Toscana
AA6	NH8403-107, NH8403-309	10	10	79	600	900	Torsk
AA7	NH8403-301, LHSG89-403	12	12	113	650	1100	Torsk
AA8	NH8403-101	11	11	95	725	1075	Torsk
AA9	NH8506-411, NH8506-305A	8	4.5	36	850	1100	Torsk
AA10	NH8403-111, NH8403-312	5	1.5	7.5	650	775	Torsk

Table 4.4: Summary of the approximate values of the different amplitude anomalies.

4.5 Morphological expressions of fluid flow on the seafloor

Several morphological circular to sub-circular depressions have been identified and mapped on the seafloor (Figure 4.44). The interpreted depressions are exclusively mapped in the 3D-cubes (SG9810, SG9804, SG9803, OMV09M01) due to uncertainty and resolution. The southwestern Barents was heavily glaciated in the Cenozoic and glacial plough marks are very common in the study area. Identification of surface-expulsion features like pockmarks are therefore difficult across 2D seismic profiles. 3D-data will also provide a much better resolution, making it easier to identify depressions on a seafloor-surface. In this thesis will the focus be on pockmarks as they represent an indication of upward fluid flow. The depressions will be divided into small-scale depressions (up to 400m wide) and mega depressions (above 400m wide).

A table of the results will be presented at the end of the chapter (Table 4.5).

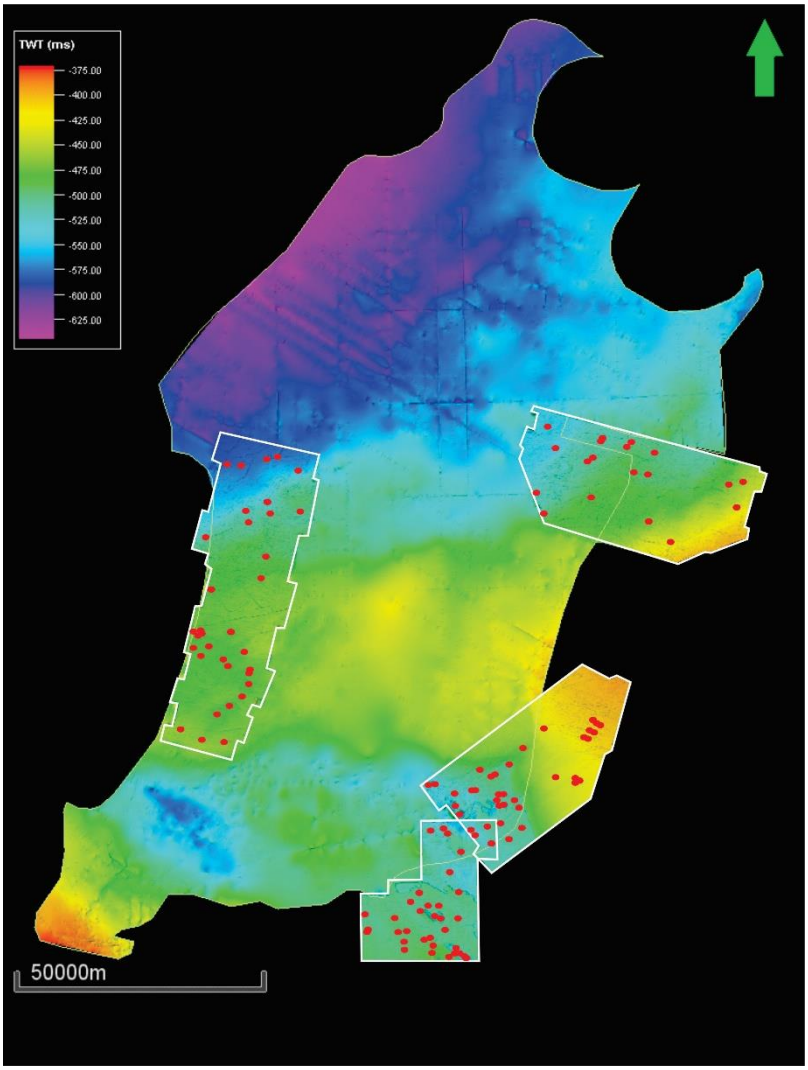

Figure 4.44: Overview of the interpreted seafloor reflection in the study area showing the position of small depressions (red circles).

4.5.1 Small-scale depressions: Pockmarks

The seafloor reflector provides information about the geomorphology of the area (Figure 4.44). It reveals the distribution and density of 124 small circular to sub-circular depressions in the Loppa High region (Figure 4.44). These occur as single features, within glacial features and as closely spaced depressions on the seabed. They often occur in chains associated with iceberg plough marks (Chand et al., 2012). Smaller depressions occur more frequently within glacial features. Many of the pockmarks are elongated, often having steep sidewalls that are U- or V-shaped. The small-scale depressions occur mostly in the deeper part of the seismic surveys (Figure 4.44). They will generally have a length of 80-320m, a width of 70-210m and a depth of 3-22.5m. Earlier studies from the southern part of Loppa High have concluded similar features to be pockmarks (Chand et al., 2012). However, erosion from plough marks makes it difficult to distinguish some of the circular to sub-circular depressions and some might be the result of icebergs piercing the seafloor rather than gas seepage and fluid flow.

The highest density of these small depressions occur in the southern part of survey SG9810, southwestern part of survey SG9803 and throughout survey OMV09M01. In the remaining data (especially survey SG9804) are the depressions spaced farther apart. It is hard to tell if there is a link between water depth and seabed depressions due to data limited to certain water depths. Still, it looks like the deeper areas (over 450 ms TWT) have a greater distribution of the circular depressions.

Artefacts are observed on the seafloor in all surveys as footprints (coherent noise) oriented along the direction of the surveys. At intersections between these footprints and plough marks, depressions may occur. These depressions are often considered to be artefacts and will not be included.

Some of the depressions occur above vertically stacked high amplitude reflections and zones of acoustic masking with push-downs. These features suggests the presence of gas and fluid flow and might be the origin to the formation of these depressions. The formation of pockmarks requires a period of sustained gas seepage followed by a less active period with burial (Løseth et al., 2009). Pockmarks only occur where soft sediments can act as a recording medium (Chand et al., 2012). Pockmarks are often connected to active chimneys and pipes in the subsurface which may migrate to shallower strata along faults (leakage). Faults extending all the way to the seafloor are not observed, but termination into the URU occurs frequently.

4.5.1.1 Depressions in Survey SG9810

In the western region (survey SG9810) are 34 pockmarks identified with the highest density in the southern part (Figure 4.44). They occur mostly as isolated depressions (Figure 4.44), but also appear in groups, often within plough marks. The pockmarks have a circular to elongated shape. In general, the longest axis measures 110-260m while the short axis measures 80-190m. The depth varies between 4-17m, assuming a water velocity of 1500 m/s (Table 3.3). High amplitude reflections are quite normal in the area while interpreted gas chimneys and potential leakage zones (along faults) are uncommon. The water depth varies from 450 to 590 ms (TWT). Depression 1 (D1) appears west in the survey and has a circular shape with a long axis of 175m, short axis of 135m and a depth of 15m (V_p = 1500 m/s)(Table 3.3) covering an area of 0.023km^2 (Figure 4.45). A high amplitude reflection is observed beneath the pockmark (Figure 4.45**c**).

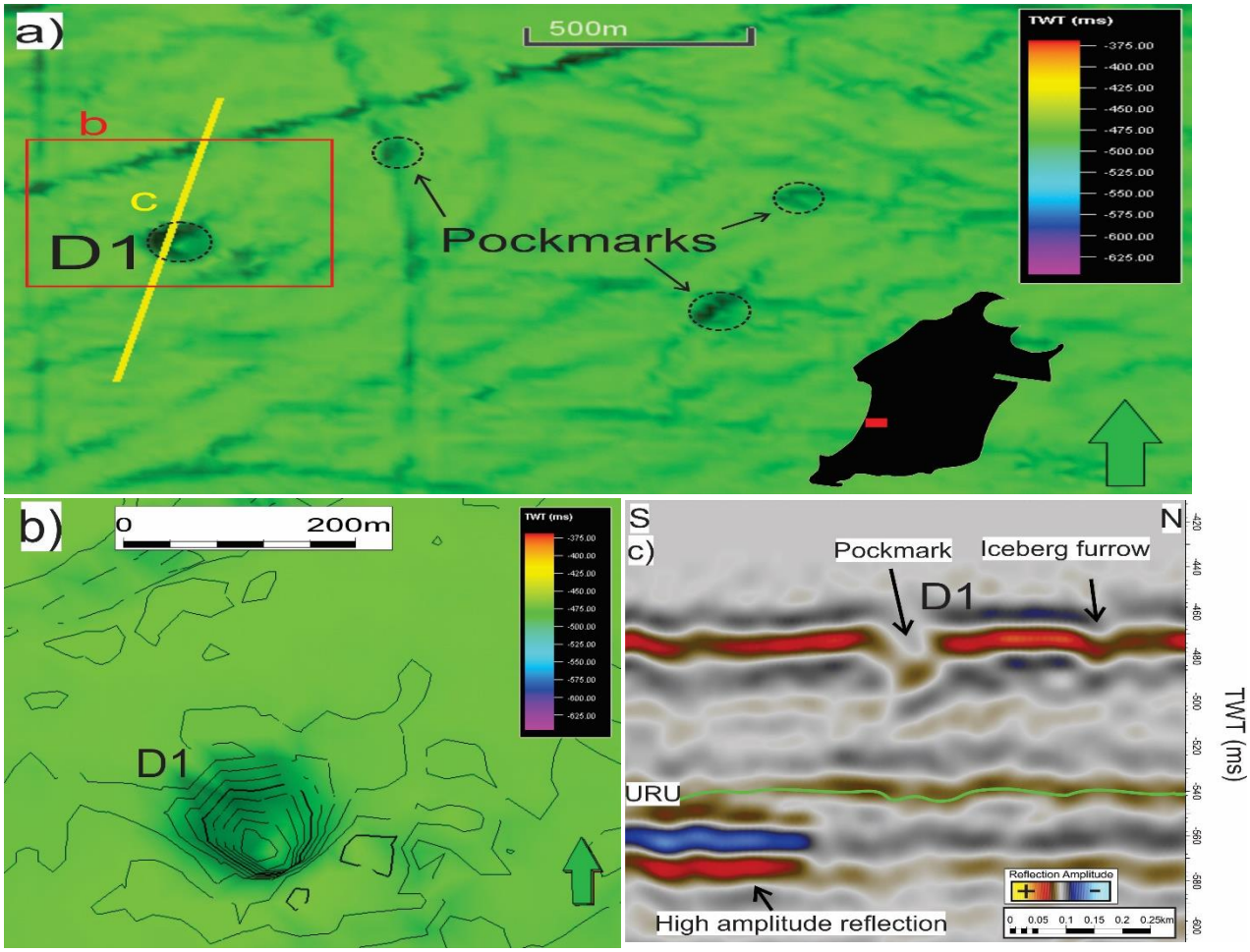

Figure 4.45: ***a)*** *Overview map of pockmarks located next to an iceberg furrow. Position of map is indicated in red inside the black polygon.* ***b)*** *Close-up picture of a prominent pockmark (D1) indicated by a red square in a.* ***c)*** *N-S oriented seismic section of pockmark (D1) indicated by the yellow line in a.*

4.5.1.2 Depressions in Survey SG9804

In the northeastern region (survey SG9804) 19 pockmarks are identified (Figure 4.44). They occur in the whole survey and appear to be similar in shape (circular to elongated) as the western region. They appear often isolated and within plough marks, and are found rarely in the dataset. The pockmarks have a long axis between 105-320m while the short axis measurers 95-205m. The depth varies between 4-22.5m (V_p = 1500 m/s)(Table 3.3). The pockmarks are in general slightly bigger compared to survey SG9810. Indications of fluids/gas like high amplitude anomalies, gas chimney and leakage zones are normal in the northwestern part of the survey which may be the reason why this area has the highest density of depressions. The water depth in the area varies from 400-550 ms (TWT).

Depression 2 (D2) is located north in the survey. It has a circular shape with a 165m long axis, 115m short axis and a depth of 11.3m (V_p = 1500 m/s)(Table 3.3) covering an area of 0.019km^2 (Figure 4.46**a,b,d**).

Depression 3 (D3) appears north in the survey (4.3km south of D2) and has a circular shape with a long axis of 125m, short axis of 110m and a depth of 13m (V_p = 1500 m/s)(Table 3.3) covering an area of 0.013km^2 (Figure 4.46**a,c,e**).

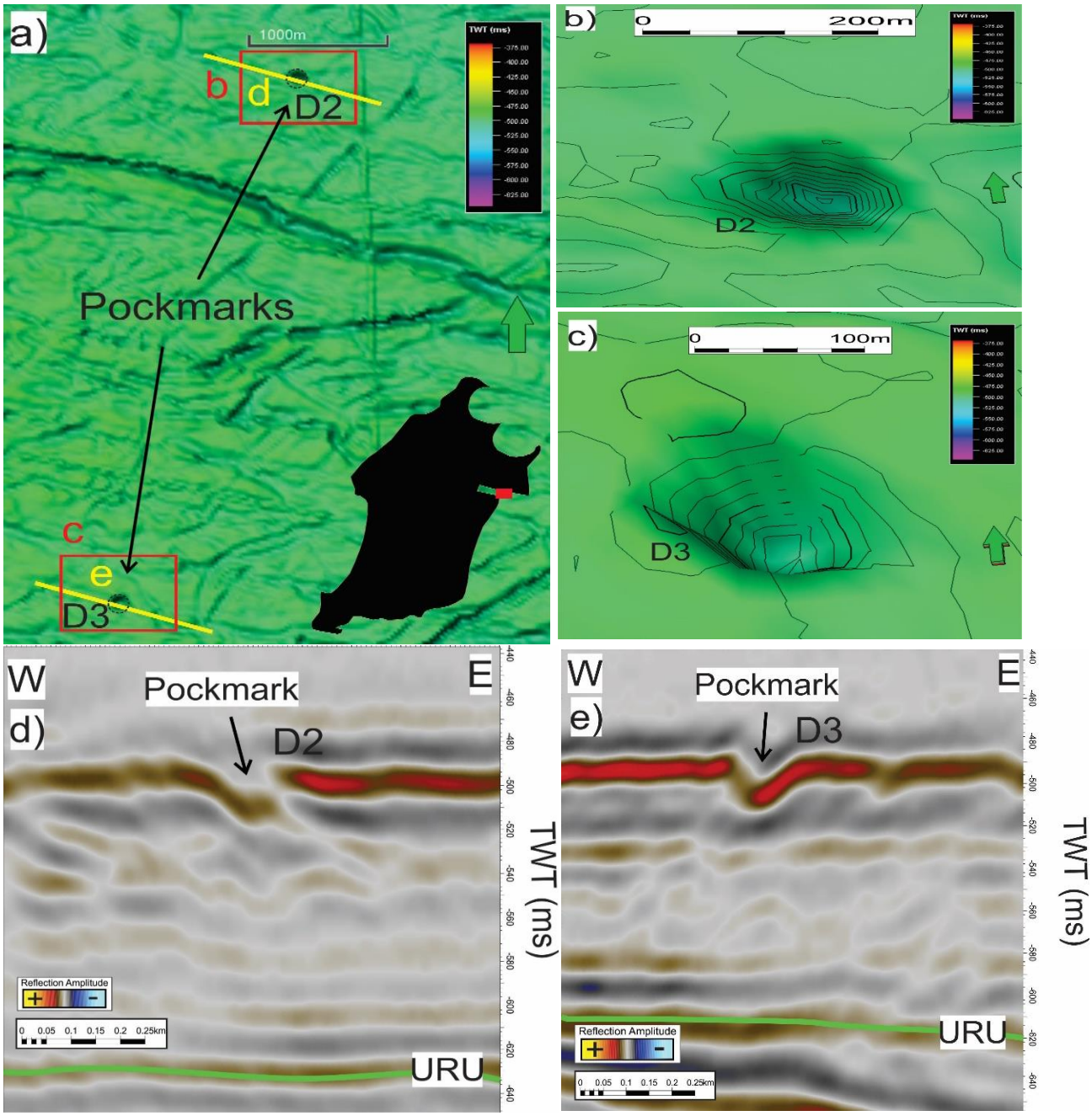

Figure 4.46: ***a)*** *Map of pockmarks (D2, D3) and plough mark. Position of map is indicated in red inside the black polygon.* ***b & c)*** *Close-up picture of pockmarks (D2, D3) indicated by the red squares in a.* ***d & e)*** *N-S oriented seismic section of pockmarks (D2, D3) indicated by the yellow lines in* ***a).***

4.5.1.3 Depressions in Survey SG9803

In the southeastern region (survey SG9803) are 34 pockmarks identified (Figure 4.44). They occur mainly in the deeper southern area, but a few depressions are also found in chains in the northern area where plough marks are more common. The southern depressions have a more elongated shape compared to the northern ones. The occurrence of pockmarks looks to be related to the presence of gas chimneys and leakage zones in the area (Figure 4.16, Figure 4.24). The pockmarks have a long axis between 80-270m while the short axis measurers 70-180m.

The depth varies between 3-21m (V_p = 1500 m/s) (Table 3.3). The water depth in the area varies from 300-431m. In the southern area are also depressions with a much greater size present which will be discussed in chapter 4.5.2. A few pockmarks are located inside these larger depressions.

Depression 4 (D4) is located south in the survey and has a sub-circular shape. It has a long axis of 180m, short axis of 130m and a depth of 20m (V_p = 1500 m/s)(Table 3.3) covering an area of 0.023km^2 (Figure 4.47).

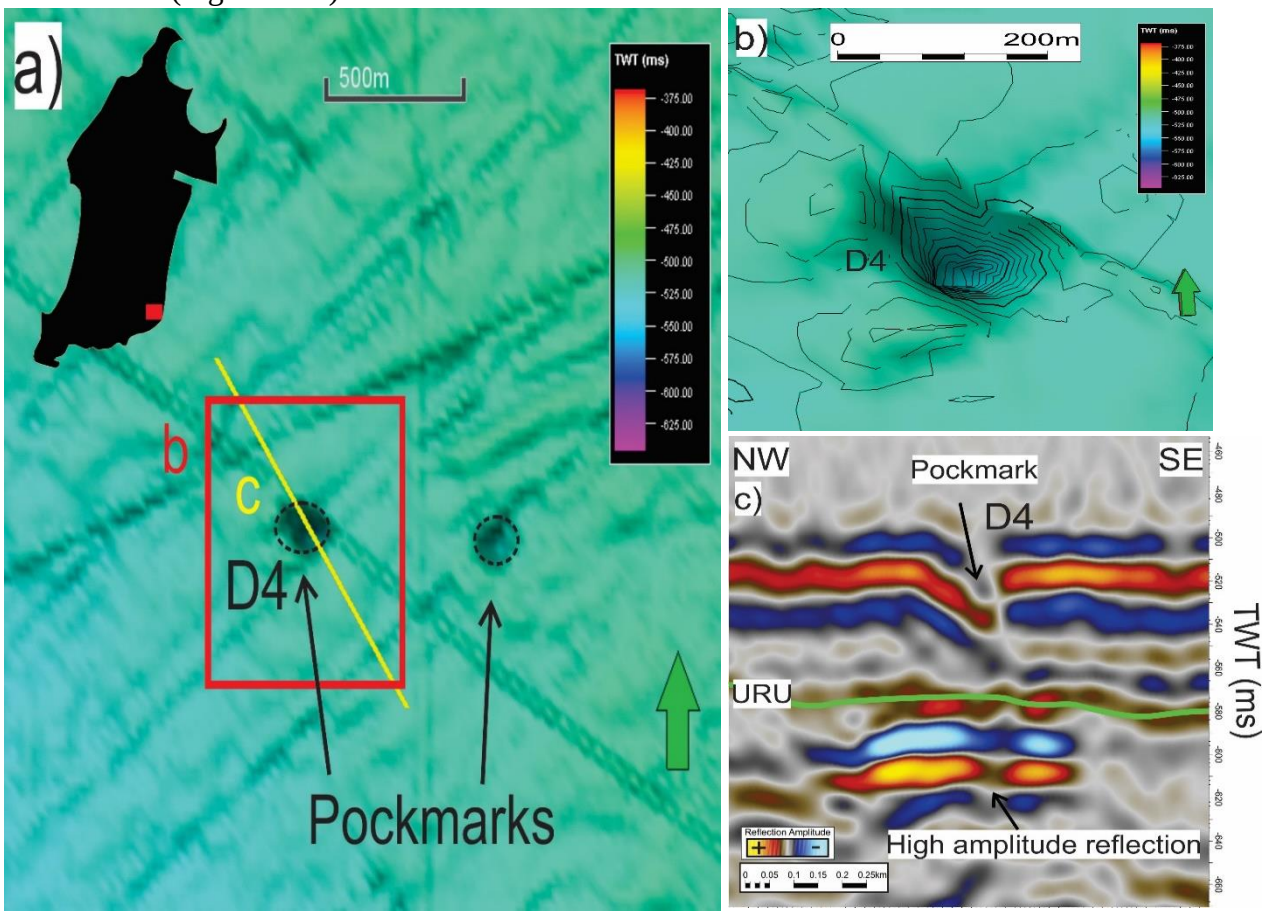

Figure 4.47: ***a)*** *Overview map of pockmarks. Position of map is indicated in red inside the black polygon.* ***b)*** *Close-up picture of a prominent pockmark (D4) indicated by a red square in a.* ***c)*** *SE-NW oriented seismic section of pockmark (D4) showing high amplitude reflections and the underlying URU. Position indicated by yellow line in* ***a).***

4.5.1.4 Depressions in Survey OMV09M01

In the southern region (survey OMV09M01) are 37 pockmarks identified (Figure 4.44). It is the survey with the most pockmarks despite covering the smallest area. They are found throughout the whole survey and appear to have the same shape as the southeastern region, being sub-circular to elongate. They are mostly not found within plough marks, although there are a few examples. They will often occur in groups of 2-5 pockmarks where the smaller ones are surrounding the larger pockmarks (Figure 4.48**a**). The pockmarks have a long axis between 80-240m while the short axis measurers 70-210m. The depth varies between 4-20m (V_p = 1500 m/s)(Table 3.3). Gas chimneys and leakage zones are rare in the area and the underlying URU reflection does not show anomalous high amplitudes. High amplitude anomalies along the URU reflection occur occasionally, but seems to not control the distribution of pockmarks. The water depth in the area varies from 475-550 ms (TWT). Like survey SG9803 do survey OMV09M01 also have larger depressions present with a few pockmarks located inside themselves.

Depression 5 (D5) is found west in the survey and has sub-circular/elongate shape. It has a long axis of 230m, short axis of 120m and a depth of 9.8m (V_p = 1500 m/s)(Table 3.3) covering an area of 0.027km^2 (Figure 4.48).

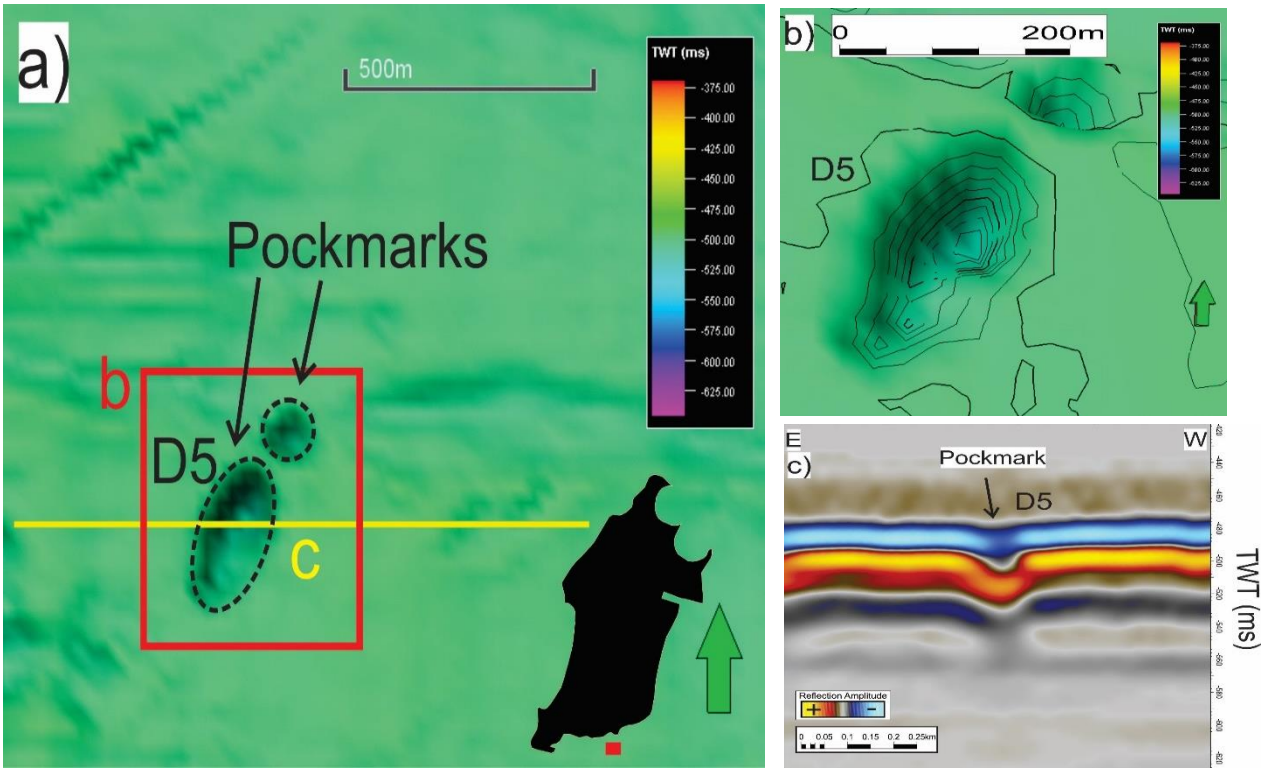

*Figure 4.48: **a)** Overview map of pockmarks. Position of map is indicated in red close to the black polygon. **b)** Close-up picture of a prominent pockmark (D5) indicated by a red square in a. **c)** W-E oriented seismic section of pockmark (D5) indicated by the yellow line in **a).***

4.5.1.5 Depressions on the URU: Paleo pockmarks

The URU reflection reveals small depressions similar to the seafloor reflection. These depressions are interpreted to be paleo-pockmarks (Judd & Hovland, 2009). They often occur in groups of 2-7 and can on occasion be found within iceberg plough marks. The depth of paleo-pockmark (P1) appears to be 6m (Vp = 1700 m/s, Table 3.3). It looks to have the same orientation and size as the pockmark located directly above which has a long axis of 210m oriented in a NW-SE direction and short axis of 125m (Figure 4.49). It has a V-shaped geometry with steep sidewalls.

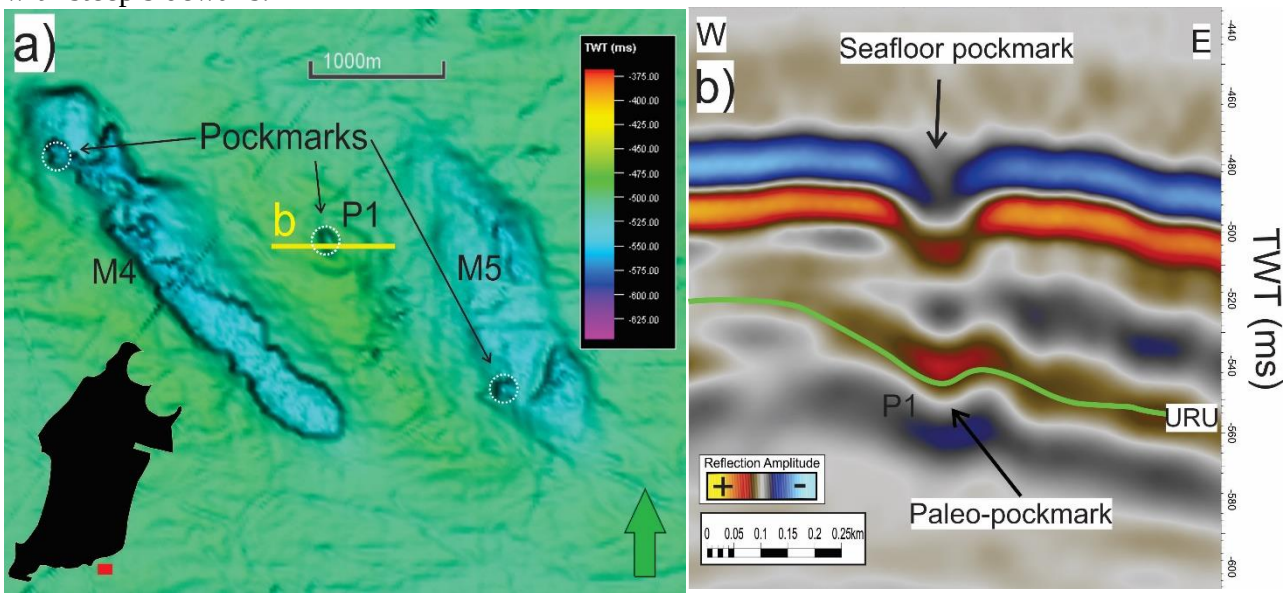

Figure 4.49: ***a)*** *Overview of pockmark located above paleo-pockmark (P1) on the interpreted seafloor reflection. Position of map is indicated in red close to the black polygon.* ***b)*** *Seismic section through P1 showing the relationship to the seafloor pockmark. Position of section indicated by yellow line in* ***a).***

4.5.2 Mega depressions

Large depressions (above 400m) are observed on the interpreted seafloor reflection in the study area. These are significantly larger than the previously described features and are found at two locations, in survey SG9803 (Figure 4.50) and OMV09M01 (Figure 4.51). The depressions are classified as mega depressions which occasionally contain small-scale depressions. The mega-depressions are termed M1-M7.

In the southern part of survey SG9803 are three mega depressions (M1-M3) identified (Figure 4.50**a**). They are located on the southeastern flank of Loppa High where the water depth (300-431m) is relatively high compared to rest of the area. The rim of the depressions appears to be irregular in plan view. M1 and M3 have an elongated shape while M2 has a more sub-circular

shape. A noteworthy meandering depression is observed east of M3. This might be an underwater channel. M1 has its longest axis striking in a SE-NW direction measuring 680m and a short axis of 450m. M2 and M3 have their long axis oriented in a N-S direction measuring 610m and 1300m with a short axis of 450m and 700m. In respect to the seafloor, M1 has a depth of 22.5m, M2 has a depth of 30m and M3 has a depth of 45m (V_p = 1500 m/s)(Table 3.3). All of them appear to have a U-shaped geometry (Figure 4.50**b,c**). M3 seems to be quite larger than M1 and M2. However, M1 and M2 are the ones reaching through the URU (Figure 4.50**c**). Underlying faults and high amplitude reflections occur beneath mega depression M2 and M3. Weak reflections (acoustic masking) are also observed. Pockmarks have been identified in all the mega depressions (Figure 4.50**a**).

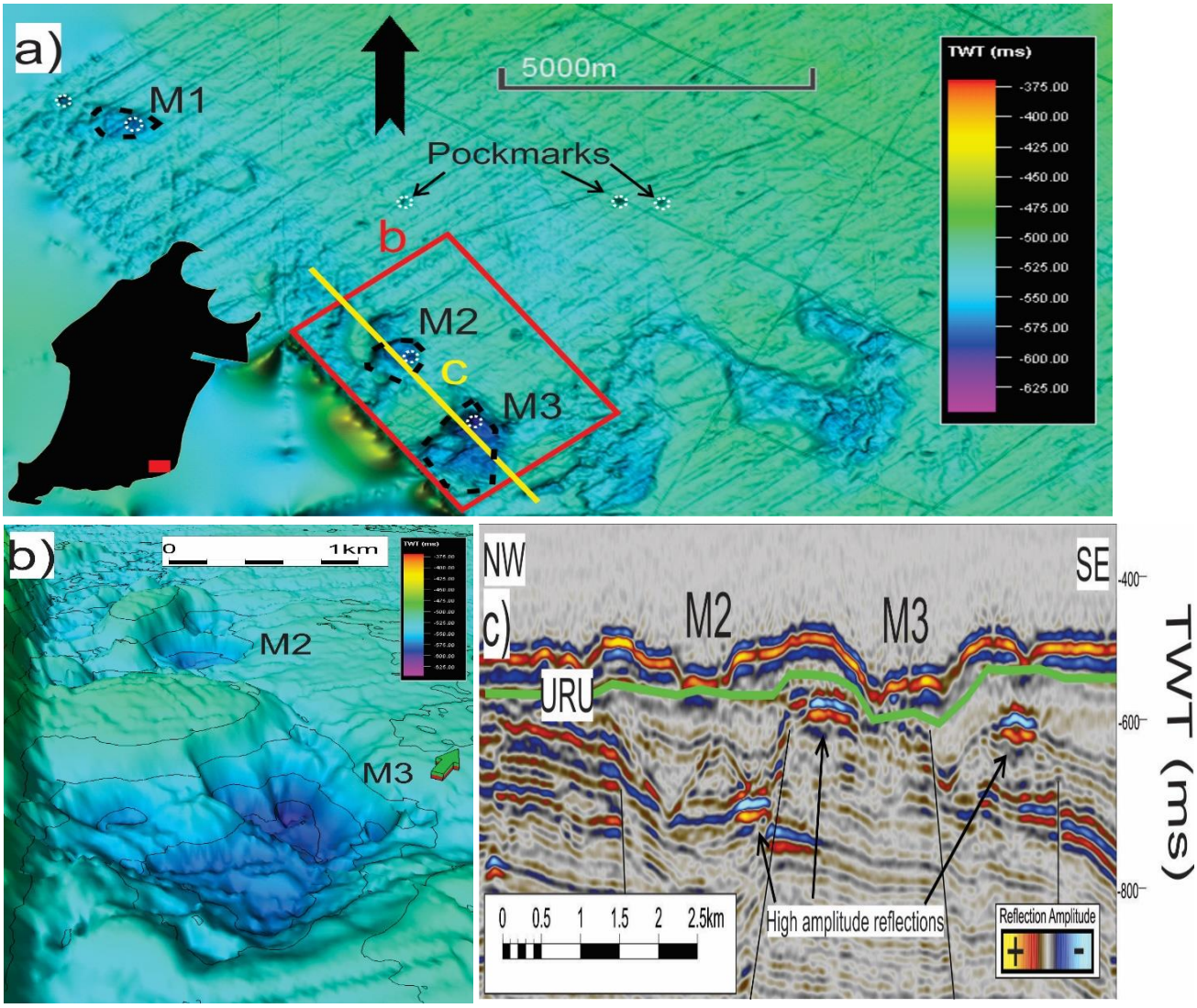

Figure 4.50: ***a)*** *Overview map of mega depressions (M1-M3) and pockmarks. Position of map is indicated in red inside the black polygon.* ***b)*** *Close-up picture of M2 and M3 indicated by a red square in a.* ***c)*** *SE-NW oriented seismic section of M2 and M3 indicated by the yellow line in a. Faults and high amplitude reflections are present.*

In the southern part of survey OMV09M01 are four mega depressions present (M4-M7) (Figure 4.51**a**). They occur at a water depths between 350-420m (V_p = 1500 m/s, Table 3.3). The two northern mega depressions (M4 and M5) have an elongated shape with their long axis striking in a SE-NW direction measuring 3300m and 2300m while the short axis measure 700 and 800m. Their depth varies between 15-22.5m (V_p = 1500 m/s, Table 3.3). A small pockmark is located between them and inside M5 (Figure 4.51**a**).

The two southern mega depressions (M6, M7) are only partly covered in the seismic data, but seems to extend further out of the dataset in a southeastern direction (Figure 4.51**a**). This makes it not possible to make exact measurements. The seismic data only covers the northern part of the features. In the available data M6 and M7 have a long axis of at least 6100m and 1400m and a short axis of 1500m and 800m. The depth of the depressions are between 22.5-37.5m (V_p = 1500 m/s, Table 3.3). M7 appear much larger in size than M6 where five small pockmark depressions occur (Figure 4.51**a**). Mega depressions M4-M6 have a V-shape geometry while M7 is more U-shaped with less steep sidewalls (Figure 4.51**c**). All of them extent to the URU, but deeper seismic analysis is not possible due to low seismic quality.

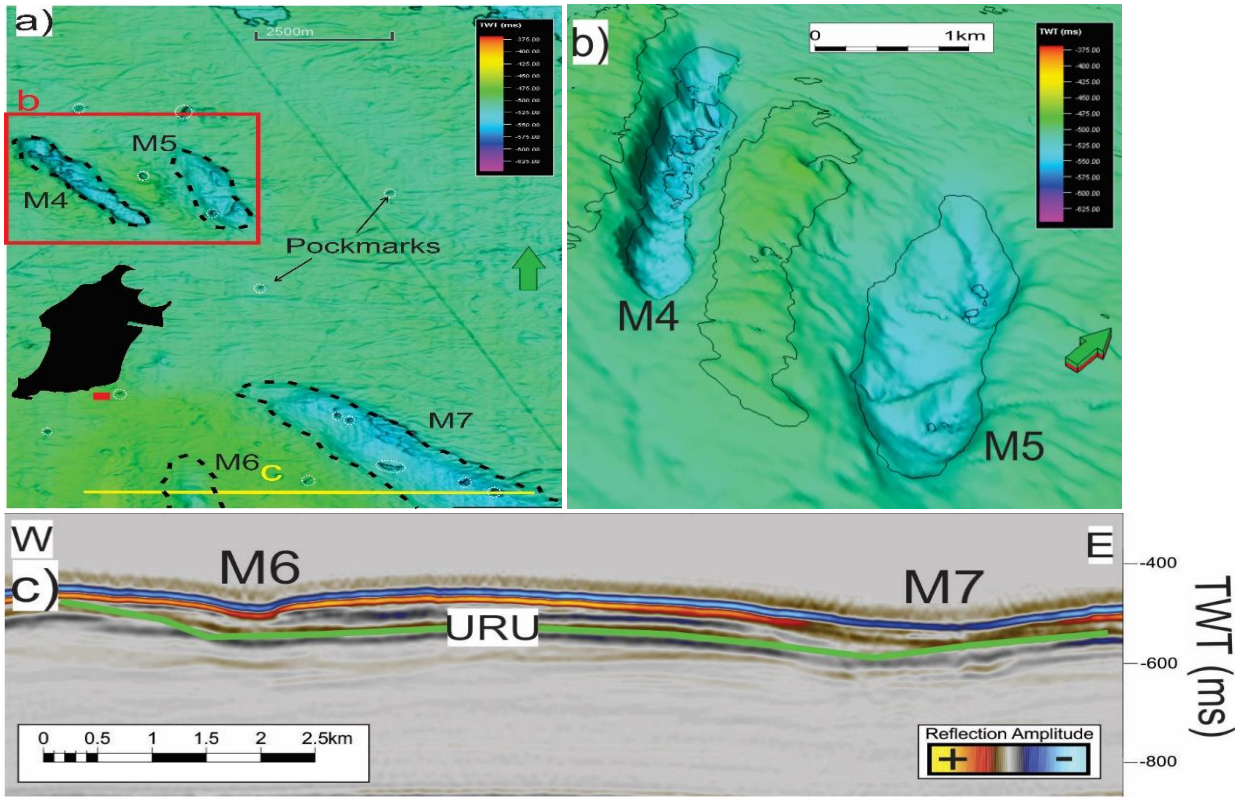

*Figure 4.51: **a)** Overview map of mega depressions (M4-M7) and pockmarks on the seafloor. Position of map is indicated in red close to the black polygon. **b)** Close-up picture of M4 and M5 indicated by a red square in a. **c)** E-W oriented seismic section of M6 and M7 indicated by the yellow line in **a).***

Depression	Long axis (m)	Short axis (m)	Short axis /long axis	Area (km^2)	Depth (ms TWT)	Depth (m, V_p=1500m/s)
D1	175	135	0.77	0.023	20	15
D2	165	115	0.7	0.019	15	11.3
D3	125	110	0.88	0.013	13	9.8
D4	180	130	0.72	0.023	20	15
D5	230	120	0.52	0.027	13	9.8
P1	210	125	0.6	0.026	7	6
M1	680	450	0.66	0.306	30	22.5
M2	610	450	0.74	0.274	40	30
M3	1300	700	0.54	0.910	60	45
M4	3300	700	0.21	2.310	20	15
M5	2300	800	0.35	1.840	30	22.5
M6	6100	1500	0.25	9.000	30	22.5
M7	1400	800	0.57	1.120	50	37.5

Table 4.5: Summary of all the measurements done related to depressions identified on the seafloor and URU.

5. Discussion

This chapter will focus on integrating the observations from the results chapter to get a better understanding of the potential source for fluid migration and dominating mechanisms controlling fluid flow in the study area.

5.1 Fluid origin

Fluid migration and fluid flow in the southwestern Barents Sea have in previous studies been documented (Chand et al., 2012; Rajan et al., 2013; Tasianas et al., 2016; Vadakkepuliyambatta, 2014; Vadakkepuliyambatta et al., 2013). In this chapter the potential source rocks for fluid flow within the study area will be discussed.

Ohm et al. (2008) presented the different source rocks in the Barents Sea based on the Total Organic Content (TOC), Hydrogen Index (HI) and the hydrocarbons potential to generate oil and gas (S2) (Figure 2.5). The lower Hekkingen Formation is regarded as the most potential source rock for oil and gas, but it is neither mature or present in the majority of the Loppa High area (Ohm et al., 2008). Other potential source rocks include formations of Triassic (Havert, Klappmyss, Kobbe, Snadd) and Carboniferous/Permian age. The maturity map of the southwestern Barents Sea (Figure 5.1) shows where the different source rocks are oil mature. However, it may not represent the correct maturation state since it is based on the pre-uplift maturities (maximum burial) of the source rocks (Ohm et al., 2008). The Cenozoic uplift prevented source rocks to be buried deeper, affecting the maturation process (A. Doré & L. Jensen, 1996). The map suggests that the different formations are eroded in a certain part on the Loppa High. This includes the Hekkingen Formation which is only present and mature in the northern, western and southern flanks. It is overmature in the Tromsø Basin to the west, but looks to progressively mature towards the RLFC and Hammerfest Basin. The formation has not yet matured in the eastern part of the Loppa High. The Triassic formations are the most widespread mature source rocks in the area, situated on most of the Loppa High where they terminate at the flanks. The Eastern flank is an exception where the Triassic formations continue to be mature to the eastern part of the Nordkapp Basin. In principle does the progressively older sequences seems to enter the oil window in an eastward direction (Ohm et al., 2008). The Triassic source rock intervals will in general become oil mature where the Hekkingen Formation is early mature and gas mature where Hekkingen is oil mature, implying that Triassic source rock intervals are overmature/gas mature in the western part of the Barents Sea (Ohm et

al., 2008). Still, the Triassic source intervals are considered to be buried too shallow to generate hydrocarbons on the Loppa High. The Carboniferous/Permian formations are mature in a relative narrow zone surrounding the eroded part of the Loppa High. The Permian Ørret Formation is considered overmature in most of the area, being only oil mature in a zone fringing the Loppa High (Ohm et al., 2008). Triassic and Permian/Carboniferous formations are considered oil mature in some of the major basins (Ohm et al., 2008; Vadakkepuliyambatta et al., 2013).

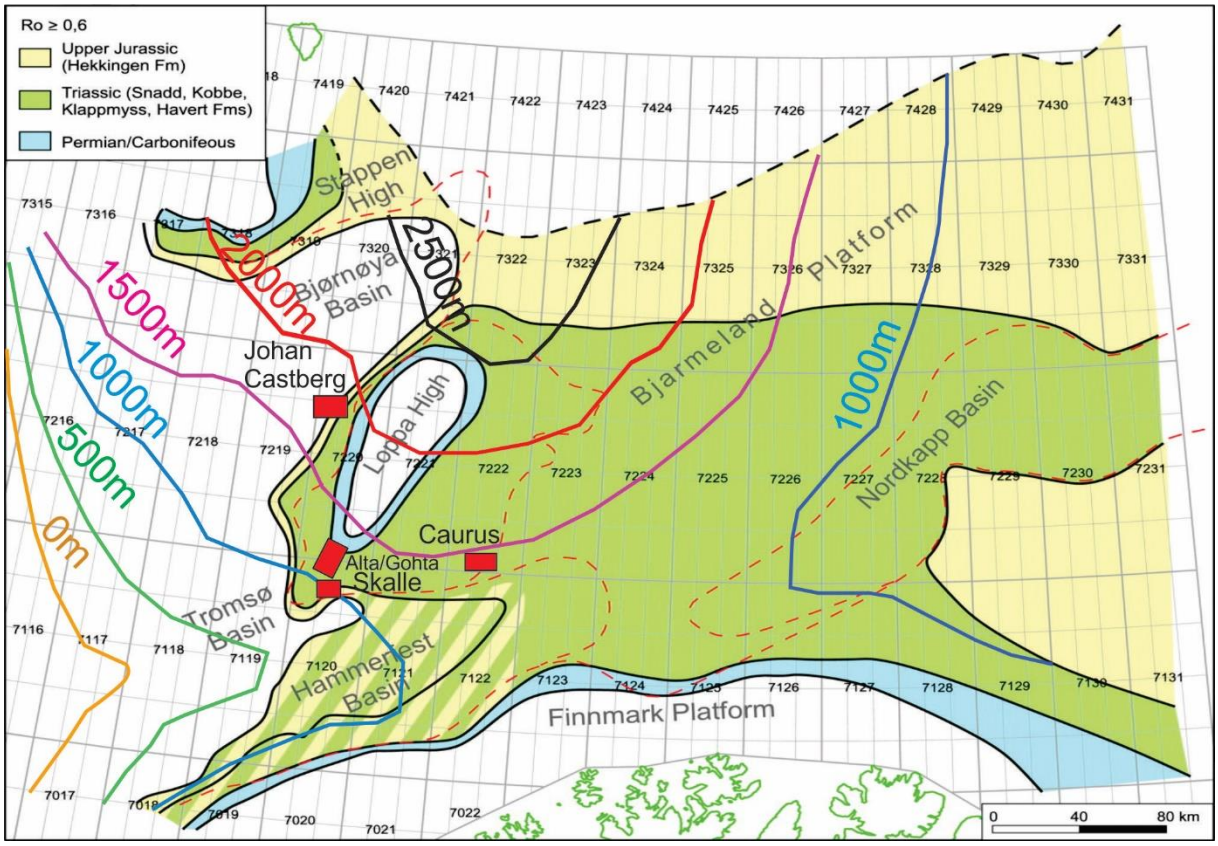

Figure 5.1: Maturity map from the southwestern Barents Sea suggesting where the Carboniferous/Permian, Triassic and Jurassic strata are oil mature. Map is based on data gathered from wells, semi regional maturity trends and depth maps. The colored lines indicate the total amount of uplift and erosion in the area based on vitrinite data. Figure modified from Ohm et al. (2008).

Even though a formation is mature in an area, does not necessarily mean that an oil accumulation originated from the same formation (Ohm et al., 2008). Repeated phases of uplift and erosion during late Cenozoic (Figure 5.1) may result in gas expansion, seal breaching and oil-spilling, which can lead to re-migration of oil into more shallow distal areas. Oil/gas is most likely resting on the flanks of basins with a partly leaking seal against the Loppa High (Ohm et al., 2008), which seems to be the case of the gas discovery Skalle located on the southern flank and the oil/gas discovery Caurus on the southeastern flank. The Alta/Gohta field is located in

the southern part of the Loppa High while the Johan Castberg field is situated west for Loppa High against the Polheim Sub-platform (Figure 5.1).

The shallow gas accumulations identified in the study area have most likely migrated from both local and distal sources. It is hard to determine the source of these accumulations due to the complex geologic history of the southwestern Barents Sea. Multiple source rocks west of Loppa High increases the chance of hydrocarbon generation and the presence of hydrocarbons from different stratigraphic levels (Ohm et al., 2008). The hydrocarbons have probably migrated and re-migrated in different time periods, originated from one or several sources along the margins of the Loppa High. However, geochemical and isotopic characterization of whole oils (saturated hydrocarbons) may be used to identify the source to some extent (Figure 5.2). For instance, the isotopic light oil from the Ladinian Reservoir in Loppa High is correlated to Triassic source rocks (Henriksen, Ryseth, et al., 2011). The same method was used for oil signatures in well 7120/2-2 (Figure 3.4) which contained oil previously argued to stem from a Triassic source rock.

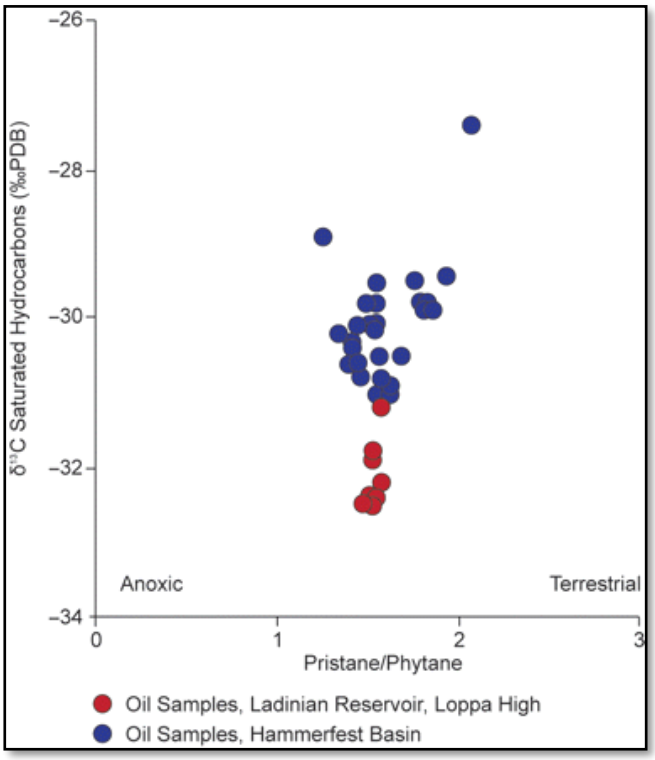

Figure 5.2: Geochemical and isotopic characterizations of saturated hydrocarbons from the Loppa High and the Hammerfest Basin. Figure from Henriksen, Ryseth, et al. (2011).

5.2 Faults

The Loppa High is a diamond shaped N-S trending structural feature, bounded by the E-W trending Asterias Fault Complex (AFC) from the asymmetric Hammerfest Basin to the south, the Ringvassøy-Loppa Fault Complex (RLFC) from the Tromsø Basin to the southwest and Bjørnøyrenna Fault Complex (BFC) from the Bjørnøya basins to the northwest (Figure 5.3). It is a high defined as a result of Late Jurassic to Early Cretaceous-Tertiary tectonism (Gabrielsen et al., 1990). The development started with a Mid-Carboniferous rift topography followed by several phases of uplift, subsidence, tilting and erosion (Gabrielsen et al., 1990). Gradual onlapping took place before the rapid subsidence and deposition of the Upper Triassic succession (Snadd Formation) (Larssen et al., 2002).

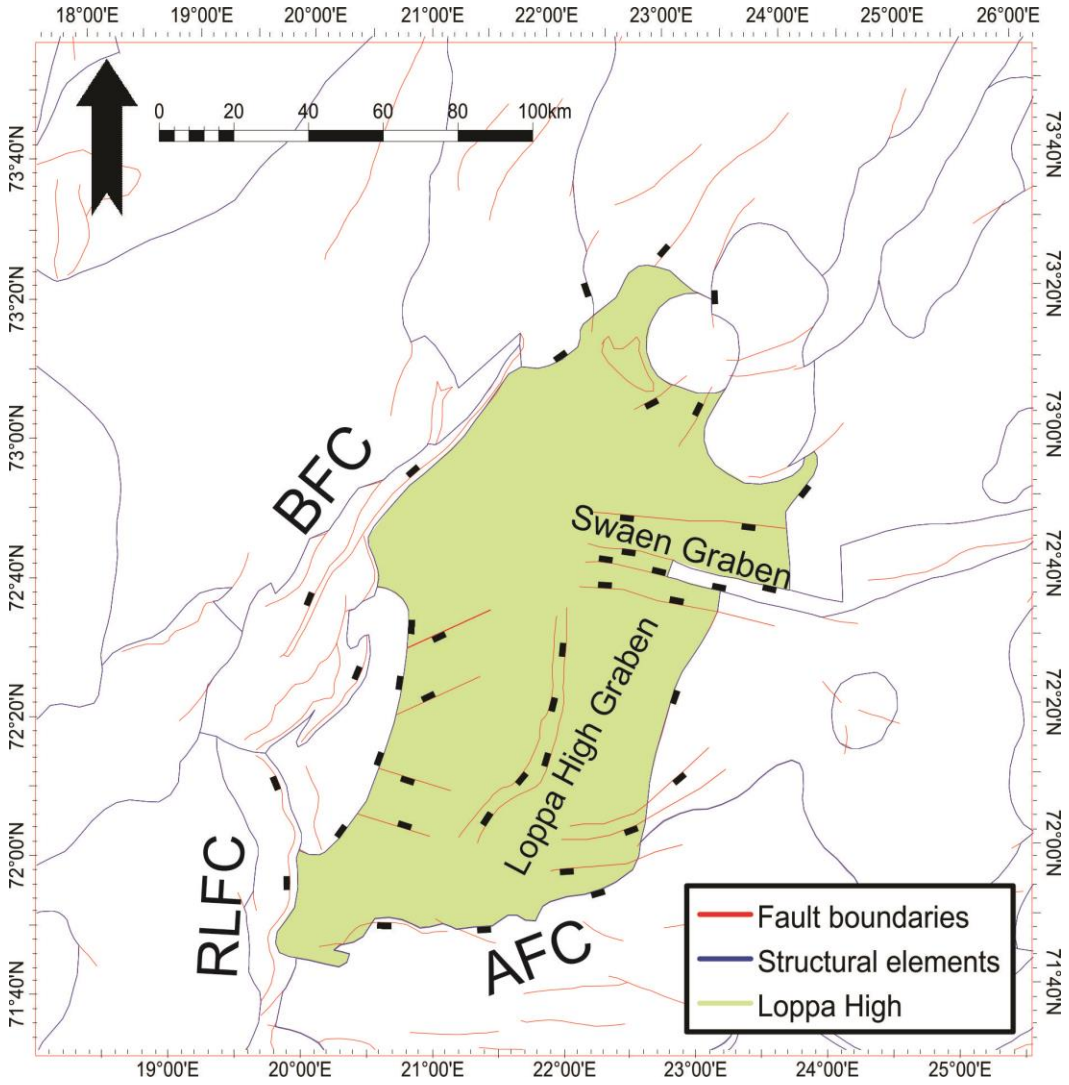

Figure 5.3: Overview map of major faults within the study area.

In Cretaceous led episodes of uplift to tectonic inversion of the rift basins (Indreværet al., 2017). The structures are reported to be of early Barremian to mid-Albian age (131 – 105 Ma) and are related to extensional boundary faults along the margins of the Loppa High (Figure 5.4)(Indreværet al., 2017). Inversion is interpreted to be the result of uplift of the high along its inclined boundary faults, resulting in space accommodation problems. The asymmetric margin configuration have probably led to a bulk clockwise rotation of the high. The cause of uplift is not fully understood, but it is suggested to be linked to the extreme lithospheric thinning in basins to the west (Indreværet al., 2017).

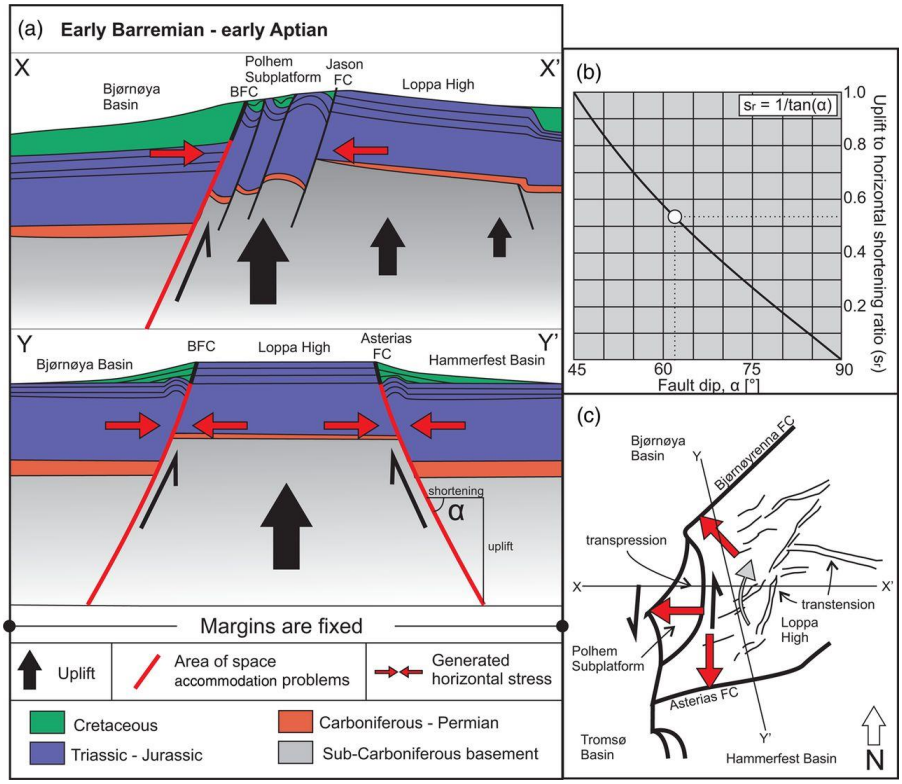

Figure 5.4: ***a)*** *Early Barremian – Early Aptian uplift of the Loppa High.* ***b)*** *Diagram showing uplift to horizontal shortening ratio.* ***c)*** *Plan view of the region showing the different orientations of the generated horizontal stress. Figure from Indreværet al. (2017).*

The western part of the Loppa High area is constituted by the Polheim Sub-platform, which is an area heavily deformed by faulting. It was downfaulted relative to the crest of Loppa High in Early-Middle Triassic (Gabrielsen, 1984). During the creation of the RLFC, the Polheim Sub-platform slid westward and formed the structural pattern of rotated fault blocks (Gabrielsen et al., 1990). Upper Permian-Lower Triassic infill of asymmetric troughs between the blocks indicate renewed movements on the fault system associated with tilting and erosion (Worsley, 2008). Its stratigraphic and structural framework probably makes it the most interesting area regarding fluid migration and fluid flow systems in the area.

In order to understand fluid leakage in the area is it essential to discuss the tectonic evolution. This will give a better overview of fault development. In the results chapter were faults subdivided into deep-seated and shallow faults, which will be classified further in the following subchapters. Gabrielsen (1984) introduced a classification of fault systems (Table 5.1) based on the degree of basement involvement, tectonic significance and reactivation. The identified deep-seated faults will be discussed in relation to this fault classification-system.

First class	Basement involved	Regional significance	Reactivated	Separate areas of different tectonic outline
Second class	Basement involved	Semi-regional	Reactivated / not reactivated	Separate areas of different tectonic outline
Third class	Basement detached	Local significance	Not reactivated	Does not separate areas of different tectonic outline

Table 5.1: Classification of fault systems. Table from Gabrielsen (1984).

5.2.1 Classification and origin of deep-seated faults

The deep-seated faults in survey SG9810 have their lower termination points below the top of the Ørn Formation, reaching the basement. They have in general an ESE-WNW and NE-SW strike orientation and are most likely linked to deeper structures. They are best defined below the top Ørn Formation and the fault throws look to be limited within the same strata. This indicates little reactivation and that they are of little regional significance. It is important to add that there is also a fault reaching the shallower strata (URU), and other faults potentially reaching the same strata are not excluded. Faults penetrating the URU may indicate a tectonically active basin after the onset of glaciations in the Plio-Pleistocene. These faults belong to the second class faults of Gabrielsen (1984).

The faults in this area are seated on top of the Loppa High in the transition to the Polheim Sub-platform, resulting in formations appearing at very shallow depths compared to areas further west. Many formations are also missing, probably due to erosion. Initiation probably occurred in Late Paleozoic by looking at the faults extent, the faults extending from Basement to the top Ørn Formation is most likely the result of Permian to Early Triassic rifting which stopped the regional subsidence in the area (Faleide et al., 1993; Gudlaugsson et al., 1998; Worsley, 2008). An earlier rift phase in the Middle Carboniferous also took place which led to fault-bounded subsidence and half-graben formation on the southern part of Loppa High (Worsley, 2008). However, the possibility of this rift phase being the origin of these faults is eliminated due to

the stratigraphic-interval affected. Faults terminating at shallow depths may have been initiated in the Middle-Late Jurassic when the Atlantic rifting propagated northwards and led to a change in the extensional stress field (Faleide et al., 1993; Gudlaugsson et al., 1998). The southern ESE-WNW faults follow the trend of the Asterias Fault Complex and may be linked to this movement. The NE-SW faults could be linked to Bjørnøyrenna Fault Complex which was most likely reactivated in Late-Cretaceous-Paleocene when the opening of the Norwegian-Greenland Sea resulted in strike-slip movement along the De Geer Zone (Faleide et al., 1993; Gudlaugsson et al., 1998; Worsley, 2008).

Deep-seated faults in survey SG9804 have a SE-NW orientation, terminating at the top Snadd Formation. They extend down to the Havert Formation and are mainly situated in the northern parts. The faults are related to the Swaen Graben which is made of two opposing normal faults trending in the same direction. The graben is found in the northeastern corner of the Loppa High, extending through the Eastern Flexure and towards the Norvarg Dome. Since Triassic formations like Havert, Klappmyss and Snadd are affected did the graben most likely form in the Jurassic. It has probably been active or reactivated multiple times since initiation, being classified as first and second class faults (Gabrielsen, 1984).

In survey SG9803 and OMV09M01 do the deep-seated faults have a NE-SW and E-W orientation. In the northern parts of survey SG9803 do the faults extend and terminate below the top Kobbe Formation while terminating at shallower depths above the top Kobbe Formation in the southern parts. This is probably due to the Asterias Fault Complex between the Loppa High and the Hammerfest Basin. The strata is clearly dipping in a southern direction forming an onlap basin. The faults in both the surveys appear to be basement involved and of regional significance, a first class fault (Gabrielsen, 1984). Since the fault throws increase with depth, have they probably been active/reactivated multiple times. The fault terminating below the top Kobbe Formation suggest an initiation older than Triassic (Anisian) age while the shallower faults suggest a younger initiation. The shallower faults most likely initiated during the onset of the Kimmerian tectonic rift phase in Middle-Late Jurassic which resulted in a transtensional regime and updoming along the AFC.

5.2.2 Origin of shallow faults

The shallow faults are normally confined to the upper part of Triassic or the Torsk Formation (Paleocene-Eocene age). These faults terminate at or right below the URU, occurring within the upper 1500 ms (TWT). This implies that some of the faults occurred prior to the onset of Plio-Pleistocene glaciations which the URU represents. Deep-seated faults can be linked to the formation of shallow faults (Ostanin et al., 2012), which is probably why the shallow faults have the same orientations. However, the occurrence of shallow faults should not be seen as completely controlled by the deep-seated faults. The shallow faults in the area might have their origin from the tectonic readjustments related to the opening of the Norwegian-Greenland Sea, in Late Eocene (Faleide et al., 1993; Ostanin et al., 2012; Vorren et al., 1991).

5.3 Fluid migration and relationship with faults

Fluid flow is mainly driven by pressure differences, where fluids will migrate from areas with high pressure to areas with lower pressures (Bjørlykke, 1993). Fluid migration is a two-phase process, where the primary expulsion of hydrocarbons happens as a result of an increased pressure inside the source rock due to kerogen being altered into petroleum (Bjørlykke, 1993). The buoyancy differences will then drive the hydrocarbons upwards if possible, either along zones of weakness (e.g. fault planes and fractures) or along carrier beds that have sufficient permeability and porosity. Continuous leakage may form accumulation in shallower strata or flow to the overlying beds and leak out at the seabed (Bjørlykke, 1993).

Several indications of fluid flow were described in the results chapter. Gas chimneys, amplitude anomalies and pockmarks are most likely related and connected in the study area (Figure 5.5). Amplitude anomalies found on top of faults, on top of gas chimneys and at shallow depths where basins and/or clinoforms truncate support this evaluation. Acoustic masking and acoustic pipes in the seismic data may be an important indicator for fluid migration (Ligtenberg, 2005; Løseth et al., 2009; Vadakkepuliyambatta et al., 2013). Structures that facilitate fluid migration will be discussed below.

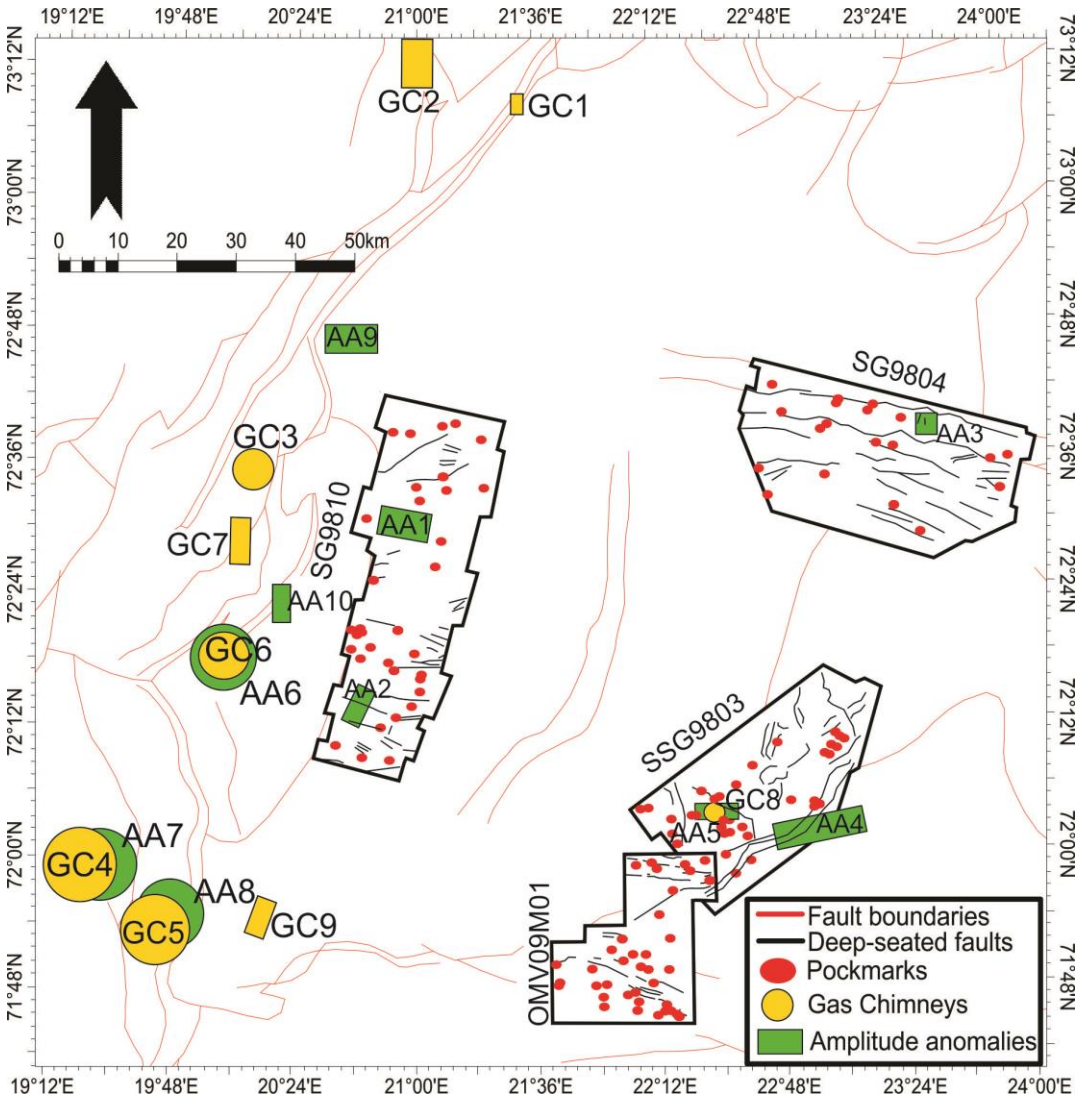

Figure 5.5: Overview of fluid flow features and faults within the study area. The distribution of fluid flow features show a relation to the faults.

5.3.1 Vertical fluid migration along gas chimneys

In chapter 4.3.2 were several gas chimneys (GC1-GC9) identified and described (Figure 4.24). Acoustic masking and chaotic reflections are often located inside these chimneys representing gas saturation and leakage pathways for upward migration of free gas from depths to shallower levels (Andreassen, 2009; Løseth et al., 2009; Rajan et al., 2013). Gas chimneys are also important in the sense that they may pose as a drilling hazard due to high-pore fluid pressures (Heggland, 1998; Løseth et al., 2002). It is important to add that attenuated seismic signals below shallow gas accumulations can result in vertical wipe-out zones and should not be mistaken as gas chimneys. By looking at the vertical extent and indications of gas like push-downs is it possible to differentiate between these two occurrences. Gas chimneys should also not be mixed with salt structures. These are quite common in the SW Barents Sea, which can

cause similar seismic signatures (Laberg & Andreassen, 1996). The main observation that differs gas chimneys with salt structures is their negative polarity at their upper termination.

Gas chimneys GC1-GC7 are situated in the western part of the study area (Figure 5.5). The south-western corner of the Loppa High is known to form a chimney-network connected to faults (Rajan et al., 2013). It is hard to tell where these chimneys terminate due to their deep origin and acoustic masking by upward migrating gas, but an estimate of 3000-4000 ms (TWT) in the Jurassic/Triassic Strata seems reasonable. GC2 is significantly smaller than the other gas chimneys and has a base at 2000 ms (TWT). How far down the gas chimneys extend is crucial for understanding their source and origin. The maturity map (Figure 5.1) from chapter 5.1 indicates that the Upper Jurassic Formation and the Triassic Formations are mature along the western fringe of the Loppa High. This suggests that the hydrocarbons in this area have a source of Jurassic and Triassic age, most likely the Hekkingen, Snadd and Kobbe formations (Ohm et al., 2008). However, the hydrocarbons also might be from a deeper source. Gas can migrate vertically through permeable faults and laterally along sub-horizontal pathways within permeable layers (Andreassen, 2009; Løseth et al., 2009).
Gas Chimney GC8 is located in the southeastern part of Loppa High (Figure 5.5). It is hard to tell where the zone of acoustic masking terminates, but a base at approximately 1500-2000 ms (TWT) in the Triassic strata (Figure 4.31) looks to be the case. The Kobbe Formation which is found at 1600 ms (TWT) is mature in the area (Figure 5.1) and could be the source of the feature. This is also most likely the scenario for Gas Chimney GC9 (GC9 terminates at 1800 ms (TWT) on top of the Kobbe Formation). An origin from another stratigraphic interval is not excluded, and the Upper Jurassic Hekkingen Formation is present and mature in a nearby basin truncating the Loppa high (Figure 4.37). It is possible that fluids have re-migrated along faults and carrier beds.

The interpreted gas chimneys have their upper termination varying from 600-1000 ms (TWT) (Table 4.3). While GC1, GC2, GC4 and GC5 terminate in Cretaceous (probably within the Kolmule Formation), terminates GC3 and GC6-GC9 within the Torsk Formation and at the URU. High amplitude reflections are observed directly above the chimneys, indicating potential presence of hydrocarbons. Push-downs are also observed within the chimney structures, which decrease in size from shallow to deeper stratigraphic levels. This probably indicates changes in the amount of gas within the chimney. Waveform changes and a lowering of both the seismic velocity and bulk density suggest a change in fluids, resulting in gas accumulation below an

impermeable barrier (Karin Andreassen et al., 2007; Ligtenberg, 2005). Since the gas is prevented from migrating to shallower depths will a migration shift from vertical to lateral take place. This evaluation is supported by the large horizontal extent of the amplitude anomalies on top of the gas chimneys, especially shown on top of gas chimneys GC3-GC7 (Figure 4.26-4.30). It is worth mentioning that a junction of faults with different orientations may enable fluids to travel through otherwise impermeable layers (Rajan et al., 2013).

The distribution of the identified gas chimneys appear to be controlled by underlying faults. Gas chimneys are often found in areas of high strain, where reactivation of faults can lead to fault seal failure and seal breaching (Rajan et al., 2013). Gas chimneys GC1-GC3, GC6-GC7 occur above major NE-SW striking fault boundaries while GC4-GC5 occur above major SE-NW striking fault boundaries (Figure 5.5). GC8 occur above a deep-seated fault striking SE-NW and GC9 do not occur above any interpreted faults. However, faults appear to occur inside the GC9 (Figure 4.32). The NE-SW striking normal faults are most likely the result of the Bjørnøyrenna Fault Complex, which follows the same structural trend. SE-NW faults are probably due to the Ringvassøy-Loppa Fault Complex. Even though GC8 is situated above a SE-NW striking fault, it is most likely related to the nearby ENE-WSW striking Asterias Fault Complex to some degree.

Since the amplitude anomalies on top of GC2-GC7 are confined to the Torsk Formation, it is a high possibility that the gas chimneys formed in Late Paleogene. Initiation probably occurred with the onset of the Plio-Pleistocene glaciations in the fault systems situated on extensional basin margins. Initiation of GC1 most likely occurred in an earlier time period by looking at the affected stratigraphic intervals. It is hard to tell when initiation started for GC8 and GC9 due to erosion. These gas chimneys have high amplitude reflections mainly confined at the URU or in the lower Triassic strata. The western part of the Loppa High is significantly more faulted than the eastern area, which looks to be correlated to the occurrence of gas chimneys.

5.3.2 Vertical fluid migration along faults

The Barents Sea is a region reported to have a large number of open faults due to removal of overburden by glaciers and resulting uplift (Chand et al., 2012). Faults and fractures tend to be more permeable than the surrounding rock, and fractures will often develop above overpressured reservoirs (Berndt et al., 2003; Cartwright et al., 2007). Faults and fractures may act as pathways for fluids across low-permeability sedimentary formations as they are very common fluid conduits (Figure 5.6) (Arntsen et al., 2007; Cartwright et al., 2007; Vadakkepuliyambatta, 2014). A petroleum system bound by fault traps can start to experience

leakage due to tectonic activities, leading to transport of fluids to a shallower subsurface or into the water column (Henriksen, Ryseth, et al., 2011). It is critical whether a structure is dry or filled with hydrocarbons in the oil and gas industry (Ligtenberg, 2005). High amplitude anomalies, indicting gas accumulations, are frequently associated with leaking faults. These anomalies occur along their fault plane or in the adjacent sedimentary bedding (Løseth et al., 2009; Vadakkepuliyambatta, 2014). A recent study from the Loppa High (Chand et al., 2012) reported seepage of gas into the water column indicating that gas migration is still active through open faults.

Figure 5.6: Schematic model of vertical fluid migration along faults ending in accumulations (amplitude anomalies). Fluids migrate along the fault planes characterized by acoustic masking. The model is based on Figure 4.20.

In chapter 4.3.1 were potential leakage zones along faults (PLZ) presented. The majority of these zones have acoustic masking along the faults with high amplitude reflections observed in the strata above or adjacent to the fault plane. This indicates that migration has taken place along the faults before the migrating gas has encountered permeable beds. Amplitude anomalies AA2-AA10 are situated on top of faults, suggesting migration pathways along these faults from deeper levels (Figure 5.5). The overview map (Figure 4.16) showed that this type of event was quite common, concentrated along the flanks of Loppa High, which represents big fault boundaries and structural elements separating the Loppa High platform with major basins. The structural geometry with enclosed basins and subsurface formations onlapping the Loppa High provide good conditions for focused fluid flow (Chand et al., 2012). In addition, the high concentration in the western part is related to the westerly-dipping extensional fault system while the eastern part is related to the Swaen Graben. Several factors are involved in leakage

along faults process. Migration along individual faults is argued to occur along zones of weakness within the fault zone, and not along the entire fault plane (Ligtenberg, 2005). These weaknesses includes irregularities on the fault plane, small-scale features associated with faults and intersections with other faults (Ligtenberg, 2005).

In the western part of the study area, where most of the large and prominent amplitude anomalies (below the URU) and gas chimneys occur, will the features in general be located above or adjacent to NE-SW and SE-NW trending faults. This coincides with the structural trends of the BFC and RLFC, suggesting a preferred fault trend in the area. Several gas flares occur along RLFC, indicating open fractures and active fluid flow (Chand et al., 2012). Observations of gas flares along regional fault complexes outside pockmark regions indicate gas only escaping from faults (Chand et al., 2012). The NE-SW trending faults were probably sealed due the opening of the Norwegian-Greenland Sea, causing a change in orientation of the stress axis in the Paleocene-Eocene (Ostanin et al., 2012). The same event led to uplift and erosion of the shelf, resulting in fault reactivation and tilting of deep reservoirs which could potentially affect the sealing ability in a negative manner (Ostanin et al., 2012; Vadakkepuliyambatta et al., 2013). Structural traps, such as faults, are thought to be quite sensitive to uplift and erosion (Henriksen, Bjørnseth, et al., 2011). Leakage along rotated fault blocks occur frequently in the area, but it is important to add that fluid leakage can also occur with the fracturing of the cap rock (Vadakkepuliyambatta et al., 2013). Seepage pipes (Figure 4.23), which is an indication of fluid leakage, can be formed if a fluid accumulation experiences a sudden release of pressure (Vadakkepuliyambatta et al., 2013). The western part of the study area is a great example on how its structural evolution affects the density of fluid flow features and fluid flow systems. Large fluid flow systems suggest the presence of significant hydrocarbon reservoirs in the subsurface (Vadakkepuliyambatta et al., 2013).

Amplitude anomalies along the URU occurs frequently on top of the Loppa High (AA1, AA2 and AA5) (Figure 4.34, 4.35 and 4.38). Shallow faults can help deeper-seated faults to transmit fluid to shallow levels (Ostanin et al., 2012), and have most likely allowed gas to re-migrate from accumulations in the Torsk Formation up to the URU. However, shallow faults are only observed related to AA2 (Figure 4.35) so another migrating process is also possible. The URU is probably acting as an impermeable barrier, resulting in horizontal fluid migration (Rajan et al., 2013). Glacial sediments are generally denser and less porous, explaining the trapping mechanism. This is illustrated in the southern amplitude anomaly in Figure 5.6.

5.3.3 Lateral fluid migration

Clinoforms truncating the URU are observed in the study area (Figure 5.7), often located at the flanks of the Loppa High with a dip towards the adjacent basins. In the western part of the study area, the seismic stratigraphy indicates shallowing from all directions toward the Loppa high at all stratigraphic levels. The base Tertiary reflector terminates at the Loppa High and only a very thin section of the Tertiary sediments overlies the Jurassic sediments.

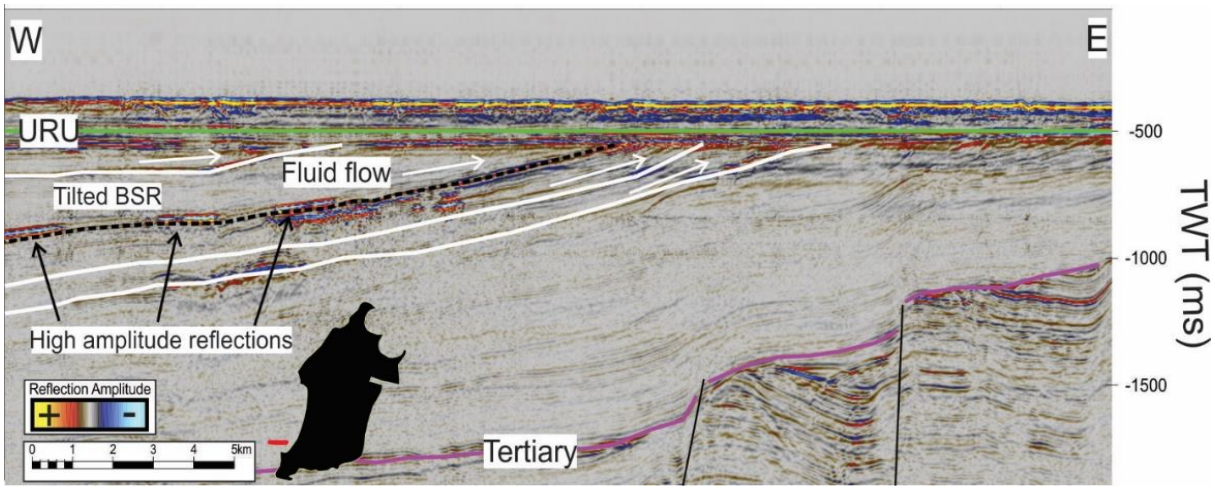

Figure 5.7: Prograding strata (clinoforms) dipping to the west. White arrows indicate direction of fluid flow along intra-Tertiary permeable formations. The black dotted shows a potential tilted BSR. Red line outside the polygon indicates the position of seismic profile.

In the Paleocene-Eocene transition, a southwards progradation commenced along the uplifted and eroded Loppa High (Vorren et al., 1991). The Loppa High has most likely served as a sediment source to the surrounding areas. Clinoforms along the south-western flank of the Loppa High indicate a south-westward transport of sediments from the Loppa High towards the Hammerfest basin (Figure 5.8)(Vorren et al., 1991).

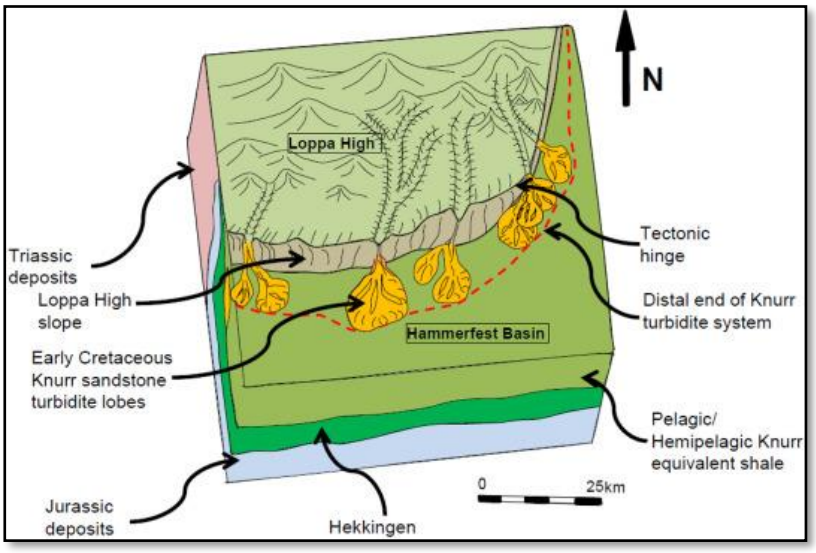

Figure 5.8: Depositional model as the result of progradation from Loppa High to the Hammerfest Basin. Figure from Sattar et al. (2017).

The clinoforms terminating at the URU are limited to the Cenozoic era. This succession is mainly comprised of horizontal layers of siltstone, claystone and sandstone (Vorren et al., 1991). The siltstone and claystone may act as impermeable barriers, preventing fluids/gas to migrate further while sandstones, known to have good reservoir qualities (being porous and permeable), can work as migration pathways. Amplitude anomalies (AA1, AA7, AA8 and AA9) are found along these clinoforms, promoting lateral fluid migration in the area (Figure 4.34, 4.40, 4.41, 4.42). This is also the case for amplitude anomalies on top of certain gas chimneys (Figure 4.26, 4.27, 4.28**b**). The clinoforms in the western and south-western part of the study area will often have anomalous strong amplitudes that can be traced down to the lower Torsk Formation. These high amplitudes will occasionally mimic the clinoforms (Figure 5.7), indicating that gas has not only migrated vertically, but also has followed the sub-horizontal pathways within the dipping layers. The steep clinoforms in the western area have most likely less potential migrating over longer distances than the more gently dipping clinoforms in the eastern area. The Western area is known to be highly faulted and have supposedly fed fluids into the clinoforms in the area. The occurrence of high amplitude anomalies in the eastern area could be due to the gentle dipping clinoforms, transporting fluids from more faulted areas.

5.4 Shallow gas accumulations and gas hydrates

The SW Barents Sea is a unique area due to its evolution-history with unloading, mostly caused by erosion and deglaciation, removing thick layers of sediment from the seabed (Chand et al., 2012). This resulted in uplift, opening of pre-existing faults and creation of new ones, leading to fluid migration which led to patchy, high amplitude reflections representing the BSR (Chand et al., 2012; Rajan et al., 2013). The BSR represents the transition between gas hydrates and the underlying free gas, and marks the base of the GHSZ (Andreassen, 2009; Chand & Minshull, 2003; Rajan et al., 2013). The origin of shallow gas accumulations relies on the presence of a source rock within the same area or from gas accumulated through secondary migration from stratigraphic and structural traps. Studies have shown that gas hydrates and shallow gas are widely distributed in the Barents Sea, existing in conjunction with deep-hydrocarbon reservoir leakage (Chand et al., 2012; Rajan et al., 2013).

The amplitude anomalies and the termination of gas chimneys occur mostly within intra-Tertiary formations (Torsk Formation) and along the URU, but they are also found in different formations. This suggests that the study area has impermeable barriers situated at several stratigraphic levels, preventing fluids from migrating further. Erosion of different formations

have also most likely played a major role. Their significant lateral amplitude variations probably indicates a heterogeneous distribution of shallow gas.

The amplitude anomalies in the Torsk Formation west for Loppa High occasionally crosscut the westerly dipping clinoforms, and are for the most part phase-reversed and not parallel to the seabed reflection (Figure 4.39). However, other amplitude anomalies like AA1, AA5 and AA10 (Figure 4.34, 4.38 and 4.43) all occur as a sub-horizontal events that mimic the seabed reflection. BSRs normally mimic the seafloor in areas of stable and constant local heat flow where the depth of the BSR is mainly controlled by geothermal gradient and pressure conditions (Rajan et al., 2013). This suggests that there is a change in the gas hydrate stability conditions where unparallel (with respect to the seafloor) amplitude anomalies occur. Variations of fluid flux across deep-seated fault complexes might have caused changes in heat flow, resulting in a shoaling of the BSR, making it tilted (Figure 5.7) (Rajan et al., 2013). Fluid flow along faults is known to induce lateral variations in geothermal gradients, resulting in a significantly varied depth-distribution of the base GHSZ (Rajan et al., 2013). Other studies suggest that the tilted BSR is a shallow gas anomaly due to tectonic uplift after erosion, and not due to gas hydrates or changes in heatflow (Chand et al., 2014). It is most likely part of a diagenetic reflector. The architecture of fluid accumulation and pathways to the surface is possibly controlled by the Opal A to Opal CT transition zone (Chand et al., 2014). This event is especially normal between the Loppa high and the RLFC/BFC where most of the BSRs are located (Rajan et al., 2013; Vadakkepuliyambatta et al., 2017). The largest BSR situated at the western part of the Polheim subplatform is reported to has a total aerial extent of approximately 100km^2 (Vadakkepuliyambatta et al., 2017).

Gas hydrates are only stable given the correct temperatures and pressures and are also affected by factors like water salinity and the composition and charge of the hydrocarbon gases. Stable gas hydrates have the potential to represent impermeable barriers, which explains why accumulations of gas below hydrate layers are common. AA7 (Figure 4.40) and AA8 (Figure 4.41) are examples of this event. As a result occur several shallow gas pockets along the dipping reflectors below the URU, where the strata has been truncated (Rajan et al., 2013). The presence of acoustic masking and pipe structures below the BSR suggests free gas in the area.

The glacial–interglacial cycles in the Cenozoic did in addition to causing fluid expulsion and hydrocarbon migration, also influence the presence of gas hydrates and their stability field depth by causing pressure changes, fluctuations in the sea level and water bottom temperatures (Løseth et al., 2009; Rajan et al., 2013).The onset of glaciations resulted in the Cenozoic gas expansion and reservoir tilting, allowing gas to migrate along faults, chimneys and permeable carrier beds up to the base of the GHSZ and develop gas hydrates (Laberg et al., 1998; Laberg & Andreassen, 1996; Rajan et al., 2013). Fault and chimneys have most likely acted as migration pathways for gas accumulating in hydrates once it enters the hydrate stability zone. In other words, the distribution of the BSR is controlled by focused fluid flow features. Their presence close to the interpreted BSR emphasize the importance of gas source and gas composition in the formation of hydrates (Vadakkepuliyambatta et al., 2017).

5.4.1 GHSZ modeling

The Barents Sea region excluding the Bear Island Trough is reported to be outside the methane hydrate stability field (structure I) due to a shallow water depth (Chand et al., 2008). This is why only structure II gas hydrates are formed where higher order hydrocarbon gases or CO_2 are present along with methane (Chand et al., 2008). As a result will hydrates form as patches wherever stability conditions are met. However, the lack of a clear BSR makes them hard to identify (Chand et al., 2008). The presence of gas-hydrate structure II has been modeled, giving a thickness variation of the GHSZ between 100-900m depending on the gas composition and geothermal gradient (Chand et al., 2008; Rajan et al., 2013). The tilted BSR in Figure 5.7 occurs approximately at a water depth of 340m, coinciding within the range of the modeled GHSZ thickness. The tilt being the result of heat flow and gas hydrates are therefore not completely excluded.

Rajan et al. (2013) argued that gas hydrates are stable at approximately 225-345m depth using the stability model for thermogenic gas compositions. This corresponds to variations in the geothermal gradient for the upper BSR (28.7 °C/km and 23.4 °C/km) and lower BSR levels (37 °C/km and 28.3 °C/km) (Figure 5.9) (Rajan et al., 2013). The gas hydrates are predominantly gas of thermogenic origin since fluid flow is widespread and related to deep-seated faults (Vadakkepuliyambatta et al., 2013).

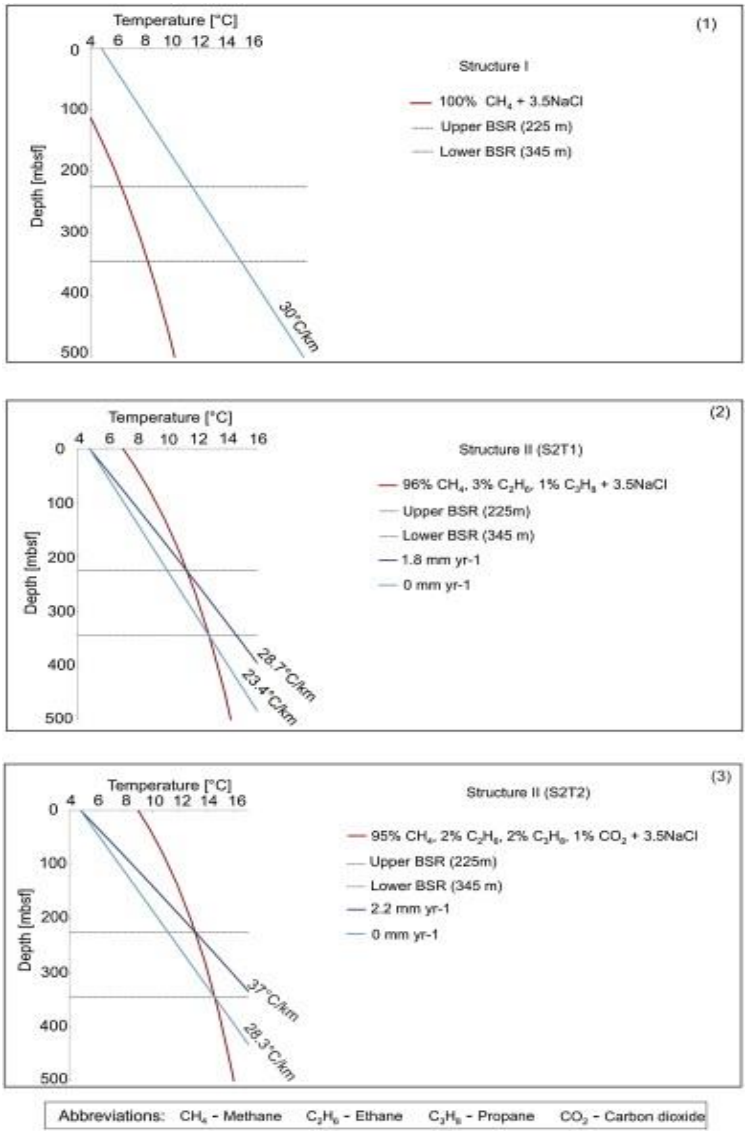

Figure 5.9: GHSZ modeling using different gas compositions and pore water salinity using CSMHYD (Sloan, 1998). The study area is within the stability zone of the gas hydrates formed from high order hydrocarbons (graph 2 and 3) along with methane. Figure from Rajan et al. (2013).

Amplitude anomalies AA2, AA3, AA4, and AA9 (Figure 4.35, 4.36, 4.37 and 4.42) are not related to gas hydrates, as they are present below the GHSZ. Most likely is an impermeable barrier in the formation preventing fluid migration to shallower levels. These anomalies could also simply be due to lithology changes. It is hard to tell if AA3 and AA4 are phase-reversed, but AA2 and AA9 are definitely not. AA2 is located on top of a marginal high, AA3 marks the base of the Swaen Graben while AA4 and AA9 are found in truncating basins, where a lithology change is expected.

The URU occur above the base of the GHSZ, indicating that shallow gas accumulations along the URU could in fact be trapped by a lithological barrier rather than impermeable gas hydrates as stated earlier. Free gas located below the gas hydrates could have migrated along faults and fractures before ultimately being trapped below the URU. This looks to be the case for the amplitude anomalies AA1, AA5, AA6 and partly AA7 (Figure 4.34, 4.38, 4.39 and 4.40),

explaining why many amplitude anomalies along the URU occur directly above deeper anomalies. AA10 is situated above two faults, 100 ms (TWT) below the URU (Figure 4.43). In areas where the URU is absent or lacking thickness, are gas released directly into the water column instead of being trapped, making the URU crucial for shallow gas accumulations in the area.

5.5 Morphological features on the seabed

In chapter 4.5 were several depressions on the seabed identified. These depressions will now be discussed to get a better understanding of their origin and how they are related to fluid flow.

5.5.1 Pockmarks

The circular to sub-circular depressions on the seabed have been interpreted to be pockmark depressions. Pockmarks are widely distributed in the Barents Sea (Chand et al., 2012) and have been identified in all the 3D seismic surveys (Figure 4.44) where they occur frequently.

5.5.1.1 Origin

The SW Barents Sea is known to be affected by uplift and erosion in response to glacial cycles during Cenozoic times (Dimakis et al., 1998; Vadakkepuliyambatta et al., 2013). This resulted in migration of hydrocarbons and spillage where fluids started to migrate into shallow sediments and eventually seeping into the ocean through the seafloor (Doré, 1995; A. Doré & L. Jensen, 1996; Henriksen, Bjørnseth, et al., 2011; Vadakkepuliyambatta et al., 2013). Since the area was heavily glaciated in the past is the appearance of iceberg plough marks and furrows (scours) normal in the study area, which are great examples on how glaciers and detached icebergs can alter the seabed. The plough marks can be tens of kilometers long, giving an idea of the forces behind these processes. The elongated depressions are similar to the circular to sub-circular depressions (pockmarks) in terms of depth and width, but not in length. Pockmarks are occasionally located within plough marks (Figure 5.10), probably due to plough marks releasing pressure from the subsurface, triggering gas to migrate (Judd & Hovland, 2009). It is important not to mix these two kind of features. While plough marks have a glacigenic origin are the pockmarks thought to be a result from seepage of gas and pore fluids in soft sediments (Chand et al., 2009; Judd & Hovland, 2009; Vadakkepuliyambatta et al., 2013). This is also most likely the case for depressions on the URU (paleo-pockmarks).

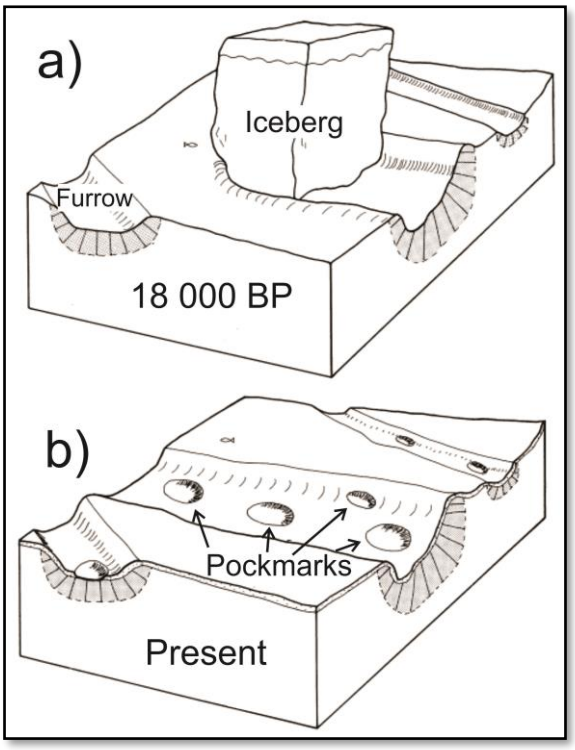

Figure 5.10: ***a)*** *Iceberg ploughs the seabed, creating furrows. This is assumed to be the case in the Barents Sea 18 000 years BP.* ***b)*** *A thin layer of fine-grained sediments remain at the ice-ploughed surface in present time. Pockmarks are located within the furrows. Figure modified from Hovland and Judd (1988).*

Even though pockmarks are most likely the result of focused fluid flow are other processes not completely excluded. The pockmarks could have been formed by freshwater streaming through impermeable units. Freshwater have the potential to be conducted from land to the seafloor through porous deposition with permeable units (Whiticar & Werner, 1981). However, this is unlikely due the distance between the study area and land. Pockmarks also may be caused by dewatering in soft cohesive sediments on the seafloor where slopes are too gentle to allow mass movement. Pore-water can stream up and form a depression on the seafloor if the pressure is sufficient (Harrington, 1985). Depressions formed from dewatering processes are normally 30-40m in diameter with a depth of 1-2m (Harrington, 1985). This is also unlikely the case due to the size of the interpreted pockmarks. High amplitude reflections underneath the pockmarks (Figure 4.45, 4.47) suggest the presence of gas and fluid flow. Absence of high amplitude anomalies suggests fluids ascending directly to the seabed.

Pockmarks within the study area have most likely been formed as a result of gas expulsion from formations at deeper stratigraphic levels. With the absence of impermeable layers will gas continue to migrate upwards until it reaches the seafloor where it will transport and distribute sediments to the water column or the seafloor (Chand et al., 2009; Hovland et al., 2002; Judd & Hovland, 2009). Pockmarks are absent outside fine-grained soft sediment depocentres, indicating an existence related to the presence of a recording medium (Chand et al., 2012). This

indicates that their formation is more related to the type of seabed sediment than the source path of fluid venting, such as faults (Chand et al., 2009; Chand et al., 2012). The thickness of the sediments control the distribution, size and depth of the depressions (Chand et al., 2009). Pockmarks will often have a thin sediment cover and a penetration down into glaciomarine sediments, indicating that they were formed after the deposition of these sediments and that fluid expulsion was active quite recently (Chand et al., 2012). Underlying glaciomarine deposits that are little influenced by their formation, indicate a formation by seeping fluids (Chand et al., 2012).

5.5.1.2 Distribution

Pockmarks are observed on both the URU and the seabed, indicating episodes of focused fluid flow from Quaternary to present day. The pockmarks have not the same shape and appearance, being circular to elongate, and symmetric to asymmetric. The shape of the pockmarks are most likely influenced by strong bottom currents along the seafloor (Hovland et al., 2002). These bottom currents may lead to an asymmetric appearance, which may be the reason why slumping tends to be limited to one side.

Chand et al. (2012) mentions multiple episodes of fluid flow in the Loppa High area evidenced by gas flares, pockmarks and gas hydrate accumulation. The presence of both inactive pockmarks and active acoustic gas flares demonstrate two different processes that took place after the glaciers retreated from the area. The first process is thought to be the release of gas caused by an increase in the seafloor temperature, leading to gas charged fluids creating the pockmarks. The second process is related to the gas flares where the fluids escape through focused fluid flow along stratigraphic boundaries facilitated by open faults (Chand et al., 2012). Figure 4.49 shows a pockmark on the URU occurring directly underneath a seabed pockmark. This also suggests at least two phases of fluid flow where fluid leakage during the second phase occurred at the same location, using the same conduits. The burial of the URU pockmark suggests that fluid flow ceased before the deposition of Quaternary sediments (Ostanin et al., 2013).

Occurrences of fluid migration along faults, gas chimneys and clinoforms are all represented in the study area. Leakage along these features are thought to be an important factor regarding the formation of pockmarks (Chand et al., 2012; Hovland et al., 2002; Judd & Hovland, 2009). To differentiate between pockmarks formed by these different occurrences is a difficult task, but

Hovland et al. (2002) suggested that pockmarks occurring in chains are the result of fault leakage. This is observed on a few occasions (Figure 4.44). Both shallow and deep-seated faults (mainly oriented in a NE-SW and an E-W direction) are identified in the area, probably related to the distribution of pockmarks to some degree (Figure 5.5).

High amplitude reflections are mentioned earlier to appear below pockmarks (Figure 4.45, 4.47). Some of the high amplitude reflections most likely represent free gas accumulated below impermeable barriers, such as gas hydrates and the URU (Figure 5.11). In time, the gas hydrate layer of accumulated gas may be penetrated by shallow faults, leading to the transport of gas below the GHSZ towards the seabed. The pockmarks are not only distributed above the high amplitude reflections, but tend to be spread out over a large area, suggesting that other migration mechanisms are involved. Lateral migration along clinoforms has possibly allowed gas to migrate large distances away from its source (Figure 5.11).

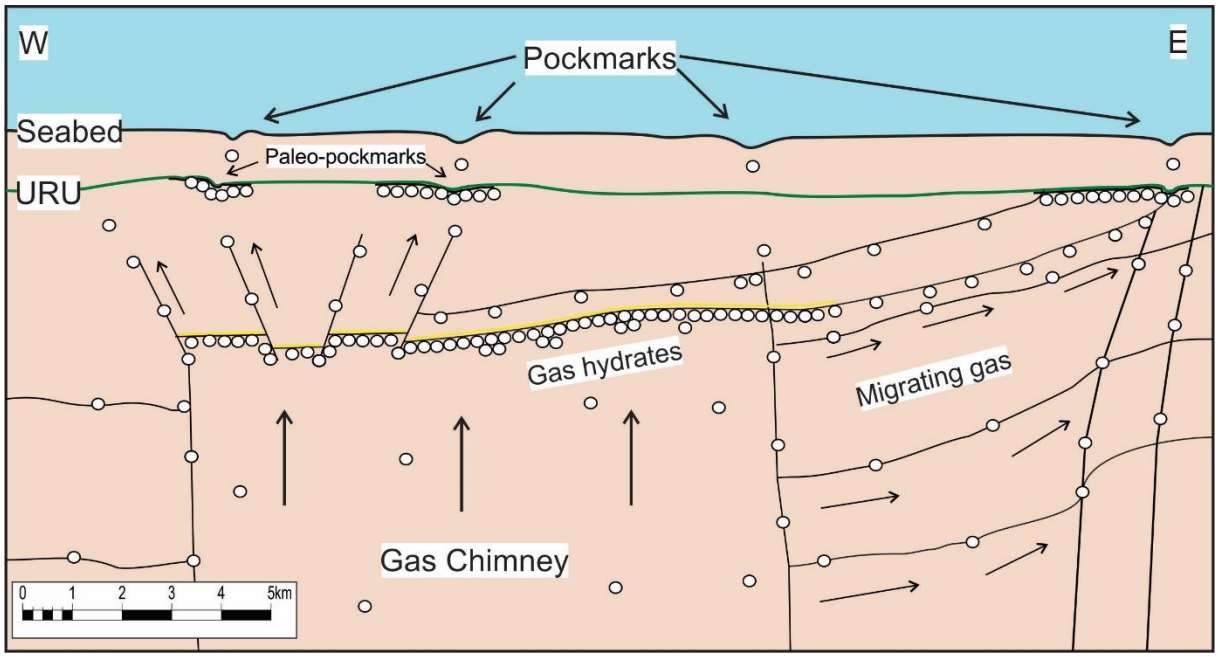

Figure 5.11: Schematic model of the formation of pockmarks. The URU and gas hydrates may create impermeable barriers allowing gas to accumulate. Lateral remigration occurs along clinoforms while vertical remigration occurs along faults. The model is based on amplitude anomaly 8 (Figure 4.41).

The thermodynamic stability of gas hydrates is potentially linked to the formation of pockmarks in the study area. Multiple glacial cycles resulted in temperature and pressure fluctuations, allowing gas hydrates to form (Cavanagh et al., 2006; Solheim & Elverhøi, 1993). The formation of pockmarks in the central Hammerfest Basin is proposed to be related to the loading of a marine ice sheet during last glacial maximum (Figure 5.12**a**)(Ostanin et al., 2013). This also might the case for some pockmarks in survey OMV09M01, which is located on the border

between the southern part of Loppa High and the central northern part of the Hammerfest Basin. During the deglaciation of the ice sheet, the water column pressure dominated the stability of hydrates and an increased seabed temperature probably developed an upward shift of the GHSZ and destabilization of the gas hydrates (Figure 5.12**b**)(Solheim & Elverhøi, 1993). This caused overpressure to develop as gas hydrates melted, resulting in upward migration of free gas, creating the observed pockmarks on the seafloor (Figure 5.12**c**)(Ostanin et al., 2013).

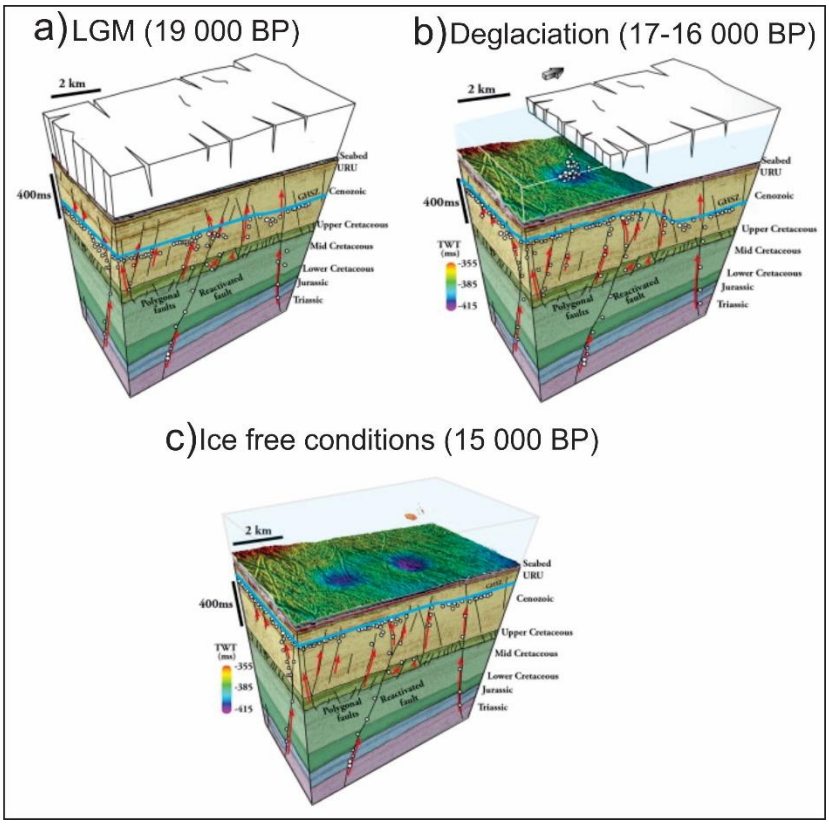

*Figure 5.12: Conceptual model for fluid flow, gas leakage and gas hydrate destabilization during **a)** Last Glacial Maximum: The ice sheet increases the pressure and forms gas hydrates. **b)** Deglaciation: A decrease in pressure causes destabilization of gas hydrates. **c)** Ice free conditions and present day scenario: Fluid migration to the seafloor. Figure modified from Ostanin et al. (2013).*

5.5.2 Mega depressions

The mega depressions identified in chapter 4.5.2 are too large to be classified as pockmarks. They also do most likely not represent mega scale glacial lineations as they appear too local with a geometry not characterizing this type of feature (mega scale glacial lineations are long elongated landforms, typically with a length-width ratio greater than 15:1) (Dowdeswell et al., 2008). While mega depressions M4-M7 appear not to be linked to underlying structures or fluid flow, do M1-M3 have faults, zones of acoustic masking and high amplitude reflections underneath (Figure 4.50**c**). However, the seismic quality related to M4-M7 is low so it should not be completely rejected. Pockmarks are located inside M1-M5 and M7 (Figure 4.49, 4.50, 4.51) arguing for potential fluid flow in the area. The mega depressions are located at water depths between 300-431m. During last glacial maximum did the water depths get shallower as a result of the eustatic sea level change (Butt et al., 2002). Even though indications of fluid flow are observed related to these mega depressions, are they most likely the result of glacial processes. This will be more elaborated in the next section.

The seafloor morphology in the Barents Sea has been described earlier by several authors (Andreassen et al., 2008; Dowdeswell et al., 2008; Knies et al., 2009; Landvik et al., 1998; Ottesen et al., 2005) where mega depressions have been reported to occur (Ottesen et al., 2005). Mega depressions M1-M3 (Figure 4.50) have a sub-circular geometry, which could be interpreted to represent kettle holes (Figure 5.13). These features are formed by the melting of a detached mass of glacial ice that became wholly or partly buried (Bennett & Glasser, 2011).

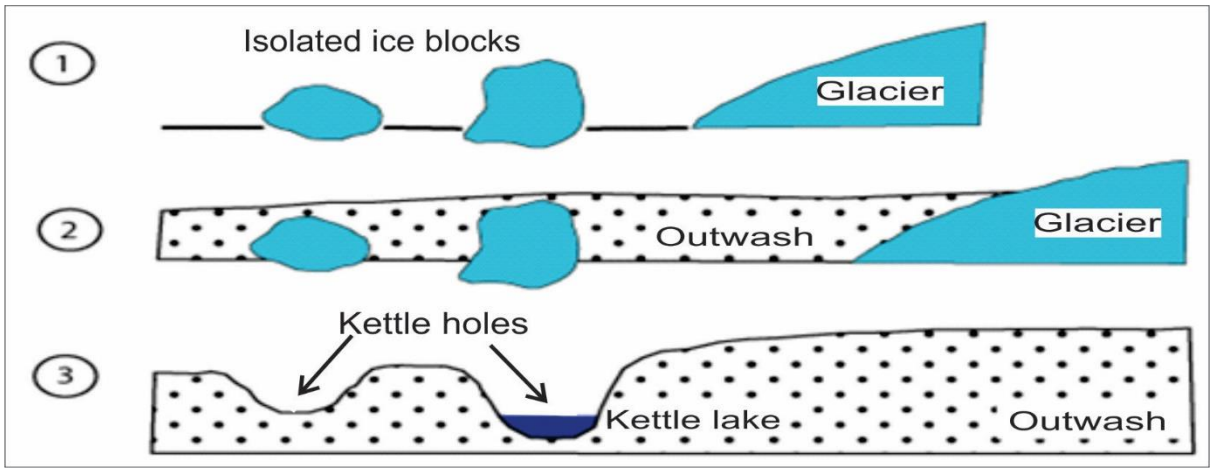

Figure 5.13: The formation of kettle holes: ***1)*** *Ice blocks are separated from the glacier.* ***2)*** *The isolated blocks of ice become wholly or partially buried in outwash if the conditions are right.* ***3)*** *Ice blocks melt, leaving behind holes or depressions which can be filled with water to become kettle hole lakes. Figure modified from Landforms.eu (2018).*

M1-M3 might also be erosive features due to what seems to be displaced material to the surroundings. Hill-hole pairs, which are glacitectonic landforms representing a basic combination of an ice-scooped basin and an ice-shoved hill (Aber et al., 2012), share the characteristics of M1-M3. The hill related to this landform is most likely formed by ice shoved material from the hole, providing indication of ice flow (Ostanin et al., 2013; Ottesen et al., 2005). Similar features have also been described and identified elsewhere in the Barents Sea (Ostanin et al., 2013).

Mega depressions M4-M7 (Figure 4.51) are probably the result of erosional processes since material from the seabed have been removed to some degree. They also show the same orientation (SE-NW) as ice streams in the area (Andreassen et al., 2008; K Andreassen et al., 2007; Ottesen et al., 2005). No distinct hills are observed in relation to these features, decreasing the likelihood of the depressions representing hill-hole pair landforms. However, it is possible that the lack of hills in the area is the result from both glaceiotectonic erosion and long distance material transportation by grounded ice or ice streams (Ostanin et al., 2013).

5.6 Conceptual model

The western part of the Loppa High region is probably the most interesting area regarding fluid migration and fluid flow systems in the area (Figure 5.14). A high concentration of amplitude anomalies related to multiple large gas chimneys support this idea. These features are found in a complex extensional fault system, which has created significant hydrocarbon plays. The distribution of reservoirs and source rocks from the Late Palaeozoic to the Palaeogene in the Barents Sea can according to Henriksen, Ryseth, et al. (2011) be related to three tectonic phases: (1) The Palaeozoic Caledonian Orogeny, which caused uplift to the west, followed by eastward sediment distribution across the shelf, (2) The Late Palaeozoic-Mesozoic Uralide Orogeny which caused widespread clastic deposition and reversal of the sediment distribution pattern, and (3) The Late Mesozoic-Cenozoic rifting and crustal breakup of the western Barents Sea which led to the current basin configuration.

Multiple tectonic episodes then caused the formation of a variety of trap types where extensional fault blocks and gently folded domes have been most prospective (Henriksen, Ryseth, et al., 2011).

The Cenozoic uplift and erosion are related to gas expansion and is probably the main drive mechanism for remobilization of different fluids (Laberg & Andreassen, 1996). This event has

most likely led to fracturing of the sealing rocks (A. Doré & L. Jensen, 1996). The migrating fluids are assumed to have originated from both accumulated reservoirs (secondary migration) and deeper-seated source rocks (primary migration) within Jurassic, Triassic and/or Permian/Carboniferous formations.

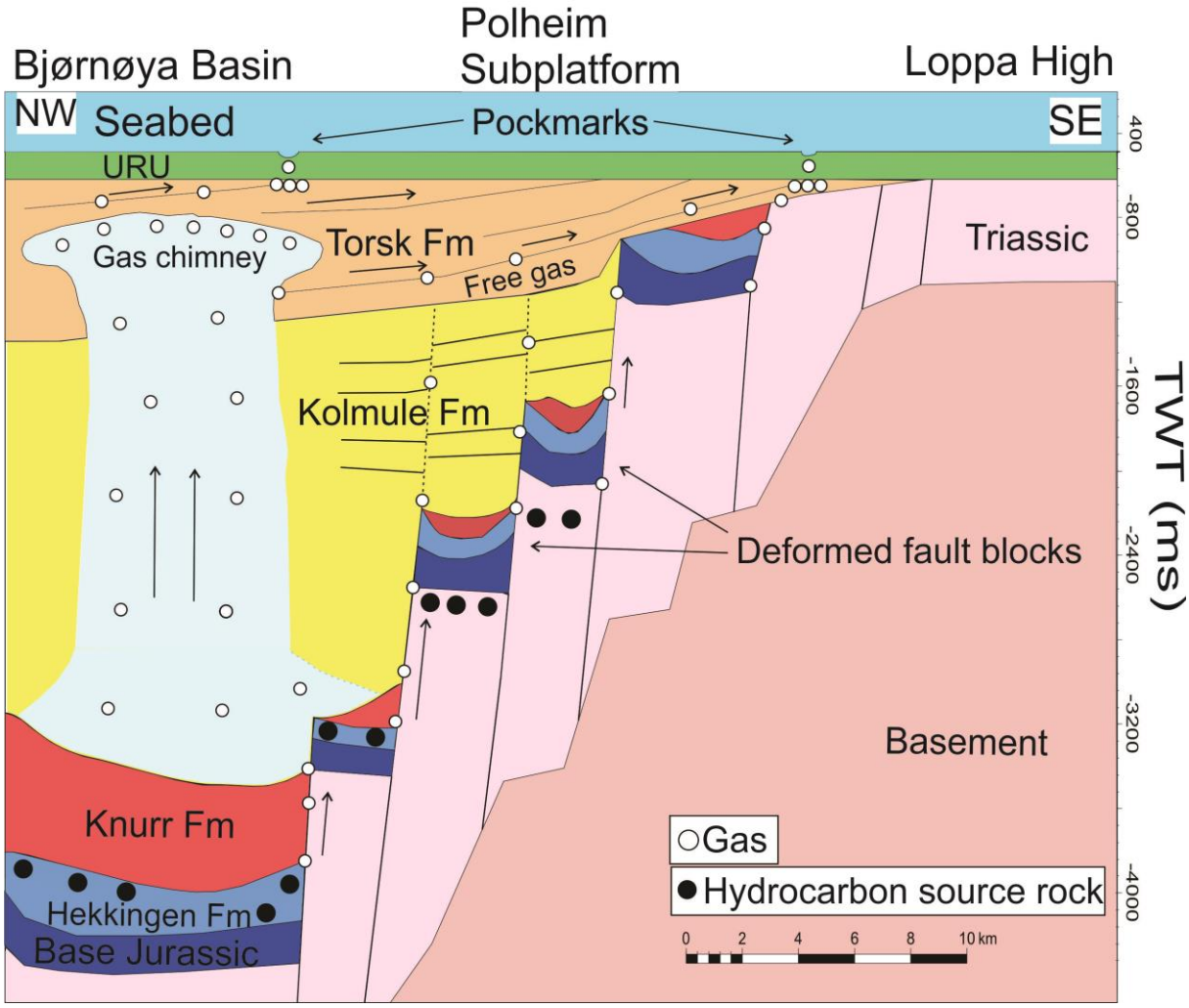

Figure 5.14: Conceptual model showing fluid migration and the stratigraphic- and structural framework in the western Loppa High region. Cretaceous syn-rift fans onlap the underlying marginal marine Jurassic pre-rift reservoirs on the deformed extensional fault blocks. This model can be applied for the Johan Castberg field which is located in the area. The Upper Jurassic (Hekkingen FM) is mature in the northwest while Triassic formations are mature in the southeastern part.

6. Summary and conclusion

Fluid flow is abundant and widespread in the study area (Loppa High region). Interpretion of 3D/2D seismic data allowed mapping of faults, fluid migration features, amplitude anomalies (accumulations) and seabed depressions. A correlation between potential leakage zones along faults (PLZ), gas chimneys and amplitude anomalies in the area show that fluid flow is highly concentrated along the flanks and in the western part. A possible link between the fluid flow features is proposed as their distribution shows a direct relationship to the structural setting of the SW Barents Sea.

- The faults are divided into deep-seated faults and shallow faults, based on their vertical extent and the strata they are confined in. The deep-seated faults were probably initiated during the Permian - Early Triassic rifting and/or the Kimmerian tectonic phase in the Middle – Late Jurassic when the Atlantic rifting propagated northwards. The shallow faults are most likely the result from tectonic readjustments related to the opening of the Norwegian-Greenland Sea, in Late Cretaceous – Paleocene. This event and multiple glacial cycles resulted in multiple episodes of reactivation.
- Mapping of faults, amplitude anomalies and pockmarks suggest that vertical fluid migration occurs mainly along the fault planes of NE-SW and E-W trending faults, often associated with zones of acoustic masking (gas chimneys) at multiple stratigraphic levels.
- Lateral fluid migration, which is primarily observed in the western region, occurs along westerly-dipping Paleogene clinoforms. This allowed fluids to migrate away from the upper termination of faults. Leakage along shallow faults and clinoforms has allowed fluids to reach the seabed.
- Strucutral traps, especially faults, are highly sensitive to glaciations, uplift and erosion, and could have problems to effectively seal the trapped hydrocarbons. This suggests that fluid leakage is influenced by extensional tectonics and by uplift and erosion in response to glacial cycles in Late Cenozoic.
- Other factors controlling the distribution of fluid flow features could be:

  1) The presence of multiple source rocks (the western part has oil mature, gas mature and over-mature source rocks from different stratigraphic intervals).

  2) The occurrence of structural traps (faults).

3) The evolution of sedimentary basins.

- Gas chimneys probably developed after the onset of the Plio-Pleistocene glaciation when uplift and tilting of deeper reservoirs caused spillage of hydrocarbons. These features will often show a BSR at their upper termination, indicating the presence of gas hydrates. The tilted BSR is probably the result of changes in heat flow or might be a diagenetic reflector (an Opal A/CT reflection). The study area is within the stability zone of the gas hydrates formed from high order hydrocarbons (Structure II) along with methane.
- The shallow amplitude anomalies observed in the Torsk Formation might represent accumulations of free gas below a sealing layer of gas hydrates. Accumulations of free gas are also present at the URU, where glacigenic sediments may act as an impermeable barrier. Most of the shallow gas accumulations are related to faults, which may act as conduits for the migration of gas-bearing fluids.
- AA6-AA10 are situated on 2D profiles where no pockmarks have been mapped due to uncertainty and resolutuion. However, AA1-AA5 are located in areas where pockmarks have been established.
- Pockmarks are formed in association with fluid expulsion events, probably where soft sediments can act as a recording medium.
- The thermodynamic stability of gas hydrates is probably linked to the formation of pockmarks in the study area. During glacial-interglacial cycles, the water column pressure and the seabed temperature may develop a shift of the GHSZ, leading to destabilization of the gas hydrates. As a result will high overpressure values allow an upward migration of free gas, creating the observed pockmarks on the seafloor.
- The mega depressions (M1-M7) are thought to be the result of glacial processes, not focused fluid flow. They may represent kettle holes and/or hill-hole pairs. Kettle holes are formed by the melting of a detached mass of glacial ice that became wholly or partly buried while hill-hole pairs represent a basic combination of an ice-scooped basin and an ice-shoved hill.

7. References

Aber, J. S., Croot, D. G., & Fenton, M. M. (2012). *Glaciotectonic landforms and structures* (Vol. 5): Springer Science & Business Media.

Andreassen, K. (2009). Marine Geophysics, lecture notes for Geo-3123. *University of Tromsø, 106*.

Andreassen, K., Hogstad, K., & Berteussen, K. A. (1990). Gas hydrate in the southern Barents Sea, indicated by a shallow seismic anomaly. *First Break, 8*(6), 235-245.

Andreassen, K., Hubbard, A., Winsborrow, M., Patton, H., Vadakkepuliyambatta, S., Plaza-Faverola, A., . . . Mattingsdal, R. (2017). Massive blow-out craters formed by hydrate-controlled methane expulsion from the Arctic seafloor. *Science, 356*(6341), 948-953.

Andreassen, K., Laberg, J. S., & Vorren, T. O. (2008). Seafloor geomorphology of the SW Barents Sea and its glaci-dynamic implications. *Geomorphology, 97*(1-2), 157-177.

Andreassen, K., Nilssen, E. G., & Ødegaard, C. M. (2007). Analysis of shallow gas and fluid migration within the Plio-Pleistocene sedimentary succession of the SW Barents Sea continental margin using 3D seismic data. *Geo-Marine Letters, 27*(2-4), 155-171.

Andreassen, K., Ødegaard, C., & Rafaelsen, B. (2007). Imprints of former ice streams, imaged and interpreted using industry three-dimensional seismic data from the south-western Barents Sea. *Geological Society, London, Special Publications, 277*(1), 151-169.

Arntsen, B., Wensaas, L., Løseth, H., & Hermanrud, C. (2007). Seismic modeling of gas chimneys. *Geophysics, 72*(5), SM251-SM259.

Bennett, M. M., & Glasser, N. F. (2011). *Glacial geology: ice sheets and landforms*: John Wiley & Sons.

Berndt, C. (2005). Focused fluid flow in passive continental margins. *Philosophical Transactions of the Royal Society of London A: Mathematical, Physical and Engineering Sciences, 363*(1837), 2855-2871.

Berndt, C., Bünz, S., & Mienert, J. (2003). Polygonal fault systems on the mid-Norwegian margin: a long-term source for fluid flow. *Geological Society, London, Special Publications, 216*(1), 283-290.

Bjørlykke, K. (1993). Fluid flow in sedimentary basins. *Sedimentary Geology, 86*(1-2), 137-158.

Brown, A. R. (2011). *Interpretation of three-dimensional seismic data*: Society of Exploration Geophysicists and American Association of Petroleum Geologists.

Bulat, J. (2005). Some considerations on the interpretation of seabed images based on commercial 3D seismic in the Faroe‐Shetland Channel. *Basin Research, 17*(1), 21-42.

Butt, F. A., Drange, H., Elverhøi, A., Otterå, O. H., & Solheim, A. (2002). Modelling Late Cenozoic isostatic elevation changes in the Barents Sea and their implications for oceanic and climatic regimes: preliminary results. *Quaternary Science Reviews, 21*(14-15), 1643-1660.

Cartwright. (2011). Diagenetically induced shear failure of fine-grained sediments and the development of polygonal fault systems. *Marine and Petroleum Geology, 28*(9), 1593-1610.

Cartwright, J., Huuse, M., & Aplin, A. (2007). Seal bypass systems. *AAPG Bulletin, 91*(8), 1141-1166.

Cartwright, J., & Lonergan, L. (1996). Volumetric contraction during the compaction of mudrocks: A mechanism for the development of regional - scale polygonal fault systems. . *Basin Research, 8*, 183-193.

Cathles, L., Su, Z., & Chen, D. (2010). The physics of gas chimney and pockmark formation, with implications for assessment of seafloor hazards and gas sequestration. *Marine and Petroleum Geology, 27*(1), 82-91.

Cavanagh, A. J., Di Primio, R., Scheck-Wenderoth, M., & Horsfield, B. (2006). Severity and timing of Cenozoic exhumation in the southwestern Barents Sea. *Journal of the Geological Society, 163*(5), 761-774.

Chand, S., Knies, J., Baranwal, S., Jensen, H., & Klug, M. (2014). Structural and stratigraphic controls on subsurface fluid flow at the Veslemøy High, SW Barents Sea. *Marine and Petroleum Geology, 57*, 494-508.

Chand, S., Mienert, J., Andreassen, K., Knies, J., Plassen, L., & Fotland, B. (2008). Gas hydrate stability zone modelling in areas of salt tectonics and pockmarks of the Barents Sea suggests an active hydrocarbon venting system. *Marine and Petroleum Geology, 25*(7), 625-636.

Chand, S., & Minshull, T. (2003). Seismic constraints on the effects of gas hydrate on sediment physical properties and fluid flow: a review. *Geofluids, 3*(4), 275-289.

Chand, S., Rise, L., Ottesen, D., Dolan, M., Bellec, V., & Bøe, R. (2009). Pockmark-like depressions near the Goliat hydrocarbon field, Barents Sea: morphology and genesis. *Marine and Petroleum Geology, 26*(7), 1035-1042.

Chand, S., Thorsnes, T., Rise, L., Brunstad, H., Stoddart, D., Bøe, R., . . . Svolsbru, T. (2012). Multiple episodes of fluid flow in the SW Barents Sea (Loppa High) evidenced by gas flares, pockmarks and gas hydrate accumulation. *Earth and Planetary Science Letters, 331*, 305-314.

Chopra, S., & Marfurt, K. J. (2005). Seismic attributes—A historical perspective. *Geophysics, 70*(5), 3SO-28SO.

Dewhurst, D. N., Cartwright, J. A., & Lonergan, L. (1999). The development of polygonal fault systems by syneresis of colloidal sediments. *Marine and Petroleum Geology, 16*(8), 793-810.

Dimakis, P., Braathen, B. I., Faleide, J. I., Elverhøi, A., & Gudlaugsson, S. T. (1998). Cenozoic erosion and the preglacial uplift of the Svalbard–Barents Sea region. *Tectonophysics, 300*(1), 311-327.

Doré, A. (1991). The structural foundation and evolution of Mesozoic seaways between Europe and the Arctic. *Palaeogeography, Palaeoclimatology, Palaeoecology, 87*(1-4), 441-492.

Doré, A. (1995). Barents Sea geology, petroleum resources and commercial potential. *Arctic*, 207-221.

Doré, A., & Jensen, L. (1996). The impact of late Cenozoic uplift and erosion on hydrocarbon exploration: offshore Norway and some other uplifted basins. *Global and Planetary Change, 12*(1-4), 415-436.

Doré, A. G., & Jensen, L. N. (1996). The impact of late Cenozoic uplift and erosion on hydrocarbon exploration: offshore Norway and some other uplifted basins. *Global and Planetary Change, 12*(1-4), 415-436. doi:10.1016/0921-8181(95)00031-3

Dowdeswell, J., Ottesen, D., Evans, J., Cofaigh, C., & Anderson, J. (2008). Submarine glacial landforms and rates of ice-stream collapse. *Geology, 36*(10), 819-822.

England, W., Mackenzie, A., Mann, D., & Quigley, T. (1987). The movement and entrapment of petroleum fluids in the subsurface. *Journal of the Geological Society, 144*(2), 327-347.

Faleide, Solheim, A., Fiedler, A., Hjelstuen, B. O., Andersen, E. S., & Vanneste, K. (1996). Late Cenozoic evolution of the western Barents Sea-Svalbard continental margin. *Global and Planetary Change, 12*(1-4), 53-74.

Faleide, J. I., Gudlaugsson, S. T., & Jacquart, G. (1984). Evolution of the western Barents Sea. *Marine and Petroleum Geology, 1*(2), 123IN1129IN5137-1128IN4136IN8150.

Faleide, J. I., Solheim, A., Fiedler, A., Hjelstuen, B. O., Andersen, E. S., & Vanneste, K. (1996). Late Cenozoic evolution of the western Barents Sea-Svalbard continental margin. *Global and Planetary Change, 12*(1-4), 53-74.

Faleide, J. I., Vågnes, E., & Gudlaugsson, S. T. (1993). Late Mesozoic-Cenozoic evolution of the south-western Barents Sea in a regional rift-shear tectonic setting. *Marine and Petroleum Geology, 10*(3), 186-214.

Fossen, H., & Gabrielsen, R. H. (2005). Strukturgeologi. *Fagbokforlaget Vigmostad & Bjørke AS*.

Gabrielsen, R. (1984). Long-lived fault zones and their influence on the tectonic development of the southwestern Barents Sea. *Journal of the Geological Society, 141*(4), 651-662.

Gabrielsen, R. H., Faerseth, R. B., & Jensen, L. N. (1990). *Structural Elements of the Norwegian Continental Shelf. Pt. 1. The Barents Sea Region*: Norwegian Petroleum Directorate.

Goulty, N. (2008). Geomechanics of polygonal fault systems: a review. *Petroleum Geoscience, 14*(4), 389-397.

Gudlaugsson, S., Faleide, J., Johansen, S., & Breivik, A. (1998). Late Palaeozoic structural development of the south-western Barents Sea. *Marine and Petroleum Geology, 15*(1), 73-102.

Guzzetta, G., & Cinquegrana, R. (1987). "Fluid tectonics": a little appreciated facet of buoyancy tectonics. *Tectonophysics, 139*(3-4), 321-324.

Harland, W. B., Anderson, L. M., Manasrah, D., Butterfield, N. J., Challinor, A., Doubleday, P. A., . . . Kelly, S. R. (1997). *The geology of Svalbard*: Geological Society.

Harrington, P. (1985). Formation of pockmarks by pore-water escape. *Geo-Marine Letters, 5*(3), 193-197.

Heggland, R. (1998). Gas seepage as an indicator of deeper prospective reservoirs. A study based on exploration 3D seismic data. *Marine and Petroleum Geology, 15*(1), 1-9.

Henriet, J., De Batist, M., De Bruyne, H., Heldens, P., Huylebroeck, J., Mostaert, F., . . . D'OLIER, B. (1989). Preliminary seismic-stratigraphic maps and type sections of the Paleogene deposits in the Southern Bight of the North Sea. *The Quaternary and Tertiary Geology of the Southern Bight, North Sea. Belgian Geological Survey, Ministry Economic Affairs (Brussels)*, 29-44.

Henriksen, E., Bjørnseth, H., Hals, T., Heide, T., Kiryukhina, T., Kløvjan, O., . . . Sollid, K. (2011). Uplift and erosion of the greater Barents Sea: impact on prospectivity and petroleum systems. *Geological Society, London, Memoirs, 35*(1), 271-281.

Henriksen, E., Ryseth, A., Larssen, G., Heide, T., Rønning, K., Sollid, K., & Stoupakova, A. (2011). Tectonostratigraphy of the greater Barents Sea: implications for petroleum systems. *Geological Society, London, Memoirs, 35*(1), 163-195.

Hindle, A. D. (1997). Petroleum migration pathways and charge concentration: A three-dimensional model. *AAPG Bulletin, 81*(9), 1451-1481.

Hovland, M., Gardner, J. V., & Judd, A. (2002). The significance of pockmarks to understanding fluid flow processes and geohazards. *Geofluids, 2*(2), 127-136.

Hovland, M., & Judd, A. (1988). *Seabed pockmarks and seepages: impact on geology, biology, and the marine environment*: Springer.

Indrevær, K., Gabrielsen, R. H., & Faleide, J. I. (2017). Early Cretaceous synrift uplift and tectonic inversion in the Loppa High area, southwestern Barents Sea, Norwegian shelf. *Journal of the Geological Society, 174*(2), 242-254.

Jakobsson, M., Mayer, L., Coakley, B., Dowdeswell, J. A., Forbes, S., Fridman, B., . . . Rebesco, M. (2012). The international bathymetric chart of the Arctic Ocean (IBCAO) version 3.0. *Geophysical Research Letters, 39*(12).

Judd, A., & Hovland, M. (2009). *Seabed fluid flow: the impact on geology, biology and the marine environment*: Cambridge University Press.

Knies, J., Matthiessen, J., Vogt, C., Laberg, J. S., Hjelstuen, B. O., Smelror, M., . . . Vorren, T. O. (2009). The Plio-Pleistocene glaciation of the Barents Sea–Svalbard region: a new model based on revised chronostratigraphy. *Quaternary Science Reviews, 28*(9), 812-829.

Laberg, J., Andreassen, K., & Knutsen, S.-M. (1998). Inferred gas hydrate on the Barents Sea shelf—a model for its formation and a volume estimate. *Geo-Marine Letters, 18*(1), 26-33.

Laberg, J. S., & Andreassen, K. (1996). Gas hydrate and free gas indications within the Cenozoic succession of the Bjørnøya Basin, western Barents Sea. *Marine and Petroleum Geology, 13*(8), 921-940.

Landforms.eu. (2018). Kettle Hole. *Available: http://www.landforms.eu/cairngorms/kettle%20hole.htm (Accessed: April 2018)*.

Landvik, J. Y., Bondevik, S., Elverhøi, A., Fjeldskaar, W., Mangerud, J., Salvigsen, O., . . . Vorren, T. O. (1998). The last glacial maximum of Svalbard and the Barents Sea area: ice sheet extent and configuration. *Quaternary Science Reviews, 17*(1-3), 43-75.

Larsen, D. S. (2011). *Fluid flow features along the Bjørnøyrenna Fault Complex west of West Loppa High, SW Barents Sea.* Universitetet i Tromsø,

Larssen, G., Elvebakk, G., Henriksen, L. B., Kristensen, S., Nilsson, I., Samuelsberg, T., . . . Worsley, D. (2002). Upper Palaeozoic lithostratigraphy of the Southern Norwegian Barents Sea. *Norwegian Petroleum Directorate Bulletin, 9*, 76.

Ligtenberg, J. (2005). Detection of fluid migration pathways in seismic data: implications for fault seal analysis. *Basin Research, 17*(1), 141-153.

Løseth, H., Gading, M., & Wensaas, L. (2009). Hydrocarbon leakage interpreted on seismic data. *Marine and Petroleum Geology, 26*(7), 1304-1319.

Løseth, H., Wensaas, L., & Arntsen, B. (2002). *Gas chimneys–indicating fractured cap rocks.* Paper presented at the Extended abstract presented at the AAPG Hedberg conference 'Near Surface Hydrocarbon Migration.

Magoon, E. (2003). Petroleum systems Exploring for oil and gas traps. *V. Chapter 3*.

Magoon, L. B., & Dow, W. G. (1994). The Petroleum System: Chapter 1: Part I. Introduction.

Mangerud, J., Jansen, E., & Landvik, J. Y. (1996). Late Cenozoic history of the Scandinavian and Barents Sea ice sheets. *Global and Planetary Change, 12*(1-4), 11-26.

NPD. (2017). Geologisk vurdering av petroleumsressursene i østlige deler av Barentshavet Nord 2017. *Available: http://www.npd.no/Global/Norsk/3-*

Publikasjoner/Rapporter/Geologisk-vurdering-BH-nord-2017/GeologivurderingBHn-nett.pdf *(Accessed: January 2018)*.

NPD. (2018a). Geology of the Barents Sea. . *Available:* http://www.npd.no/en/Publications/Reports/Compiled-CO2-atlas/6-The-Barents-Sea/61-Geology-of-the-Barents-Sea/ *(Accessed January 2018)*.

NPD. (2018b). Lithostratigraphy. *Available:* http://www.npd.no/en/Topics/Geology/Lithostratigraphy/ *(Accessed: January 2018)*.

NPD. (2018c). Norwegian Petroleum Directorate Factpages (Online). *Avilable:* http://factpages.npd.no/factpages/Default.aspx?culture=en *(Accessed: January 2018)*.

Nøttvedt, A., Cecchi, M., Gjelberg, J., Kristensen, S., Lønøy, A., Rasmussen, A., . . . Van Veen, P. (1993). Svalbard-Barents Sea correlation: a short review. *Arctic Geology and Petroleum Potential, Norwegian Petroleum Society (NPF), Special Publication, 2*, 363-375.

Ohm, S. E., Karlsen, D. A., & Austin, T. (2008). Geochemically driven exploration models in uplifted areas: Examples from the Norwegian Barents Sea. *AAPG Bulletin, 92*(9), 1191-1223.

Osborne, M. J., & Swarbrick, R. E. (1997). Mechanisms for generating overpressure in sedimentary basins: A reevaluation. *AAPG Bulletin, 81*(6), 1023-1041. doi:10.1306/522B49C9-1727-11D7-8645000102C1865D

Ostanin, I., Anka, Z., di Primio, R., & Bernal, A. (2013). Hydrocarbon plumbing systems above the Snøhvit gas field: structural control and implications for thermogenic methane leakage in the Hammerfest Basin, SW Barents Sea. *Marine and Petroleum Geology, 43*, 127-146.

Ostanin, I., Anka, Z., di Primio, R., Bernal, A., Anka, Z., Berndt, C., & Gay, A. (2012). Identification of a large Upper Cretaceous polygonal fault network in the Hammerfest Basin; implications on the reactivation of regional faulting and gas leakage dynamics, SW Barents Sea. In (Vol. 332-334, pp. 109-125). Amsterdam: Amsterdam, Netherlands: Elsevier.

Ottesen, D., Dowdeswell, J., & Rise, L. (2005). Submarine landforms and the reconstruction of fast-flowing ice streams within a large Quaternary ice sheet: the 2500-km-long Norwegian-Svalbard margin (57–80 N). *Geological Society of America Bulletin, 117*(7-8), 1033-1050.

Rajan, A., Bünz, S., Mienert, J., & Smith, A. J. (2013). Gas hydrate systems in petroleum provinces of the SW-Barents Sea. *Marine and Petroleum Geology, 46*, 92-106.

Ryseth, A., Augustson, J. H., Charnock, M., Haugerud, O., Knutsen, S.-M., Midbøe, P. S., . . . Sundsbø, G. (2003). Cenozoic stratigraphy and evolution of the Sørvestsnaget Basin, southwestern Barents Sea. *Norwegian Journal of Geology/Norsk Geologisk Forening, 83*(2).

Sattar, N., Juhlin, C., Koyi, H., & Ahmad, N. (2017). Seismic stratigraphy and hydrocarbon prospectivity of the Lower Cretaceous Knurr Sandstone lobes along the southern margin of Loppa High, Hammerfest Basin, Barents Sea. *Marine and Petroleum Geology, 85*, 54-69.

Schlumberger. (2018a). http://www.glossary.oilfield.slb.com/Terms/h/hydrocarbon_indicator.aspx (Accessed: January 2018).

Schlumberger. (2018b). http://www.glossary.oilfield.slb.com/Terms/r/reservoir_pressure.aspx (Accessed: January 2018).
Selley, R. C., & Sonnenberg, S. A. (2014). *Elements of petroleum geology*: Academic Press.
Sheriff, R. (1985). Aspects of Seismic Resolution: Chapter 1.
Sheriff, R. (2006). Encyclopedic Dictionary of Exploration Geophysics. *Society of Exploration Geophysics, Tulsa, 5th. Ed.* .
Sloan, E. D. J. (1998). Clathrate Hydrates of Natural Gases. *New York & Basel, Marcel Dekker Inc*, 705 p.
Smelror, M., Petrov, O., Larssen, G. B., & Werner, S. (2009). Geological history of the Barents Sea. *Norges Geol. undersøkelse*, 1-135.
Solheim, A., & Elverhøi, A. (1993). Gas-related sea floor craters in the Barents Sea. *Geo-Marine Letters, 13*(4), 235-243.
Steel, R. J., & Worsley, D. (1984). Svalbard's post-Caledonian strata—an atlas of sedimentational patterns and palaeogeographic evolution. In *Petroleum geology of the North European margin* (pp. 109-135): Springer.
Storvoll, V., Bjrlykke, K., & Mondol, N. H. (2005). Velocity-depth trends in Mesozoic and Cenozoic sediments from the Norwegian Shelf. *AAPG bulletin, 89*(3), 359-381.
Studentenergy. (2018). Available: https://www.studentenergy.org/topics/hydrates (Accessed: January 2018).
Tasianas, A., Martens, I., Bünz, S., & Mienert, J. (2016). Mechanisms initiating fluid migration at Snøhvit and Albatross fields, Barents Sea. *arktos, 2*(1), 26.
Thrasher, J., Fleet, A. J., Hay, S. J., Hovland, M., & Düppenbecker, S. (1996). Understanding geology as the key to using seepage in exploration: the spectrum of seepage styles.
Tissot, B. P., & Welte, D. H. (1984). Diagenesis, catagenesis and metagenesis of organic matter. In *Petroleum Formation and Occurrence* (pp. 69-73): Springer.
Torsvik, T. H., & Cocks, L. R. M. (2005). Norway in space and time: a centennial cavalcade. *Norwegian Journal of Geology/Norsk Geologisk Forening, 85*.
Twiss, R. J., & Moores, E. M. (2007). *Structural geology* (2nd ed. ed.). New York: W.H. Freeman Co.
Vadakkepuliyambatta, S. (2014). Sub-seabed fluid-flow systems and gas hydrates of the SW Barents Sea and North Sea margins.
Vadakkepuliyambatta, S., Bünz, S., Mienert, J., & Chand, S. (2013). Distribution of subsurface fluid-flow systems in the SW Barents Sea. *Marine and Petroleum Geology, 43*, 208-221.
Vadakkepuliyambatta, S., Chand, S., & Bünz, S. (2017). The history and future trends of ocean warming‐induced gas hydrate dissociation in the SW Barents Sea. *Geophysical Research Letters, 44*(2), 835-844.
Veeken, P. C. (2013). *Seismic stratigraphy and depositional facies models*: Academic Press.
Vorren, T. O., Richardsen, G., Knutsen, S.-M., & Henriksen, E. (1991). Cenozoic erosion and sedimentation in the western Barents Sea. *Marine and Petroleum Geology, 8*(3), 317-340.
Whiticar, M., & Werner, F. (1981). Pockmarks: Submarine vents of natural gas or freshwater seeps? *Geo-Marine Letters, 1*(3-4), 193-199.
Worsley, D. (2008). The post‐Caledonian development of Svalbard and the western Barents Sea. *Polar Research, 27*(3), 298-317.

References

Worsley, D., Johansen, R., & Kristensen, S. (1988). The mesozoic and cenozoic succession of Tromsøflaket. *A lithostratigraphic scheme for the Mesozoic and Cenozoic succession offshore mid-and northern Norway. Norwegian Petroleum Directorate Bulletin, 4*, 42-65.